JAERI-M
6320

REACTOR ENGINEERING DIVISION ANNUAL REPORT

(April 1, 1974 ~ March 31, 1975)

November 1975

Division of Reactor Engineering

日本原子力研究所
Japan Atomic Energy Research Institute

この報告書は，日本原子力研究所がJAERI-Mレポートとして，不定期に刊行している研究報告書です．入手，複製などのお問合わせは，日本原子力研究所技術情報部（茨城県那珂郡東海村）あて，お申しこしください．

JAERI-M reports, issued irregularly, describe the results of research works carried out in JAERI. Inquiries about the availability of reports and their reproduction should be addressed to Division of Technical Information, Japan Atomic Energy Research Institute, Tokai-mura, Naka-gun, Ibaraki-ken, Japan.

JAERI-M 6320

Reactor Engineering Division
Annual Report
(April 1, 1974 ∿ March 31, 1975)

Division of Reactor Engineering, Tokai, JAERI

(Received November 6, 1975)

Research activities in fiscal 1974 in Reactor Engineering Division of eight laboratories and computing center are described.

Works in the division are closely related with the development of a multi-purpose High-temperature Gas Cooled Reactor, the development of a Liquid Metal Fast Breeder Reactor in Power Reactor and Nuclear Fuel Development Corporation, and engineering of thermonuclear fusion reactors. They cover nuclear data and group constants, theoretical method and code development, integral experiment and analysis, shielding, heat transfer and fluid dynamics, reactor and nuclear instrumentation, dynamics analysis and control method development, fusion reactor technology and aspects of the computing center.

JAERI－M 6320

昭和49年度原子炉工学部年報

日本原子力研究所東海研究所原子炉工学部

（1975年11月6日受理）

本報告書は，原子炉工学部の8研究室と計算センターにおいて昭和49年度に得られた主要な研究成果をとりまとめたものである。

原子炉工学部の研究計画は，多目的高温ガス炉の開発，動燃事業団による液体金属高速増殖炉の開発，および核融合炉のための炉工学的研究に密接に関連している。核データと群定数，炉理論とコード開発，積分実験と解析，遮蔽，熱伝達と流動，炉計装と核計装，動特性解析と制御法の開発，核融合炉技術，および計算センターの活動の各分野にわたって，多くの成果が述べられている。

Foreword

This is the annual report of Reactor Engineering Division, Japan Atomic Energy Research Institute, and covers the one year period, April 1974-March 1975.

The research activities of the Division extend the broad area of reactor engineering. The major fields are thermal and fast reactor physics, shielding, reactor instrumentation and controls, heat transfer and fluid dynamics, and numerical analysis.

The total number of people working in the Division at the end of the period was 116. Expenditures during the period under review in this report totalled about 1.23 billion yen. In addition to this, a considerable amount of expenditures was covered under research contracts with outside organizations, among which Power Reactor and Nuclear Fuel Development Corporation offered the largest contribution.

Some researches were conducted under research collaborations with universities and research organizations.

The research activities were conducted in eight Laboratories and Computing Center.

The Laboratories are

Reactor Physics Analytical Laboratory
Fast Reactor Physics Laboratory
Thermal Reactor Physics Laboratory
Reactor Instrumentation Laboratory
Reactor Control Laboratory
Heat Transfer Laboratory
Shielding Laboratory
Numerical Analysis Laboratory.

The major research and development projects, with which some research programmes in the Division are closely associated, are

1) Development of Experimental High Temperature Gas Cooled Reactor (HTGR) for Multi-purpose Use
2) Development of Liquid Metal Fast Breeder Reactor as a national project conducted by Power Reactor and Nuclear Fuel Development Corporation (PNC).
3) Some Engineering Research Programmes for Thermonuclear Fusion Reactor.

The research programmes associated with the second subject of the above three have been mainly conducted through research contracts between JAERI and PNC.

A small scale helium gas loop and a large scale helium gas loop have been operated for HTGR development. In particular, since 1973 the large loop has been operated at 1,000 °C and 40 kg/cm^2 for 450 hours and the total operating time amounts to 1800 hrs. Out-of-pile test of in-pile gas loop OGL-1, to be installed in JMTR, has been conducted in the large loop.

In the field of LMFBR, the critical experiment and some integral experiments on the Fast Critical Assembly (FCA) have been made to support the design of the prototype fast breeder reactor. A number of analyses related with the above experiments have also been made. In the latter half of the period, the modification work on FCA core was initiated in order to increase the core diameter of FCA.

Concerning the thermo-nuclear fusion reactor, studies have been made on integral experiments on a spherical lithium metal blanket system, on heat transfer of electrically conductive fluids under a strong magnetic field, and on fusion reactor stability and feedback control. X-ray energy spectrum of plasma in JFT-2 was measured by Si(Li) detector, through which electron temperature was deduced.

A number of researches are being made other than those closely related with the projects mentioned above.

In the field of nuclear data and group constants, emphases are placed on the development of the methods and computer codes for the evaluation to establish a simple means to revisions of these data and constants.

For developing theories and calculation codes, stresses are laid on analyses of sodium-void effect and plate lattice heterogeneity effect. In addition, the finite element method has been developed for dealing with stationary neutron transport in cylindrical systems and the point-reactor kinetics. The development of Monte Carlo method has been continued to obtain the reactor eigenvalue with less computing time as well as to analyze neutral particle transport in torus plasma.

In the field of reactor and nuclear instrumentation, some improvements of nuclear instrumentations and portable semiconductor detector developments for gamma spectrometry have been made and a high temperature neutron detector has successfully been tested up to 600 °C. Studies on thermoluminescence dosimeters for measuring neutron have been made.

In the field of dynamic analyses and control methods development, a new method of load-following control for BWR plant and a diagnostic technique for analyzing the nuclear reactors have been developed. The dynamic analyses of gas diffusion plant have been made by the hybrid computer system which has been installed in this period.

Developments of software and hardware for the computer in the computing center have been achieved for the expected growth both in number and size of demands for the computer system. In addition, discussions had been made on the selection of a new computer in larger scale for replacing the present machine.

Some studies on gas cooled fast breeder reactors are being made on experimental facilities for HTGR.

Junichi MIIDA, Head
Division of Reactor Engineering

CONTENTS

1. Nuclear Data and Group Constants

1.1 Production of Group Constants for ^{235}U, ^{238}U and ^{239}Pu in Resonance Energy Region

H. Takano and S. Katsuragi

The resonance parameters for ^{238}U, ^{235}U and ^{239}Pu were evaluated and the group constants of 25 and 70 group structures were produced [1] as the function of temperature, σ_0 and R, where σ_0 is the admixture cross section of Bondarenko type and R is the ratio of the number density of ^{238}U to that of ^{235}U or ^{239}Pu. The evaluation of the average resonance parameters for the unresolved resonance region was performed by the least squares fit of the pre-evaluated infinitely dilute cross sections.[2] The calculation of the fitting was performed by using the ARCFIT [3] code in which the resonance parameters were searched by the iterative method. The average resonance parameters obtained for ^{235}U, ^{238}U and ^{239}Pu are shown in Table 1.1.1. The fitted cross section curves are compared with the measured cross sections in Figs. 1.1.1-1.1.3.

In order to take exactly the effects of mutual and self-interference between resonance levels into consideration, the individual resonance parameters were generated by the random sampling method. The ladders of resonance parameters were selected [3] so as to reproduce accurately the pre-evaluated infinitely dilute cross sections [2] of 70 group structures. The produced α-values of ^{239}Pu are shown in Fig.1.1.4 with the pre-evaluated values as an example.

The effective cross sections were accurately calculated by solving numerically the neutron slowing down equation.[4] [5] The resonance shielding factors of ^{238}U, ^{235}U and ^{239}Pu were provided for 4 temperatures of 300, 900, 2100 and 3500°k and for 4 σ_0

of 1000, 100, 10 and 1. The calculated energy ranges were 46.5 keV - 0.215 eV for ^{238}U, 21.5 keV - 0.215 eV for ^{239}Pu and 10 keV - 0.215 eV for ^{235}U, respectively. The upper energy range were extended for ^{238}U from 21.5 keV to 46.5 keV in the present revision work, since it was found [6] that the Doppler effects above 21.5 keV could not be neglected.

Table 1.1.1 Average resonance parameters obtained by using the ARCFIT [3] code

	Do (meV)	$\langle \Gamma_\gamma \rangle$ meV	So ($\times 10^{-4}$)	S1 ($\times 10^{-4}$)	r ($\times 10^{-13}$ cm)
^{238}U	41.6	23.0	0.928	1.4	8.8
^{235}U	8.0	47.9	1.05	2.48	8.3
^{239}Pu	8.8	41.6	0.95	3.04	8.28

r is the atomic radius. The fission widths of ^{235}U and of ^{239}Pu were obtained from using the fission channel schemes in Ref. (7).

References

1) Takano, H., Katsuragi, S.: JAERI-memo 6158 (1975).

2) Takano, H., Hasegawa. A., Katsuragi, S.: Reactor Engineering Division Annual Report, JAERI-M 5955, p.4, 1975.

3) Takano, H., Ogawa, S.: A code of the average resonance cross section fits., (to be published).

4) Takano, H. JAERI-M 4721 (1972)

5) Nakagawa, H., Katsuragi, S.: JAERI-memo 3907 (1969)

6) Takano, H., et al.: JAERI-memo 4934 (1972).

7) Katsuragi, S., et al.: JAERI-1199 (1970).

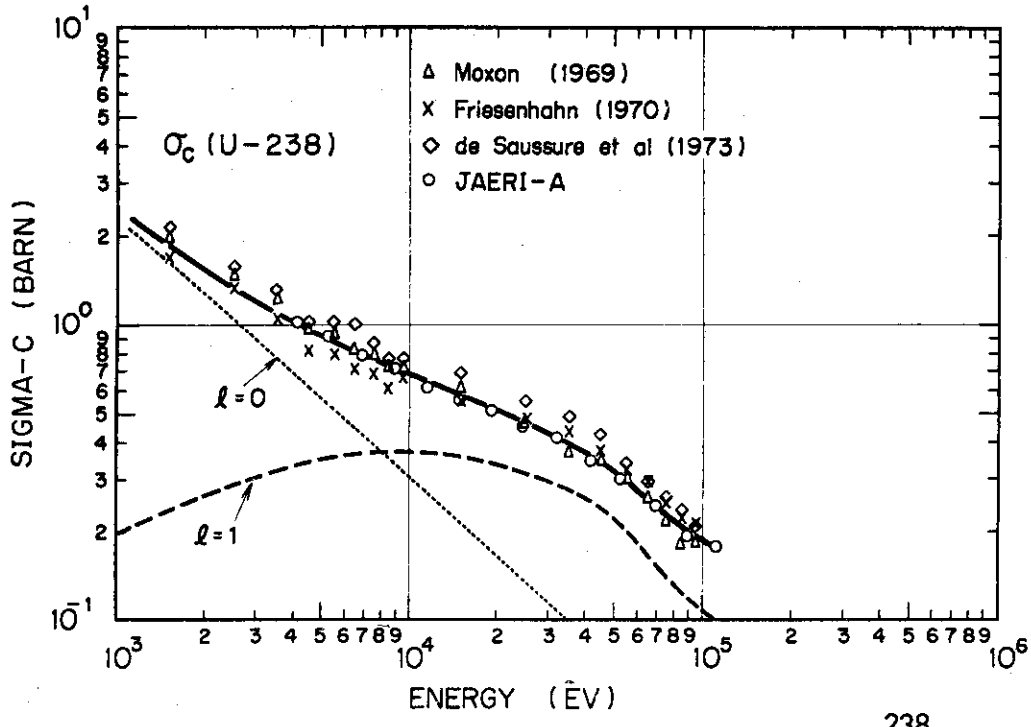

Fig.1.1.1 Comparison of capture cross sections for ^{238}U

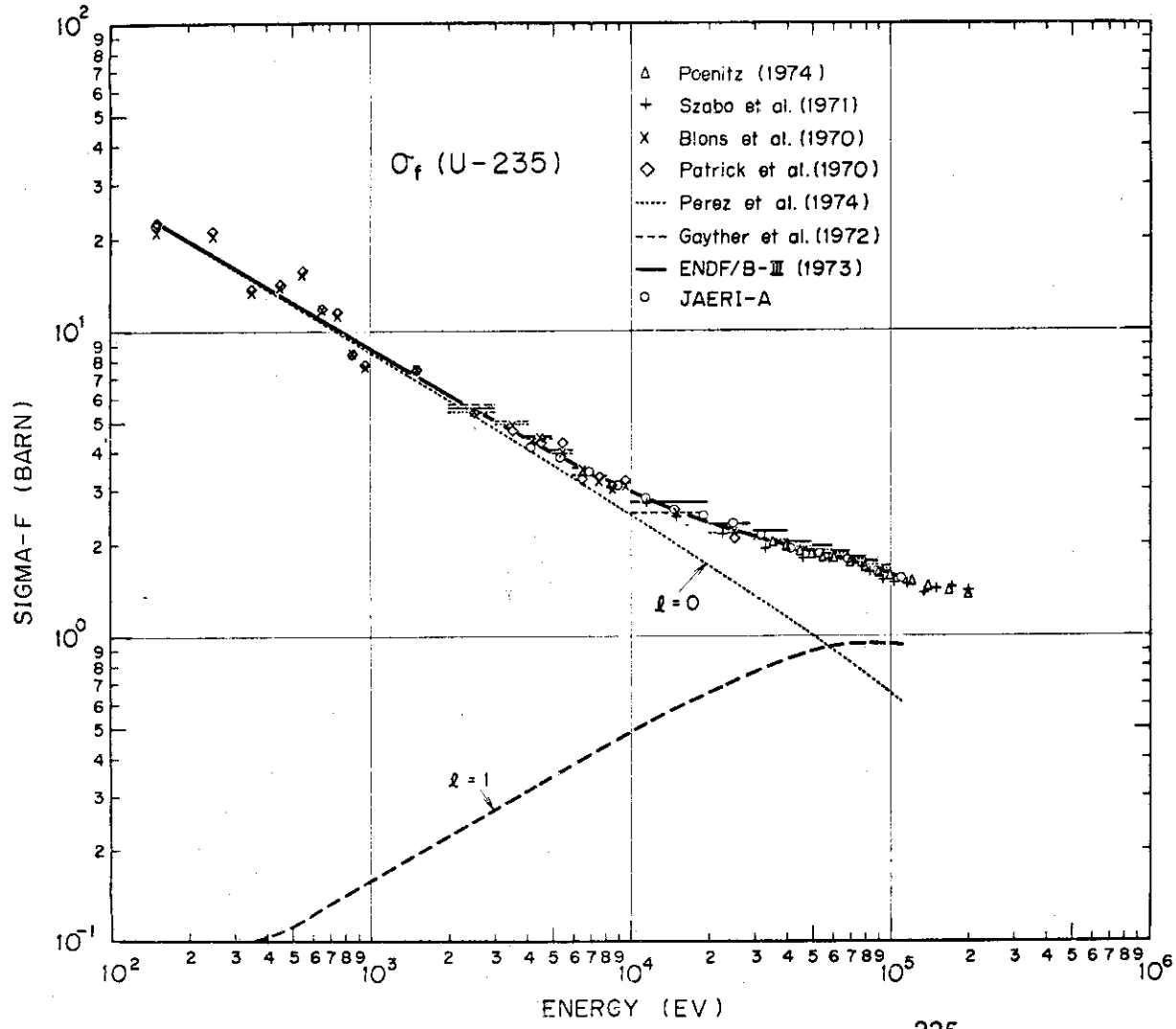

Fig.1.1.2 Comparison of fission cross sections for ^{235}U

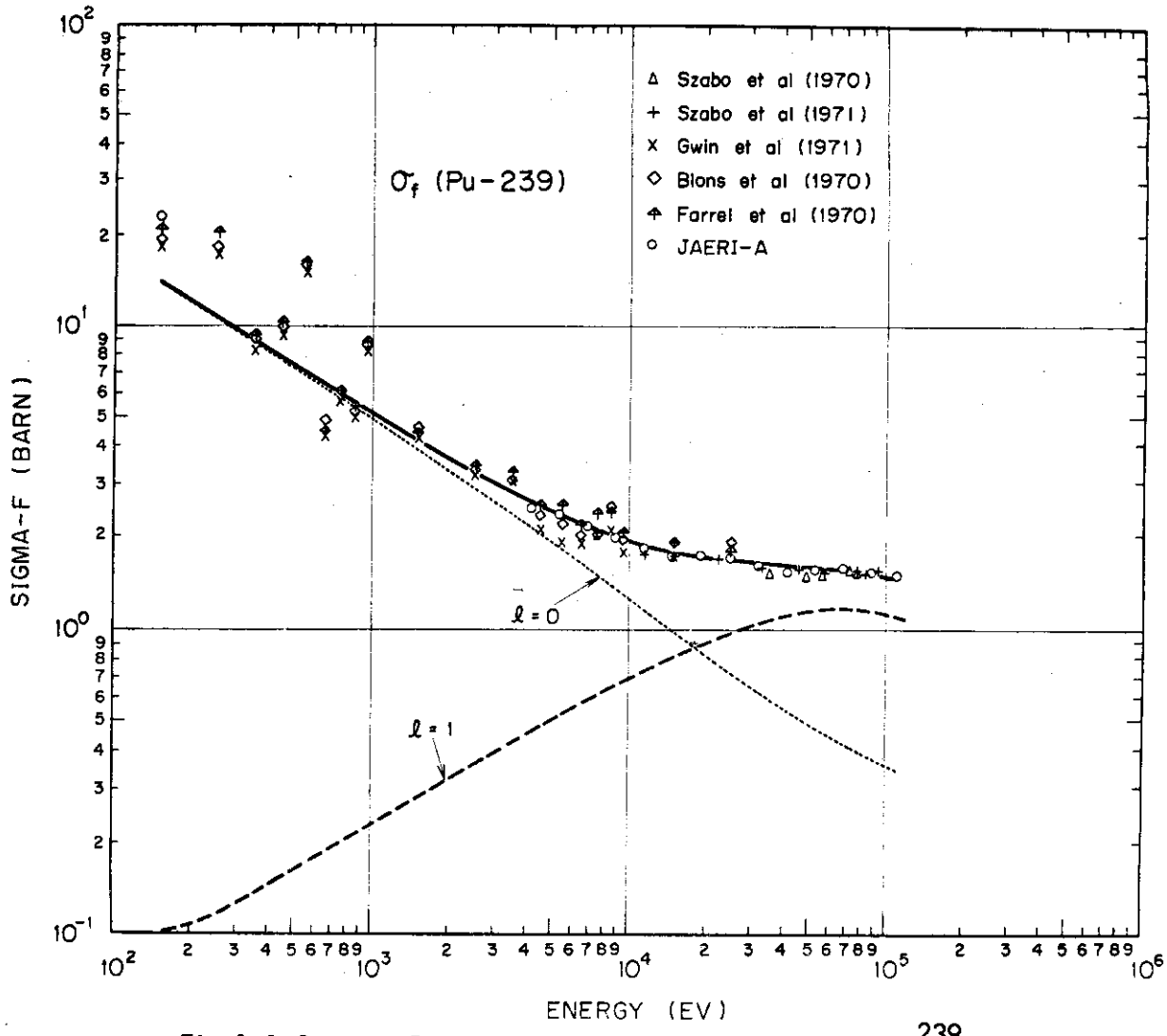

Fig.1.1.3 Comparison of fission cross sections for ^{239}Pu

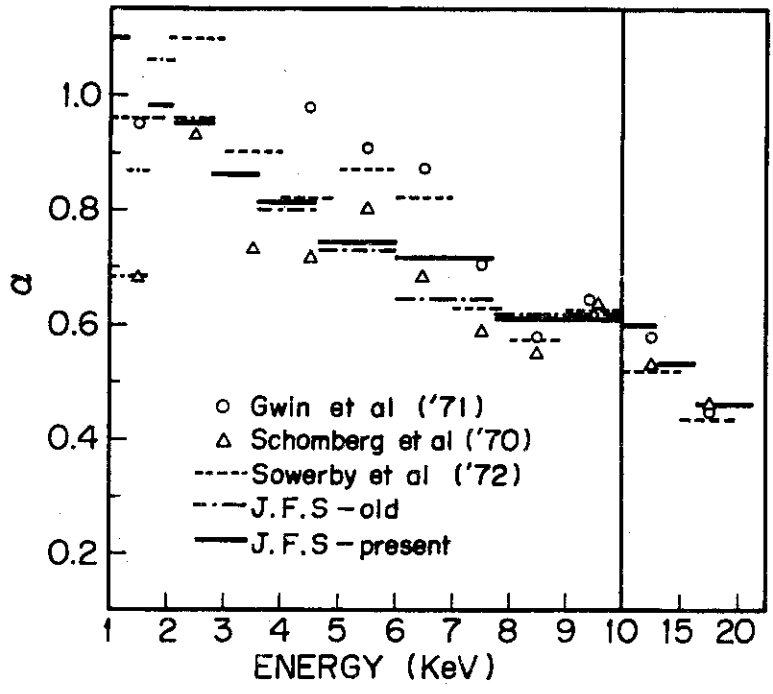

Fig.1.1.4 α - value of Pu-239

1.2 Development of PROF. GROUCH G-II System

(A system of fully automated generation routine of multigroup cross section set)

A. Hasegawa and S. Katsuragi

In JAERI, the processing code, PROF-GROUCH-G[1], was commonly used to prepare multigroup cross section set hitherto. This code is, however, programmed to treat only the ENDF/A format data for the input nuclear data file. Nowadays, ENDF/B format data has been mainly used, while the ENDF/A format has been minor format. From the trends of nuclear data file in the world, ENDF/B format was adopted for the Japanese Evaluated Nuclear Data Library (JENDL) which is under development.

A new code system, PROF-GROUCH-G-II[2], producing multigroup cross section set has been developed. This code system is designed to produce fully automatically a JAERI-Fast Set type multigroup cross section set (which is similar to the Russian set) from any input nuclear data file with ENDF/B format including the Version IV. This code can also prepare the multigroup cross section library tape that is used in a diffusion calculation code such as the EXPANDA 70D.

This code system consists of three main parts: (A) File control system, (B) Nuclear-Data-File processing system and (C) Data (multigroup constants) update and retrieval system. Main features of each part are as follows: (A) Setting of direct accessable data set and control of these files. (B) ENDF/B format data (up to Version IV data) are processed. In the calculation of the inelastic scattering matrices, this code processes exactly secondary neutron angular distribution data. Upper limit of the point-wise data is enlarged up to 20000 points per reaction. The effective cross section depending on σ_0 parameter can be produced, and therefore it is very easy to produce self-shielding factor tables. For elastic and inelastic matrices calculation, general

tabulated secondary neutron angular distribution data is processable. (C) Any data in the direct access data set can be updated and retrieved in any moment in this system. Therefore users will be able to produce a library tape composed of only necessary data.

Owing to the capability of flexible data processing, this code system requires a fairly large computer core memory, say 317 K words, in standard overlay structure. Typical running time for one nuclide by processing a set of multigroup constants including σ_{aa}, $\sigma_e^{i\to j}$, $\sigma_{in}^{i\to j}$, $\sigma_{2n}^{i\to j}$, σ_{eff} (σ_0 parameter 6 cases) is about 15 minutes on FACOM-230/75 Monitor VII in the case of the 6000 points data per primary reaction.

This code is fully free from tedious input data preparation, so it is a very powerful tool for the production of group constants set.

References

1) Tone, T., Katsuragi, S. : "PROF GROUCH G: A Processing Code for Group Constants for a Fast Reactor", JAERI-1192 (1970).

2) Hasegawa, A., Katsuragi, S. : to be published.

1.3 Tests of FP Group Constants with Integral Experiments

Y. Kikuchi and A. Hasegawa

Tests of FP group constants produced from the preliminary version of JNDC evaluated data[1] have been performed, while the revision of evaluation has been carried out. It was found[2] from the integral tests for FP mixtures that the preliminary version of JNDC group constants might give too large capture cross section. It is difficult, however, to discuss the reliability of the cross section set from the integral data of mixtures, since the mixtures are composed of so many isotopes.

On the other hand, the reactivity worths of 57 isotopic samples were measured at STEK cores in RCN-Petten, and the preliminary results were already published[3,4]. The correction of self-shielding effect is difficult in these experiments, and these experimental results are noted to be preliminary. It is worthwhile, however, to check our set with these integral data. The flux and the adjoint flux were informed as a private communication.

The calculated reactivities with the JNDC set are compared with the experimental data, and the followings can be said :

1) The calculated values with the JNDC set are a little larger than the experimental ones for

Mo-95, Mo-97, Ru-101, Cs-133, Nd-143,

Nd-145, Pm-147, Sm-147, Eu-153. (category 1)

2) The calculated values are a little smaller for

Tc-99, Rh-103, Pd-105, Pd-107, Ag-109, Sm-149.
(category 2)

3) The calculated values are much larger than the experimental ones for

Ru-102, Ru-104, I-129, Nd-144. (category 3)

4) The calculated values are much smaller for

Sm-151. (category 4)

5) The core dependence of the calculated values does not agree at all with the experimental ones for

Zr-93, Cs-135. (category 5)

The agreement is satisfactory for the nuclides of category 1 and 2. The tendency of these slight disagreements was taken into account in the revision work for these nuclides so as to improve the agreement. The disagreement for the nuclides of category 3 may be partly explained with our rough treatment of inelastic scattering. As for Sm-151, the JNDC evaluated curve is very different from the other evaluated data and might be in error. The disagreement of the core dependence for the nuclides of category 5 is not understandable.

It is concluded that the disagreement for categories 3, 4 and 5 seems too large to be explained as due to the error of the nuclear data. Therefore these results were used in the revision work only as references. The detailed discussion concerning various tests of JNDC FP group constants (preliminary version) is given in Ref. 2.

References :

1) JNDC, Evaluation of Fission Product Nuclear Data for Fast Reactor, JAERI-M5752 (1974)

2) Kikuchi, Y., Hasegawa, A., Tasaka, K., Nishimura, H., Otake, I. and Katsuragi,S., JNDC Fission Product Group Constants-Preliminary Version-, JAERI-M 6001 (1975)

3) Hoekstra, E. K., Fast Reactor Programme, Second Quarter 1973, Progress Report RCN-190 (1973)

4) Hoekstra, E. K., Fast Reactor Programme, Third Quarter 1973, Progress Report RCN-199 (1973)

1.4 Gamma-ray Energy Release in the Decay of Fission Products[1)]

N. Sasamoto and T. Nemoto*)

Fission Product decay gammas will not dictate the thickness of the shield surrounding a reactor in operation, they are, however, considered to be the only gamma sources in the shield after reactor shutdown. These gamma rays, therefore, will provide design criteria for shields in the waste disposal facility, reprocessing plant, spent fuel storage equipment and transport cask for spent fuels.

The purpose of this study was to evaluate the gamma-ray spectra for the fission product more precisely than those by Perkins and King[2)], following the representation of them. The points of revision are as follows :

(1) updating of the gamma-ray and decay scheme data for fission products;

(2) consideration of the more precise disintegration rate of fission products, using Bateman's solution and its integral form;

(3) division of the energy spectrum into 10 groups, Perkins' six groups for $E \leq 2.6$ MeV, and four groups for $E > 2.6$ MeV;

(4) extension of the operating time to 10 years; and

(5) consideration of eight kinds of fission types; i.e. ^{235}U, ^{239}Pu, ^{241}Pu and ^{233}U by thermal neutrons and of ^{235}U, ^{238}U, ^{239}Pu and ^{232}Th by fission spectrum neutrons.

The decay scheme considered in this study are for 289 radioactive fission products, plus 125 stable ones. The nuclear data of decay scheme are mainly taken from the Table of

*) Toyo Eng.Cooporation, Kasumigaseki 3-2-5, Chiyodaku, Tokyo

Isotopes[3]. Independent fission yields used in the evaluation are obtained using the extensive cummulative fission yield data by Meek and Rider[4]. Gamma-ray energy and the absolute value of the branching ratio of gamma-ray emission for each fission product were taken mainly from the compilation in ref.[5], supplemented by the data from ref.[6].

A part of the results of extensive evaluation in this study were presented in Fig.1.4.1 and Fig.1.4.2 for gamma-ray energy decay rates due to burst thermal neutron fission of ^{235}U and due to thermal fission of ^{235}U for 10 years of reactor operation, respectively.

References

1) Sasamoto, N., Nemoto, T.: "Gamma-ray Energy Release in the Decay of Fission Products," Nucl. Eng. Design 32,252(1975).

2) Perkins, J.F., King, R.W.: "Energy Release from the Decay of Fission Products," Nucl. Sci. Eng. 3,726(1958).

3) Lederer, C.M. et al.: Table of Isotopes, 6th edition, John Wiley(1968).

4) Meek, M.E., Rider, B.F.: "Compilation of Fission Product Yields," NEDO-12154(1972).

5) Wachter, J.W.: "DKDATA:subroutine for retrieving radionuclide gamma-ray decay data from RSIC data set DLC-19/DECAYGAM," ORNL-TM-4095(1973).

6) Wakat, M.A.: "Catalogue of γ-rays emitted by radionuclides, Nuclear Data Tables, section A, vol.8, nos5-6(1971).

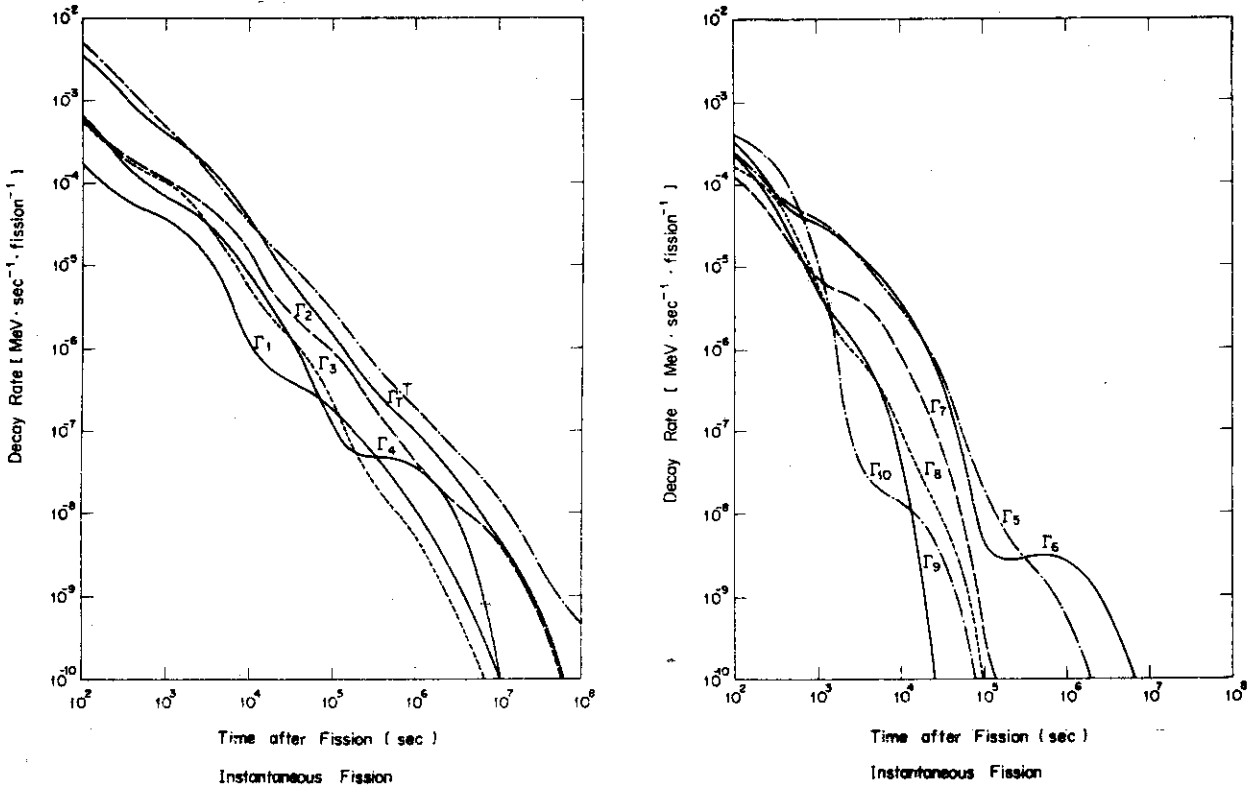

Fig.1.4.1 Gamma-ray energy decay rates due to burst thermal neutron fission of ^{235}U

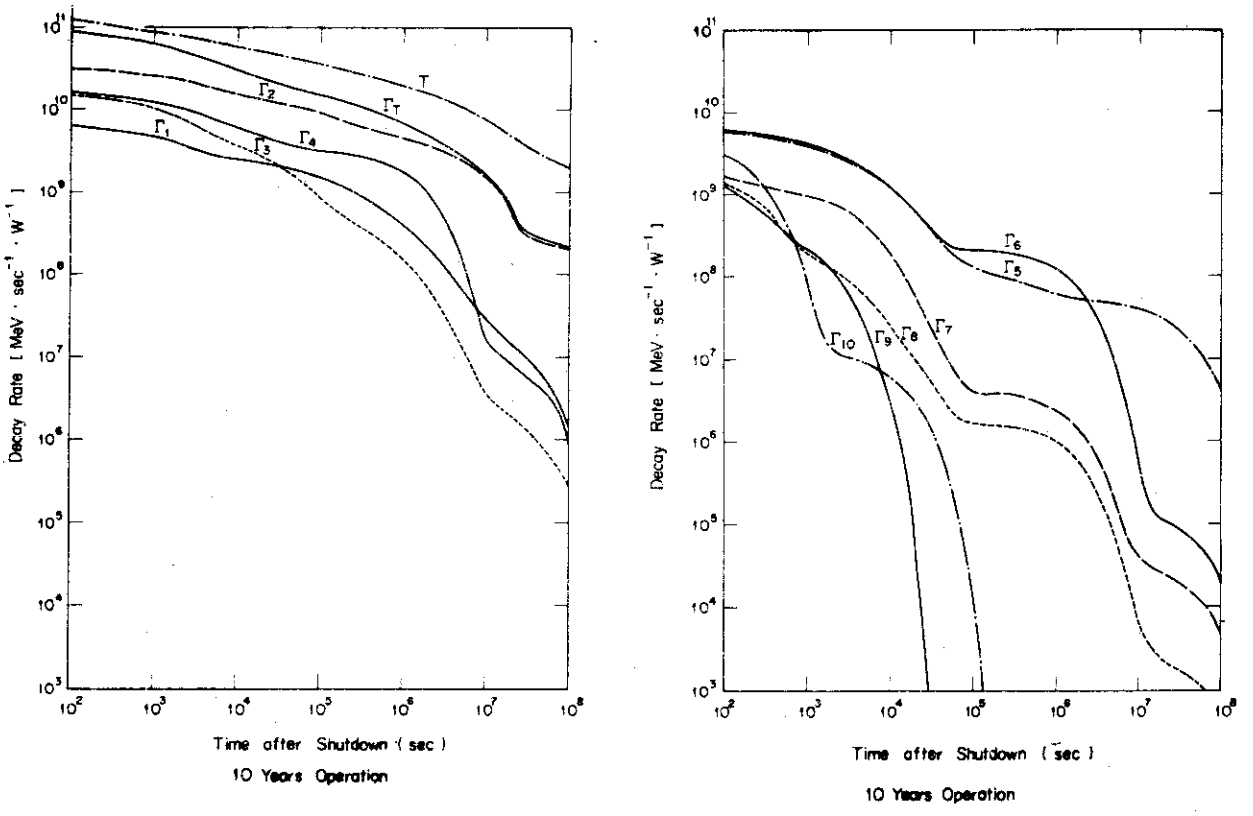

Fig.1.4.2 Gamma-ray energy decay rates due to thermal neutron fission of ^{235}U for 10 years of reactor operation

1.5 Calculation of the Decay Power of Fission Products Considering the Neutron Capture Transformation

K. Tasaka

The decay power of fission products has been calculated taking into consideration the neutron capture transformation of each nuclide and its beta decay.[1] The nuclear data library[2] contains 1114 nuclides of which 144 are stable, and neutron capture transformation is considered for 56 nuclides, 30 of which are stable. A statistical array of unknown, short-life nuclides is included in the library to achieve agreement with experimental data at short cooling time. The atom number of each FP nuclide was calculated analytically by using the DCHAIN computer code.

The effect of neutron capture transformation in the decay power of fission products was examined by varying the neutron spectrum, neutron flux, fissioning nuclide, and irradiation and cooling time. The results for the thermal neutron fission of ^{235}U and the fast neutron fission of ^{239}Pu are shown in Fig. 1.5.1. ^{235}U was irradiated for one year in the core of thermal reactor with epithermal index of 0.2 and thermal neutron flux of 3×10^{13} n/cm^2.sec. ^{239}Pu was irradiated for one year in the core of 1000 MWe LMFBR with neutron flux of 3×10^{15} n/cm^2.sec. From the results obtained the following were revealed: The neutron capture transformation generally increases the decay power. The effect increases with neutron flux and irradiation time, and it becomes salient beyond 10^5 sec in cooling time. It is small for less than 10^4 sec which is important for the design of ECCS(emergency core cooling system) of a light-

water reactor. In this region the decay power changes less than 0.2 % for the thermal fission of ^{235}U. Around 10^3 sec the neutron capture transformation of ^{135}Xe reduces the decay power in the thermal reactor. The effect of neutron capture has peaks around 10^6 sec and 10^8 sec; it is negligible beyond 10^9 sec. The changes in decay power are 2.4 %, 10.5 % and 0.2 % at cooling time 10^6 sec, 10^8 sec and 10^9 sec respectively for the thermal fission of ^{235}U. These values are 1.3 %, 3.2 % and 0.2 % for the fast fission of ^{239}Pu. Around 10^6 sec, the change in decay power is mainly from the contributions of ^{103}Ru, ^{134}Cs, ^{136}Cs, ^{148m}Pm and ^{148}Pm. Around 10^8 sec ^{134}Cs alone contributes to the change in decay power in the thermal fission of ^{235}U, and ^{154}Eu also contributes considerably in the fast fission of ^{239}Pu.

Reference

1) Tasaka, K. : "Calculation of the Decay Power of Fission Products Considering Neutron Capture Transformation," JAERI-M 5972 (1975).

2) Tasaka, K. : "Nuclear Data for Calculation of the Decay Power of Fission Products," JAERI-M 5997 (1975).

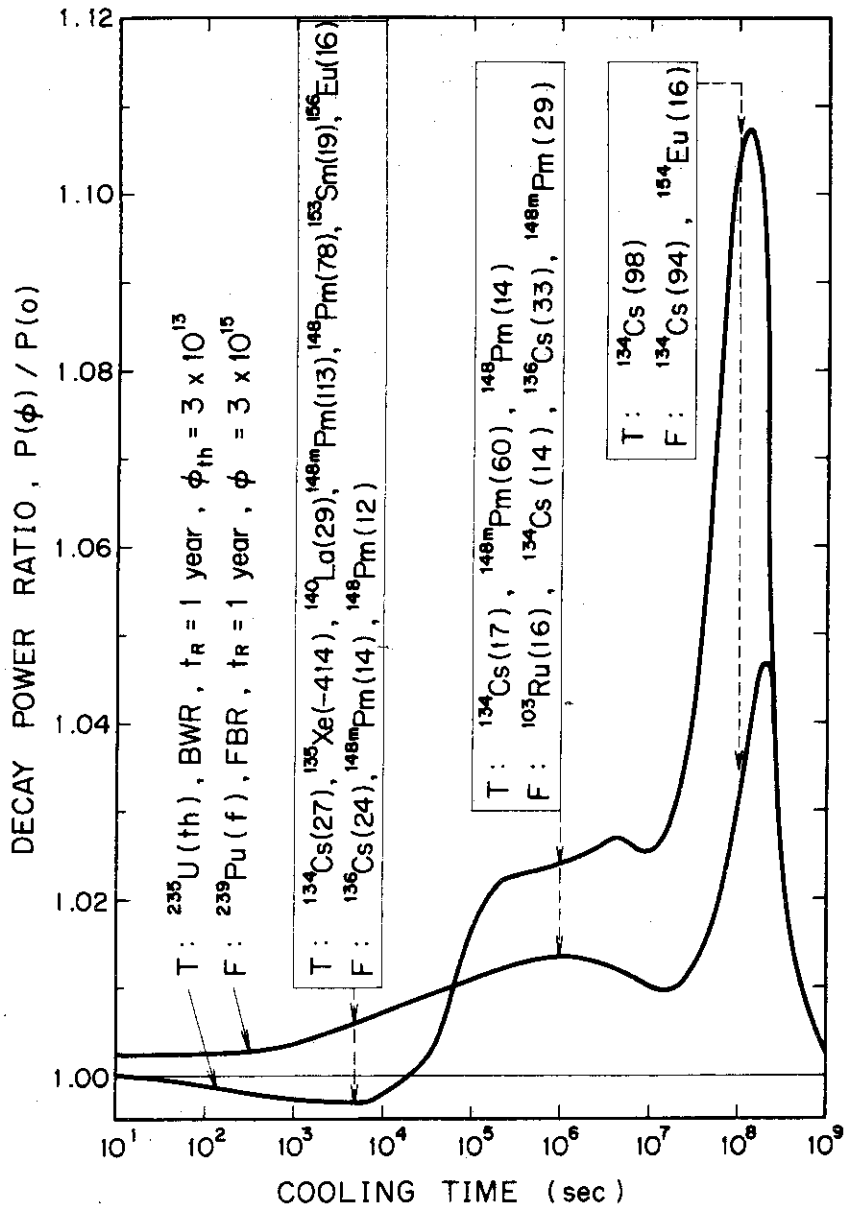

Fig. 1.5.1 The decay power of fission products was calculated considering the neutron capture transformation for the thermal neutron fission of ^{235}U irradiated for one year with thermal neutron flux of 3×10^{13}, and for the fast neutron fission of ^{239}Pu irradiated for one year in the core of 1000 MW_e LMFBR with neutron flux of 3×10^{15}. The results are shown as the ratio to those without consideration for the neutron capture transformation.

2. Theoretical Method and Code Development

2.1 Treatment of the Elastic Removal Cross Sections in Na-Fe Resonance Region and One-Dimensional Code EXPANDA-70 DRA

A. Hasegawa, S. Tsuruta* and Y. Ishiguro

A code EXPANDA-70DRA[1] has been developed to remove a drawback usually encountered when preparing effective elastic removal cross sections for a set of group constants. This code is designed to treat exactly the effective elastic removal cross sections in the resonance energy regions of light and medium-weight nuclides. The procedure is as follows: The fine spectrum of each region (the region as homogeneous) is obtained by purely numerical calculation using a recurrence formula[2], considering the anisotropy up to P1 component in the center of mass system. The effective removal cross sections are then calculated by using the fine group spectrum as a weighting function, and finally the one-dimensional diffusion criticality or perturbation calculation is performed.

The simple description of this code is as follows: The lethargy steps of 0.0085 is taken for solving the slowing down equation in the energy range from 70 keV down to 1 keV, where the resonance scatterings of sodium and iron are dominant. The pointwise elastic scattering cross sections were taken from ENDF/B-III file, while the JAERI-Fast Set with 70-group[3] was used for the various cross sections of other elements and also for those of other reactions of sodium and iron.

In order to see the difference between this exact treatment and conventional

---

* Nippon Information Service Co., Ltd., Chiyoda-ku, Tokyo

table-look-up method, the calculations were made for some integral quantities such as sample worth of Na and Na-void reactivity coefficient in typical Fast Critical Assemblies. The difference of 10-15% was found between these two methods in the calculations of both the Na-sample and the Na-void reactivity coefficient. The results for the Na-void reactivity coefficient in ZPR III-48 are shown in Table 2.1.1 as an example. These differences were, however, found to be the same magnitude as those caused by using different evaluated nuclear data for the primary cross sections of heavy nuclides, or by different treatments of fluxes in the perturbed region. The influence of the removal cross sections on effective multiplication factor was at most 0.05%, which is no problem at present as long as the group constant set with 70 groups is used.

References

1) Hasegawa, A., Tsuruta, S., Ishiguro, Y.: "Treatment of the Elastic Removal Cross Sections in Na-Fe Resonance Region and One-Dimensional Code EXPANDA-70DRA", JAERI-M6081 (1975) (in Japanese)

2) Ohkubo, Y., Ishiguro, Y., Tsuruta, S.: "Numerical Solution of the Slowing Down Equation with P1 Approximation by Recurrence Formula", J. Nucl. Sci. Technol., 11, 348 (1974) (Short Note).

3) Katsuragi, S., Tone, T., Hasegawa, A.: "JAERI Fast Reactor Group Constants Systems, Part I", JAERI-1195 (1970)

Katsuragi, S., et al.: "JAERI Fast Reactor Group Constants Systems, Part II-1", JAERI-1199 (1970)

Table 2.1.1 Na-void reactivity coefficient calculated from several cross section sets and methods

(ZPR - Ⅲ - 48)

SET NO	No	METHOD	C/E	C	k_{eff}	(δk/k) COMPONENT					
						$\nu\Sigma_f$	Σ_r	Σ_a	Σ_{in}	Σ_D	SUM
I	1	F.O.PD	1.97	11.003	0.99768	-5.0450-5	-1.2847-4	2.8288-4	2.6985-4	-8.6441-5	2.8734-4
	2	F.O.PR	1.75	9.813	0.99780	-4.6844-5	-1.3149-4	2.5742-4	2.6361-4	-8.6416-5	2.5623-4
II	3	F.O.PD	1.63	9.133	1.00353	-5.3845-5	-1.7121-4	2.9485-4	2.5422-4	-8.5466-5	2.3854-4
	4	F.O.PR	1.33	7.459	1.00390	-5.0212-5	-1.8362-4	2.6874-4	2.4537-4	-8.5477-5	1.9480-4
III	5	F.O.PD	1.81	10.120	0.99407	-5.5238-5	-1.8075-4	3.0360-4	2.8170-4	-3.5009-5	2.6431-4
	6	F.O.PR	1.55	8.686	0.99416	-5.1562-5	-1.8786-4	2.7682-4	2.7446-4	-8.4994-5	2.2685-4
	7	E. P D	1.56	8.734	0.99407	-5.3366-5	-2.4379-4	3.2142-4	2.8642-4	-8.2598-5	2.2809-4
	8	E. P R	1.35	7.539	0.99416	-5.1142-5	-2.6237-4	3.1173-4	2.8321-4	-8.4035-5	1.9639-4
	9	E. P R1	1.36	7.612	0.99404	-5.0795-5	-2.5900-4	3.1023-4	2.8241-4	-8.4038-5	1.9881-4
	10	E. P R2	1.37	7.662	0.99397	-5.0568-5	-2.5644-4	3.0924-4	2.8191-4	-8.4039-5	2.0011-4
	11	D. K D	1.43	8.029	Na IN k_{eff} =	0.99407035		Na OUT k_{eff} =	0.99427760		2.0725-4
	12	D. K R	1.21	6.797	〃	0.99415746		〃	0.99433289		1.7753-4
	13	D. K R1	1.23	6.871	〃	0.99404159		〃	0.99421893		1.7944-4
	14	D. K R2	1.24	6.925	〃	0.99396524		〃	0.99414395		1.8085-4

SET NO Ⅰ : Na, Fe ENDF/B - Ⅲ, OTHERS JAERI - FAST 72.6 V.
Ⅱ : Na, Fe ENDF/B - Ⅲ, OTHERS JAERI - FAST 74.1 T.
Ⅲ : Na, Fe ENDF/B - Ⅲ, OTHERS JAERI - FAST 74.6 V.

D : EXP 70 D
R : EXP 70 DR
R1: EXP 70 DR
R2: EXP 70 DR

B^2 = 0.
= 3.0E - 3
= 5.0E - 3

F.O.P 1-st Order Perturbation
E. P Exact Perturbation
D. K Direct k Calculation

C : IH / Kg

E = 5.6 ± 0.3 IH / Kg

2.2 Analysis of Plate Lattice Heterogeneity Effect with Coarse Group Constants

Y. Kikuchi

The method to analyze the plate lattice heterogeneity effect with the coarse group constants[1] has been further improved during this period and a one-dimensional diffusion code EXPANDA-75 was published[2].

The flux heterogeneity is obtained by solving the multi-region integral transport equation in which the net leakage from the unit cell is taken into account by renormalizing the first flight collision probability. The fission source of each plate is calculated with the spectrum for the homogenized cell, and it was found that the fission source iteration was not necessary in the heterogeneous cell calculation under most of conditions for fast reactors.

The effective admixture cross sections (σ_0) were defined[1,2] for each plate by considering the interference with the other plates. The effective cross sections were calculated with these admixture cross sections in EXPANDA-75 and were compared with the exact results calculated by SDR[3]. The agreement was excellent except for the capture cross section of ^{238}U below 500 eV. This drawback below 500 eV was extensively investigated and it was concluded that this error was caused by the interpolation of the self-shielding factor from the tabulated values. EXPANDA-75 adopts the conventional interpolation with a quadratic function. This method gives considerable errors when the self-shielding factor depends strongly on σ_0 . However, the energy range below 500 eV is not very important for fast reactors. Therefore we did not improve the interpolation in EXPANDA-75, since more precise interpolation with a hyperbolic tangent function requires the iteration and therefore considarable computing time.

The elastic removal cross sections near the 2.85 keV resonance of sodium should

be corrected, since the values contained in the JAERI-Fast set were calculated with assuming the asymptotic 1/E spectrum. We have developed a simple analytical expression[4] of flux shape near a wide scattering resonance. It is well known that the collision density is not flat in lethargy unit for a composite medium near such a resonance. The present method expresses fairly well such a behavior of collision density, by treating the mixture as a pseudo nuclide which has an appropriate α value, which can be obtained analytically from the slowing down equation. The elastic removal cross sections are numerically corrected with the collision density thus obtained.

The flux heterogeneities of 4 plate cell, whose number density is the same as given in ref. 1 are shown in Fig 2.2.1. The exact values with SDR and the values without correction of the elastic removal cross sections are also given for comparison. The improvement due to the correction is remarkable near the sodium resonance. It is concluded that the multi-region plate lattice heterogeneity effect can be analyzed accurately enough with EXPANDA-75.

References

1) Kikuchi, Y. and Katsuragi, S.: Reactor Engineering Annual Report (April 1, 1973 to March 31, 1974), p.24, JAERI-M5955 (1975)

2) Kikuchi, Y., Katsuragi, S., Ogitsu, M. and Suzuki, T.: EXPANDA-75, JAERI-1239 (1975)

3) Bressenden, R. J. and Durston, C.: Proc. Conf. Application of Computing Methods to Reactor Problems, ANL, May 17-19, 1965, p.51, ANL-7050 (1965)

4) Kikuchi, Y. and Katsuragi, S.: Approximate Expression of Collision Density and Correction of Group Elastic Removal Cross Section near a Wide Scattering Resonance, JAERI-M5963 (1975)

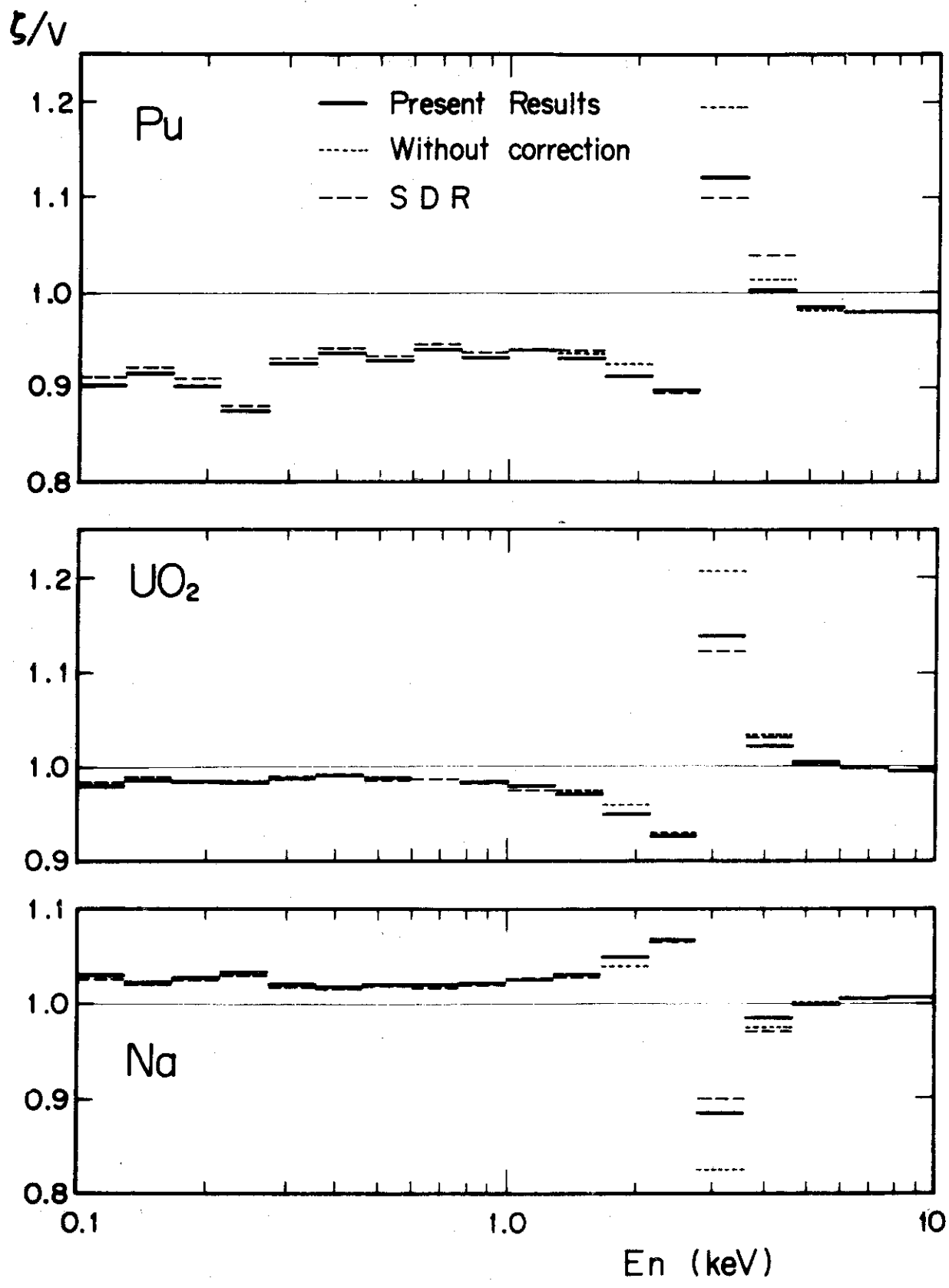

Fig. 2.2.1. Flux heterogeneity of 4 plate cell.

$$\zeta_i = \phi_i V_i$$

2.3 The Resonance Integral of Coated Particles

K. Tsuchihashi and Y. Gotoh

Plans are in progress to develop a multipurpose high-temperature gas-cooled reactor (HTGCR) at the Japan Atomic Energy Research Institute (JAERI) with coated particle fuels. The kernel of UO_2 with a diameter of $\sim$500μ is coated with layers of pyrocarbon and SiC. The fuel rods consist of these particles mixed with a graphite binder, and they are inserted into a graphite block. One of the physical problems associated with this type of fuel matrix is double heterogeneity due to the self-shielding of the grain and the lattice configuration of fuel rods.

The grain-shielding factor has been the subject of several papers that intended, in the first step, to obtain the equivalent homogenized cross section in the fuel rod, and then to treat the rod lattice configuration.

The effective resonance absorplion of coated particles, which are embedded in a graphite matrix, is studied. The effect of a random arrangement of particles on the resonance integral is examined using the radial distribution function derived from the Percus-Yevick equation. A differential equation is proposs-ed to obtain the neutron-beam current from a source particle in a medium in which the distribution function of coated particles is specified. By the use of the neutron beamcurrent and the distribution function as the weight, the fuel-to-fuel collision probability is defined. This collision probability is applied to a RICM-type resonance integral code. The depression of the resonance integral of ^{238}U due to grain structure amounts 5 %

in a design study of the multi-purpose high-temperature gas-cooled reactor (HTGCR) at the Japan Atomic Energy Research Institute. The applicabilities of the spherical cell model and of the collision probability in the high-dilution approximation of Lane et al. are tested. These simple procedures give satisfactory results for the treatment of microscopic heterogeneity in the range of the HTGCR design.

Reference

1) Tsuchihashi, T., Gotoh, Y. "The Resonance Integral of Coated Particles," Nucl. Sci. Eng. 58 213 (1975).

2.4 A Study on the Convergence and Error Estimate of the Perturbation Method in Reactor Calculations

H. Mitani

A general theory to obtain the higher order perturbation terms up to any desired order was given by the present author.[1] However, the perturbation series is not always convergent for all the problems and it is generally not so easy to obtain the convergence criterion for the perturbation method in a strict mathematical sense. It is, however, possible to treat this problem strictly in one-group diffusion approximation if we use Kato's theorem developed for linear operators in the Hilbert space.[2]

The unperturbed and perturbed systems are described by the equations

$$H_0\Phi_0 = \lambda_0\Phi_0 \quad , \qquad H_\varepsilon\Phi_\varepsilon = \lambda_\varepsilon\Phi_\varepsilon \quad , \tag{1}$$

where λ_0 and λ_ε are eigenvalues of each system, and it is assumed that H_0 is a self-adjoint operator and also H_ε is given in a general form as

$$H_\varepsilon = H_0 + \varepsilon H^{(1)} + \varepsilon^2 H^{(2)} + \cdots \tag{2}$$

Here, it is also assumed that λ_ε and ϕ_ε in Eq.(1) can be expanded formally in ε

$$\lambda_\varepsilon = \lambda_0 + \varepsilon \lambda^{(1)} + \varepsilon^2 \lambda^{(2)} + \cdots \quad , \tag{3}$$

$$\Phi_\varepsilon = \Phi_0 + \varepsilon \Phi^{(1)} + \varepsilon^2 \Phi^{(2)} + \cdots \quad . \tag{4}$$

Then, the criterion for a regular perturbation given by T. Kato is as follows:[2] If there are non-negative constants a, b, c, such that

$$\| H^{(n)} f \| \leq C^{n-1} \left(a \| f \| + b \| H_0 f \| \right) \quad , \tag{5}$$

for every $f \in D(H_0)$, H_ε is self-adjoint with the same domain as H_0 and regular for $|\varepsilon| < (b+c)^{-1}$. In this case, if the condition (5) is satisfied, the values of λ_ε and ϕ_ε in Eqs.(3) and (4) are absolutely convergent for

$$1 > \left\{ 2\frac{a}{d} + 2b\left(1 + \frac{|\lambda_0|}{d}\right) + C \right\} \quad , \tag{6}$$

where d is the level distance of eigenvalue λ_0, i.e., the distance of λ_0 from the rest of spectrum of H_0.

In order to apply Kato's theorem to a reactor system, let us consider

the reactor equation with one-group diffusion approximation. In this case, the unperturbed and perturbed reactor equations are described by

$$H_0 \Phi_0 = 0 \quad , \qquad H_\varepsilon \Phi_\varepsilon = \rho_\varepsilon \Phi_\varepsilon \quad , \tag{7}$$

where $$H_0 = \frac{1}{\nu\Sigma_f}\left[D\left(\frac{d^2}{dr^2} + \frac{P}{r}\frac{d}{dr}\right) + (\nu\Sigma_f - \Sigma_a)\right] \quad , \tag{8}$$

$$H_\varepsilon = \frac{1}{\nu\Sigma_f + \varepsilon\delta(\nu\Sigma_f)}\left[D\left(\frac{d^2}{dr^2} + \frac{P}{r}\frac{d}{dr}\right) + (\nu\Sigma_f - \Sigma_a) + \varepsilon\left(\delta(\nu\Sigma_f) - \delta\Sigma_a\right)\right] \quad . \tag{9}$$

From Eq.(9), each of the expansion terms in Eq.(2) is given by

$$H^{(1)} = \frac{\delta(\nu\Sigma_f)}{\nu\Sigma_f} - \frac{\delta\Sigma_a}{\nu\Sigma_f} - H_0\frac{\delta(\nu\Sigma_f)}{\nu\Sigma_f} \quad , \tag{10}$$

$$\vdots$$

$$H^{(n)} = (-1)^n\left(\frac{\delta(\nu\Sigma_f)}{\nu\Sigma_f}\right)^{n-1}\left[\frac{\delta(\nu\Sigma_f)}{\nu\Sigma_f} - \frac{\delta\Sigma_a}{\nu\Sigma_f} - H_0\frac{\delta(\nu\Sigma_f)}{\nu\Sigma_f}\right] \quad . \tag{11}$$

Substituting Eq.(11) into Eq.(5), the values of a, b, c, can be obtained as $a = |\rho^{(1)}|$, $b = c = |\rho_f^{(1)}|$. Therefore, the convergence criterion can be calculated from Eq.(6) using the above a, b, c.

$$1 > \left(\frac{2}{d}|\rho_f^{(1)} + \rho_a^{(1)}| + 3|\rho_f^{(1)}|\right) \quad , \tag{12}$$

where $\rho_f^{(1)}$ and $\rho_a^{(1)}$ are the first order reactivity worths when fission and absoption cross sections are respectively changed. The convergence domain of $(\rho_f^{(1)}, \rho_a^{(1)})$ is shown in Fig. 2.4.1 From Eq.(12), it is apparent that the convergence criterion is $d/2 > |\rho_a^{(1)}|$ when only absorption cross section is changed and also $(d/2)/(1+3(d/2)) > |\rho_f^{(1)}|$ when only fission cross section is changed.

Furthermore, when only absorption cross section is changed, the higher order perturbation method contains the following error if it is truncated with the first n terms.[3]

$$\varepsilon_n \leq |\rho_a^{(1)}| \frac{\left(\frac{2}{d}|\rho_a^{(1)}|\right)^n}{\left(1 - \frac{2}{d}|\rho_a^{(1)}|\right)} \quad . \tag{13}$$

In Eqs.(12) and (13), half the level distance plays an important role. The first few eigenvalues ρ_n, $K_{eff,n}$ and d/2, (d/2)/(1+3(d/2)) for the prototype and 1000MWe fast reactors are given in Table 2.4.1. From this table, it is concluded that the perturbation series is convergent for almost all perturbation experiments in the former system and for $|\rho_a^{(1)}| < 0.12$ and $|\rho_f^{(1)}| < 0.09$ $\Delta K/K$ in the latter system. However, it does not always mean that the perturbation method cannot be used if the convergence condition is not satisfied. This reason is that it is regarded as an asymptotic expansion.

References

1) Mitani, H.: Nucl. Sci. Eng., 51, 180 (1973).

2) Kato, T.: " Perturbation Theory for Linear Operators," (1966), Springer-Verlag, New York.

3) Mitani, H.: " On the convergence and Error Estimate of the Perturbation Method in Reactor Calculations," to be published.

Table 2.4.1 The first few eigenvalues and half the level distance in the proto-type and 1000MWe fast reactors

Number of levels n	Proto-type reactor		1000MWe reactor	
	ρ_n	$K_{eff,n}$	ρ_n	$K_{eff,n}$
0	0.0	1.0000	0.0	1.0000
1	- 0.5827	0.6318	- 0.2396	0.8067
2	- 1.6987	0.3706	- 0.6899	0.5918
3	- 3.2560	0.2350	- 1.3653	0.4228
d/2	0.2914	------	0.1198	------
(d/2)/(1+3d/2)	0.1555	------	0.0881	------

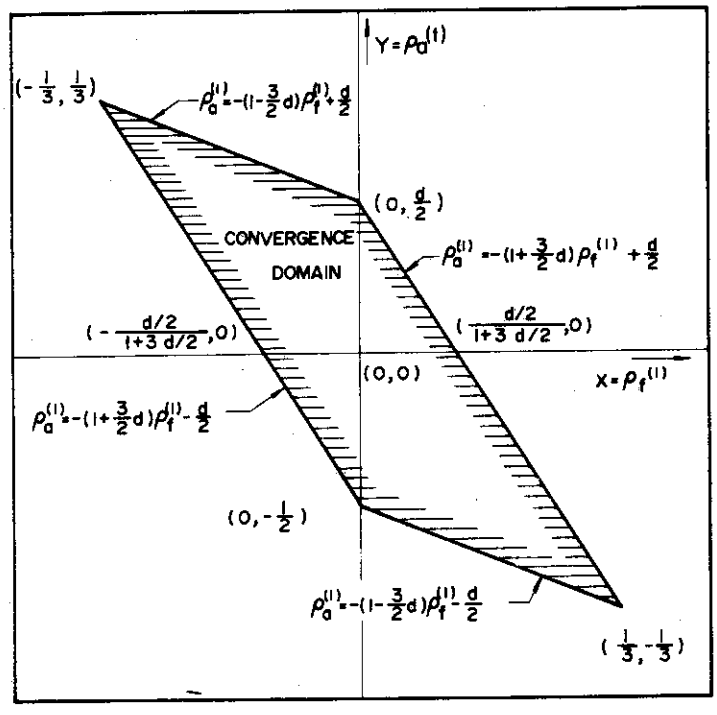

Fig.2.4.1 Convergence domain of the perturbation series for the case where both absorptin and fission cross sections are changed

2.5 Improvements of the HONEYCOMB Code System Concerning Accuracy and Computational Efficiency

T. Suzuki, A. Hasegawa and S. Katsuragi

HONEYCOMB, the 3-dimensional diffusion criticality and burn-up calculation system for fast reactors,[1] has been improved in accuracy and efficiency.

1. The accuracy of the neutron fluxes in and around the control rod has been raised by using a modified diffusion coefficient in the usual coarse mesh difference diffusion scheme dealing with the hexagonal-z geometry. This modified diffusion coefficient is locally prepared as the ratio of "the net current into the control rod" to "the gradient of the 'mean' fluxes averaged in the coarse meshes in and out of the control rod". The preparatory calculation of these current and fluxes is made using the integral transport model in a simplified slab cell, with the functional approximation and the variational method. As the results of criticality calculation by the usual coarse mesh difference method, neutron fluxes are obtained with the transport accuracy (in the sense of average value in each coarse mesh) without any increase of computation time.

2. As to the γ-heating calculation, the photon production constants are prepared by using LAPHANO code and ENDF/B-IV data file.

3. The total cpu time of executing the whole system of HONEYCOMB has been reduced to about 80% by using the H-compiler for some subroutines. It was found that there are subroutines suitable for the G-compiler rather than H-compiler.

4. An efficient method has been devised in order to obtain the detailed power distribution within the fuel assemblies, that is, the power emission rate from each fuel pin. The one-group, two-dimensional diffusion equation is solved in each coarse volume segment. The boundary condition b(s) is given on the hexagonal boundary by the coarse

mesh fluxes which are previously obtained. This boundary value problem is solved by using the Green's function of infinite medium (Yo (x) or Ko (x)), that is, by the potential theory,[2] superposing some image source of double layer along the hexagonal boundary. The solution of

$$\nabla^2\phi + B^2\phi = 0$$

is given by

$$\phi(\vec{r}) = \int_C f(s)\, \nabla_\nu\, Y_0(BR)\, ds$$

where $\int_C ds$ means the line integration along the hexagonal boundary, ∇_ν the gradient to the outward normal direction and $R = \| \vec{r} - \vec{s} \|$ is the distance between the inner point $\vec{r}$ and boundary point $\vec{s}$. The density distribution of the image source $f(s)$ is directly determined from the boundary condition $b(s)$ by solving an integral equation

$$2 f(s) - B \cdot P \int_C f(s') \cos\gamma\, Y_1(BR)\, ds' = b(s)$$

where P means the principal value and $\gamma = \vec{\nu}_\wedge (\vec{s}' - \vec{s})$, $R = \| \vec{s}' - \vec{s} \|$.

By this method, the power distribution for each fuel pin is accurately obtained with much reduction of computation time (1/50 ~ 1/100), compared with the fine mesh difference method. This reduction is mainly because the resolvent kernels need to be calculated only once for each value of B, and they can be applied to many volume segments having the same value of B.

The next problem to be solved is how to calculate the effective macroscopic cross sections of the control rod assemblies, in which 7 rods of B_4C are arranged hexagonally.

References

1) Div. of Reactor Engng.: 1974's Annual Report, JAERI-M 5955, pp.45-47 (1975).

2) Courant, R. and Hilbert, D. : "Methods of Mathematical Physics", vol. II, "Partial Differential Equations" by R. Courant, Chap. IV, (1962), Interscience Publishers.

2.6 Solution of Two-Dimensional Neutron Transport Equation in Cylindrical Geometry by the Finite Element Method

T. Fujimura, K. Horikami, Y. Nakahara, T. Tsutsui and T. Ohnishi*

The finite element method (so called FEM) has been well known as a powerful tool to get the numerical solution of many physical problems. With the main purpose to decrease the mesh points by utilizing the merit of a higher order approximation inherent to the FEM, we proposed a formulation based on it for solving the two-dimensional multi-group neutron transport equation in (r,z) geometry.[1)]

Progress has been made in developing a computer code FEMRZ and some calculations have been performed for both sample and real scale problems. These results have been compared to the solutions of an excellent diamond difference discrete ordinate S_N code TWOTRAN-II.[2)]

In our algorithms the FEM is used only for spatial variables. With traditional notations, an approximate angular flux $\hat{\psi}_m^g(r,z)$ are expanded in each rectangular subregion using p-th order Lagrange's polynomial $L_p(r,z)$ and nodal value ψ_m^{gl};

$$\hat{\psi}_m^g(r,z) = \sum_{l=1}^{N_p} \psi_m^{gl} L_p(r,z). \qquad (1)$$

Use has been made of first or second order approximation in which the number of nodes N_p in each subregion is four or nine, respectively.

Substituting (1) to the original equation, we can define the

---

* Atomic Energy Research Laboratory, Hitachi Ltd.

residue $R_m^g(r,z)$. We have used a discontinuous-type explicit iterative scheme along neutron flight direction. In this case, Galerkin's method which satisfies the inner product relations;

$$<L_p^l\ (r,z),\ R_m^g\ (r,z)> \ = 0$$

is adequate for deciding new nodal values. The linear equations for them are solved by Crout's method. Other computational methods and code options are much the same as those in TWOTRAN-II.

Figs. 2.6.1 and 2 show the configuration and the result of eigenvalue calculation of a sample problem, respectively. It is not surprising that the first order approximation and the diamond difference scheme shows a good coincidence with each other, since these schemes may be expected to give the same order of accuracy. In the case of the second order approximation, reasonable solutions are gained with coarser mesh calculations.

Fig. 2.6.4 shows the scalar flux in a fast reactor, whose configuration is given in Fig. 2.6.3. It gives the isotropic component of the first group flux along a radial direction. The solution based on the second order approximation is well fitted for the fine mesh solution with TWOTRAN-II.

Our conclusion is as follows:

(1) Stable solutions can be obtained always even with coarse mesh calculations.

(2) Further improvements are necessary for saving computing time.

References

1) Horikami, K., et al. : "Finite Element Method for Solving

Neutron Transport Problems in Two-Dimensional Cylindrical Geometry," JAERI-M 5793 (1974).

2) Lathrop, K.D., Brinkley, F.W. : "TWOTRAN-II: An Interfaced Exportable Version of the TWOTRAN Code for Two-Dimensional Transport," LA-4848-MS (1973).

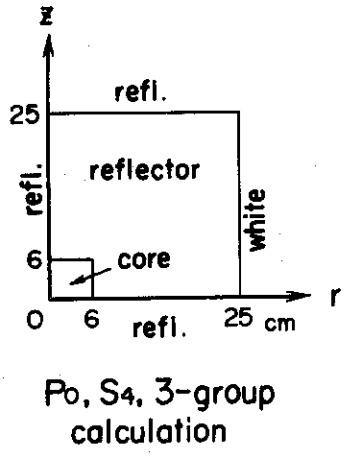

Fig. 2.6.1 A sample problem configuration

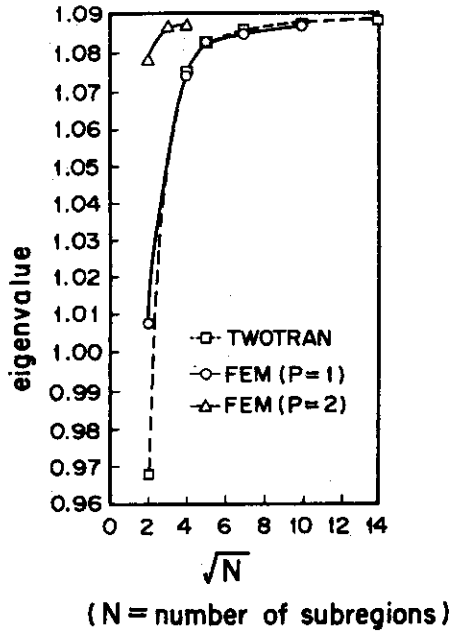

Fig. 2.6.2 Dependence of the eigenvalue on the number of sub-regions

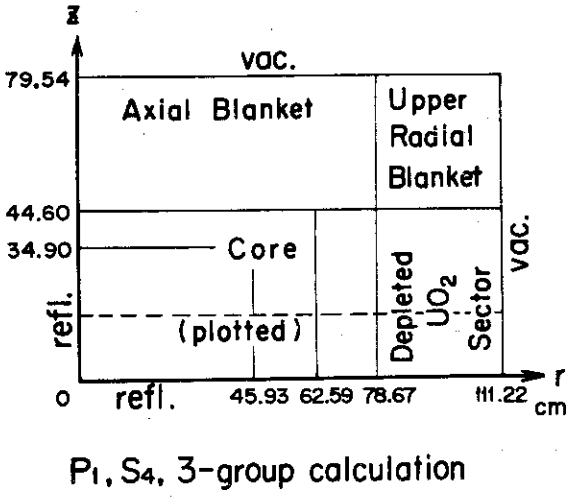

Fig. 2.6.3 A fast reactor configuration

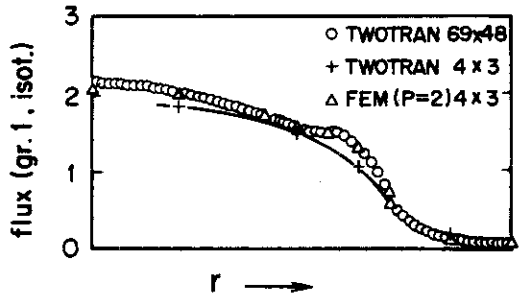

Fig. 2.6.4 Comparison of scalar fluxes along radial direction

2.7 Acceleration of S_N Transport Computations

T. Asaoka, T. Fujimura and T. Tsutsui

It has been found that the introduction of the coarse-mesh rebalancing method into the one-dimensional S_N code ANISN[1] results in the reductions of the number of required iterations and computation time by 20 ∿ 40 % and 10 ∿ 20 %, respectively.[2] The further studies have shown that the use of the coarse-mesh rebalance at the first and third inner iterations gives a minimum computation time for obtaining the reactor eigenvalue with a given precision. [In the original ANISN, the pointwise scaling (fine-mesh rebalance) is used at every three iterations.] A simultaneous use of the fine, coarse and whole system rebalance for the first few iterations is very effective to reduce the maximum relative deviation of the neutron fluxes.

The advantage of the coarse-mesh rebalance over pointwise scaling is naturally increased for two-dimensional computations compared to one-dimensional cases. One of two-dimensional S_N codes, TWOTRAN-2[3] has already been equipped with the coarse-mesh rebalance acceleration, but the DOT-3 code[4] has not adopted it. A modification has therefore been performed in the DOT so as to have the coarse-mesh rebalance option, in addition to the successive overrelaxation, Chebyshev acceleration, fine-mesh and whole system rebalancing options.

Fig. 2.7.1 shows the maximum relative deviation of the 1-group neutron flux due to a fission source placed in the air over ground, as a function of the number of inner iterations. Compared to the pointwise scaling, the computation time for one iteration of calculating the coarse-mesh rebalance factors is

reduced by a factor of the ratio of the number of fine-meshes to coarse-meshes. In addition, as is seen from Fig. 2.7.1, the coarse-mesh rebalance gives a more stable convergence than the pointwise scaling, though the whole system rebalance is the best for this problem.

In Fig. 2.7.2, however, the coarse-mesh rebalance has given, as expected, a better convergence than the whole system rebalance. This figure shows the maximum deviation of the first-group neutron flux in a spent fuel container calculated with 21 x 10 coarse-meshes and 105 x 50 fine-meshes. The coarse-mesh rebalance calculation takes a less computation time by about 20 % compared to the pointwise scaling.

The TWOTRAN-2 code, on the other hand, is not suited to shielding calculations due mainly to the lack of the capability to output the fluxes at exterior or interior boundaries for use in very large problems to be run in overlapping regions (bootstrap problems). We have therefore modified the code to be able to output the boundary angular flux along any internal radial or axial boundary. This flux can be used directly as a boundary source for bootstrapping very large calculations. The present option is especially useful for problems where fission sources exist only within limited regions and hence the outer (source) iterations are required only for the first run.

References

1) Engle, W.W., Jr. : "A User's Manual for ANISN, A One Dimensional Discrete Ordinates Transport Code with Anisotropic Scattering," K-1693 (1967).

2) Nishida, T., et al. : "Evaluation of Convergence Properties

of the S_N Algorithm," in JAERI-M 5955 "Reactor Engineering Division Annual Report," p. 39 (1975).

3) Lathrop, K.D., Brinkley, F.W. : "TWOTRAN-II : An Interfaced, Exportable Version of the TWOTRAN Code for Two-Dimensional Transport," LA-4848-MS (1973).

4) Mynatt, F.R., et al. : "The DOT-III Two-Dimensional Discrete Ordinates Transport Code," ORNL-TM-4280 (1973).

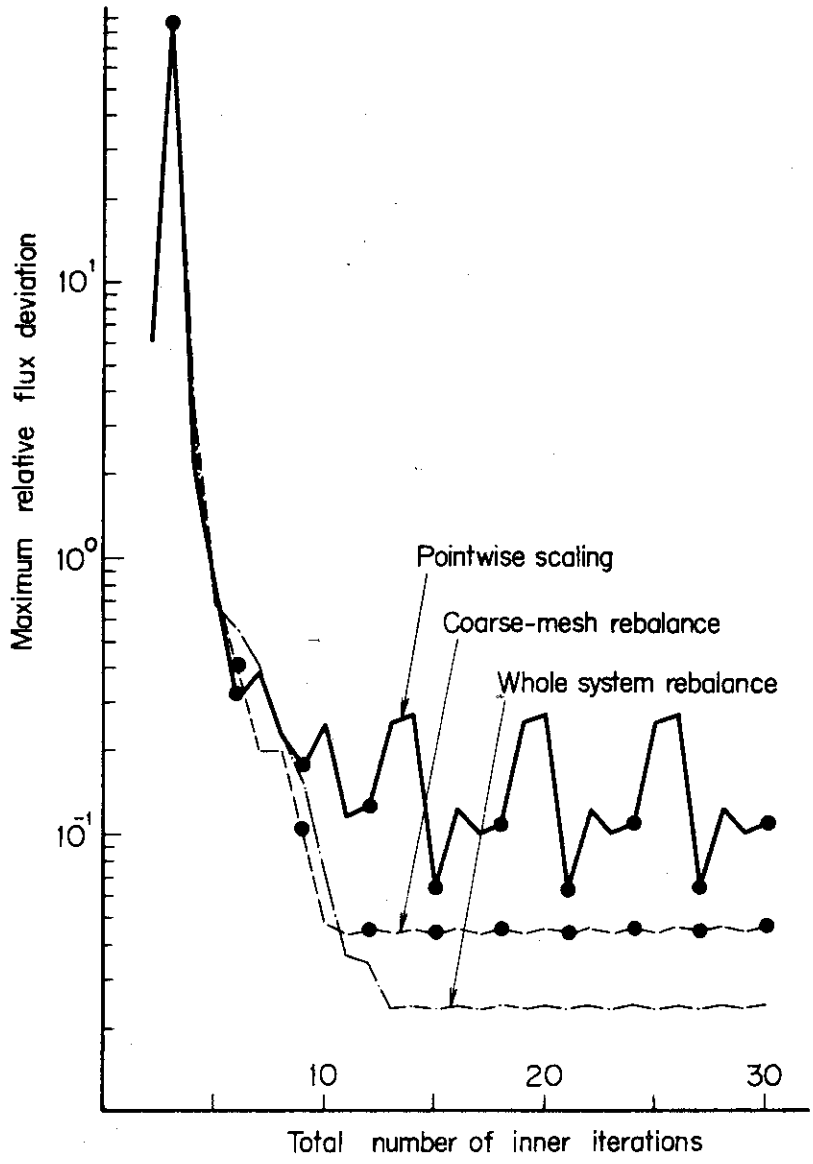

Fig. 2.7.1 Convergence of the flux due to a fission source in the air over ground in DOT-3 calculations

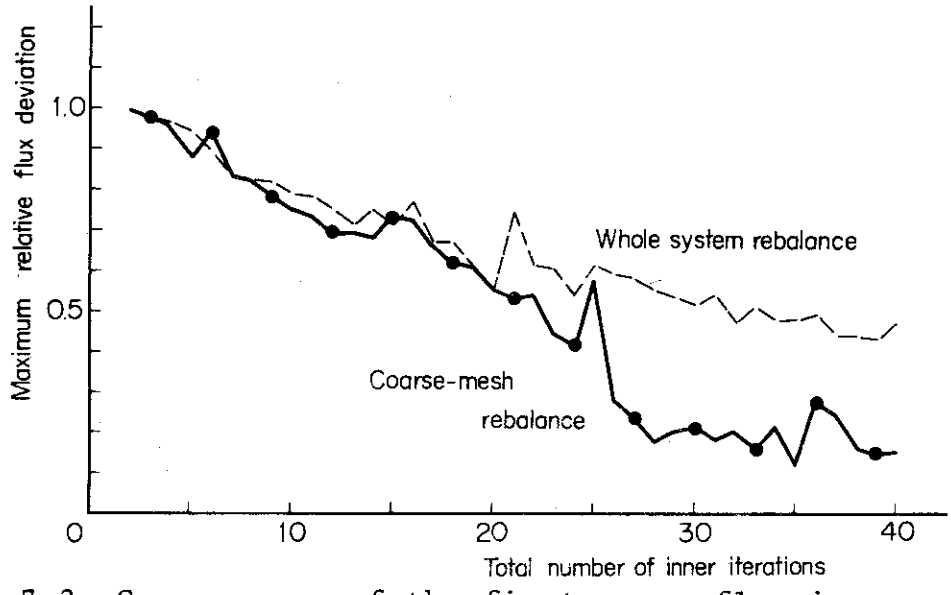

Fig. 2.7.2 Convergence of the first group flux in a spent fuel container in DOT-3 calculations

2.8 Analysis of Reactivity Perturbation by Correlated Sampling Monte Carlo Method

T. Asaoka, M. Nakagawa, Y. Seki, T. Suzuki, Y. Taji,
Y. Nakahara, S. Miyasaka and J. Hirota

It is well known that the correlated Monte Carlo technique can be used for estimating the reactivity perturbation in nuclear reactors due to changes of the geometry or composition.[1)-3)] By following an identical set of neutron histories for both unperturbed and perturbed systems, the error of the differential reactivity can drastically reduced independently of the error of the total reactivity.

This method of similar flight paths has been introduced to the general purpose Monte Carlo code MORSE.[4)] After having achieved a nearly converged fission source distribution, each neutron which enters for the first time the region to be perturbed is marked and no longer subject to the Russian roulette procedure. In this batch of calculations, a simple splitting process can be used to increase the number of neutrons crossing the perturbed regions. These marked neutrons are then followed for the perturbed system with the same chain of random numbers as for the unperturbed case.

After completed a pair of the unperturbed and perturbed calculations, one can start the next pair of the calculations using the resulting fission source distribution from the unperturbed run. Upon repeating these correlated runs, the number of sampled neutrons is increased and the error of the calculated reactivity change can not only be reduced but also be estimated easily.

It should be noted however that the present technique neglects the effect due to the change of the fission source distribution caused by the perturbation.

To test the accuracy of the present method, a calculation was performed on a cylindrical fast reactor without the axial blanket, the cross section of which is illustrated in Fig. 2.8.1. The central part with a radius of 12.458 cm is composed of 8 concentric cylindrical cells of 0.90 cm thick plutonium oxide fuel and 0.6572 cm thick mixture of stainless steel and sodium. The height of the system is 121.5 cm.

Table 2.8.1 shows the results for the reactivity change caused by the replacement of the mixture shells of stainless steel and sodium to stainless steel layers (no sodium in them) with a reduced density of 1/10. In Table 2.8.1 are given also the reactivity changes due to the homogenization of 8 concentric cells with the normal or reduced density mixture shells.

It is seen that for all three cases the variances are small enough for relying on the average values, though the total number of sampled neutrons seems still too small. The reactivity change due to the density reduction is rather in agreement with the S_8 value obtained from the TWOTRAN computer code[5] but the reactivity changes for two homogenized cases are too small compared to the S_8 values. Since the disagreement seems to come mainly from the difference in the fission source distribution, the present MORSE code will be modified to take into account also the effect due to the change of the source distribution caused by the perturbation.

References

1) Kschwendt, K., Rief, H. : "TIMOC, A General Purpose Monte Carlo Code for Stationary and Time Dependent Neutron Transport," EUR 4519e(1970).

2) Schmidt, F.A.R. : "Status of the Monte Carlo Development," in "Proc. Seminar on Numerical Reactor Calculations," IAEA, Vienna (1972).

3) Bernnat, W. : "A Monte Carlo Technique for Local Perturbations in Multiplying Systems," in "Proc. NEACRP Meeting of a Monte Carlo Study Group," ANL-75-2 (NEACRP-L-118) (1974).

4) Straker, E.A., et al. : "The MORSE Code, A Multigroup Neutron and Gamma-Ray Monte Carlo Transport Code," ORNL-4585 (1970).

5) Lathrop, K.D., Brinkley, F.W. : "TWOTRAN-II: An Interfaced, Exportable Version of the TWOTRAN Code for Two-Dimensional Transport," LA-4848-MS (1973).

Table 2.8.1 Reactivity changes due to density reduction and homogenization of the central region of a cylindrical fast reactor by correlated sampling Monte Carlo calculations

Unperturbed batch No.	No. of marked neutrons	Density reduction	Homogenization	
			Normal density	Reduced density
13	309	-0.0006	-0.0146	-0.0140
14	349	0.0001	-0.0158	-0.0163
15	334	0.0057	-0.0140	-0.0080
16	357	0.0060	-0.0138	-0.0087
Average	1349	0.0029	-0.0145	-0.0117
Standard deviation		0.0018	0.0007	0.0020
S_8 result	——	0.0035	-0.0237	-0.0225

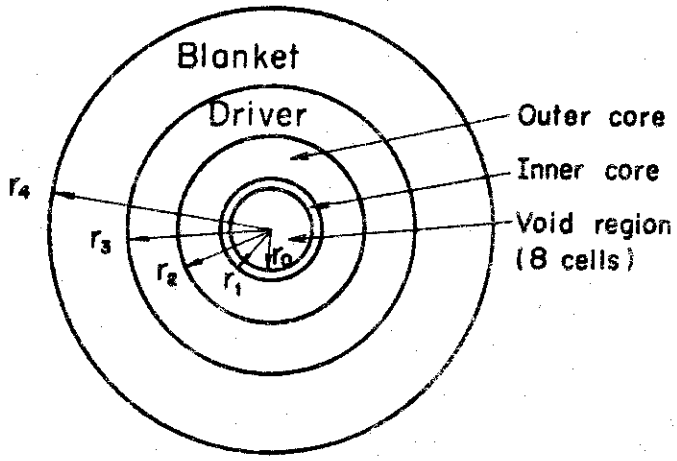

r_0 = 12.458 cm, r_1 = 15.57 cm,
r_2 = 29.38 cm, r_3 = 46.70 cm,
r_4 = 72.17 cm,

Fig. 2.8.1 Cylindrical fast reactor with a height of 121.5 cm

2.9 Application of Coarse-Mesh Rebalancing Acceleration to Monte Carlo Eigenvalue Problems

T. Asaoka, Y. Nakahara, K. Horikami, T. Nishida,
T. Suzuki, Y. Taji, S. Miyasaka and J. Hirota

The coarse-mesh rebalance method has successfully been applied to accelerate the convergence of source iterations in Monte Carlo eigenvalue calculations for spherical reactors.[1] This technique has been extended to deal with two-dimensional cylindrical systems.

To test the effectiveness of the method, 5-energy-group calculations were performed on a cylindrical fast reactor shown in Fig. 2.9.1 by using a modified MORSE computer code[2] with the coarse-mesh rebalance option. In the core surrounded completely by the blanket (the shadowed region in Fig. 2.9.1), small regions just outside of 3, 11 and 20 represent the control and safety rods, and another small regions inside of 7, 15 and 24 are filled with sodium. All 29 regions illustrated in Fig. 2.9.1 are treated as the coarse-mesh zones.

The average values of k_{eff} and their standard deviations are shown in Fig. 2.9.2 as a function of the total number of neutron histories, where the first batch of 1,000 histories is excluded from calculating the averages. An excellent convergency is seen in the result obtained from the coarse-mesh rebalance Monte Carlo. Already after 10 batches of about 1,000 histories, the k_{eff} is almost converged (0.990 ± 0.002) to the S_4 value 0.9924 obtained from the TWOTRAN computer code[3] (k_{eff} = 0.994 ± 0.003 after 20 batches). On the other hand, the standard Monte Carlo using the original MORSE gives 0.984 ±

0.005 after 10 batches and 0.985 ± 0.003 after 20 batches, which are still two small compared to the S_4 value.

Since the coarse-mesh rebalance is expected to improve also the estimate of the neutron flux obtained from the point detector estimator of the SAMBO code,[4] the values are compared in Table 2.9.1 for each energy-group at the middle of the inner core (r=10 and z=61 cm in Fig. 2.9.1). It is seen that the coarse-mesh rebalance gives certainly a better estimate of the flux, though the standard deviation is still large. In the present calculations where only one point detector estimator is placed, the rebalance Monte Carlo takes a computation time more per collision by about 30 % than the standard calculation.

It is noted that the present technique is by no means limited to spherical and cylindrical geometries but can easily be applied to general three-dimensional geometries.

References

1) Asaoka, T., et al. : "Application of an Acceleration Technique to Monte Carlo Eigenvalue Problems," in JAERI-M 5955 "Reactor Engineering Division Annual Report," p. 36 (1975).

2) Straker, E.A., et al; : "The MORSE Code – A Multigroup Neutron and Gamma-Ray Monte Carlo Transport Code," ORNL-4585 (1970).

3) Lathrop, K.D., Brinkley, F.W. : "TWOTRAN-II : An Interfaced, Exportable Version of the TWOTRAN Code for Two-Dimensional Transport," LA-4848-MS (1973).

4) Cain, V.R. : "SAMBO, A Collision Analysis Packages for Monte Carlo Doses," ORNL-TM-3203 (1970).

Table 2.9.1 Five-energy-group neutron fluxes and their standard deviations at the middle of the inner core of a 29-zone cylindrical fast reactor

Energy group	Standard Monte Carlo	Coarse-mesh Monte Carlo	S_4 result
1	0.051 ± 0.014	0.077 ± 0.020	0.074
2	0.940 ± 0.069	1.419 ± 0.160	1.533
3	3.575 ± 0.247	6.527 ± 1.155	4.769
4	3.486 ± 0.844	3.868 ± 0.580	3.718
5	0.119 ± 0.059	0.132 ± 0.047	0.171
Total	8.171 ± 0.936	12.022 ± 1.396	10.265

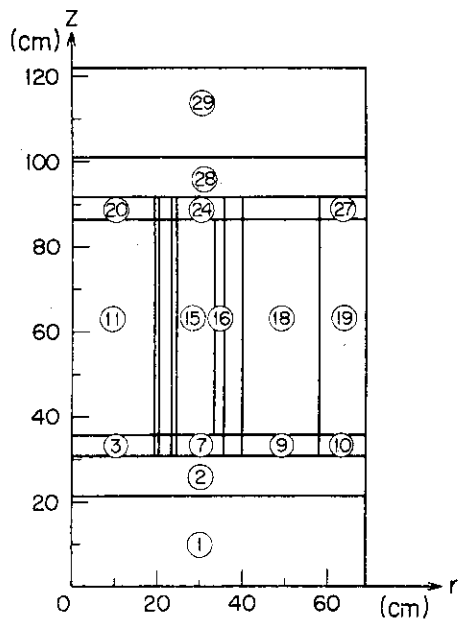

Fig. 2.9.1 Cylindrical fast reactor with 29 coarse-mesh zones

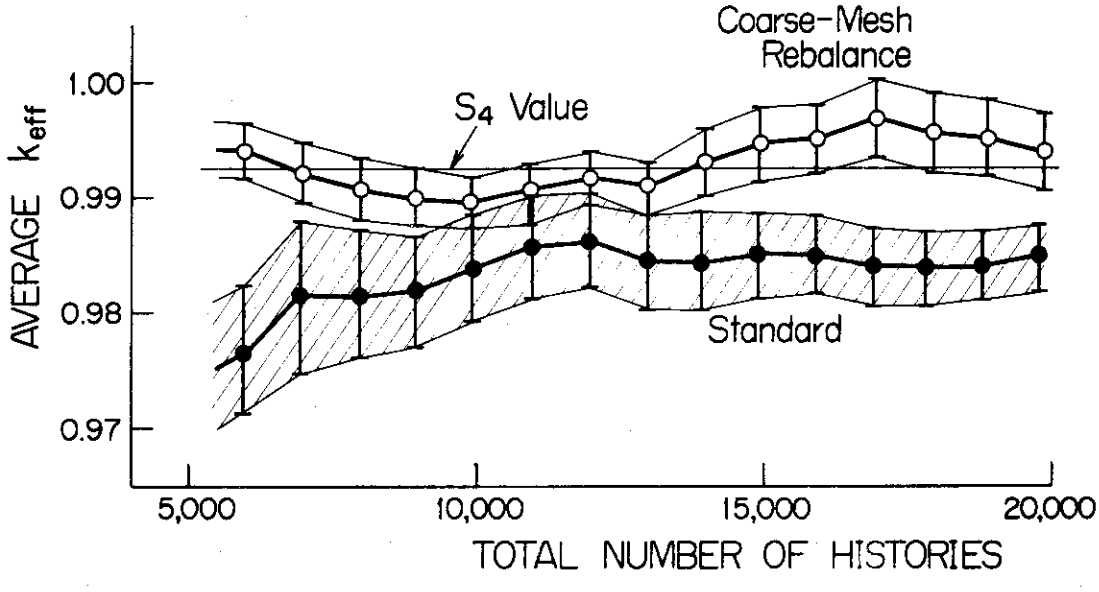

Fig. 2.9.2 Average value of k_{eff} and its standard deviation of a 29-zone cylindrical fast reactor

2.10 Direct Method for Numerical Solution of a Nonlinear Volterra Integro-Differential Equation and its Application to Nonlinear Point Reactor Kinetics

Y. Nakahara, T. Ise and K. Kobayashi

A new method has been developed for the numerical solution of a class of nonlinear Volterra integro-differential equation with quadratic nonlinearity, which can be written as follows;

$$\frac{d}{dt} n(t) = F(n(t), \int_0^t dsK(t,s,n(s)), n(t)\int_0^t ds\ n(s)), \quad (1)$$

where K is a linear Volterra kernel.

Let R(t) be the region defined by $R(t) = \{ t;\ 0 \leq t \leq Tmax \}$ and $[0, T_{max}]$ be divoded into N equal subintevals of a width of h. We apply piece-wise approximations over these subintervals. At first, let us integrate Eq. (1) over t in the interval $[t_i, t_{i+1}]$. Then we have

$$n(t_{i+1})-n(t_i) = F\Big(\int_{t_i}^{t_{i+1}} dt\ n(t), \int_{t_i}^{t_{i+1}} dt \int_0^t ds\ K,$$

$$\int_{t_c}^{t_{i+1}} dt\ n(t) \int_0^t ds\ n(s) \Big) . \quad (2)$$

Six approximate treatments have been applied to Eq. (2), i.e., fully explicit, fully implicit, Crank-Nicolson, linear interpolation, quadratic and cubic spline methods. Using these approximations and performing elementary analytical integrations, we obtain algebraic quadratic equations for unknowns $n_{i+1} = n(t_{i+1})$:

$$A(n_{i+1})^2 + Bn_{i+1} + C = 0. \tag{3}$$

In our algorithm the numerical solution at each time step is thus obtained directly as a positive root of Eq. (3).

The point reactor kinetics equation with ramp reactivity insertion, linear temperature feedback and delayed neutrons belongs to Eq. (1) and can be written as follows;

$$\frac{d}{dt} n(t) = \frac{\alpha}{\ell} tn(t) - \frac{\gamma}{C\ell} n(t) \int_0^t dsn(s) - \frac{\beta}{\ell} n(t) + \sum_j \lambda_j \left\{ C_{jo} e^{-\lambda j t} + \frac{\beta_j}{\ell} - \int_0^t dsn(s) e^{-\lambda_j (t-s)} \right\}, \tag{4}$$

where conventional nomenclatures are used. We applied our algorithm to the Argonne Benchmark Problem ID. 7-A1, for which standard solutions are given in the prompt approximation.[1)]

In our algorithm for Eq. (4) without delayed neutrons, the fully implicit method has been found to be unconditionally stable in a sense that it gives positive real roots always. The cubic spline method is divergent. Fig. 2.10.1 shows the convergency of these numerical solutions at 0.5 sec after the start of ramp reactivity insertion. From the estimation of stability, convergency, accuracy and CPU time it is concluded that the best is the Crank-Nicolson method and the linear interpolation comes closely next to it.

Reference

1) Argonne Code Center : "Argonne Code Center Benchmark Problem Book," ANL-7416 (Supl. 1) (1972).

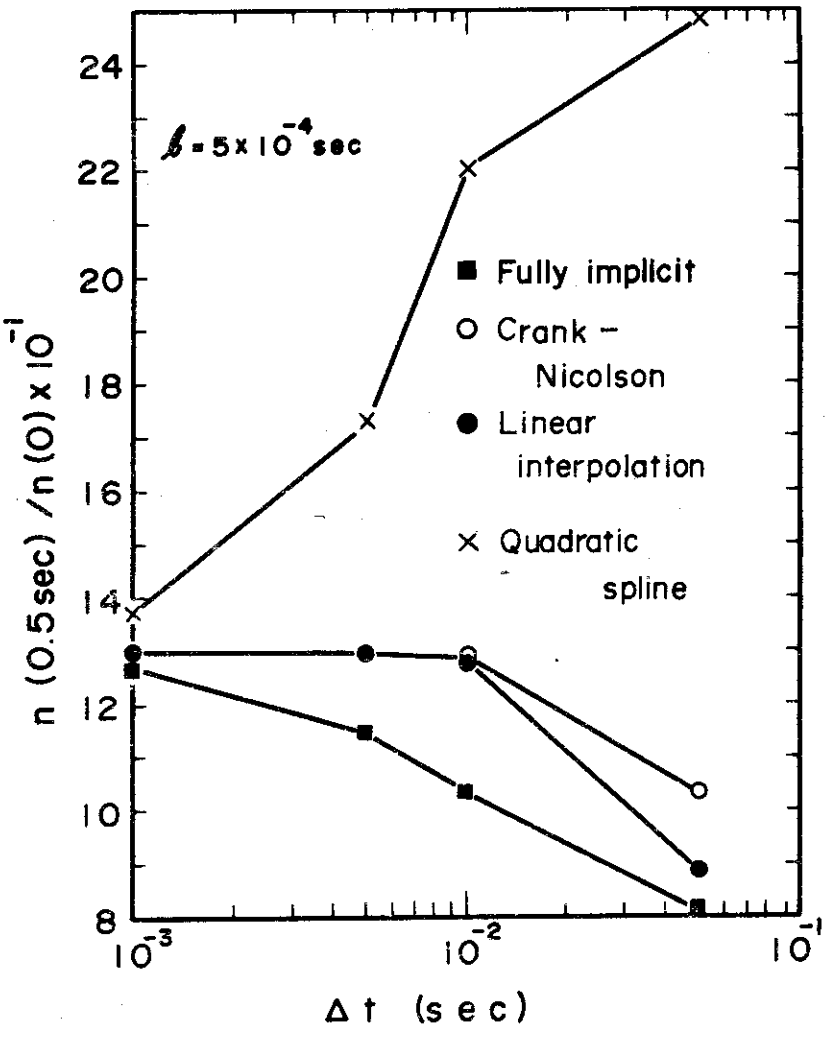

Fig. 2.10.1 Comparison of convergencies for a thermal reactor problem

2.11 Study of the Power Spectral Density by a Nonlinear Response to the Stochastic Input

Y. Gotoh

It is well known that a reactor responds nonlinearly to a periodic reactivity change. Hence, it is desirable to extend it to a stochastic input. In the usual method of noise analysis the basic equation is linearized about the mean and the fluctuating part is treated as an inhomogeneous source term.

Few works have been done on the neutron fluctuation in a reactor arising from the stochastic reactivity change.

We have studied the non-linear response of reactor to the stochastic reactivity input. The kinetic equation of an integral type of which the kernel is to defined as to include a small negative reactivity, and a graphical interpretation of the solution are useful to investigate the effects of an random reactivity input on the neutron density. The conditions for the stabilization of the mean and the Gaussian steady and the white noise, respectively. Taking the ensemble average of neutron density and its covariance, and through the Fourier transformation of the equation for the auto-correlation function, an integral equation was derived for the power spectral density, which includes the effect of a non-linear response on the random reactivity input. However, it was assumed that the mean or the mean square of neutron density changes gradually, as compared with the correlation time of the neutron density correlation function. The zeroth approximation to the solution corresponds to the usual P.S.D. by the non-linear response, in slightly over or below the critical state, is the same as in

just critical state, if the systematic variation of neutron density with time is taken into consideration.

Reference

1) Gotoh, Y. "Study of the Power Spectral Density by a Non-linear Response to the Stochastic Input," Annals of Nuclear Energy, 2, 119 (1975).

2.12 Development of a Program for Nuclear Energy System Analysis

S. Katsuragi

In these days, impacts of various industries on social and environmental spheres become strong and even fatal for nation, particularly in chemical industries. These fatal situation resulted from ignorance of system analysis or a lack of technology assessment considering unfavorable consequences of technology development.

For establishing strategies in research and development of nuclear energy, we must recall thoroughly the above situation. There is a powerful opinion stressing that we must establish philosophy on development of nuclear energy before making any analysis of nuclear energy production systems. However it seems true that we cannot make any philosophical statements on the problem in the sense of responsibility without knowing consequences of research and development in nuclear energy.

There are four types of method used for technology assessment, that is, intuitive, explorative, normative and feed back methods. Because scientific and technological resources are known rather definitely for nuclear energy production systems, we adopt a normative method. We can define rather clearly social objectives in stages of impacts of technology development on the society.

Following the above argument, development of simulation program for nuclear energy production systems is in progress. At first stage, conservation of resources and money is set as an important objective, aiming at an optimum allocation of various types of reactors. For this purpose, we are developing the simulation program shown in Fig. 2.12.1. Last year the program for calculating nuclear power cost has been prepared. The test of this program will be made by the end of 1975. In 1976 the program estimating fuel cycle cost will be developed.

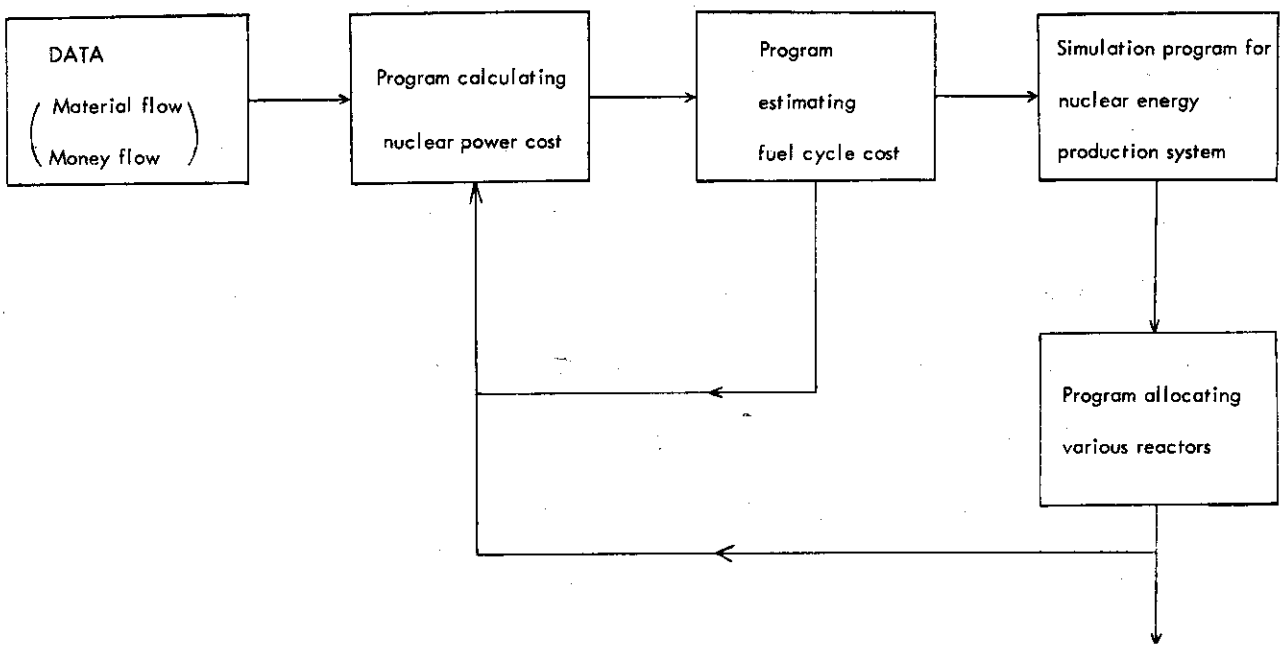

Fig. 2.12.1 Simulation program for nuclear energy production system

2.13 Calculation of Image Contrast of Dislocation Loop by Many Wave Dynamical Theory of Electron Diffraction

T. Nishida and K. Izui

In the present work, using the dynamical theory of electron diffraction based on the column approximation, we have calculated the image contrasts due to a prismatic dislocation loop, grown on (100) plane between atomic planes in a Ge crystal, and simulated the contrasts by computer. Stress field around the loop is expressed by Eshelby's formula. The coordinate system used here is shown in Fig. 2.13.1. The elastic displacement $R^I(x,y.z)$ due to the dislocation loop are given by (R^I_z is similar to R^I_y)

$$R^I_x = \frac{b}{8\pi(1-\nu)} \iint_L \left[(1-2\nu)\frac{x}{r^3} + 3\frac{x^3}{r^5}\right] dy'dz',$$

$$R^I_y = \frac{b}{8\pi(1-\nu)} \iint_L \left[(1-2\nu)\frac{y-y'}{r^3} + 3\frac{(y-y')x^2}{r^5}\right] dy'dz', \qquad (1)$$

$$r = \sqrt{x^2+(y-y')^2+(z-z')^2},$$

where $b = |b|$, ν is Poisson ratio and integration L is over the surface of loop.[1),3)] At the points sufficiently far from the loop, the expression (1) takes a simpler form R^{II} excluding integral, called I.L. approximation. Fig. 2.13.2 shows the contours of R^I_x, R^I_y, and R^{II}_y around the loop at Z_t = 1000 Å and $b = \frac{a}{2}$ (a: lattice constant).[4)] The difference between R^I and R^{II} is sufficiently small where the distance from the center of a loop becomes much longer than 2 r_1. On the other hand, a column approximation in a deformed crystal assumes that a crystal is a pile of many thin slices having constant displacement $R^m(x,y,z)$ in each slice. P_m is a scattering matrix for the

m-th slice of a deformed crystal, defined in the dynamical theory and is given by

$$P_m = Q_m^{-1} \cdot P_o \cdot Q_m,$$

$$Q_m = \begin{pmatrix} 1 & e^{2\pi i \beta_1^m} & & 0 \\ & e^{2\pi i \beta_2^m} & & \\ & & \ddots & \\ 0 & & & e^{2\pi i \beta_{j-1}^m} \end{pmatrix}, \quad \beta_j^m = g_j R_m , \tag{3}$$

where g_j is the j-th reciprocal lattice vector and R_m is the displacement of the m-th slice. P_o is a scattering matrix for a perfect crystal.[2] Applying the approximation, we have calculated the image contrasts of dislocation loops under various specified conditions. The value of phase factor β at a distance of less than 2 r_1 from the center of loop is approximated by $\beta^I = g.R^I$ and, outside the region, by $\beta^{II} = g.R^{II}$. Intensity profiles along the X-axis are calculated using four wave approximation at the exact (400) Bragg positon. Two dimensional images are also simulated (see Figs. 2.13.3 and 2.13.4). The dark and bright contrasts seen in these images imply the difference of phase changes of diffracted waves on both sides of the loop. The spot patterns (bright-dark, dark-dark etc.) are observed in the electron microscope images and present a possibility of determining whether the loop is interstitial or vacancy type after many computations on various conditions have been completed. A new subroutine, which integrates numerically R^I, has therefore been added to the code MSCOPE-I.[5]

References

1) Eshelby, J.D. : Proc. Roy. Soc., 241, 376 (1957).

2) Howie, A., Whelan, M.J. : Proc. Roy. Soc., A263, 217 (1961).

3) Ashby, M.F., Brown, L.M. : Phil. Mag., 8, 1649 (1963).

4) Ohr, S.M. : Phil. Mag., 26, 1307 (1972).

5) Nishida, T., Izui, K., : JAERI-M 5441, (1973).

6) Izui, K., Nishida, T., Furuno, S. : Jour. Elec. Micro., 22, No. 4, 329 (1973).

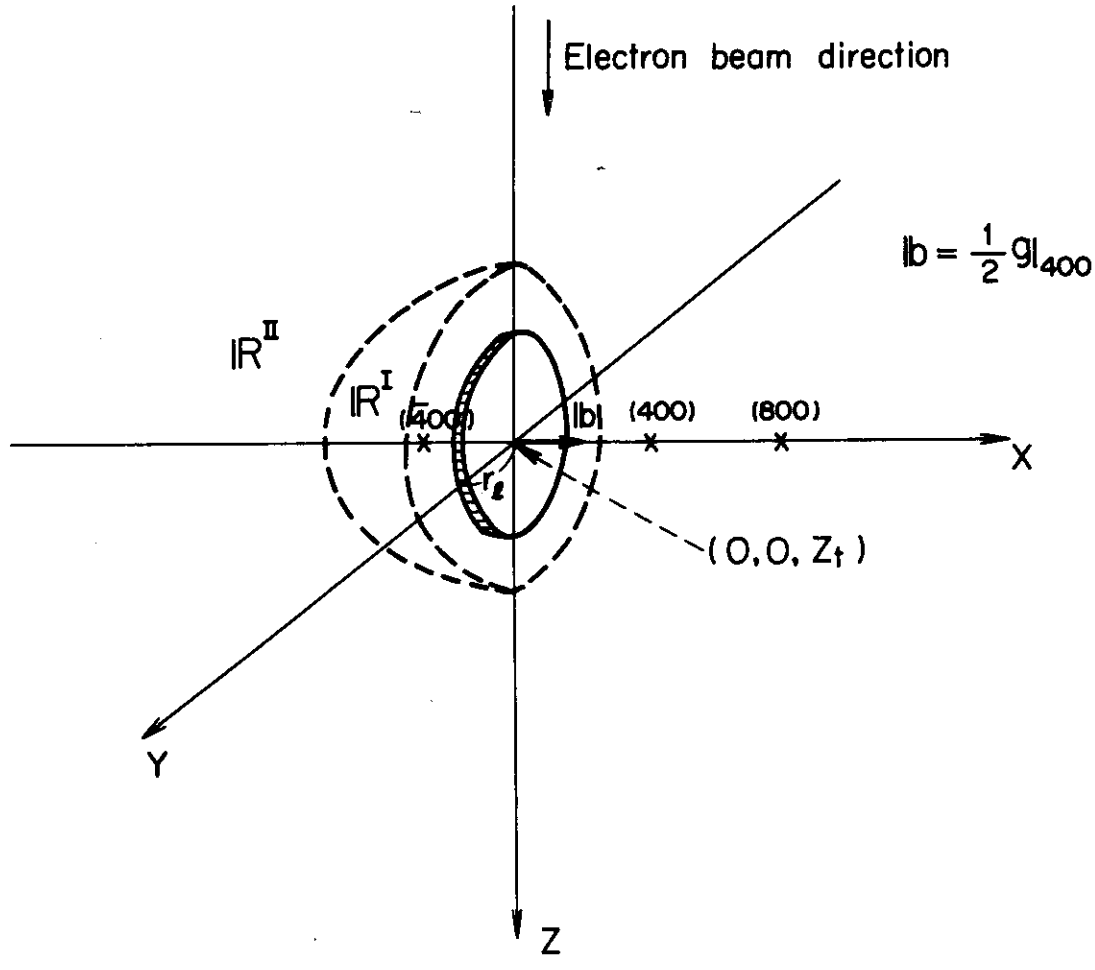

Fig. 2.13.1 Coordinate system for loop

$Z_f = 1000$, $b = \frac{a}{2}$, $\upsilon = \frac{1}{3}$

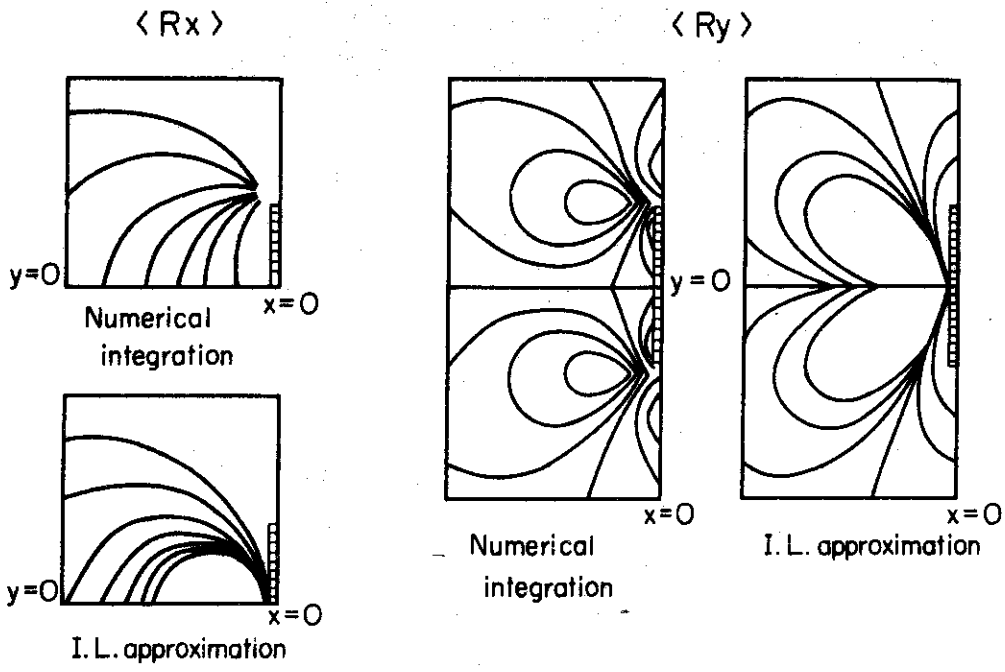

Fig. 2.13.2 Contours of displacement around loop

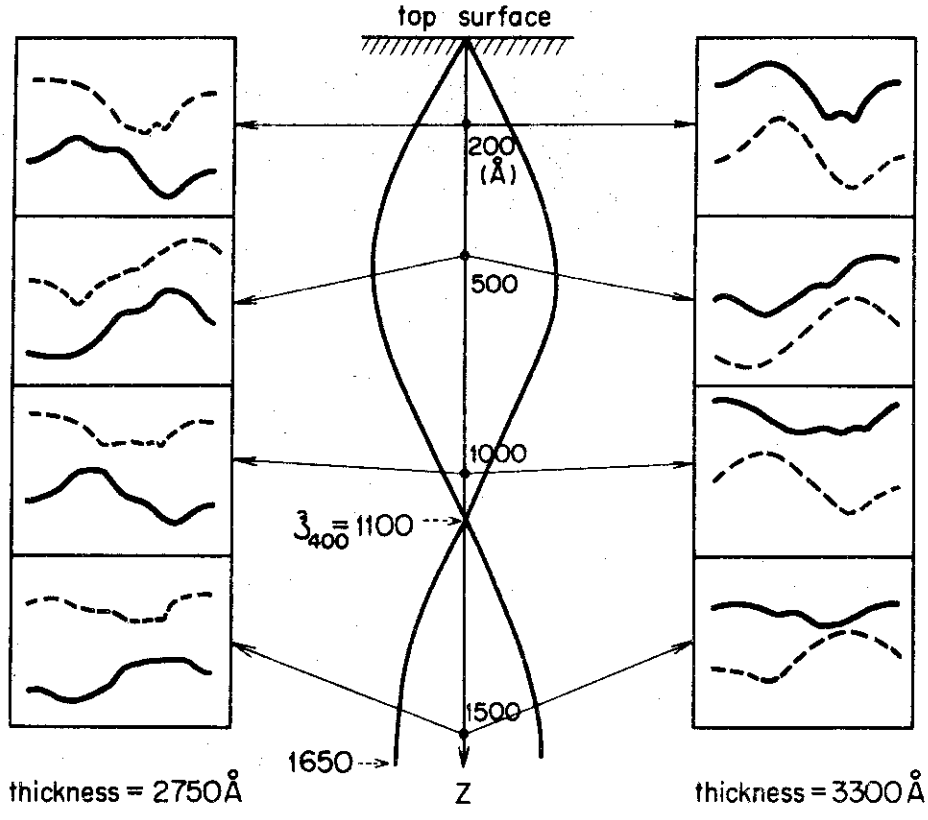

——— bright field, ---- dark field, • loop position

ζ_{400} = extinction distance, loop radius : 50 Å

Fig. 2.13.3 Intensity profile on the X-axis

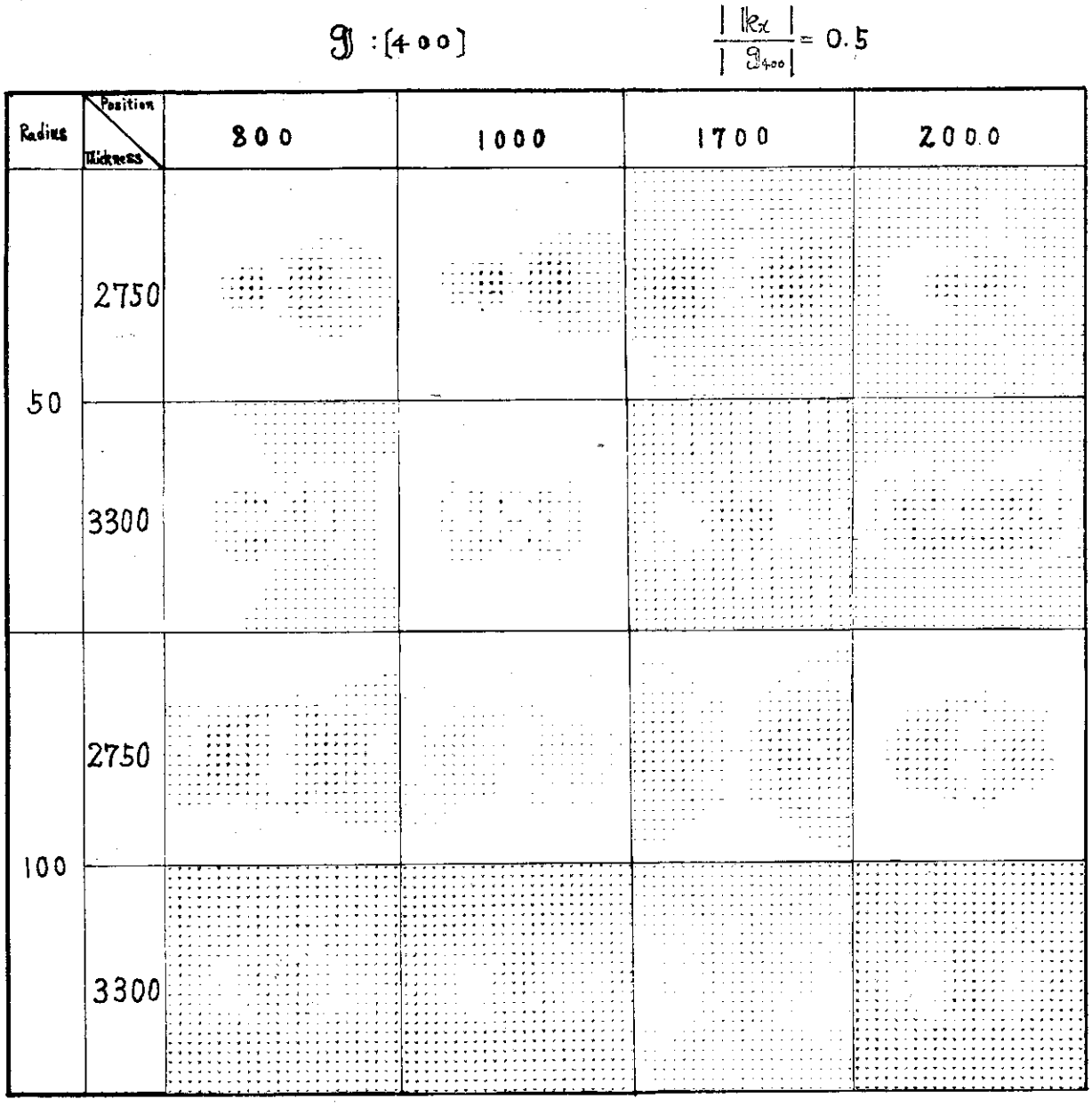

Fig. 2.13.4 Two dimensional simulation of image contrast

2.14 Development of Scientific Subroutine Library

T. Nishida, T. Fujimura, T. Asaoka, Y. Nakahara, T. Ise, K. Horikami, S. Inoue, T. Suzuki, T. Ideta and T. Tsutsui

It is well known that Scientific Subroutine Library (so called S.S.L.) plays an important role in physics and engineering calculations. In order to respond to various increasing requests from users, new informations on the development in algorithms of numerical analysis have to be collected for updating the S.S.L. continuously.

We have therefore systematically surveyed new theories, their applications to the numerical analysis, new topics and algorithms as a basis of renewing and improving the S.S.L.. The results have been summerized as internal reports. The followings are brief reviews on each field.

(1) General and special functions; It is necessary to test the accuracy and computation speed of the available different subroutines.

(2) Algebraic and transcendental equations (including polynomial operations); not yet reported.

(3) Linear equations; There exist various algorithms based on the direct method, which are ready for use, but the iteration method should be developed further.

(4) Matrix operations (mainly eigenvalue problems); Traditional algorithms for solving $Ax = \lambda x$ are mainly based on the direct method but recent algorithms based on the iteration method have an advantage over them.

(5) Linear programming; This gives a simple and sound method to be able to always use for obtaining an

optimal solution for linear systems as well as an approximate solution for nonlinear systems.

(6) Integral equations; Subroutines should be prepared for solving the first and third kind equations, and algorithms should be developed for solving nonlinear equations.

(7) Ordinary differential equations; Existing algorithms should be programmed and compared with each other from the viewpoint of the efficiency, definition of which needs to be established.

(8) Partial differential equations; Algorithms should carefully be checked with each other or further be developed for dealing with the hyperbolic, parabolic or nonlinear type, though algorithms have been established for the elliptic type.

(9) Numerical differentiations and integrations; Newly developed algorithms need to be adopted in the subroutine library.

(10) Fast Fourier transformations; It is necessary to develop subroutines to be able to treat any number of sampled data.

(11) Approximations of functions (interpolations, least-squares and minimax approximations); There exist many new algorithms and hence the subroutine library should be enlarged by adopting these algorithms.

(12) Statistics (including random number and Monte Carlo method); not yet reported.

At the next stage, we will perform the benchmark tests between computer programs of the S.S.L. for aiming at ascertaining the accuracy, speed and stability of some proven methods as

well as developing the advanced methods. A part of this work is now in progress.

3. Integral Experiment and Analysis

3.1 Reactivity Measurement in a Far-Subcritical Fast System[1),2),3)]

N. Mizoo, M. Nakano, T. Mukaiyama, T. Nakamura and M. Cho*

Reliable knowledge of the subcriticality of a fast reactor system is important for safety and economy in operation of an LMFBR. Experimental and theoretical studies have been made for the negative reactivities of a far-subcritical system with singularity, on FCA Assembly VI-2 B2.

Subcritical system of having singularity at core center (BC-7, BC-16 and BC-32) or at periphery (BP-7 and BP-32) were constructed, using three kinds of 90% and 80% enriched B_4C pin clusters. The reactivities of those subcitical systems range from -2$ to 7$. Critical balance technique (CBT), source multiplication (SM), pulsed neutron source (PNS), source jerk (SJ) and rod drop (RD) methods were used for the experiments. Spontaneous fission neutrons from Pu^{240} in the core region were utilized as external neutron source for SM and RD experiments, 14 MeV neutrons from Cockcroft accelerator being provided for PNS and SJ experiments. Neutron detectors were placed up to 11 points in and around the assembly.

Kinetic parameters and reactivities were calculated with 2-dimensional diffusion code CITATION using 6 energy group constants condensed from JAERI-Fast-2[4)], with the effective cross sections for B_4C pin clusters obtained by collision probability code CLUP[5)]. Reactivity of a system is defined by multiplication factor k_{eff} as $\rho = (k_{eff} - 1)/k_{eff}$.

Experimental data were analyzed under the assumption of one-point reactor theory. The resulting measured reactivities by SM method have large spatial effect due to singularity of B_4C pin cluster for the detectors set in and near the assembly. However, the detectors far from the assembly show

* Korea Atomic Energy Research Institute

position-independent results, which also agree with those by CBT method and by calculation in each system. SJ method is affected by the relation in the positions between the detector and the neutron source. SJ-integral and PNS-area methods give smaller values than those by SM method.

Each reactivity is given by the countrate measurements of two states e.g., those with and without neutron source for SJ method. Therfore, the difference of reactor parameters and detector efficiency ε between two states has to be corrected. Our definition of ε is as follows.

$\varepsilon = \int CR\, dt \,/\, \int F\, dt$ (= CR/F for steady state),

where CR is countrate and $F = \int\int \chi \phi^{\dagger} \nu\Sigma_f \Phi dEdr$ (Φ and $\phi^{\dagger}$ are the solutions of time dependent reactor equation and adjoint eigen function, respectively). Then, ε is obtained by solving time-integrated equation using multigroup diffusion code with fixed source, where the reactor constants and external source are evaluated for each state.

The results of SM, PNS-area and SJ-integral methods are shown in Table 3.1.1. The position dependence of the measured reactivities become negligible after the correction. Agreements of the corrected reactivities between these methods are also satisfactory, inspite of the fact that large corrections of up to 30% are made in the cases of far-subcritical system.

References

1) Mizoo, N., et al.: JAERI-M 6066 (1975).

2) Mukaiyama, T., et al.: JAERI-M 6067 (1975).

3) Nakano, M., et al.: JAERI-M (1975), to be published.

4) Katsuragi, S., et al.: JAERI-1195 and -1199 (1970).

5) Tsutsihashi, K.: JAERI-1196 (1971).

Table 3.1.1 Measured and corrected reactivities by SM, PNS-area and SJ-integral methods

System	Det.	SM		PNS-area		SJ-integral	
		$-\rho$ (%Δk/k)		$-\rho$ (%Δk/k)		$-\rho$ (%Δk/k)	
		Meas.	Corr.	Meas.	Corr.	Meas.	Corr.
BC-7	A	1.66 ± 0.01	1.64			1.60 ± 0.02	1.66
	B	1.67 ± 0.01	1.66			1.50 ± 0.03	1.65
	C	1.66 ± 0.01	1.65	1.51 ± 0.01	1.64	1.62 ± 0.02	1.69
	Av.		1.65		1.64		1.67
BC-32	A	4.45 ± 0.03	4.18			3.72 ± 0.16	4.15
	B	4.38 ± 0.03	4.25			3.19 ± 0.10	4.13
	C	4.19 ± 0.03	4.18	3.44 ± 0.03	4.12	3.71 ± 0.06	4.16
	Av.		4.20		4.12		4.15
BP-32	A	4.45 ± 0.03	3.23			3.28 ± 0.10	3.42
	B	3.31 ± 0.04	3.32			2.88 ± 0.05	3.45
	C	3.11 ± 0.03	3.44	3.00 ± 0.02	3.44	3.16 ± 0.06	3.40
	Av.		3.33		3.44		3.43

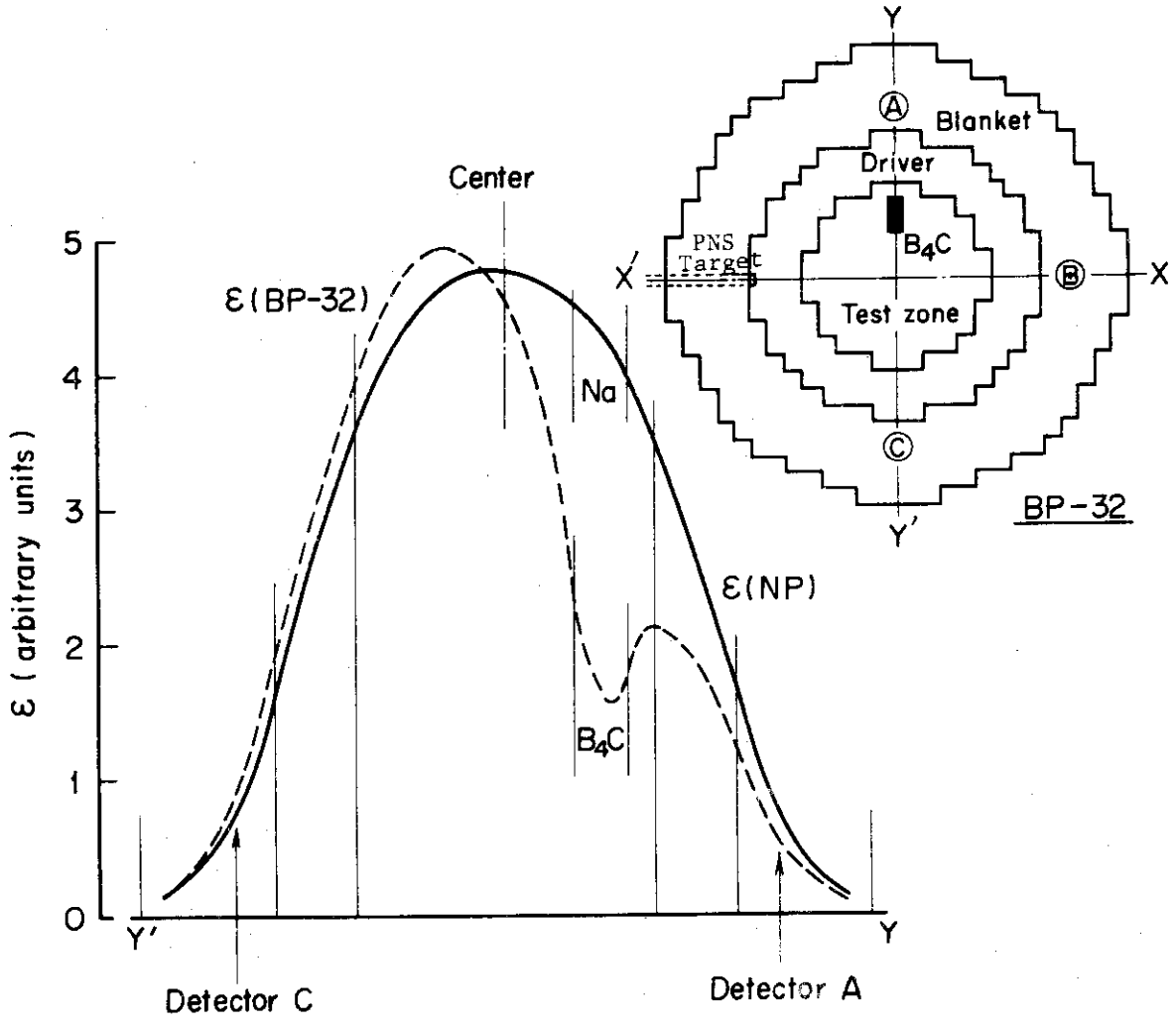

Fig. 3.1.1 Spatial distributions of detector efficiency ε for SM method (BP-32 system)

3.2 Evaluation of Neutron Leakage by the Measurement of Central Cell Reactivity Worth

T. Iijima, T. Mukaiyama and M. Nakano

In reactor calculation, the evaluation of neutron balance or criticality is made in the form of effective multiplication factor k_{eff} which is combination of the infinite multiplication factor $k\infty$ and the non-leakage probability. Therefore, cross-sections related to $k\infty$ such as fission and absorption cross-sections cannot be evaluated or adjusted, unless the neutron leakage is properly estimated.

Based on the fact that the central cell reactivity worth of a reactor system is equal to the worth of leakage neutrons from the central cell, a method to obtain the leakage fraction experimentally and to evaluate the accuracy of leakage calculation has been proposed and applied to FCA cores.

The reactivity worth of the central cell (unit cell at core center) of a reactor is expressed as

$$\rho_{cell} = \frac{\frac{1}{k_{eff}} <\phi^{\dagger} F \phi>_{cell} - <\phi^{\dagger} A \phi>_{cell}}{<\phi^{\dagger} F \phi>_{reactor}} = \frac{<\phi^{\dagger} L \phi>_{cell}}{<\phi^{\dagger} F \phi>_{reactor}} , \quad (1)$$

where L, A, and F are the operators of the reactor equation $-(L+A)\phi + \frac{F}{k_{eff}}\phi = 0$, and represent the leakage, the disappearance other than leakage and the fission source respectively. Equation (1) represents the worth of leakage neutrons from the central cell. Using the characteristic quantity k^+ defined as $k^+ = <\phi^{\dagger} F \phi>_{cell} / <\phi^{\dagger} A \phi>_{cell}$,

$$\text{Leakage fraction } X \equiv \frac{<\phi^{\dagger} L \phi>_{cell}}{<\phi^{\dagger}(L+A)\phi>_{cell}} = 1 - \frac{k_{eff}}{k^+} . \quad (2)$$

The k^+ can be determined from the measurement of the central cell reactivity worth[1]. That is, from the measured worth ratio of the central cell to a standard sample which is the main fissile material of the core composition, i.e., Pu sample, the k^+ is obtained as

$$k^+ = \frac{1}{1 - M \frac{\rho_{cell}}{\rho_{st}}} , \quad (3)$$

where the coefficient M is based on calculation, but can be calculated very accurately[1].

The k^+ values are obtained on FCA Assemblies VI-1 and VI-2 from the measurements of central cell reactivity worth (Table 3.2.1 and 3.2.2). In Table 3.2.1, the leakage fraction and its C/E values are also shown. To examine the accuracy of neutron leakage in reactor calculation, calculations by using two different cross-section sets, JAERI-Fast-II and ABBN, were performed and compared with experiments. From the results it is found that J-F-II a little overestimates the neutron leakage, while ABBN underestimates it. Using sensitivities of $k^+(\simeq k^\infty)$ and leakage fraction x to k_{eff} value, i.e., $\frac{\partial k_{eff}}{\partial k^+} = (1-x)$ and $\frac{\partial k_{eff}}{\partial \chi} = -k^+$ the differences in k^+ and leakage between the two cross-section sets lead to 4.9% and 2.0% difference in k_{eff} respectively. That is, ABBN set gives 4.9% reactive k_{eff} than J-F-II set from k^+, but 2.0% less reactive from neutron leakage. As a result, net difference in k_{eff} between the two sets (Δk_{eff} in usual meaning) is 2.9%Δk. As above, the present accuracy of neutron leakage in reactor calculation is unsatisfactory.

In Tables, there are also given the effective (one-group) diffusion coefficient $\bar{D}$. It can be seen that the difference in leakage fraction is due to the difference in $\bar{D}$. Table 3.2.3 shows that $\bar{D}$ value is determined mainly by the neutron spectrum rather than the differential cross-section D(E). Consequently, neutron spectrum has a strong influence on neutron leakage and in turn on criticality. This is due to the fact that the value of D(E) rises up more than twice in the energy rang 100KeV - 1MeV.

Reference

1) Nakano, M., Iijima, T.: J. Nucl. Sci. Technol., 10, 69 (1973).

Table 3.2.1 Characteristics of the central cell in FCA Assembly VI-1

	Experiment	Calculation J-F-II	Calculation ABBN
k^+	1.60 ± 0.01	1.581	1.659
$\frac{<\phi^\dagger L \phi>_{cell}}{<\phi^\dagger (L+A) \phi>_{cell}}$	0.375 ± 0.004	0.3705	0.3830
C/E		0.988	1.021
$\overline{D}$		1.571	1.630

Table 3.2.2 Characteristics of the central cell in FCA Assembly VI-2

	Experiment	Calculation J-F-II	Calculation ABBN
k^+	1.310 ± 0.004	1.280	1.367
$\overline{D}$		1.470	1.536

Table 3.2.3 Spectrum dependence of the effective diffusion coefficient $\overline{D}$ (FCA VI-1)

Cross-section D(E) / Spectrum φ(E)	J-F-II	ABBN
F-F-II	1.571	1.588
ABBN	1.616	1.630

3.3 Three Dimensional Benchmark Experiments on FCA VI-3 Assembly and their Analysis

K. Koyama, H. Kuroi, M. Obu, K. Shirakata, J. Hirota, N. Sasamoto, T. Ichimori*, N. Ogawa, S. Fujisaki, K. Yamagishi and H. Watanabe

Main topics on the reactor physics on prototype reactors are varing from asymptotic properties to spacially dependent ones. FCA assembly VI-3, which consists of a cylindrical core fueled with U-235 and Pu-239, and of the metallic uranium blanket of about 20 cm thick, has been built as a 3-D benchmark core to establish a reliable method for three dimensional analysis.

The main purposes of the experiments performed in the FCA VI-3 assembly are for measuring the power tilting due to B_4C control rods in the core region and for measuring the reactivity change due to sodium channels provided in the core region. For investigating the effects of power tilting, four different loading types in core region were adopted. The first one; named R-type, is a reference core without any channels except safety and control rods used for operating the critical facility. The second one; named N-type, provides two Na channels in core region as symmetry with respect to Z axis shown Fig. 3.3.1. The third one; named B1-type, provides B_4C and Pu fuel spiked channels instead of two Na channels. The criticality was achieved by adjusting fuel concentration in the Pu fuel spiked channel, without any geometrical changes. The last one; named B2-type,

---

The work performed under contracts between PNC and JAERI

* Tokyo Institute of Technology

was built to simulate the power tilting due to half-inserted control rods. This one was built by gathering the N-type applied in the fixed half of the FCA and the B1-type in the movable half of the FCA. The critical adjustment was also done by modulating fuel concentration in the Pu fuel spiked channel.

The reaction rates distributions were measured with the fission chambers of U-235 and U-238, and also by the foils of U-235 (93 %, 10φ x 0.1 t) and U-238 (400 ppm U-235, 12.7φ x 0.05 t). The reaction rates of U-235 and U-238 foils were determined from the results of photo peak analyses of γ-ray spectrum measured with Ge(Li) detector. [1] The photo peaks used for each measurement are as follows;

U-235 (n,f)	La-140	1597.1 KeV,
	I-132	954.6 " ,
	I-131	364.5 " ,
U-238 (n,f)	Xe-135	250.0 " ,
U-238 (n,r)	Np-239	334.3 " ,
		209.7 " ,

The details of the experimental results have been summarized on the JAERI-memo. [2]

These measured reaction rate distributions have been analysed by the three dimensional diffusion code in the DOYC computer code system using the AGLI/V-3 [3] cross section library. The analysis has been performed using 7 energy group structure whose cross section data were collapsed from 1950 group of AGLI library by taking into consideration of space dependent neutron spectrum given by the FCA 26 group structure.

The comparisons of the experimental results with the calculated results are performed by normalizing the valvu at the core center, for each loading type. From the comparisons of

C/E calculated by the present version of the DOYC system, following conclusions are obtained;

(1) on the N-type, the C/E shows good agreement,

(2) on the B1-and B2-types, the C/E dose not agree well especially in the neighborhood of the Pu fuel spiked channel,

(3) on all the types, the C/E for the U-238 (n,f) reaction is inferior to the others,

(4) on an average, reliability of the present data and method to predict the effect of power tilting due to control rod insertion is about 5 ∿ 8 % error.

Typical examples of the comparisons are shown in figures, Figs. 3.3.2 and 3.3.3. The studies of 3-D benchmark analysis has just been started, and more efforts should be continued to improve the data and method for predicting three dimensional power tilting due to rod insertion.

In order to investigate the reactivity change due to Na channel provided in the core region, about 40 different sets of Na channels with variety of size and positions were inserted into the core region of FCA VI-3, and the reactivity change for each set of channel was measured by the critical mass change. However, the analysis of the measured results have not been completed yet.

References

1) Sasamoto, N., Koyama, K., Tanaka, S. : "An Analysis Method of Gamma-ray Pulse-Hight Distributions obtained with a Ge(Li) Detector," N.I.M [125] p. 507 (1975).

2) Kuroi, H., et al : "Three dimensional Benchmark Experiments

(FCA VI-3 Assembly) and their Analysis," JAERI-memo 6202 (unpublished) (1975).

3) Kuroi, H., et al : "Adjusted Cross Section Library AGLI and Reliability of Analysis of Integral Data," Proceedings of International Symposium on Physics of Fast Reactors, Tokyo, Oct. 16-19, 1973, A33.

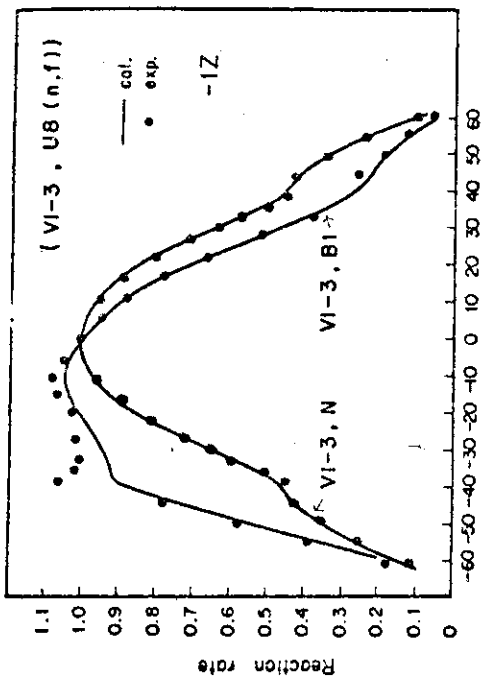

Fig. 3.3.2 Radial reaction rate distribution

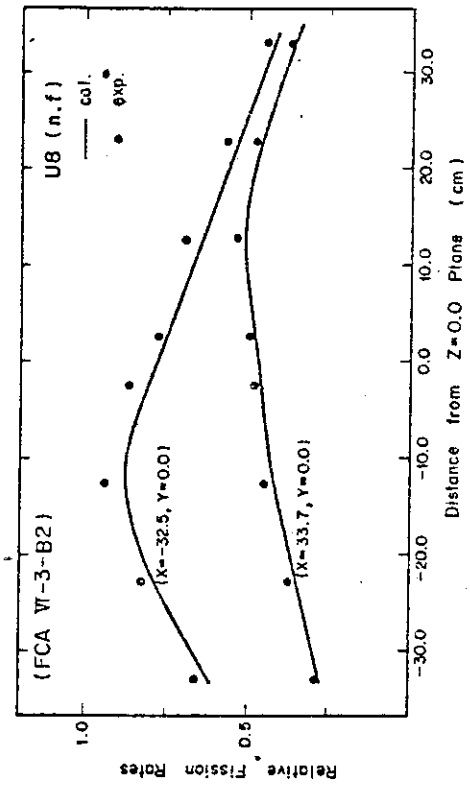

Fig. 3.3.3 Axial reaction rate distribution

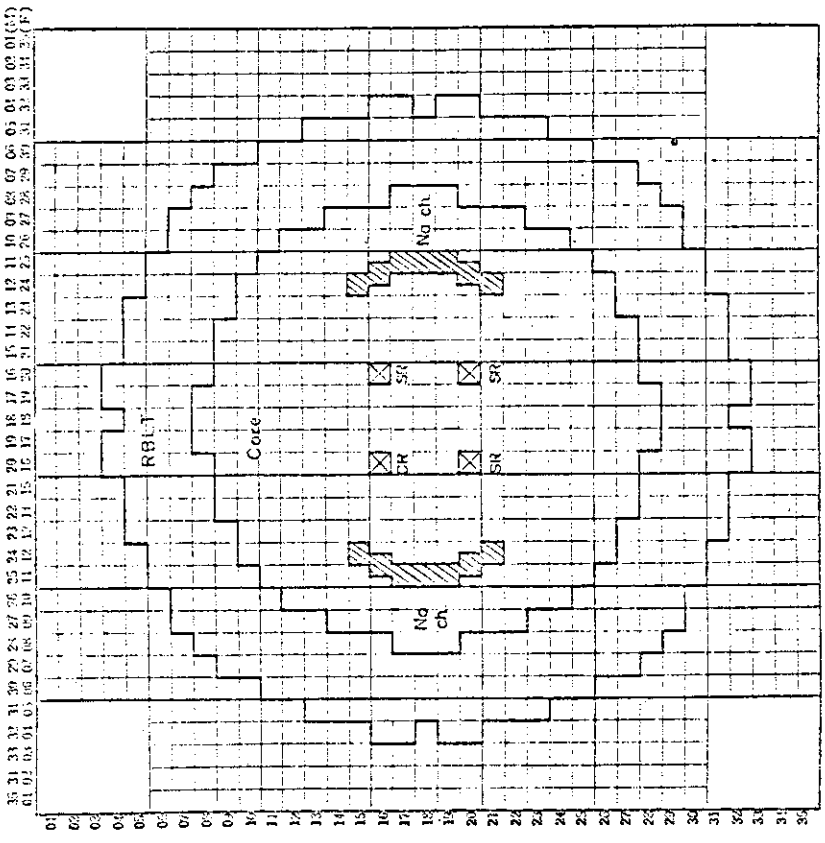

Fig. 3.3.1 Loading map (VI-3-N)

3.4 A Study of the Sector Mockup System for Prototype Fast Breeder Reactor MONJU

T. Iijima, N. Mizoo, H. Mitani, M. Nakano, K. Shirakata, T. Mukaiyama, M. Cho* and J. Hirota

A mockup experiment for MONJU has been designed in which the assembly consists of a Pu fueled sector test region simulating the MONJU core composition and a U-235 fueled driver region for the reason of the limited amount of Pu fuel inventory. The experiment will be started after the completion of enlargement of the FCA. Determination of optimum driver compositions, applicability or limit of sector type mockup, simulating accuracy of the quantities of the full mockup system by the sector system, and possible experiments in the sector mockup system have been studied.

As shown in Fig. 3.4.1, the full mockup system which the sector mockup system aims as ideal is Pu fueled two zone core. The corresponding sector system is constructed by replacing a portion of the core with the driver (D_1 and D_2). By matching the characteristics of the driver and the test region, it is expected that quantities in the test region of the sector system can be approached to those in the full mockup system. In general, to simulate the characteristics concerning distribution between two mediums of different composition is achieved by equalising the following three quantities between the two : (i) fundamental mode spectrum $\phi m(E)$, (ii) material buckling B_m^2, and (iii) diffusion coefficient $\overline{D}$. The condition (iii) is needed for the continuity of gradient at the boundary. The two regions satisfying above conditions can behave as if they were one region mdedium.

The compositions of driver regions D_1 and D_2 have been determined according to the above-mentioned principle. Especially, the three fundamental quantities (i) ~ (iii) of the inner driver D1 could be equalized to those of

* Korea Atomic Energy Research Institute

the inner test region T1 within the accuracy from cross-sections (Table 3.4.1). As for the outer driver D2, the matching to the outer test region T2 is slightly inferior due to the addition of carbon to reduce the critical mass within the U-235 inventory.

Two-dimensional diffusion calculations by X-Y or R-θ model with various sector angles were carried out and the distribution properties were compared with the full mockup system (Figs. 3.4.2, 3.4.3, and 3.4.4). From these results it has been made clear that the deviation of the neutron spectrum, the reaction rate distribution, and the reactivity worth distribution in the test region from the full mockup system are very small and are within the accuracies of measurement of these quantities. This means that the experimental results in the sector system can be analysed on the model of the full mockup system. Thus, it can be forecasted that by choosing appropriate driver composition the quantities such as power and reactivity worth distributions of the full mockup system can be obtained directly by the measurements with the sector system.

Table 3.4.1 Comparison of three fundamental quantities

	D_1-driver	T_1-test region
B_m^2 (cm^{-2})	1.195×10^{-3}	1.188×10^{-3}
$\overline{D}$ (cm)	1.485	1.468
$\sum_g \lvert \phi_g(D_1) - \phi_g(T_1) \rvert$	5.24%	

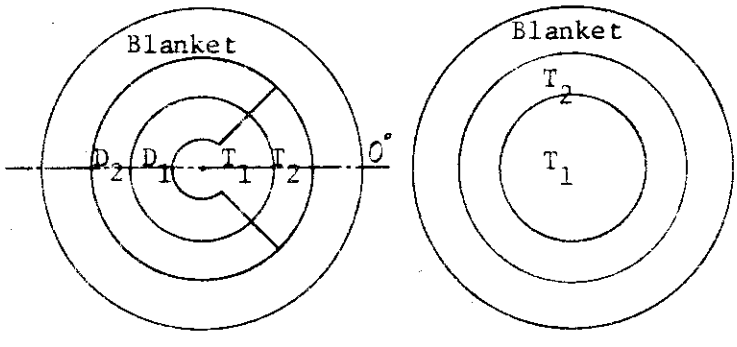

Fig. 3.4.1 Sector and full mockup system

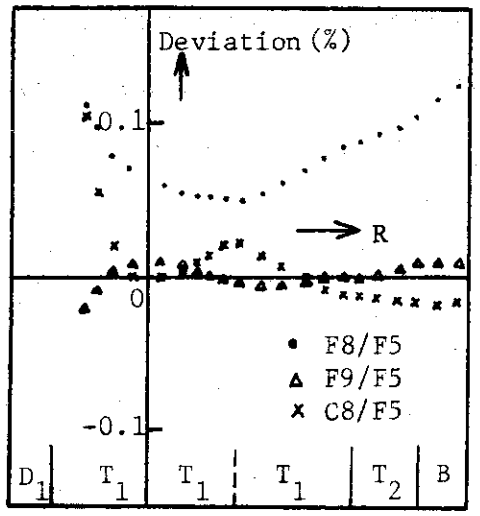

Fig. 3.4.2 Deviation of reaction rate ratio distributions in 60°-sector system from the full mockup system (Θ=0°, R-direction)

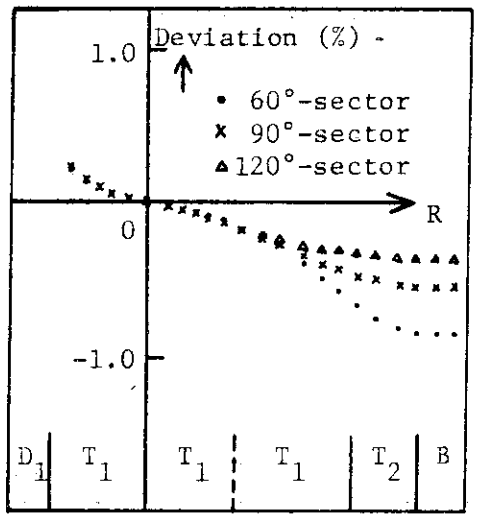

Fig. 3.4.3 Deviation of U-238 fission rate distribution from the full mockup system (Θ=0°, R-direction)

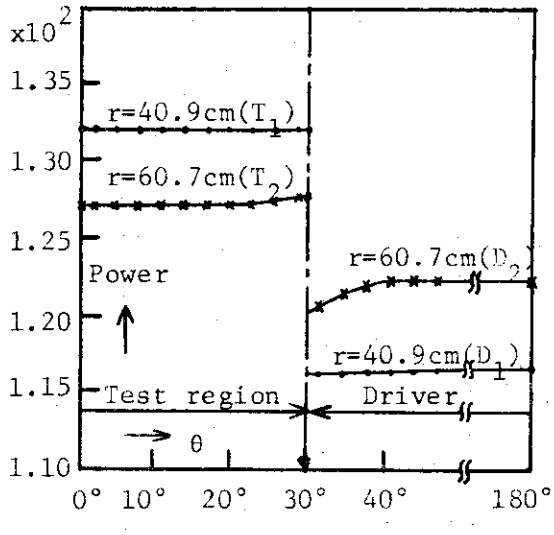

Fig. 3.4.4 Power distribution in 60°-sector system (Θ-direction)

3.5 Enlargement Work of the FCA

J. Hirota, T. Nakamura, H. Watanabe, H. Ogawa, S. Fujisaki and H. Yoshifuji

Under the contract between the PNC and JAERI, the enlargement work[1] has been proceeded at FCA since the middle of September, 1974. The FCA was originally so designed that the matrix could be enlarged from 35 rows by 35 columns to 51 rows by 51 columns. Therefore, the work is to add 8 layers of the matrix tubes on the all sides of the old matrix. It is also included to carry out the following modifications; removing the central bundle of 3 rows by 3 columns if necessary for the insertion of an experimental sample, driving two drawers instead of one by the control and safety rod drive mechanism, and increasing the number of the temperature measuring points imbedded in the matrix up to 18 for the more detailed temperature profile.

2,880 matrix tubes were newly fabricated and then, welded to form bundles of 5 rows by 5 columns or 5 rows by 3 columns for the assembling. Unexpected difficulties were experienced to fit the new bundles to the old ones resulting in the delay of the time schedule. Prior to the disassembling of the old matrix, a performance test of the bed and a preliminary test of the pair driving of the control and safety drawers were made. In October, fabrications of the frame supporting the control and safety rod drive mechanisms and the frame constraining the matrix were started. In December, an assembling test of the movable half matrix and a preliminary test of the removal of the central bundle were carried out.

Then, the work was proceeded in assembling of the fixed

half matrix, centering of the plate supporting the control and safety rod drive mechanisms, finishing of the contact surface of the fixed half matrix and setting of the air-cooling chamber. The time schedule was delayed mainly owing to the difficulties encountered in making possible the removal of the central bundle. Nevertheless, the most of the enlargement work was completed by the end of the fiscal year leaving the final performance test. It is expected that the engineering mock-up experiment for the Prototype Fast Breeder Reactor MONJU will be started in a few months.

Reference

1) Hirota, J., et al.: "The enlargement of the FCA," JAERI-M 5955 (1975) p. 67.

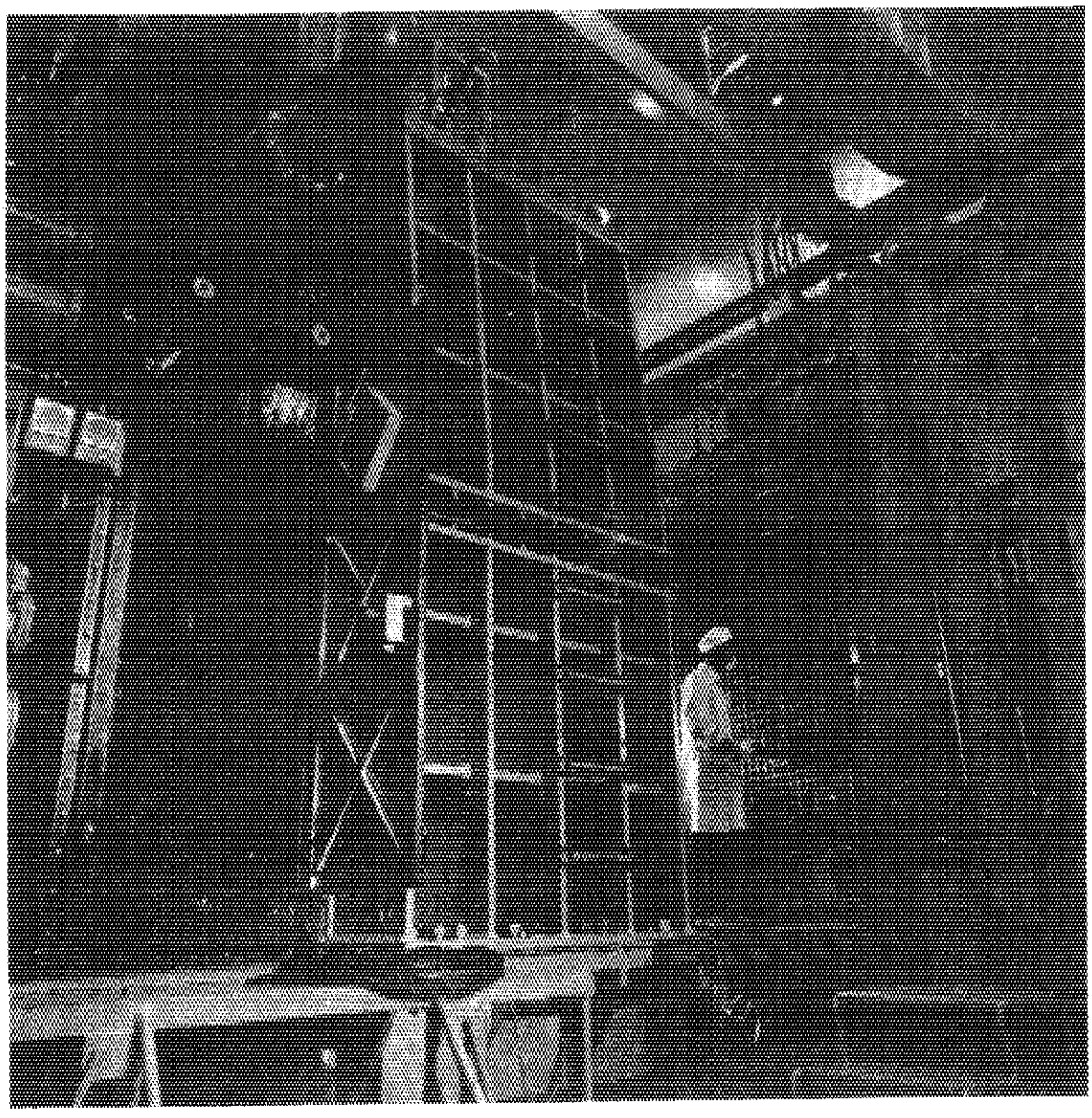

Fig. 3.5.1. The FCA enlarged to 51 rows by 51 columns .

3.6 Semi-empirical Formula for the Shape Factor of Fast Reactors

K. Koyama

The shape factor of fast reactor is a important value in order to elucidate the correlation between criticality calculated by one dimensional spherical geometry and that calculated by two dimensional cylindrical geometry.

Examining the various shape factors calculated by one-and two-dimensional DSN codes by mean of the least square method, an atempt has been made to introduce a set of semi-empirieal formulas of the shape factor to be applicable for any types of reactors, for examples, metallic fueled type, oxide fueled type, etc.. According to Davey's definition[1], the peak shape factor PSF is given in the semi-emprical formula as follows;

$$PSF = \{1.0 - 0.1 \exp(-0.00135\ R_s)\}\beta_\eta^{-\frac{1}{3}}$$

$$\beta_\eta = \beta(R_s, T) \,/\, \beta(\infty, T)$$

where $\beta(R_s, T)$ is a reflector's albedo obtained by one-group approximation for the spherical reactors with core radius R_s and reflector thickness T. The normalized shape factor NSF is given as

$$NSF = x^2 g^{-3}(x) \quad , \qquad x = Z/R_c \quad ,$$

$$g(x) = 0.3107 + 0.6905x + \gamma |x - 0.9|^3 \{1.0 - 0.54(x-0.9)^2 Y(x)\} \quad ,$$

$$Y(x) = x \qquad 0 \leq x \leq 0.9$$

$$= 1.8 - x \qquad 0.9 < x \leq 1.8 \quad ,$$

and the parameter γ depending on reactor composition is given as

$$\gamma = \frac{1}{0.729}\left(\frac{Z_0}{A_s R_s} - 0.3107\right) \quad ,$$

$$A_s = \left(\frac{2}{3}\frac{1}{PSF}\right)^{\frac{1}{3}} \quad ,$$

where Z is half the core thickness of infinite plane geometry as a extreme case of cylindrical geometry x = 0.

The comparisons of the true values with the estimated ones from the semi-empirical formulas are shown in Figs. 3.6.1 and 3.6.2 for the peak

shape factors and the function g(x) respectively. Accuracies of the shape factors estimated by these formulas are better than 0.6% in critical core volumes in the range of core height to diameter ratio x between 0.4 and 1.8.

References

1) Davey, W.G.: "K Calculations for 22 ZPR-III Fast Reactor Assemblies using ANL Cross-section Set 635", ANL-6570 (1962).

2) Koyama, K.: "Semi-empirical Formula for the Shape Factor of Fast Reactors", (to be published on J. Nucl. Sci. Technol).

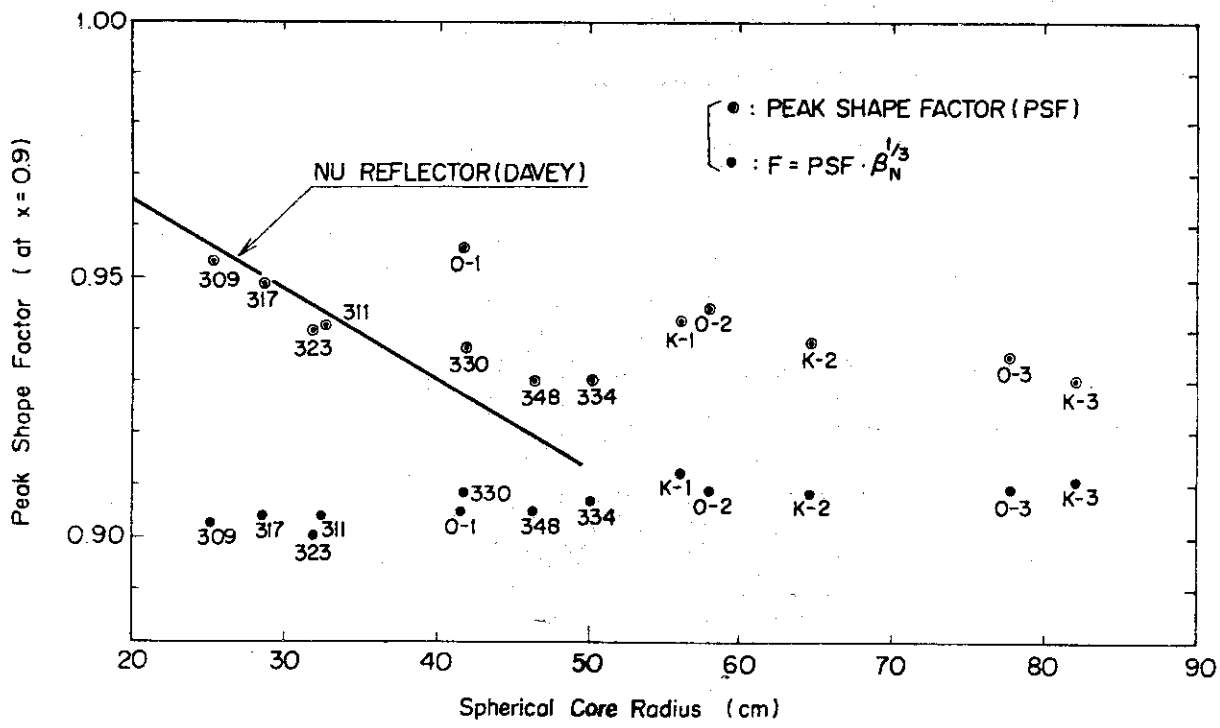

Fig. 3.6.1 Peak shape factor PSF and value of PSF·$\beta^{1/3}$ versus spherical core radius

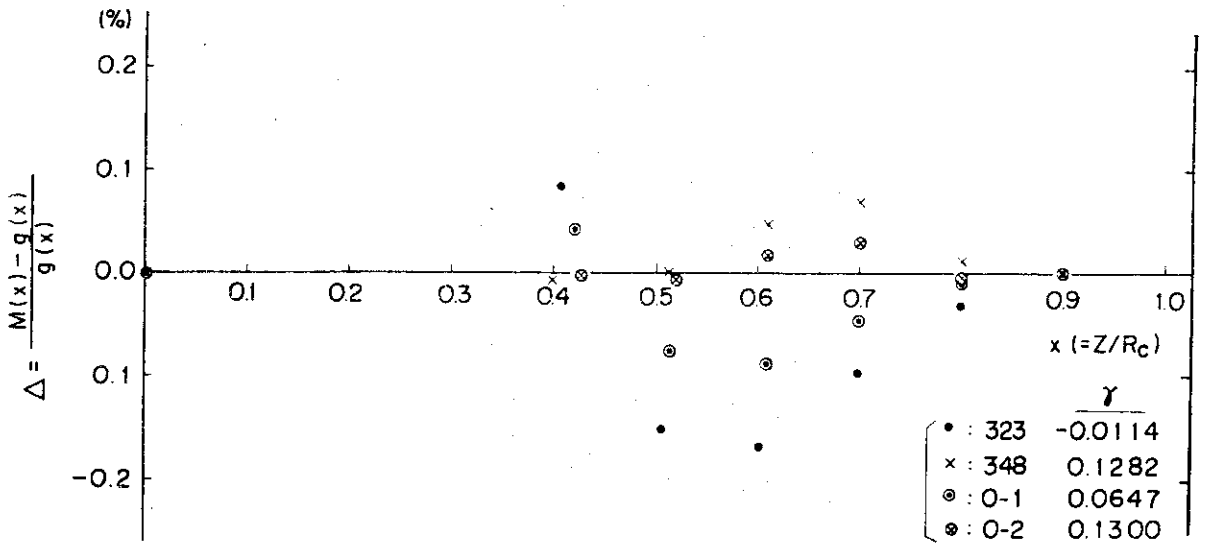

Fig. 3.6.2 Deviation of g(x) from its exact value M = $Z/(A_S \cdot R_S)$

3.7 Analysis of Critical Experiments in MZA and MZB Assemblies with the Revised JAERI-Fast Set

M. Nakagawa, A. Hasegawa, Y. Kikuchi and S. Katsuragi

The results of critical experiments in MZA and MZB assemblies are analyzed with the revised version of the JAERI-Fast set,[1] in order to investigate the differences from those analyzed with the old version and to know the reliability of the set and the accuracy of the methods for analysis.

As for the effective multiplication factor, the C/E values are 1.0055 for MZA and 0.9986 for MZB, while they were 1.0142 and 1.0114 respectively with the old version. Thus remarkable improvement in C/E is attained with the revised version.

The central reaction rate ratios are calculated for $\sigma_f^{28}/\sigma_f^{25}$, $\sigma_f^{25}/\sigma_f^{49}$, $\sigma_f^{40}/\sigma_f^{49}$, $\sigma_f^{41}/\sigma_f^{49}$ and $\sigma_c^{28}/\sigma_f^{49}$. Remarkable improvement is observed in $\sigma_f^{41}/\sigma_f^{49}$ and $\sigma_c^{28}/\sigma_f^{49}$. This suggests that the fission cross section of ^{241}Pu and the capture cross section of ^{238}U are improved in the revised version. It is also suggested that some errors may still remain in the fission cross sections above 1 MeV. These conclusions are supported by the analyses of the central reactivity worths.

As for the reaction rate distribution, the fission rates of ^{235}U and ^{239}Pu are underestimated in the radial blanket of both assemblies. This error may not be caused by the errors in the cross section set but is due to some inadequate treatment in analysis.

The sodium removal reactivities measured at MZB assembly have been analyzed with three types of JAERI Fast sets, that is, the old version (JF-O), the revised version (JF-R) and that with revised sodium cross sections (JF-N). The sodium cross sections were prepared by evaluating the recent nuclear data. The measurements were performed at the central regions along axial direction and at off-center regions (inner core, outer

core and radial blanket) for plate and pin type cells. The analysis is based on the two dimensional (X-Y, R-Z) diffusion calculations. The effective cross sections are obtained by heterogeneous cell calculations and are collappsed to 12 groups. The neutron streaming effect is considered by using Benoist's anisotropic diffusion coefficients.

Some results are shown in Table 3.7.1. The JF-R set (revised for the cross sections of heavy elements) predicts more negative values than measurements compared with those by the JF-O set. By using the JF-N set the calculations considerably approach to the measurements. Therefore it is necessary to revise the sodium group constants of original JAERI-Fast set. All the sets shows more negative values than the measurements. The leakage components obtained by perturbation calculations are in good agreement with the three dimensional calculations in AEE Winfrith.[2] The main difference between calculations and measurements may be caused by the difference in the spectrum terms. When the cross sections are averaged with fine group spectrum the C/E value at the central region is improved about 15 percents. In the calculation of the off-center regions three dimensional treatment will be necessary, because the ambiguity is large for buckling values to axial direction.

References

1) To be published
2) Stevenson, J.M., et.al. : IAEA Tokyo Conf. A19 (1973)

Table 3.7.1 Comparison of calculated and measured sodium removal reactivities for plate cells ($\times 10^{-4}$ $\Delta k/k$)

Region	Exp.	JF - O	JF - R	JF - N
Center cells	1.75 ± .02	1.22	1.07	1.32
Upper and lower cells	0.56 ± .04	-0.55	-0.70	-0.303
Blanket	-0.76 ± .03	-1.10	-1.06	-1.022
Whole core	2.31 ± .05	0.68		1.013
Element		-0.42		-0.147
Inner core	0.50 ± .05			-1.27
Outer core	-2.06 ± .05			-2.66
Radial blanket	-1.27 ± .02			-1.46

3.8 Assessment of Group Constants through Measurements and Analyses of Neutron Spectrum in Reactor Materials

M. Nakagawa, M. Ando*, K. Kobayashi**, K. Kimura** and H. Nishihara*

The multi-group constants have been used for the prediction of physical quantities in fast reactors. At present remarkable discrepancies exist among different group constants. Several works to improve the accuracy of group constants have been frequently performed through the comparison between measurements and analyses of them. The measurements of neutron distribution function in bulk assemblies have been recently performed and found to be a powerful method to assess cross sections of light and medium weight elements. The advantage of this method is that the assemblies have very simple geometries and homogeneous composition with an individual material. Therefore the analysis is simple and the anbiguity is smaller compared with measurements in fast critical assemblies.

In the present work, the energy and space distributions of neutrons have been measured for several materials by the neutron time-of-flight method using the electron linear accelerator of Research Reactor Institute, Kyoto University, as a pulse neutron source. The details of experiments can be found in the references, (1) and (2). The materials and the geometries measured are shown in Table 3.8.1. The calculations have been performed with neutron transport codes, DTFIV and ANISN, for the sherical geometry. The assumption of spherical symmetry has been convinced by measuring the spacial reaction rate distribution from the source at the center to several directions. The group constants have been taken from the JAERI Fast, ABBN sets and DLC-2D

---

* Department of Nuclear Engineering, Kyoto University

** Research Reactor Institute, Kyoto University

library, which is compiled by RSIC at ORNL. Some group constants have been produced from the ENDF/B and U.K. files.

Some results are discussed below. Fig.3.8.1 shows the comparison of angular flux between the measurement and calculations for the iron assembly at r=15cm, $\mu = 0$. The calculation with the JAERI-Fast set is apparently lower than the measurement in a few 10keV region. This is caused by the inadequate treatment for the elastic removal cross sections at resonances. The accurate self-shielding factors should be used especially at 28.5 keV resonance peak and deep window of iron. The result for the DLC-2D set seems to be in very good agreement. However the position of resonance peaks shifts from that of the measurement. This is improved by using the self-shielding factors obtained by fine group calculations as shown in Fig.3.8.1. The discrepancy at 0.8 - 2 MeV region means that the inelastic scattering cross sections are small in the ENDF B/III.

Fig.3.8.2 presents the spectra obtained for the thoria assembly by the measurement and calculations by the NNM (JAERI Fast type constants), ABBN and DLC-2D sets. All the sets show the considerably good agreement over the whole energy range. The NNM presents the best fit for the measurement among the three sets, because the effective cross sections are obtained by the most accurate method in the resonance region. In the 100 keV - 10 keV region the calculations are smaller about 20 - 30 percents than the measurement. Therefore further study will be necessary about the average resonance parameters of thorium. In the course of the analysis we noticed that the impurity of H_2O included in thoria significantly affects the shape of spectrum below 100 keV.

The discussion on the spectrum in the SUS assemblies is presented in Ref. 2 and the analyses of another materials have been continued.

References

1) Nishihara, H., Kimura, I. and Kobayashi, K., Proceedings of International Symposium on Physics of Fast Reactors, Tokyo, Vol.2, p.861 (1973)

2) Kimura, I., et al, Conf. on Neutron Cross sections and Technology, Washington DC (1975)

3) Nakagawa, M., Nishihara, H. and Miki, K. JAERI-M 4927 (1972)

Table 3.8.1 Geometry of assemblies

Material	Geometry (cm)
Iron	90 x 100 x 100
Iron oxide (Fe_2O_3)	60 (D)
Stainless steel	75 x 75 x 75
Alumina	60 (D)
Lead	70 x 70 x 70
Boron - graphite	70 x 70 x 80
Thoria (ThO_2)	60 (D)

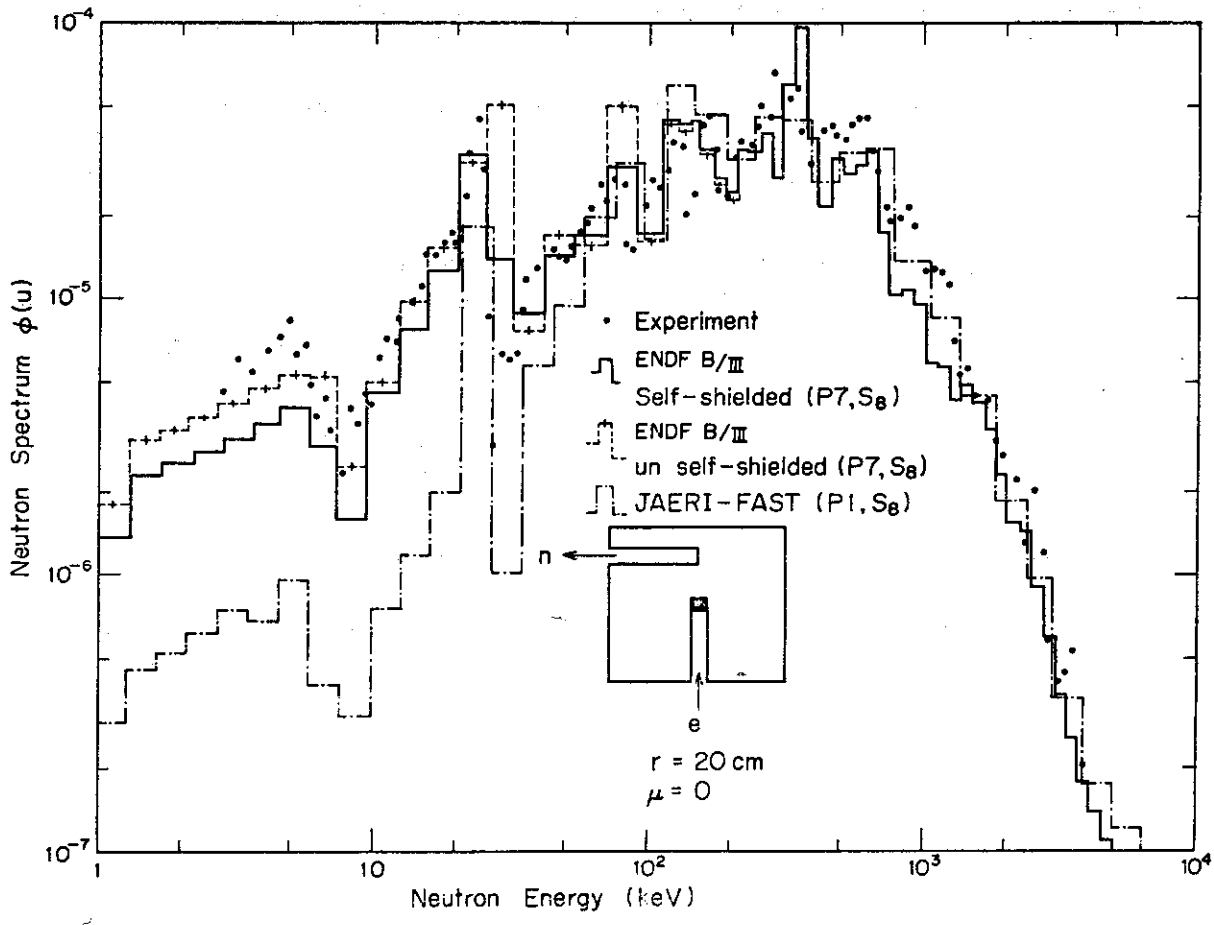

Fig.3.8.1 Neutron spectrum at r=20 cm and $\theta = 90^{\circ}$ ($\mu = 0$) in the iron assembly

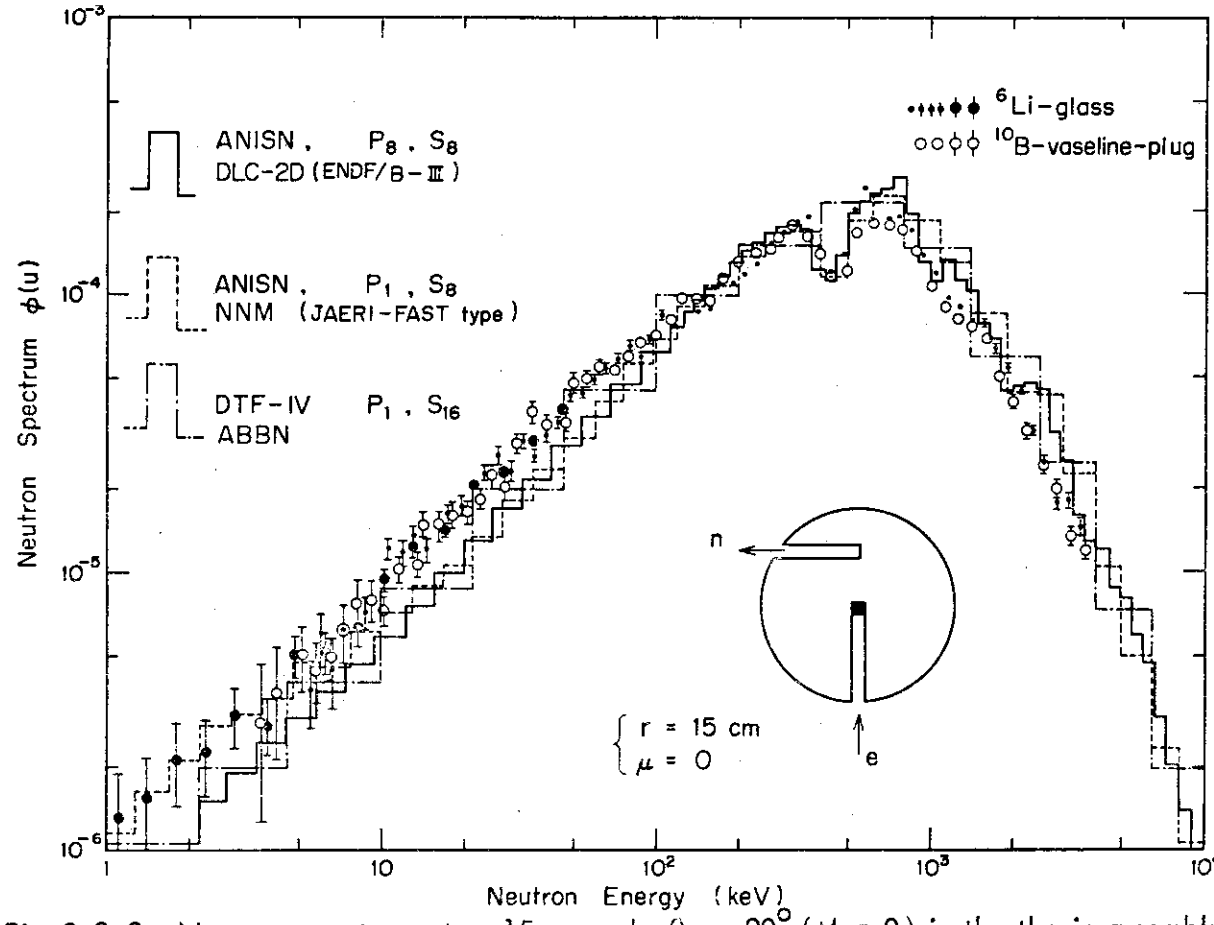

Fig.3.8.2 Neutron spectrum at r=15 cm and $\theta = 90^{\circ}$ ($\mu = 0$) in the thoria assembly

3.9 Integral-Versions of Some Kinetic Experiments for Determing Large Negative Reactivity of Reactor

Y. Kaneko

Theoretical treatments, including the methods of source-multiplication, rod-drop and source-jerk, are suggested for dealing with the spatial effects observed in several kinetic experiments for determining large negative reactivity in a reactor. An analysis by means of kinetic eigenfunctions is made on the kinetic behavior of the reactor, when these methods are applied. For each kind of experiment, a new multi-point type formula is established to replace the current single point type expressions, in order to derive the precise reactivity value by utilizing all of the neutron counting data obtained from every part of the reactor core. In the new formulas, the raw neutron counting data are integrated in reference to space and energy, weighted with the product of the static adjoint-neutron density and the static fission spectrum as shown in Table 3.9.1. This integral procedure is effective in eliminating the effects of kinetic distortion and of the spatial harmonics included in the raw counting data. In addition, using the kinetic eigenfunctions, a new formula is also presented for determining the effective intensity of the source neutrons injected in the source-neutron-introduction method for absolute measurements of reactor power.

Reference

1) Kaneko, Y. : J. Nucl. Sci. Technol., 12, 12 (1975).

Table 3.9.1 Multi-point type formulas for determining large negative reactivity and absolute power of reactors

Experimental method	One-point	Multi-point
Pulsed neutrons	$\frac{\rho}{\beta_{eff}} = -\frac{A_p(\vec{r})}{A_d(\vec{r})}$	$\frac{\rho}{\beta_{eff}} = -\frac{\bar{A}_p}{\bar{A}_d}$
Source-neutron multiplication	$\rho = \pm\frac{S \cdot d}{A_+(\vec{r})}$	$\rho = -\frac{S\, k_{os}^{+}(\vec{r}_s, \vec{r}_c)}{\bar{I}_+}$
Rod-drop (Source-jerk)	$\frac{\rho}{\beta_{eff}} = -\frac{A_c(\vec{r})}{A_r(\vec{r})}$	$\frac{\rho}{\beta_{eff}} = -\frac{\bar{A}_c}{\bar{A}_r}$
Source introduction	$\rho = \frac{S' \lambda I}{\alpha \bar{\nu}^2 \beta_{eff} I'}$	$\rho = \frac{S'_{eff} \lambda I}{\alpha \bar{\nu}^2 \beta_{eff} I'}$

Remarks: $\bar{A}_p$ and $\bar{A}_d$ means the saptial integration of neutron counting areas $A_p(\vec{r})$ and $A_d(\vec{r})$ for the prompt and delayed neutron modes respectively. This rule is valid for the other kinds of neutron counting areas.

3.10 Measurement of Space Dependent Angular Thermal Neutron Spectra in Natural Uranium-Light Water Slab Geometry

F. Akino, Y. Kaneko, K. Kitadate and R. Kurokawa

0° angular thermal neutron spectra were measured by the time of flight method at several positions in a spectrum source, which is a single natural uranium plate sandwiched between two layers of pure water.[1] Theoretical analysis was made by means of the multigroup discrete S_8 method,[2] using the Haywood's model for scattering of the thermal neutrons. The calculated thermal neutron spectra are compared with the measured plots in Fig. 3.10.1 after correction for the reentrant hole perturbation.[3] Fairly good agreement is observed between experiment and theory, and then the followings were concluded;

(1) Validity of the Haywoods model is demonstrated for description of the thermal neutrons spectra in heterogeneous multiplying media like the present spectrum source, under the condition that anisotropies in either the neutron scattering or the source neutrons the thermal neutrons are taken into consideration. Discrepancy between the measured and the calculated spectra is so small as the error in the neutron absorption of ^{235}U, induced therefrom is within 3 %.

(2) The spatial distribution of the source neutrons requires much attention, especially for the thermal neutron spectra in the light water region surrounding the natural uranium plate.

References

1) Akino, F. et al. : to be published in J. Nucl. Sci. Technol. (1975).

2) Lathrop, K.D. : LA-3373 (1965).

3) Akino, F. and Kaneko, Y. : J. Nucl. Sci. Technol., 10[1], p. 45 ∿ 53 (1973).

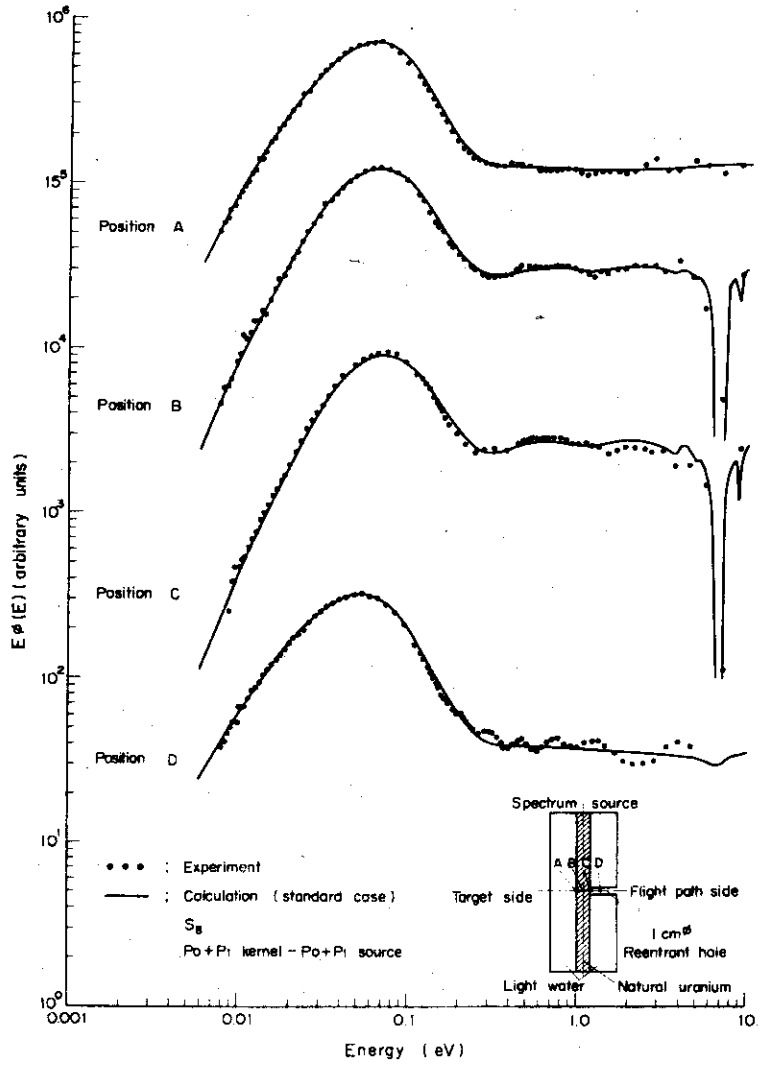

Fig. 3.10.1 Comparison of measured 0° angular thermal neutron spectra with calculated spectra for the natural uranium-light water spectrum source

4. Shielding

4.1 Measurement and Analysis of Radiation Leakage on the Nuclear Ship MUTSU

S. Miyasaka, T. Asaoka, Y. Taji, T. Tsutsui, T. Ise, I. Kobayashi, H. Ryufuku, S. Tanaka, H. Yamazaki*, K. Kabayama*, K. Takeuchi*, A Yamaji* and T. Fuse*

Radiation measurements, calibration of radiation detectors and analysis of measured data were carried out to investigate a radiation leakage on the nuclear ship MUTSU.[1)]

Radiation measurements were performed around the primary and secondary shields of MUTSU. BF_3 counters, with and without polyethylene and cadmium covers, and thermoluminescence dosimeters were mainly used as neutron detectors. Gamma-ray dose rates were measured with thermoluminescence dosimeters, pocket chambers, etc..

In order to obtain the absolute neutron flux and the dose equivalent rate, the BF_3 detector system was calibrated by comparing with a reference detector system in neutrons of a ^{252}Cf source and a light water moderated critical assembly. Calibration of thermoluminescence dosimeters was also carried out with a ^{226}Ra source and the critical assembly.

The analysis of the shielding problem utilized TWOTRAN[2)] and PALLAS-2DCY[3)] calculations in cylindrical geometry. In the TWOTRAN calculation, the ENDF/B-III data file was used for the neutron cross sections. The secondary gamma-ray production and

---

* Ship Research Institute

gamma-ray transport cross sections were obtained from the POPOP4 and the GAMLEG-JR, respectively.[4] These cross sections were collapsed to 5 neutron and 3 gamma-ray groups by one-dimensional calculations using the ANISN code.[5] The TWOTRAN calculation was performed with P_1 and S_8 approximation.

In the PALLAS-2DCY calculation, the shield region was devided into four sub-regions. The calculated neutron angular flux distributions at the outer surface of each sub-region were used as the input for a boundary condition for the calculation in the next sub-region. The neutron energy range of 13.35 - 0.1098 MeV was divided into 25 groups having the same lethargy width of 0.2. The group constants were obtained by assuming the 1/E energy spectrum in each lethargy width.

The experimental and analytical results show the importance of streaming through the gap between the reactor vessel and the primary shield. The neutron dose rate at the upper part of the reactor vessel is increased by neutrons incident on the head through cavity. The neutron dose rate at the lower part of the containment vessel is also increased by neutrons scattered by the steel structure of the vessel and the double bottom. The BF_3 counter measurement indicates that the neutron dose rate at the top of the primary shield is 10 $\sim$ 20 mrem/hr at 0.24 % output power.

References

1) Ando, Y., Miyasaka, S., Takeuchi, K. : J. At. Energy Soc. Japan, 17, 57 (1975) (in Japanese).

2) Lathrop, K.D., Brinkley, F.W. : "Theory and Use of the General-Geometry TWOTRAN Program," LA-4432 (1970).

3) Takeuchi, K., Yamaji, A. : J. Nucl. Sci. Technol., 11, 49 (1974).

4) Miyasaka, S., et al. : "Code System for the Radiation-Heating Analysis of a Nuclear Reactor, RADHEAT," JAERI-M 5794 (1974) (in Japanese).

5) Engle, W.W., Jr. : "A User's Manual for ANISN, A One Dimensional Discrete Ordinates Transport Code with Anisotropic Scattering," K-1693 (1967).

4.2 Iron Shielding Benchmark Experiments at "YAYOI"

S. Miyasaka, S. An[1], Y. Oka[1], M. Akiyama[1],
T. Hyodo[2], T. Nishibe[2], K. Shin[2] T. Fuse[3],
K. Takeuchi[3], A. Yamaji[3], T. Miura[3], S. Iwasaki[4]

Transmitted neutron spectra through up to 20 cm thick iron slab were measured using two measuring geometries at the fast neutron source reactor, "YAYOI". One was the experiment using broad beam and collimated counter. The other was the measurement using a collimated narrow beam of reactor neutron as a source together with uncollimated counter as shown in Fig. 4.2.1.

Neutron spectra in the energy range 1.5 to 14 MeV were obtained using an NE-213 scintillation counter with the aid of the unfolding code FERDO.[1)] Neutron spectra in the energy range about 10 KeV to 1.0 MeV were measured using a propotional recoil spectrometer with the aid of the unfolding code SPEC4.[2)]

The measured spectra through the iron slab were compared with calculated spectra using the discrete ordinate code, ANISN,[3)] and the Monte Carlo codes, MORSE[4)] and CYGNUS.[5)] The basic iron cross section sets used were the ENDF/B-III and -IV data file.

From the comparisons between MORSE calculations and measured spectra as shown in Fig. 4.2.2, the agreement is adequate at 0° of both iron thickness. The calculated spectra at 30° of both iron thickness, however, show discrepancy, which may be due to the treatment of the angular distributions for

---

(1) University of Tokyo, (2) Kyoto University,
(3) Ship Research Institute, (4) University of Tohoku

elastic and inelastic scattering.

From the experimental and analytical results, the following remarks are derived:

1) Concerning neutron cross section data, there is almost no difference between the results of analysis based on ENDF/B-III data file and those based on ENDF/B-IV. The reason is attributed to the fact that the values of total cross section in the experimental energy range are about the same for both data files.

2) The calculational results by Monte Carlo method agree fairly well with the experimental ones in general, except the discrepancy at 30° in MORSE calculation which may be due to the treatment of angular distributions for scattering.

3) It seems to be rather difficult to analyze the narrow beam experiments by the discrete ordinate transport codes. The usual analytical treatment using this kind of code could not well simulate the experimental conditions. The study is now continued to find a calculational procedure suited to get a good agreement with the experimental results.

References

1) Burrus, W.R., Verbinski, V.V. : ANS-SD-2 (1964).

2) Verbinski, V.V., et al. : ANS-SD-2 (1964).

3) Engle, W.W., Jr. : "A User's Manual for ANISN, A One Dimensional Discrete Ordinates Transport Code with Anisotropic Scattering," K-1693 (1967).

4) Straker, E.A., et al. : "The MORSE Code — A Multigroup Neutron and Gamma-Ray Monte Carlo Transport Code," ORNL-4585 (1970).

5) Hirayama, H., Nakamura, T. : The Memories of the Faculty of Engineering, Kyoto University, 34, part 2 (1972).

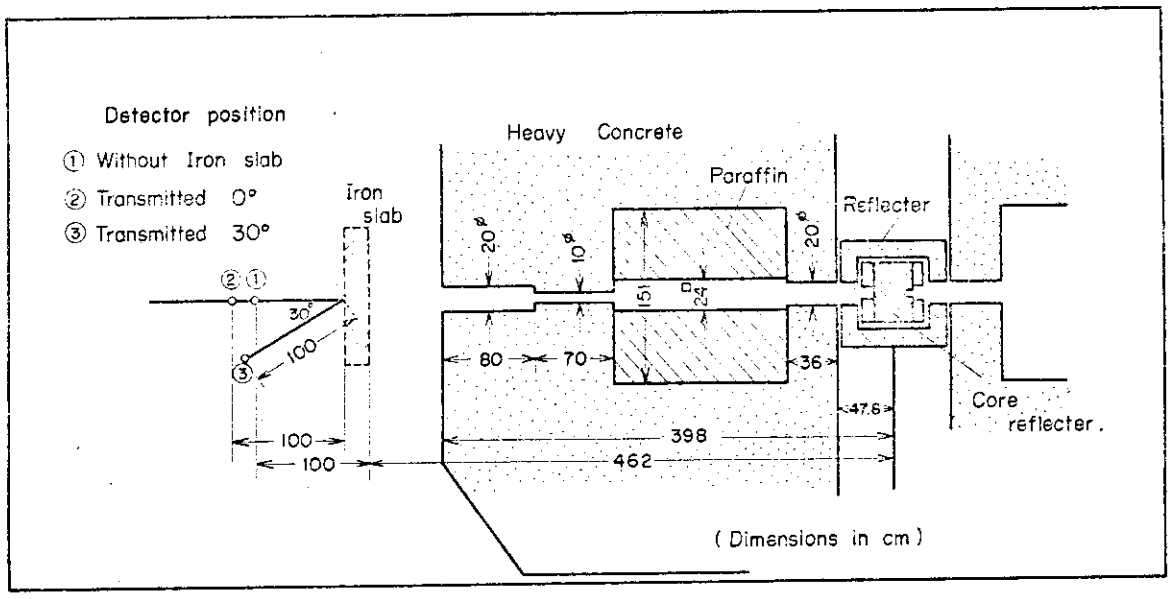

Fig. 4.2.1 Experimental arrangement for experiment 2

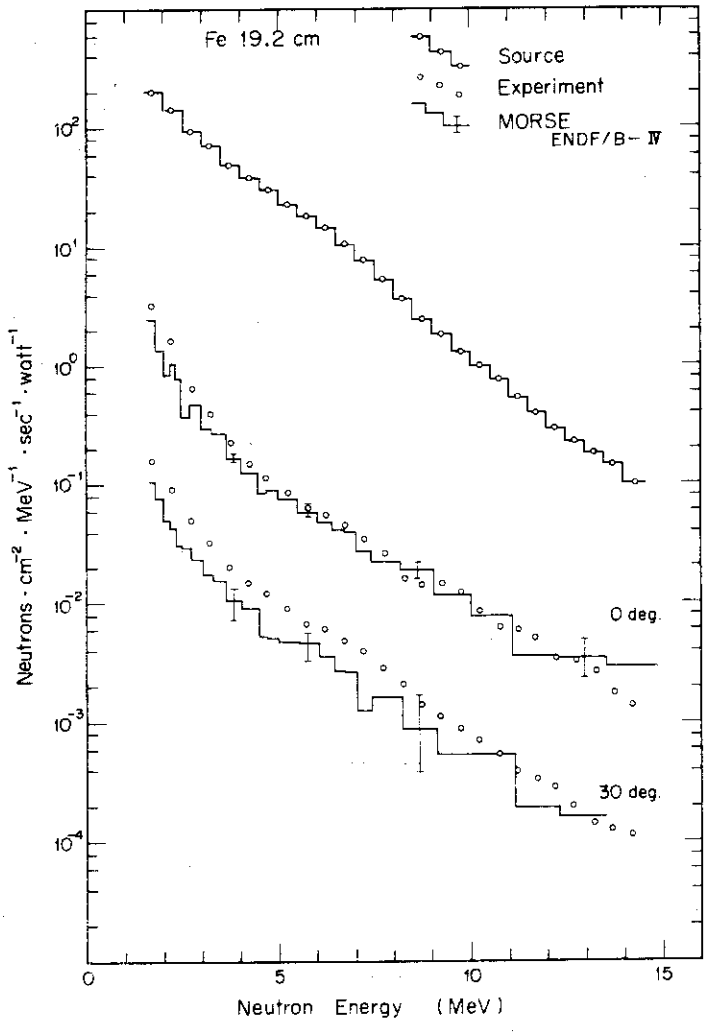

Fig. 4.2.2 Comparison of measured and calculated neutron energy spectra

4.3 Sensitivity and Uncertainty Analysis for Iron Cross Sections

S. Miyasaka, T. Minami*, H. Kuroi and J. Hirota

The present work is to investigate the following two items. The first is to estimate the uncertainties of the group cross sections of iron in the energy range above 1.5 MeV using the NE-213 spectra obtained from the YAYOI benchmark experiment[1] and the linear purturbation theory. The second is to survey how results of shield calculations are susceptible to value of level density parameter adopting the calculation of inelastic scattering energy transfer matrix.

For this work, a sensitivity analysis code, ROSETTA, has been written. The code system consists of (1) preparation of group cross sections by using SUPERTOG-V3,[2] (2) forward and adjoint transport calculations by ANISN,[3] (3) sensitivity analysis based on the linear purturbation theory and (4) calculation of uncertainties of the group cross sections from measured reaction rate.

The definition of the uncertainties of the group cross sections is as follows:

$$- \frac{\langle \phi_c^*(\bar{\xi}),\ \delta M \phi_c(\bar{\xi}) \rangle}{\langle \Sigma_D(\bar{\xi}) \phi_c(\bar{\xi}) \rangle} = \frac{\langle \Sigma_D(\bar{\xi}) \{ \phi_{EXP}(\bar{\xi}) \pm \Delta\phi_{EXP}(\bar{\xi}) \} \rangle}{\langle \Sigma_D(\bar{\xi}) \phi_c(\bar{\xi}) \rangle} - 1$$

where $\phi_c(\bar{\xi})$ and $\phi_c^*(\bar{\xi})$ are the result of a properly-performed transport forward and adjoint calculation, and the deviation;

---

* Fujitsu Limited

$\Delta\phi_C(\bar{\xi})$, caused by the uncertainties in the group cross sections; $\phi_{EXP}(\bar{\xi})$ and $\Delta\phi_{EXP}(\bar{\xi})$ are the measured spectrum and the error due to both counting statistics and unfolding uncertainties; δM is a change of the Boltzmann operator due to variation of cross section in the shield, and $\Sigma_D(\bar{\xi})$ is the response function of the counter which gives the angular flux response.

Fig. 4.3.1 presents the results of the uncertainty calculations for the elastic and inelastic cross sections of iron in the energy range above 1.5 MeV using the NE-213 spectra obtained from the YAYOI experiment. And Fig. 4.3.2 shows the comparison between the measured spectra and the recalculated ones using the elastic cross sections adjusted by the uncertainties shown in Fig. 4.3.1.

From the analysis of the YAYOI benchmark experiment, it is possible to estimate the uncertainties of group cross sections using the measured reaction rate with considerable accuracy, if the approximations in the forward and adjoint transport calculations represent correctly the experimental conditions. For assessing the uncertainty of the group cross sections using this method, it is necessary to accumlate a large number of results of well-defined benchmark experiments, and it is also necessary to check on unsuspected source of systematic error in a measurement by applying two or more independent techniques to the measurement.

It may be also necessary, in addition, to take the correlation between reaction cross sections into account. Further it may be important, especially for the inelastic scattering cross section, to take the correlation among cross section errors into account, because the shape of the inelastic scattering cross section may be to some extent defined theoretical-

ly.[4),5)]

Finally, from the analysis of 14 MeV neutron transmitted through the iron sphere,[6)] it was shown that the spectra calculated by different inelastic scattering models differ very markedly from each other above about 3 MeV, and that the sensitivity for group cross sections is closely related to the way of processing the basic cross sections.

Reference

1) Miyasaka, S., et al. : "Iron Shielding Benchmark Experiments at YAYOI," in the present report, 4.2 (1976).

2) Wright, R.Q., et al. : "Data Generator : Fine Group Constants and P_n Scattering Matrices from ENDF/B," ORNL-TM-2679 (1969).

3) Engle, W.W., et al. : "A User's Manual for ANISN, A One Dimensional Discrete Ordinates Transport Code with Anisotropic Scattering," K-1693 (1967).

4) Mitani, H., Kuroi, H. : J. Nucl. Sci. Technol., 7, 56 (1970).

5) Gandini, A., Petilli, M., Salvatores, M. : "Nuclear Data and Integral Measurement Correlation for Fast Reactors. Statistical Formulation and Analysis of Methods. The Consistent Approach," International Symposium on Physics of Fast Reactor. Vol, II, 612 (1973).

6) Hanse, L.H., et al. : Nucl. Sci. Eng., 51, 278 (1973).

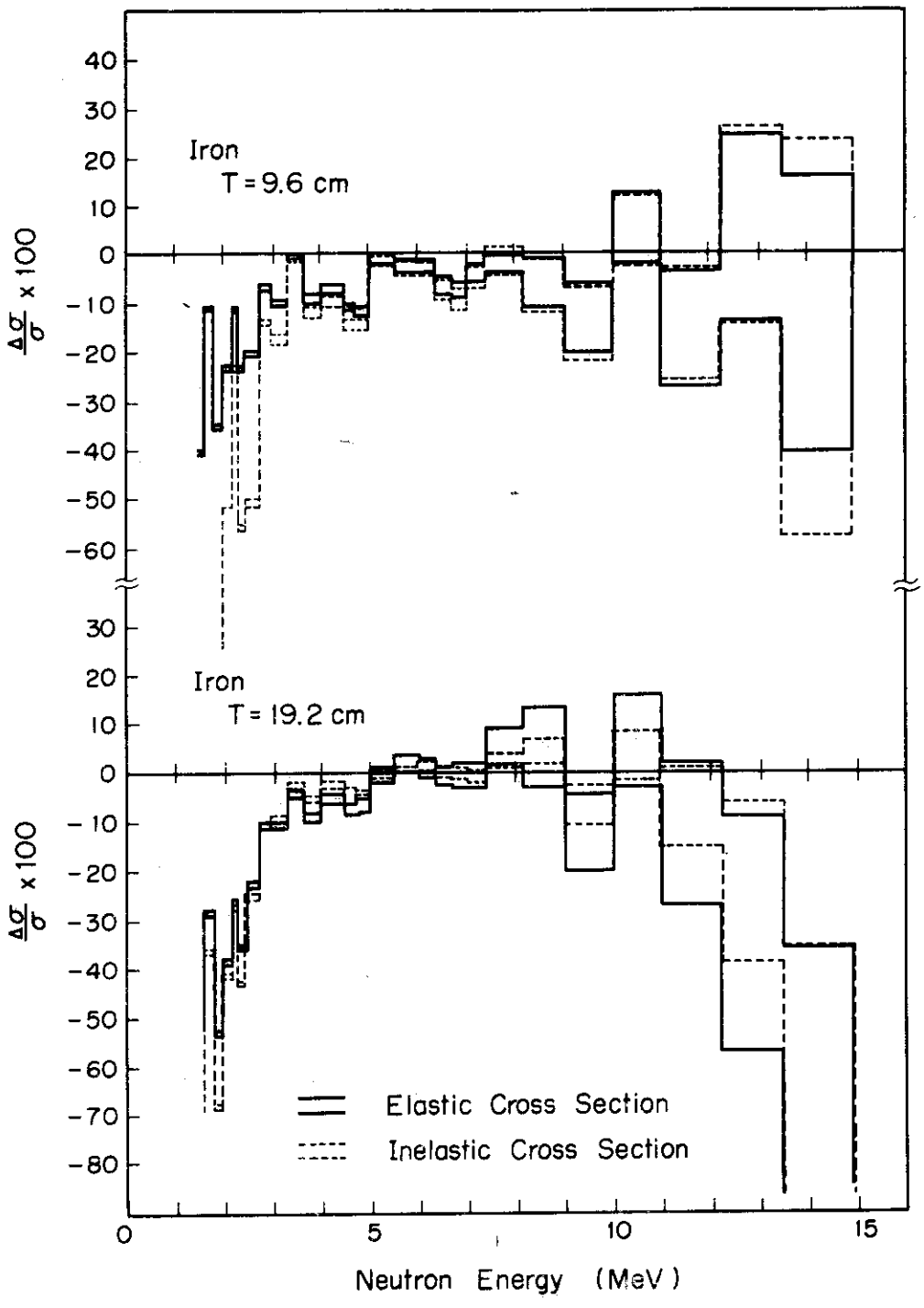

Fig. 4.3.1 Uncertainties for elastic and inelastic cross sections of iron in the energy range above 1.5 MeV

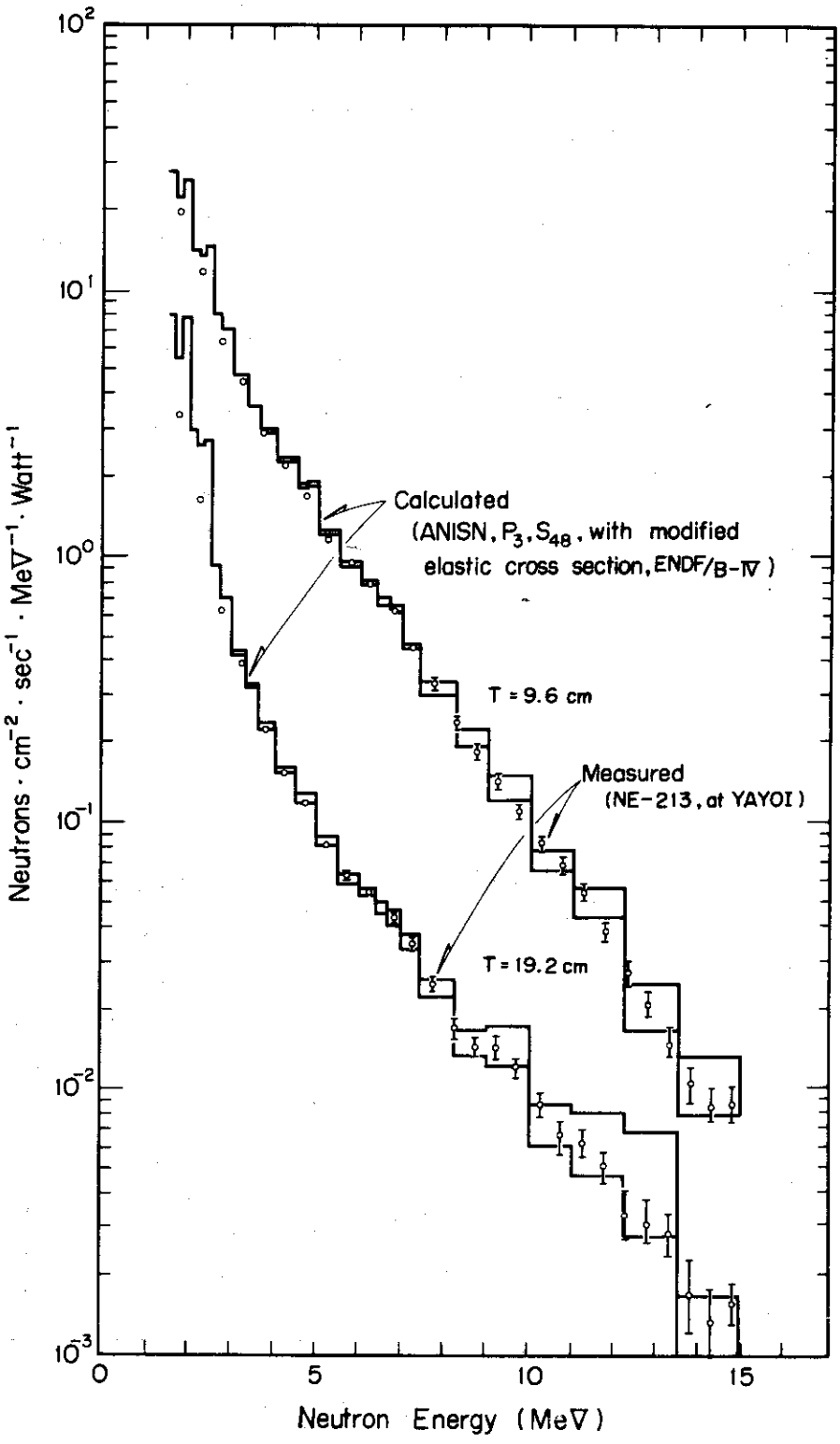

Fig. 4.3.2 Comparison between measured spectra and recalculated ones using the elastic cross sections adjusted by the uncertainties shown in Fig. 4.3.1

4.4 Development of a Computer Code System for Two-Dimensional Shielding Calculations

T. Asaoka, S. Miyasaka, T. Tsutsui and T. Fujimura

A computer code system has been developed for detailed shielding calculations with the help of two-dimensional S_N code, DOT-3,[1] to deal accurately with the transport and heating of neutrons and gamma rays in a fast reactor system. We have introduced the coarse-mesh rebalance option to DOT-3 for accelerating the convergence of iterative processes. This has resulted in the reduction of computation time by about 30 % compared to the original pointwise scaling option. In addition, the JAERI-FAST set[2),3)] is adopted for neutron group constants to have a close relation with the nuclear design calculation.

The flow diagram of the present code system is shown in Fig. 4.2.1. The JAERI-FAST 70 group cross sections are collapsed into, for example, 39-group constants by the use of the JFUSER program of the utility code system, J-FAST-70U.[4)] These 39-group cross sections are used for producing the secondary gamma-ray production constants and nuclear heating cross sections through the SPMOD program which has replaced the SUPERTOG-V3-JR and THERMOS-JR in the RADHEAT code system for radiation heating analyses.[5)] The ANISN code[6)] is adopted for one-dimensional transport calculations and for the cross section collapsing for two-dimensional analyses. For ANISN calculations, the thermal-group constants of JAERI-FAST set can be replaced by any values with the use of input cards as illustrated in Fig. 4.2.1. The form of the collapsed cross sections is then converted into the format for the DOT-3 (or for the

TWOTRAN-2[7]).

The present code system is tested through analyses of the ORNL benchmark experiment for neutron transport through sodium [8] and the shielding experiments performed on a zero power fast reactor in the MOZART project.[9] The results have shown that the S_4 approximation can be used for practical purposes with 4 – 5 collapsed neutron groups and 3 gamma-ray groups by using space-mesh intervals smaller than about one mean-free-path of radiations in media. It is shown also that the present system can be applied to the shielding calculations for a spent fuel container.

References

1) Mynatt, F.R., et al. : "The DOT-III Two-Dimensional Discrete Ordinates Transport Code," ORNL-TM-4280 (1973).

2) Katsuragi, S., et al. : "JAERI Fast Reactor Group Constants Systems, Part I," JAERI 1195 (1970).

3) Katsuragi, S., et al. : "JAERI Fast Reactor Group Constants Systems, Part II," JAERI 1199 (1970) & 1199 (Supplement) (1971).

4) Hasegawa, A., Katsuragi, S. : "An Utility Code System for JAERI-Fast 70-Group Set : J-FAST-70U," JAERI-M 5381 (1973) (in Japanese).

5) Miyasaka, S., et al. : "Code System for the Radiation-Heating Analysis of a Nuclear Reactor, RADHEAT," JAERI-M 5794 (1974) (in Japanese).

6) Engle, W.W., Jr. : "A User's Manual for ANISN, A One Dimensional Discrete Ordinates Transport Code with Anisotropic Scattering," K-1693 (1967).

7) Lathrop, K.D., Brinkley, F.W. : "TWOTRAN-II : An Interfaced, Exportable Version of the TWOTRAN Code for Two-Dimensional Transport," LA-4848-MS (1973).

8) Maerker, R.E., et al. : "The ORNL Benchmark Experiment for Neutron Transport in Thick Sodium," E-1, the Fourth International Conference on Reactor Shielding (1972).

9) Campbell, C.G., et al. : "The Scope of the MOZART Programme and the General Conclusions Drawn from It," International Symposium on Physics of Fast Reactors, Tokyo (1973).

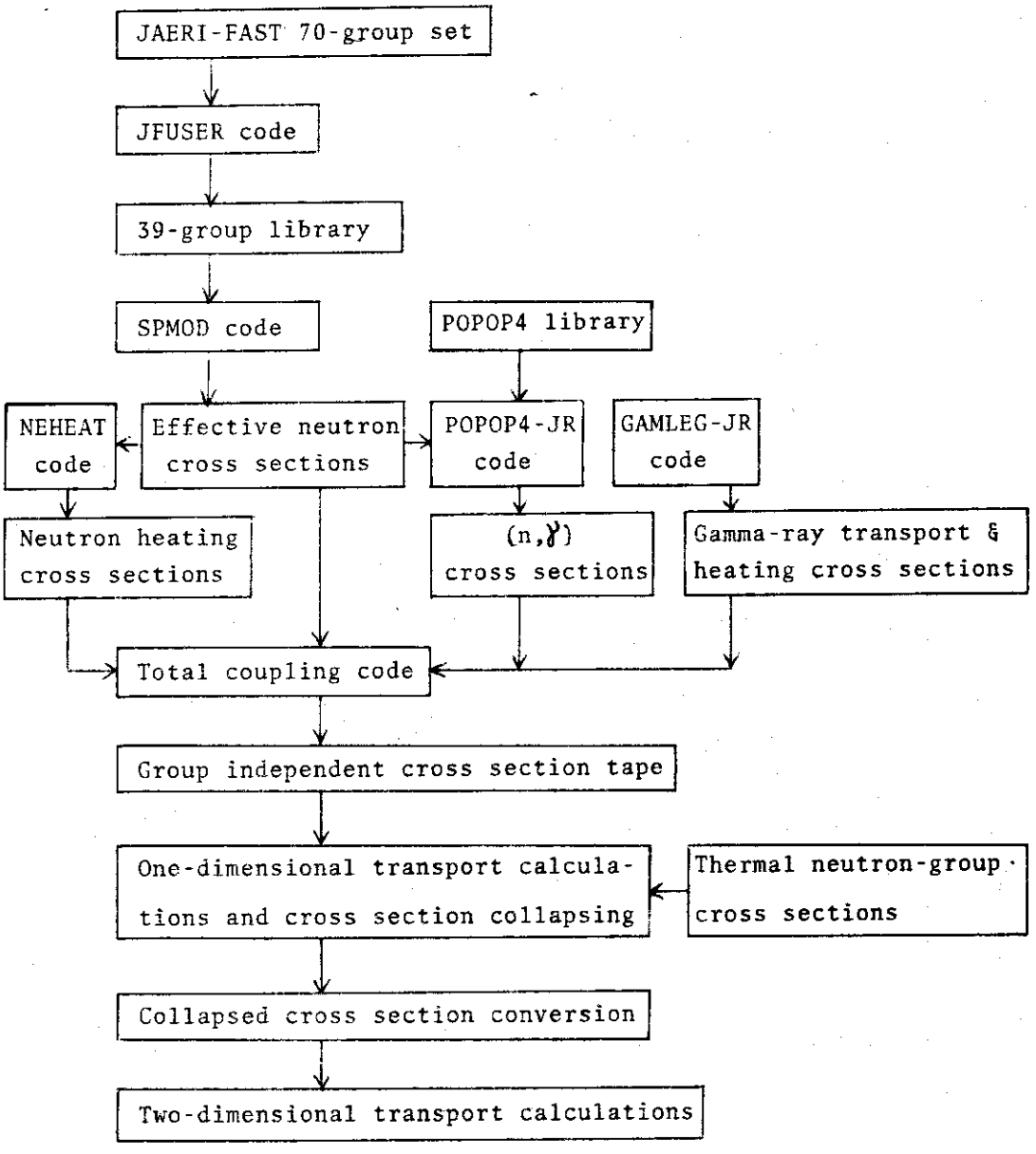

Fig. 4.4.1 Flow diagram of neutron and gamma-ray transport calculations

5. Heat Transfer and Fluid Dynamics

5.1 Heat Transfer Study of GCR Fuels by Using High-Temperature Helium Gas Loops

Y. Okamoto, K. Sanokawa, H. Shimomura, N. Akino, M. Hishida, M. Ouchi
S. Nekoya, H. Kawamura, M. Seki, K. Emori and Y. Shiina

In order to obtain a demonstration correlation curves on laminarization and transient instability under simulated reactor operating conditions of GCR reactor core, a mock-up fuel element has been constructed and tested by using high temperature helium gas loops (SGL and HTGL).[1] The loops provided a wide range of testing condition at high temperature and high pressure.

Fig. 5.1.1 shows the flow diagram of the small helium gas loop. A fuel test section is located in the outlet of compressor, which is connected to the pre-heater in series.

The laminarization condition of helium flow at the temperature of up to 1100 °C is planned to test by the loop SGL.

Fig. 5.1.2 shows the flow diagram of HTGL loop. The HTGL loop was selected to provide an installation for testing the thermal mock up fuel elements of VHTR under simulated reactor operating conditions of 42 kg/cm^2 and 1000 °C.

Helium gas of 900 °C is generated from the tantalum heater and flows into the fuel element test section.

The high-temperature fuel element test section is shown in Fig. 5.1.3. Tantalum heating rod was installed in a graphite channel and heated by electric heater. Helium gas flows downward from an upper nozzle into the test channel, and goes out to the lower nozzle at the temperature of 1000 °C. To avoid the heat loss from the high

temperature channel, seven-segmented compensation heaters ($MoSi_2$) were installed around the channel.

The simulated fuel element is used to derive the correlation equation of determining laminarization and transient critical heat flux at high-temperature and high-pressure simulated condition of GCR reactors.

Reference

1) H. Shimomura et. al., "Thermal and Hydraulic Performance of High Temperature Helium Gas Loop" ASME Paper 74-WA/HT-3 (1974).

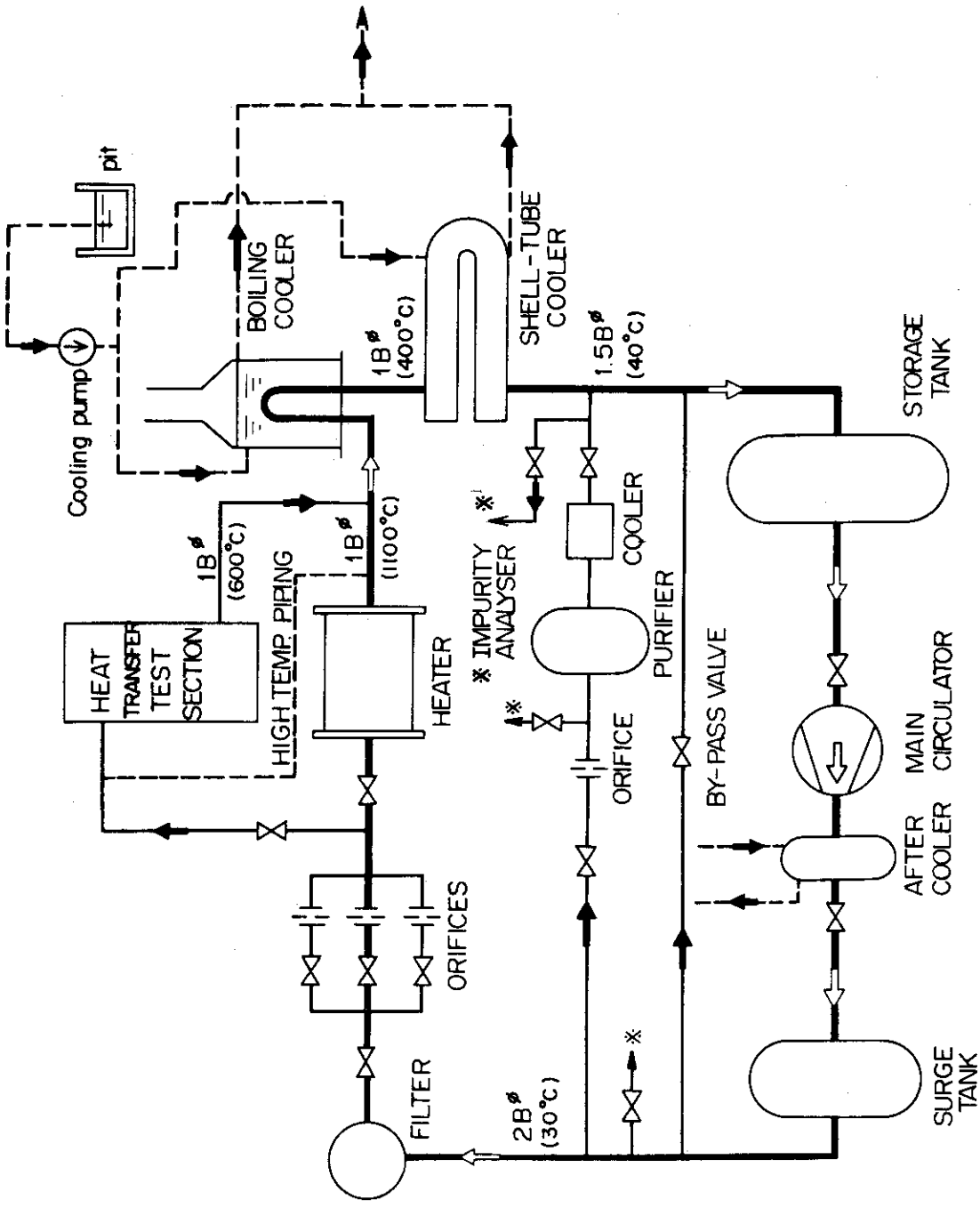

MAIN SPECIFICATION

fluid	Helium
pressure (kg/cm²)	2
temperature (C)	1100
flow rate (g/s)	10
heat input (KW)	150
purification	Ti bed

Fig. 5.1.1 Flow diagram of Small Helium Gas Loop (SGL)

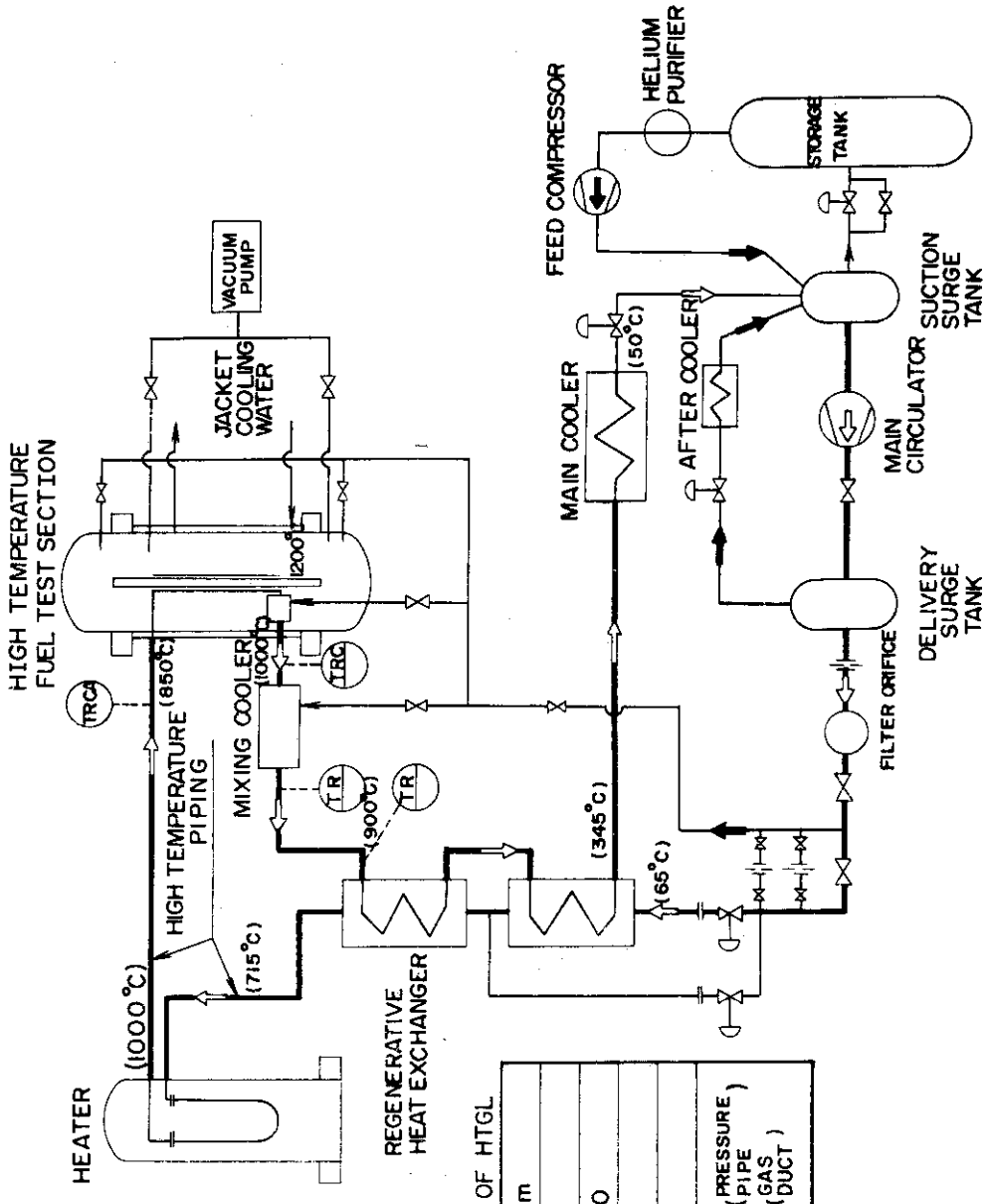

MAIN SPECIFICATION OF HTGL

fluid	Helium
pressure (kg/cm²)	40
temperature (℃)	1000
flow rate (g/s)	100
heater input (KW)	270
high temperature pipe diameter (cmφ)	21.6 (PRESSURE PIPE) 3.8 (GAS DUCT)

Fig. 5.1.2 Flow diagram of High Temperature Gas Loop (HTGL)

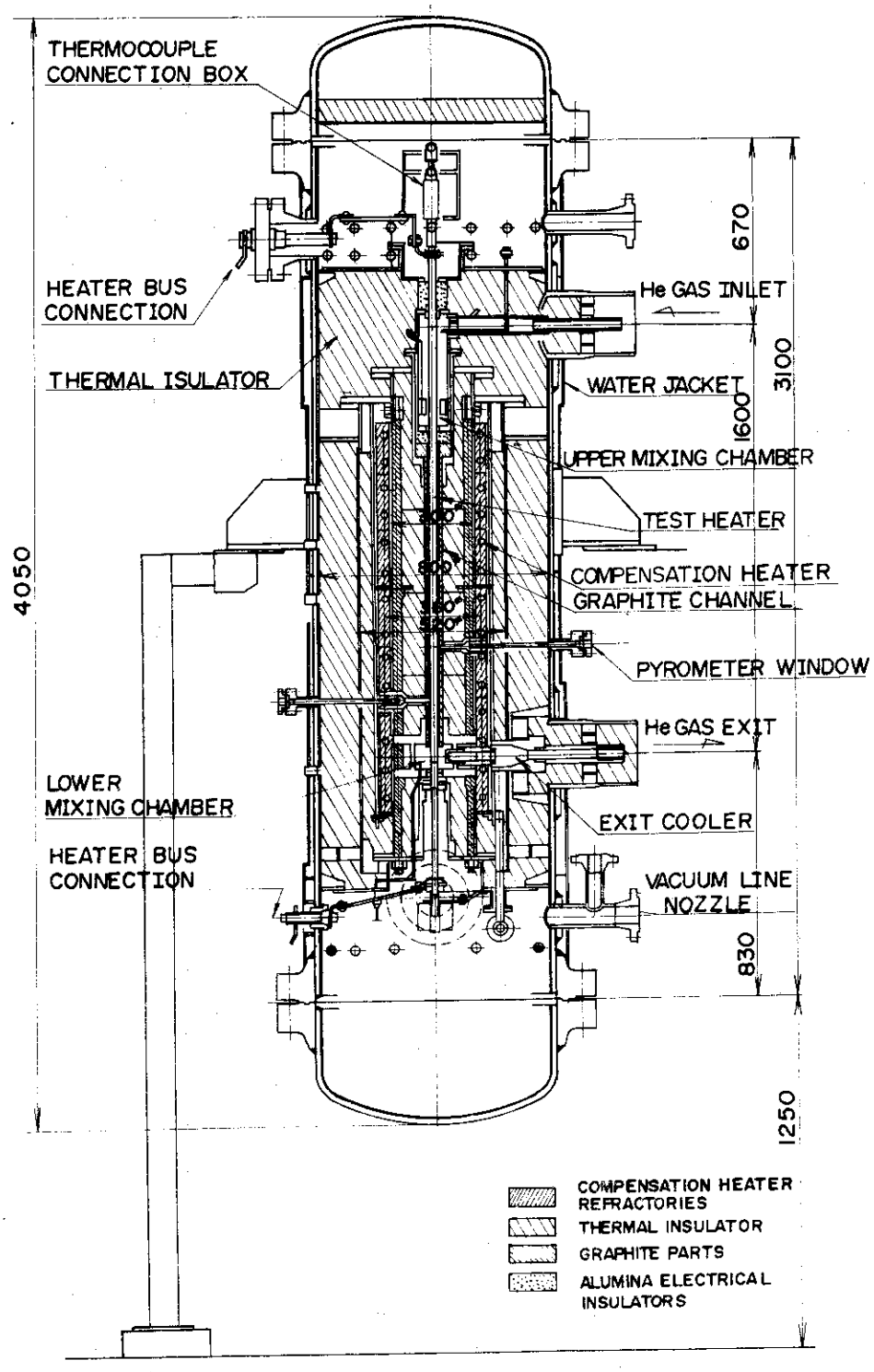

Fig. 5.1.3 High-temperature fuel element test section

5.2 Enhanced Heat Transfer of Roughened Surface at Low Reynolds Number

M. Hishida, Y. Shiina, J. Hanawa and Y. Okamoto

Heat transfer characteristics of turbulence promoters at low Reynolds number has been studied very little[1,2]. We studied the heat transfer and pressure drop characteristics of the parallel channel with wired promoters to improve the heat transfer of GCR fuel elements at low Reynolds number. The experiments were performed at Reynolds number of 500-4000[3].

To realize the heat transfer and fluids dynamics of the promoter surface, the vortex flow pattern behind the promoters was visualized by aluminum tracer method.

Figure 5.2.1 shows the relation between average Nusselt number and Reynolds number as a parameter of d/De (p/d=10). In case when Reynolds number is larger than 2000, Nusselt number of a-surface with promoters Nu_a is 2.7 to 3.8 times larger than that of smooth channel, and Nusselt number of another surface Nu_b is 1.7 to 2.3 times larger than that of smooth one.

In case when Reynolds number is smaller than 2000, Nu_a decreases steeply with decrease in Reynolds number and becomes smaller than Nu_b at $Re < 800$-1000. These values are less than the laminar Nusselt number of the smooth channel.

Figure 5.2.2 shows the relation between the friction factor and Reynolds number. Friction factor of our study shows 3 to 6 times larger than that of smooth channel.

Figure 5.2.3 shows the relation between the performance factor P and Reynolds number at both surface. The mountainous curves of the performance factor P_a at a-surface become maximum

at Reynolds number of about 3000. The maximum value of P_a is 1.8 to 2.3, and exceeds the value of 1 at $Re > 1500$.

These results show that the promoter surface is quite effective at transition region.

Figure 5.2.4 shows the streak-line flow pattern arround the one-side promoters at low Reynolds number The results show that unstable and separated vortices augument the heat transfer at Reynolds number of over 900, as shown in Fig. (b), (c), (d), while steady and stable vortices are creeping into downstream at $Re < 500$-600.

The unstable vortices change their pattern to be stable with decrease in Reynolds number. And, these stable vortices become a thermal barrier from the heated surface to the coolant flow. Then, heat transfer at a base surface becomes steeply smaller than that of the smooth channel at lower Reynolds number.

References

1) Nunner, W.: "Wärmeübergang und Druckabfall in Rauhen Rchren" VDI-Forschungsheft 455, 1956.

2) Sams, E. W.: "Experimental Investigation of Average Heat Transfer and Friction Coefficients for Air Flowing in Circular Tubes Having Square-thread-type Roughness" NACA RME 52 D 17, 1952.

3) Hishida, M., et al.: "Enhanced Heat Transfer of Fuel at Low Reynolds number" Europian Nuclear Conference, Paris 1975.

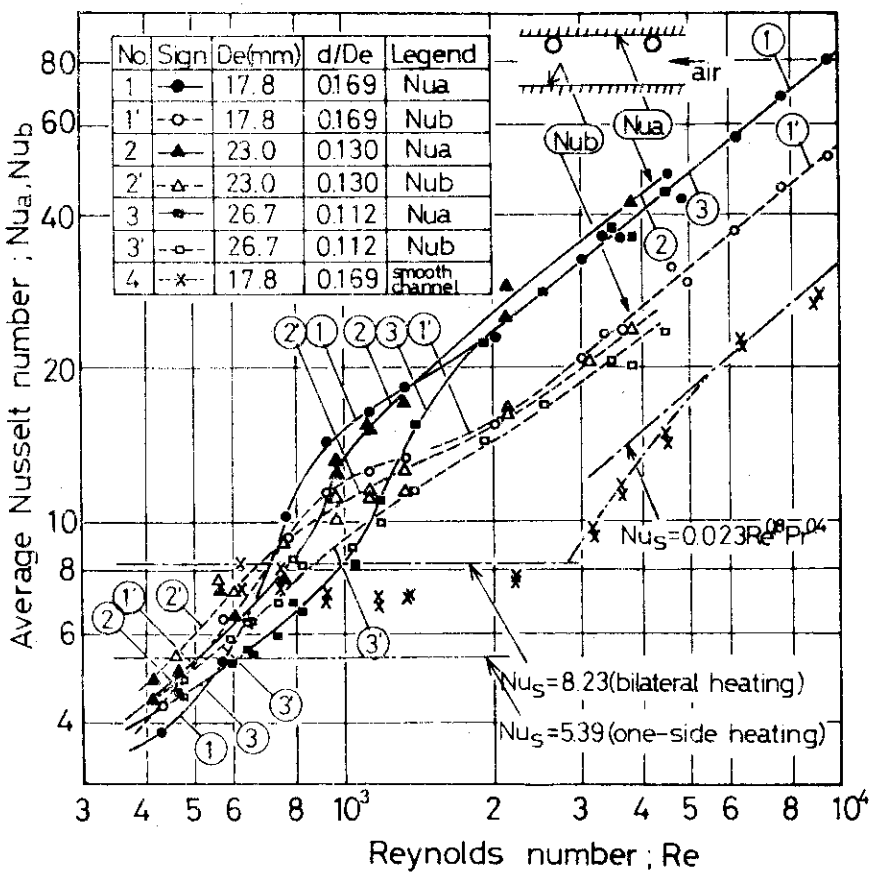

Fig.5.2.1 The relation between the average Nusselt number and Reynolds number (p/d = 10)

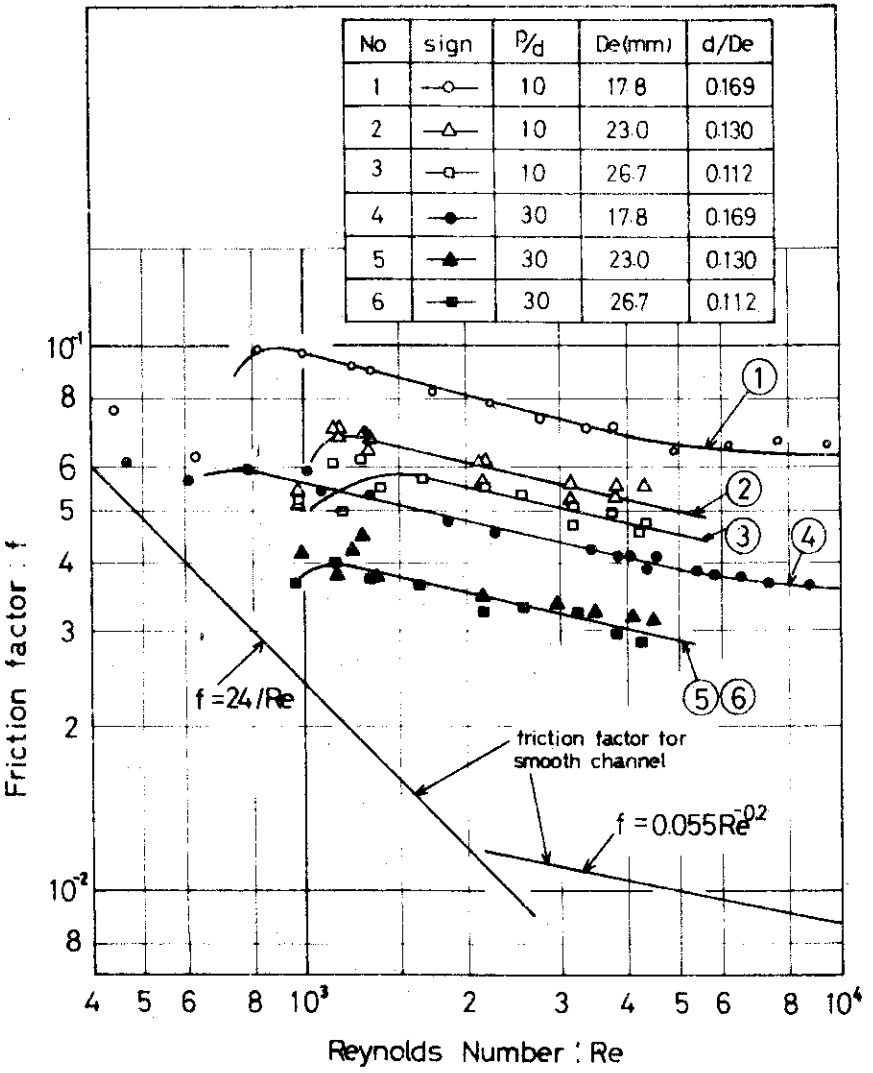

Fig.5.2.2 The relation between the friction factor and Reynolds number

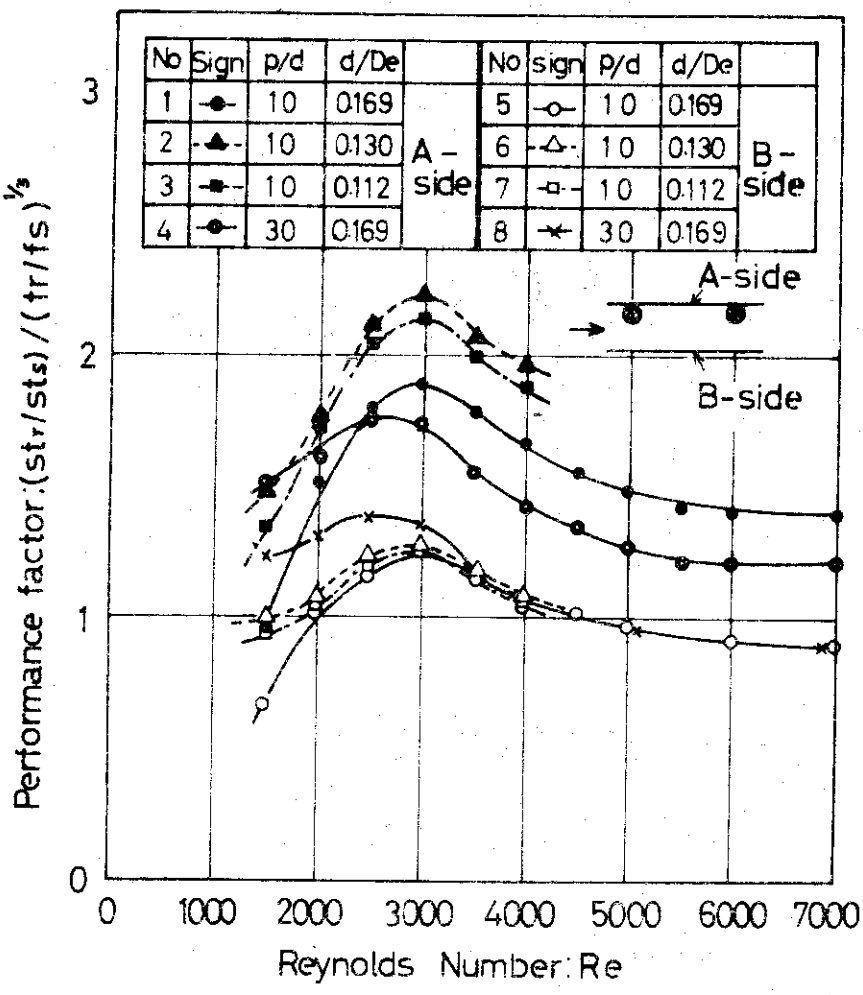

Fig.5.2.3 The relation between the performance factor $(St_r/St_s) / (f_r/f_s)^{1/3}$ and Reynolds number

(a) Re = 500

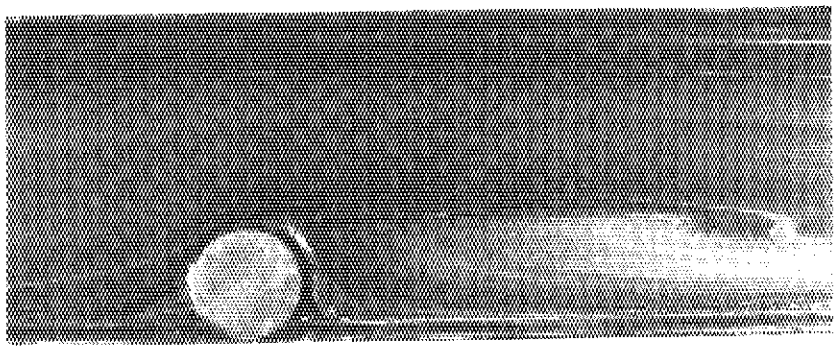

(b) Re = 880

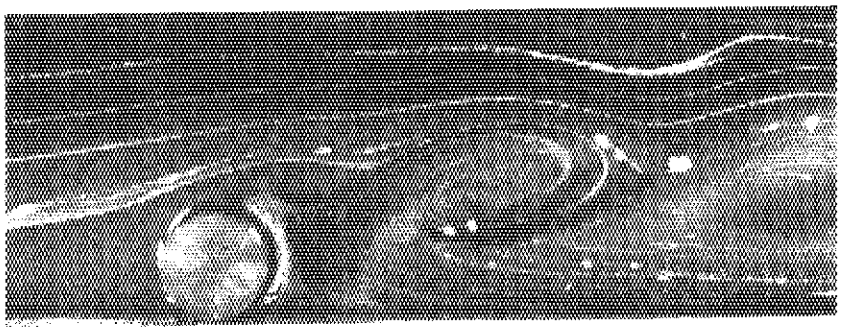

(c) Re = 1500

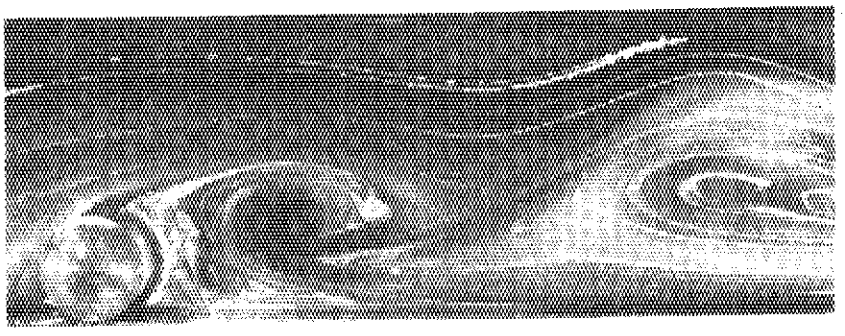

(d) Re = 3600

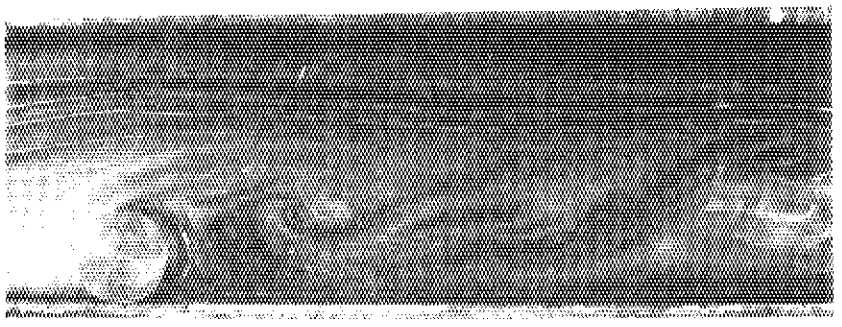

Fig. 5.2.4 Flow pattern arround the promoters (p/d=10)

5.3 Temperature Distribution and Thermal Stress of GCFR Roughened Fuel Elements

M.Hishida, Y.Okamoto, K.Miya*, M.Hashimoto* and S.An*

Generalized solution of the temperature and thermal stress of the roughened surface in case of GCFR fuel can has been studied very little [1]. The steady/unsteady equations of heat conduction and stress [2] were solved numerically by using the finite element method in several spscified cases.

Steady state temperature and thermal stress distributions in the fuel can with transverse rectangular ribs were obtained. Transient temperature and stress in case of sudden change of heat flux were also studied.

Figure 5.3.1 shows the calculated temperature and thermal stress distribution in the GCFR fuel can.

Figure 5.3.2 shows the transient distribution of temperature and stress at points where the tensile and compressive stresses become maximum.

The results were summarized in the followings,

(1) The temperature in the rib is considerably smaller than the temperature in the can tube, because the average heat transfer coefficient at the rib surface is several times greater than that of the can surface.

(2) The tangential stress becomes maximum at the front tip of the rib, while the surface temperature becomes minimum at the point. The outside surface temperature becomes maximum at the point of 1.5e downstream from the rib.(e; rib height)

---

* Tokyo University

The compressive stress becomes maximum at the point of inside surface, corresponds to the center of the two ribes.

(3) The maximum values of the temperature and stress at the outside and inside surface in case of the uniform h distribution becomes smaller than those of non-uniform h distribution [3]. These results show the necessity of the local heat transfer coefficients on the rib surface to analyse the detail behaviour in the thermal stress of the fuel can.

(4) The axial and radial thermal stress are practically smaller than the tangential stress.

(5) The stepwise transient calculation shows that the time constant becomes less than 1 sec. The time dependent change is so rapid.

References

1) Barnett,P.G.:"The Influence of Wall Thickness, Thermal Conductivity and Method of Heat Input on the Heat Transfer Performance of Some Ribbed Surface." Int. J. Heat and Mass Transfer, Vol. 15, p.p. 1159-1169 (1972)

2) Miya.K., Hashimoto,M. and Ando,A.:"Application of Finite Element Method to Transient Thermal Contact Problem of Fuel Element and Experimrnts in Fast Neutron Source Reactor" 3rd Int. Conf. on SMiRT (1975)

3) Williams,F. and Watts,J.:"The Development of Rough Surfaces with Improved Heat Transfer Performance and a Study of the Mechanics Involved." Heat Transfer 1970, Vol.II, F.C. (1970)

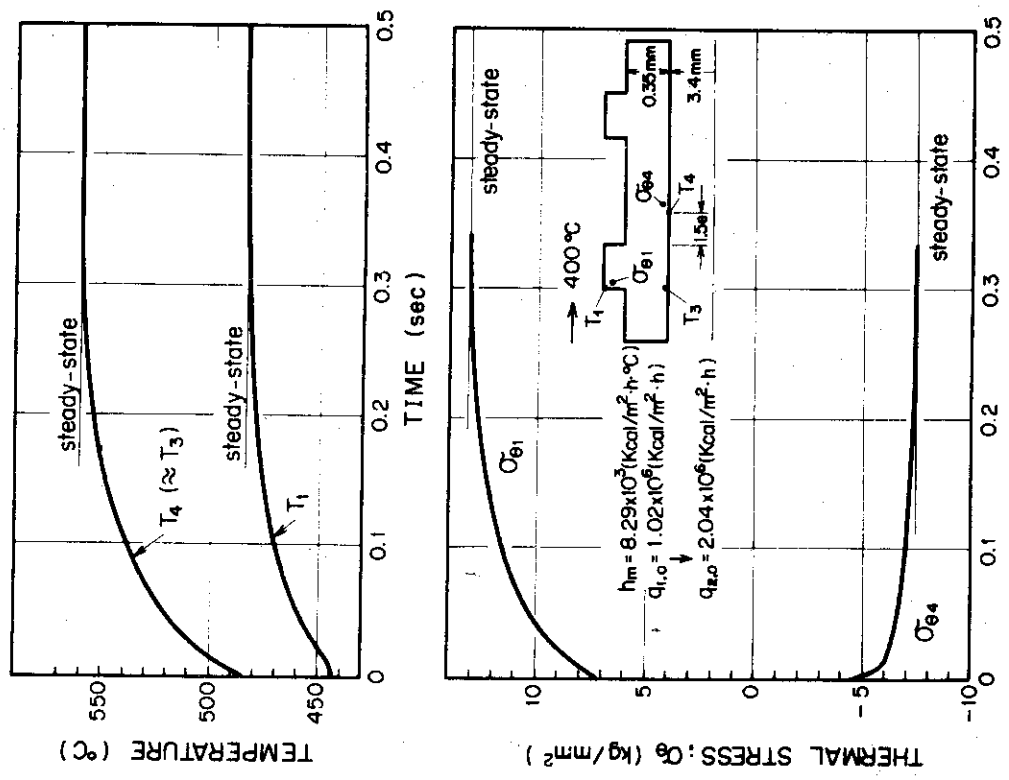

Fig.5.3.2 TRANGIENT TEMPERATURE AND THERMAL STRESS OF THE CAN OF GCFR FUEL ELEMENTS

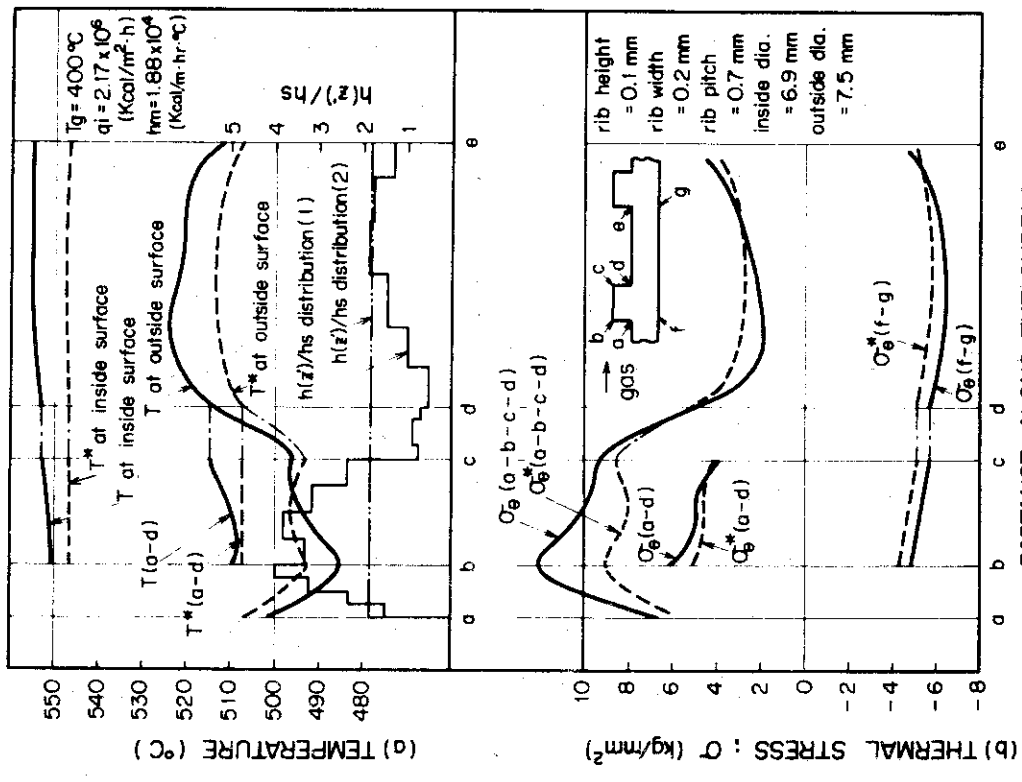

Fig.5.3.1 TEMPERATURE AND THERMAL STRESS DISTRIBUTION IN THE CAN OF GCFR FUEL.(T,σ…calculated result with h(z')/hs distribution(1), T*,σ*…calculated result with h(z')/hs distribution(2))

5.4 Heat Transfer and Fluid Dynamics of Annular Duct at Transient Flow

M. Hishida, Y. Shiina, M. Ouchi, K. Emori, Y. Okamoto and N. Akino

In order to analyse the time-dependent behavior of heat transfer and fluid dynamics in a transient regime from turbulent to laminar flow, an experimental work of an annular duct has been examined by using an atomospheric open circuits testing rigs. The annualr duct consists of Ni-Cr steel alloy, 43 mm in outer diameter, and 32 mm in inner diameter and 1200 mm in length. Nu, f, and temperature fluctuation ratio τ was measured by using an electric heater, thermocouples and pressure taps.

The result are shown in Figure 5.4.1, where the τ is represented by

$$\tau = \frac{(T_{gmax} - T_{gmin})_{out}}{(T_w - \overline{T}_g)_{out}} \qquad (1)$$

Transient region of Nu, f is located in Re = 2000 $\sim$ 6000. In this transient regime, temperature of gas is fluctuated for time duration. Heater wall temperature is constant. The fact shows that heat transfer coefficient is fluctuating between laminar and turbulent values at the frequency of about 3 $\sim$ 5 Hz. This causes severe thermal cycle at GCR outlet core structure. To avoid this instability in transient regime, an orifice plate was installed at the inlet of the channel. The fluctuation ratio τ becomes extremely smaller, because the free flow becomes turbulent by pro-turbulence effect of the orifice.

Lastly, it is concluded that the pro-turbulence and self-turbulence promoters are quite useful to avoid hydraulic problems on the transient regime in the free flow, such as temperature fluctuation and instability.

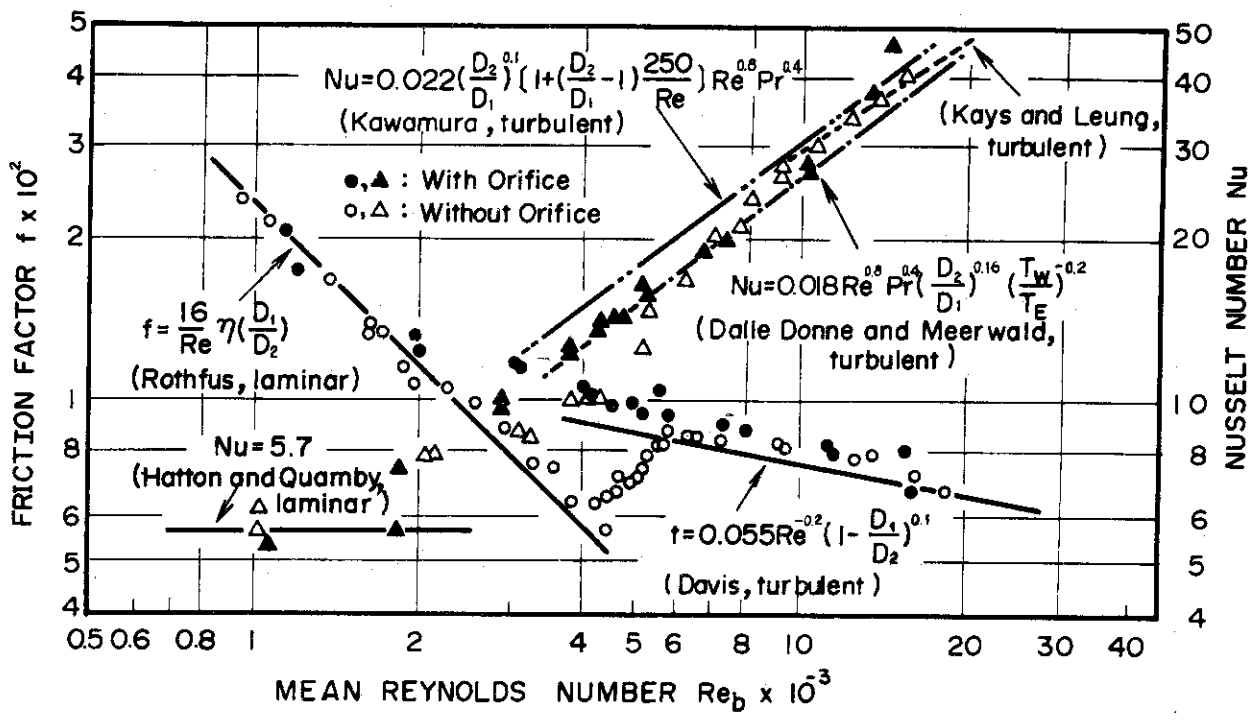

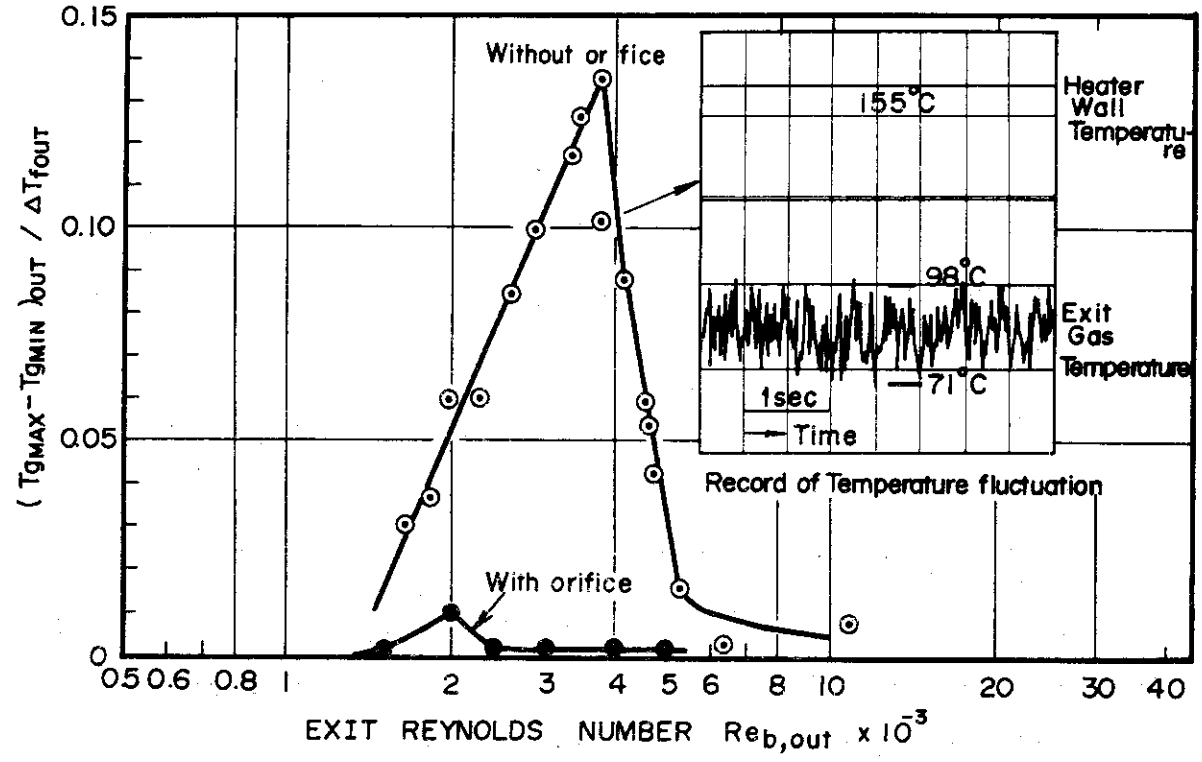

Fig 5.4.1 $Re_b \sim Nu, f, \Delta\bar{T}g/\Delta Tf$

5.5 Enhanced Heat Transfer by Roughened Surface for Free Stream Turbulence

M. Hishida, Y. Shiina, Y. Okamoto and N. Akino

Experimental data are presented for enhanced heat transfer by wired promoters for various rates of free stream acceleration. In case of free stream acceleration dimensionless acceleration parameter K is disignated by[1]

$$K = \frac{\nu}{v^2}\frac{dv}{dx} \tag{1}$$

Free stream acceleration can be regulated by a rectangular duct the height of which is continuously varied and decreasing along the flow direction. Fig. 5.5.1 shows the diagram of two-dimensional convergent channel.

The test channel consists of a rectangular duct, the lower wall of which is heated for heat transfer measurement and the upper wall of which is designed to provide any desired acceleration rate by regulating the value of convergent ratio.

The rectangular testing channel consists of acrylic walls, 600 mm in length and 100 mm in width. The lower heating surface consists of a stainless foil, as already described in 3.2.

Flow acceleration was obtained by three tapered and convergent channels, 147 mm and 300 mm in length, as shown in Exp 1, 2, 3, of the Fig. 5.5.1. The surface temperature distribution along the flow was measured by 79 alumel-chromel thermocouples.

Those test sections were connected into the atomospheric wind tunnel.

Reynolds number Re is denoted by

$$Re = \frac{2vH}{\nu} \tag{2}$$

where H is channel height.

In case of the convergent channel

$$vH = \text{const} \tag{3}$$

and then, Reynolds number becomes constant with accelerated flow.

Fig. 5.5.2 shows the results of heat transfer data for free stream acceleration.

In case of acceleration without promoters, as shown in Fig. 5.5.2, the heat transfer coefficient is constant along the flow and does not affected by acceleration, but the Nusselt number Nu was continuously decreasing at given value of K. The result shows that the Nu is gradually approaching to the asymptotic value along the duct.

Fig. 5.5.3 shows the relation between Reynolds number and Nusselt number ratio Nu/Nu_s with x/H value as a parameter. In case of no promoter surface, the greater Re is, the smaller Nu/Nu_s becomes, and, Nu/Nu_s becomes constant at Re > 7000.

In case of the promoter surface, the greater x/H is, the more steep increasing the Nu/Nu_s is. In this case, the Nu/Nu_s becomes constant from the two-pitch position after the starting promoter.

Heat transfer correlation of the heat transfer surface with the promoter was analysed systematically.

Fig. 5.5.4 shows the relation between $Re_{x'}$ and Nu/Nu_s with the K as a parameter. Where, Re_x is represented by

$$Re_{x'} = \int_0^{x'} \frac{v}{\nu} \, dx' \tag{4}$$

The promoter surface was quite useful to avoid the heat

transfer deterioration by flow laminarization at the value of $K = 10^{-4}$.

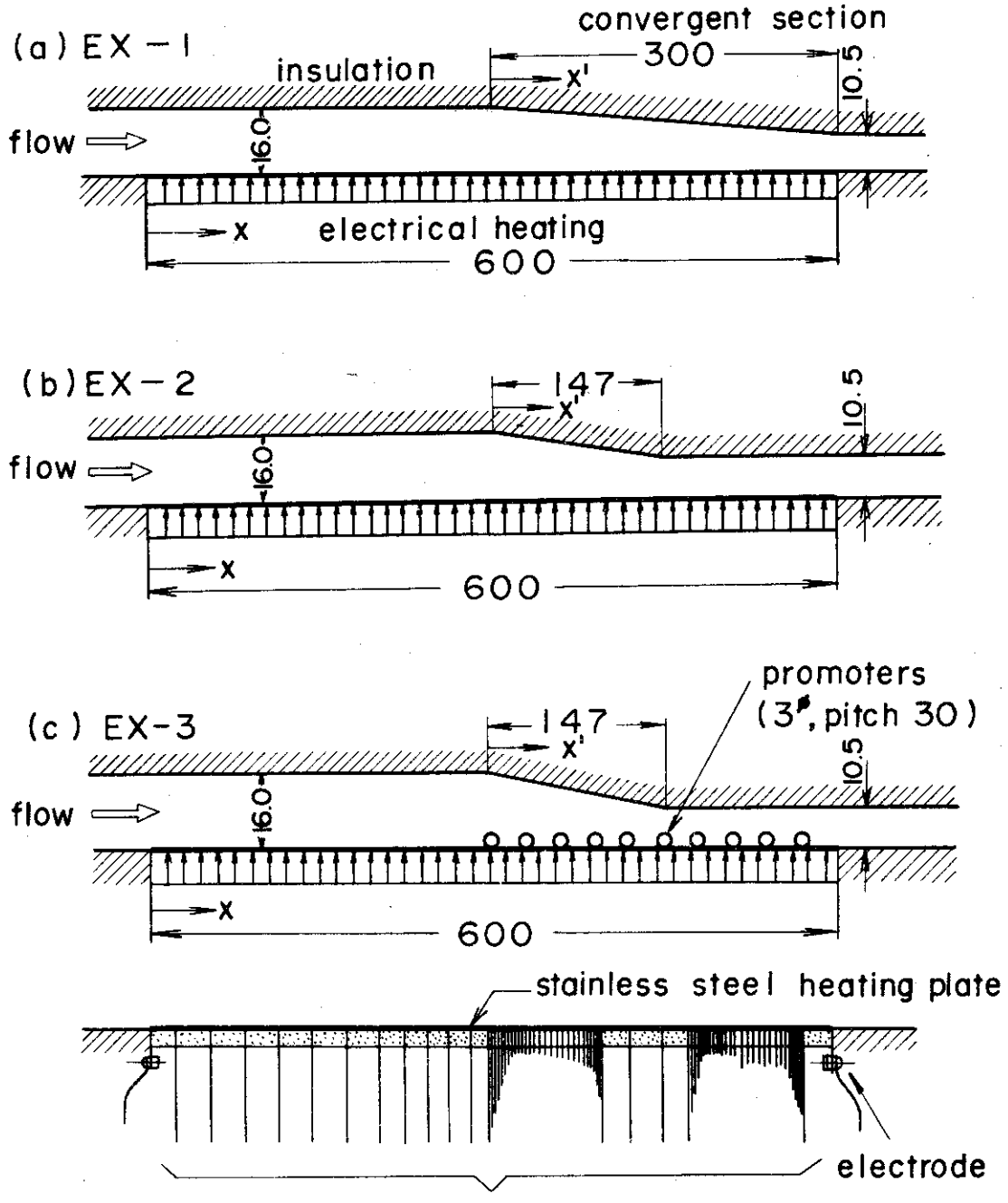

Fig.5.5.1 Diagram of two-dimensional convergent channel for free stream acceleration.

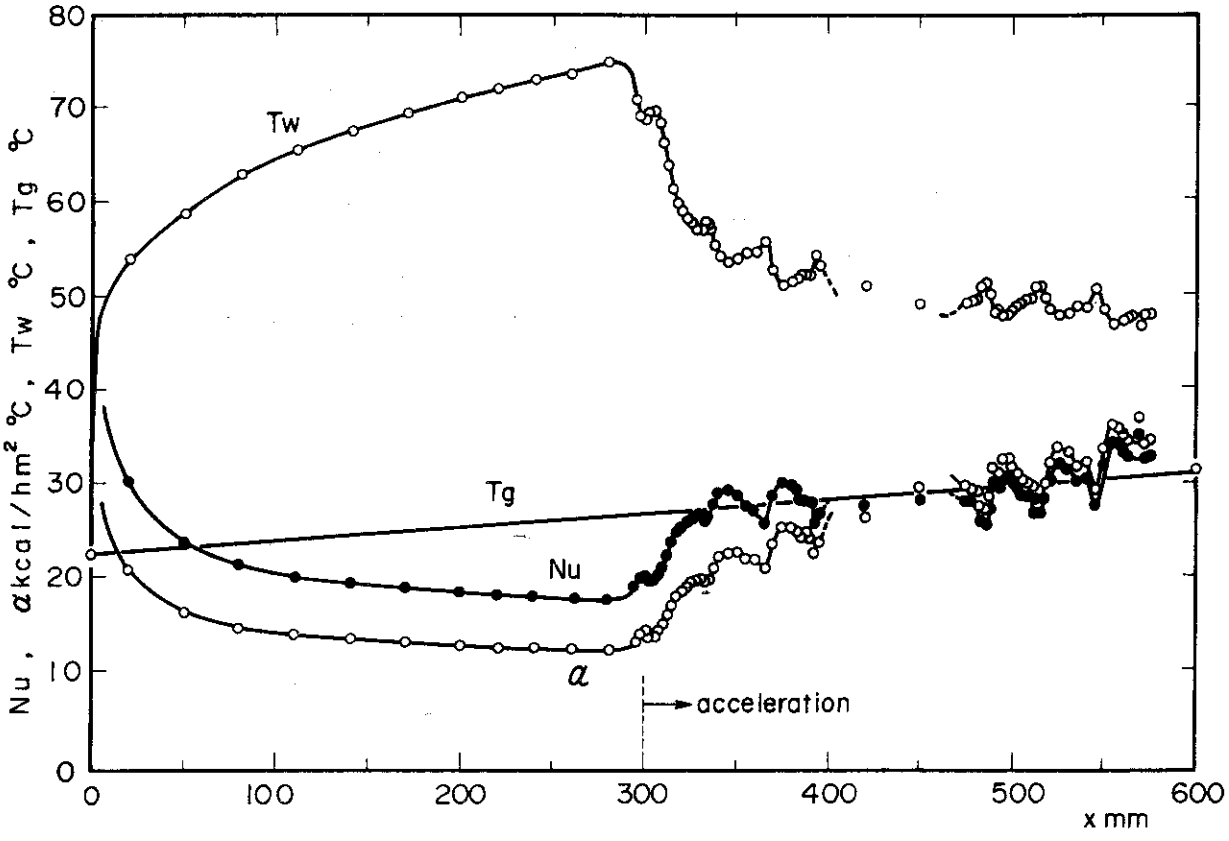

Fig. 5.5.2 Free stream acceleration with promoters
(EX－3 , Re = 5080 , K = 14.7 x 10^{-6})

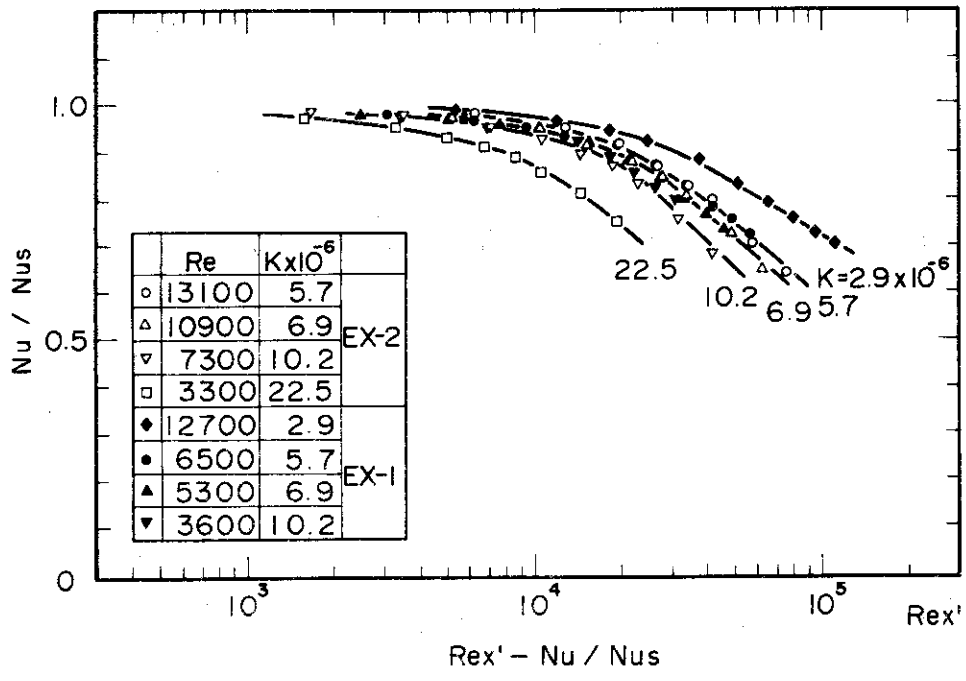

Fig. 5.5.4 Heat transfer correlation without promoters.

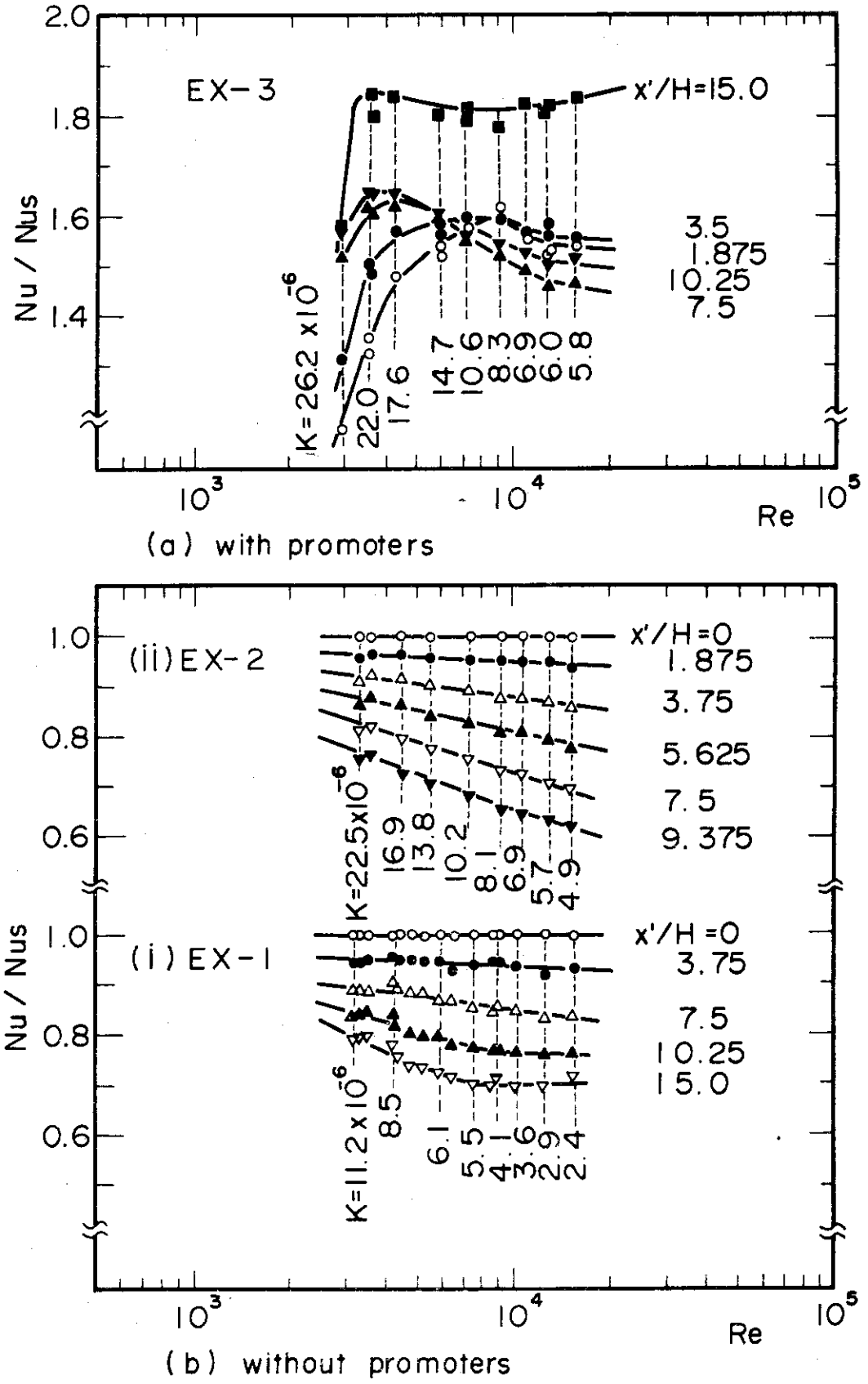

Fig. 5.5.3 Nu/Nus – Re as a parameter of x'/H

6. Reactor and Nuclear Instrumentation

6.1 Fast-Response Nuclear Instrumentation for Pulse Reactors

N. Wakayama, T. Iida and H. Yamagishi

Developmental studies of fast response nuclear power monitoring system was continued for power transient measurement of pulse reactor NSRR (maximum peak power: 23Gw, minimum reactor period: 1.1msec) and JLB (Linac booster, under planning).

Development of a Linear Power Channel having response of 2μsec rise time was completed and, as next stage of studies, the efforts to reduce response time of Log-N amplifier were made.

As results of these studies, three types of fast response logarithmic amplification methods were developed.

Although improvement of response of conventional type Log-N amplifier was limited by the instability of the whole system including chamber and input cable capacitance, in new type Log-N amplifiers, response time of several hundred microsecond were obtained at 10^{-9}A even the same operational amplifier had been used.

Table 6.1.1 shows response of new Log-N amplifiers of type-A, type-B and type-C connected with a chamber and a chamber cable of 40m. No overshoot and/or instability were observed in any input current region in these amplifiers.

The response characteristics of conventional type Log-N amplifier using the same operational amplifier are also shown in Table 6.1.1 for comparison with new type ones.

Fig. 6.1.1 shows the response characteristics of Log-N amplifiers of type-A, type-B, type-C and conventional one as a function of input current.

Fast period amplifiers having measuring ranges of 0.1msec, 0.3msec,

1 msec,----- and 1 sec for full scale were also made and connected with new Log-N amplifiers.

In order to test the overall performance of fast Log-N-Period channels, a exponential current generator was made. The generator can generate exponentially increasing and decreasing current signal from 10^{-11}A to 10^{-3}A con continuously and period of the signal is adjustable in the range between 100 μsec and 100sec.

In the Log-N-Period channels, overshoot of period indication may be appear at low current region because of change of time constant of Log-N amplifiers as shown in Fig. 6.1.2 even both Log-N amplifier and period amplifier have no overshoot characteristics. However overshoot of period indication can be eliminated by means of adjusting of initial current of Log-N amplifier to cerain value depending on the period of input signal.

Fig. 6.1.3 shows initial current suitable for reactor period measurement as a function of input-signal period for type-A Log-N-Period channel.

The NSRR will be in operation at beginning of next year and it is expected that very rapid reactor period will be measured accurately as a function of time with the fast Log-N-Period channels and reactor power with the Fast Linear channels developed.

Types of LogN Amplifiers	Response Time							
	10^{-10} A	10^{-9} A	10^{-8} A	10^{-7} A	10^{-6} A	10^{-5} A	10^{-4} A	10^{-3} A
Type A	7.8 ms	780 μs	78 μs	15 μs	15 μs	15 μs	15 μs	15 μs
Type B	2.8 ms	300 μs	120 μs	80 μs	60 μs	15 μs	3 μs	3 μs
Type C	800 μs	200 μs	180 μs	180 μs	180 μs	15 μs	8 μs	3 μs
Conventional (Critical Damping)	900 ms	90 ms	9 ms	900 μs	90 μs	9 μs	3 μs	3 μs
Conventional (Under Damping)	27 ms	2.7 ms	270 μs	Overshoot	Ringing	Ringing	Oscillation	Oscillation

Table 6.1.1 Response of new-type Log-N amplifiers connected with a chamber and chamber cable of 40m

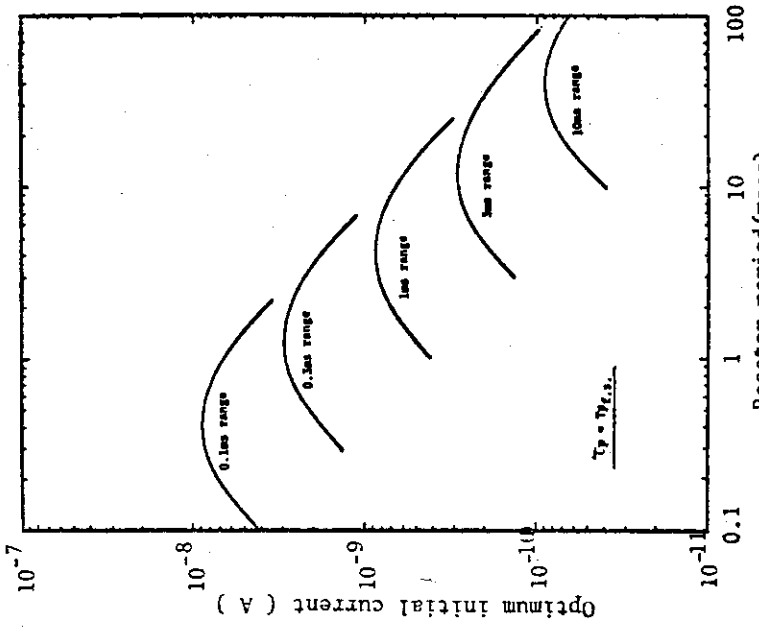

Fig. 6.1.3 Optimum initial current of Log-N-Period channel type-A connecting with a chamber and input cable of 40m

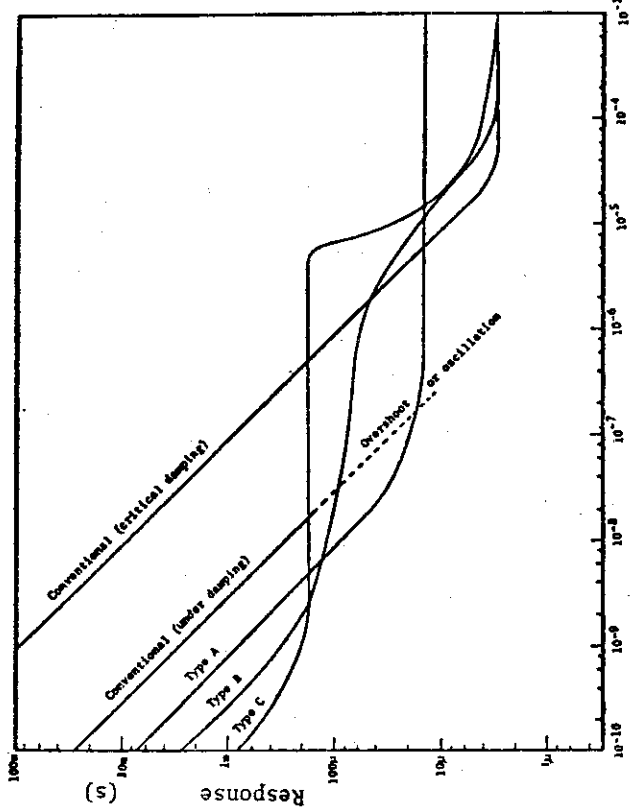

Fig. 6.1.1 Response characteristics of new-type Log-N amplifiers as a function of input current

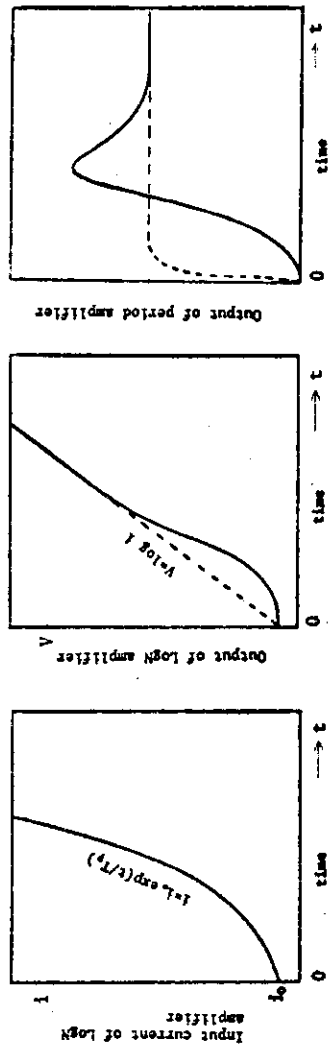

Fig. 6.1.2 Period overshoot caused by delay of response of Log-N amplifier

6.2 High-Temperature Neutron Detector Development

N. Wakayama, T. Tomoda*, H. Yamagishi and H. Gotoh

In this field of work, neutron detectors which can be used in high temperature environment such as inside of reactor vessel of the HTGR's and FBR's are being developed satisfactorily.

Fission counter-chambers named FX-2 which had been designed last year were manufactured on an experimental basis and performance test of these fission counter-chambers has been finished successfully.

FX-2's were tested in ambient temperature range up to 640°C (1184°F) and worked stably in all temperature range tested.

Almost all operating characteristics necessary as a sencer of neutron flux monitoring system for reactor control have been measured minutely.

General characteristics of the fission counter-chamber FX-2 are shown in Table 6.2.1.

Good agreement was obtained between designed characteristics and measured ones as shown in the table.

As an example of the characteristics of FX-2, the effect of ambient temperature on integral bias curve is shown in Fig. 6.2.1.

Since FX-2 has double electrically shielding screens (an outer pressure vessel and electrically insulated inner vessel) and is fitted up with mineral insulated triaxial cables, the sensitivity of electric interference is very low and good signal to noise ratio was easily obtained at the characteristics measurements.

Neutron and γ-ray irradiation test of FX-2 at 600°C will be initiated in May, 1975 in a material testing reactor JMTR.**

Design of heat-resisting C.I.C. and high-sensitivity fission counter

have been finished and manufacturing of these detectors will be completed by end of next year.

Effort to improve on manufacturing technics for these detector production was also continued.

---

* Central Laboratory of Mitsubishi Electric Corporation

** A FX-2 was irradiated 1.7×10^{18}nvt of neutrons and 1.5×10^{10}R of γ-ray at 600 ~ 620°C in JMTR core up to end of June, 1975 and no trouble was occurred in this period. Further irradiation is continued until end of 1975.

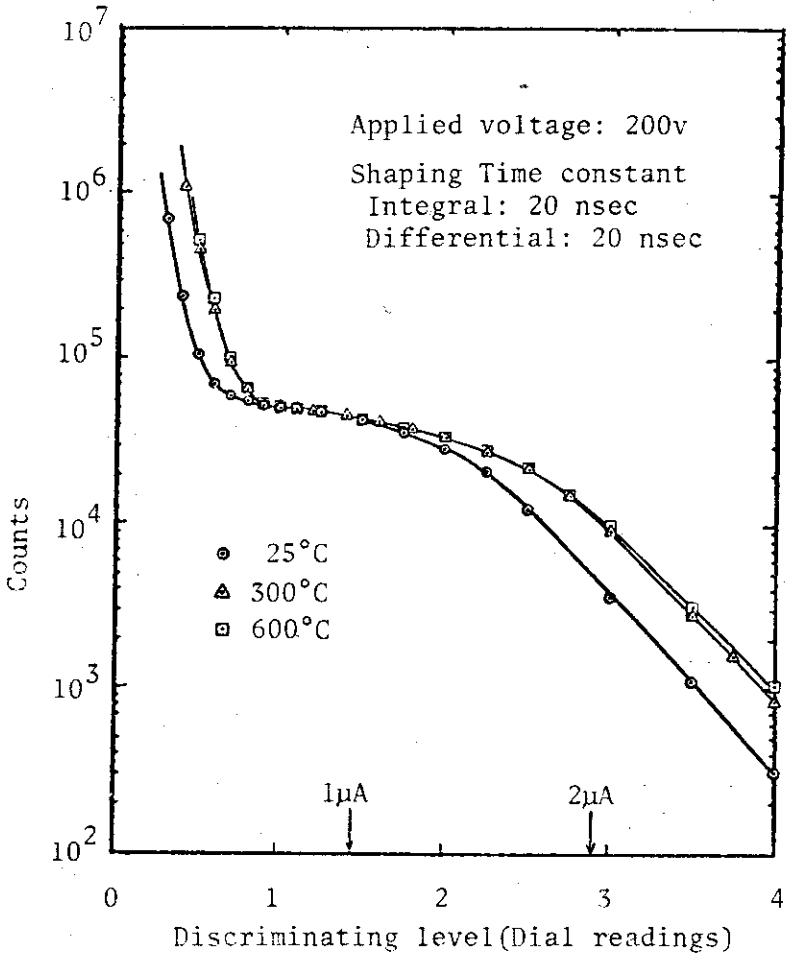

Fig. 6.2.1 Effect of ambient temperature on integral bias curve of FX-2

Table 6.2.1 Characteristics of fission counter-chambers developed for use in high temperature environment

Type	FX-1 (1972)	FX-2 (1974)	
	Characteristics measured	Characteristics designed	Characteristics measured
Detector size(mm)	38ϕ x 360	38ϕ x 340	
Cables	4.8mm mineral insulated triaxial cables, Ro=33Ω		
Max. temperature(°C)	550	650	650
Max. operating temperature(°C)	500	600	640
Applied voltage(V) for characteristics test	200	200	200
Electron collection time (nsec)	50	105	100
Output pulse current (Mode, μA)	2.0(500°C) 1.8(25°C)	2.1	2.2(600°C) 1.9(25°C)
Output pulse charge (Mode, C)	0.45×10^{-13}	1.1×10^{-13}	0.95×10^{-13}
Neutron sensitivity (1) as counter (cps/nv)	0.1	0.13	0.12
(2) as d.c. chamber (A/nv)	——	2.8×10^{-14}	2.2×10^{-14}
(3) as m.s. chamber (Arms/nv$^{\frac{1}{2}}$)	——	——	6.5×10^{-11}
γ-ray sensitivity (A/R/hr)	——	1.3×10^{-11}	1.2×10^{-11}

6.3 High-temperature Tests of Ceramic-insulated Wires and Ceramic Cements

T. Kakuta, M. Yamada and K. Ara

Among in-core instruments, there are some instruments which utilize phenomenon of electromagnetic induction, such as a differential transformer, an eddy-current displacement sensor, an eddycurrent flowmeter, and so on. In these instruments, coils are generally used for energizing themselves and for picking up output signals. Since the instruments are used in environments of high temperature and of strong gamma and neutron radiations, the coils as well as other components of the instruments must stand these severe conditions.

Ceramic-insulated wires and ceramic cements have been already developed by several manufacturers for use under high-temperature and nuclear environments, and are commercially available. In using them as coil wire and a sealing- or potting- cement of the coil, however, it is necessary to investigate in details their actual performance and behavior in in-core environments, though some performance characteristics are presented by the manufacturers. Therefore, ceramic-insulated wires and ceramic cements were tested at high temperatures.

Three types of specimens as shown in Fig. 6.3.1 were prepared. Type 1 was made of two ceramic-insulated wires (Ceramatemp; now manufactured by HY-Temp Transducers, U.S.A.), each about 0.15 mm or 0.3 mm in diameter, and these two wires were twisted together to 30 turns in 100 mm. This specimen was prepared for testing insulation resistance between the wires themselves.

Type 2 was made by covering wholly twisted portion of the same specimen as type 1 with a ceramic cement. The ceramic cements used were Sauereisen (made in Germany), Ceramacast 505 (Aremco Products, U.S.A.) and Ultratemp 516 (Aremco Products). These specimens were prepared not only for testing insulation resistances but also for compatibility between the wires and cement from standpoint of electrical insulation ability at high temperatures.

Type 3 was prepared for testing insulation resistances of the ceramic cement itself. As shown in Fig. 6.3.1, the ceramic cement was potted into a quartz tube to have the diameter of 8 mm and the length of 10 mm and both ends of the section was contacted with the respective electrodes. Since insulation resistance between the electrodes include also that of the qualtz tube, a test specimen containing dry air instead of the cement was also prepared so as to subtract this effect from the value of measured insulation resistance, when necessary. Several different cements were selected for the tests.

All Specimens were then heated from room temperature up to 550 °C in a furnace, and insulation resistances between the wires or electrodes were measured at several temperatures with applying DC 1 volt. The results are shown in Figs. 6.3.2 to 6.3.4. There is not much difference in insulation resistances between the wires of 0.15 mm dia. and 0.3 mm dia. in type 1, and also between Ceramacast 505, Ultratemp 516 and Sauereisen in type 2. It should be noticed, however, that the insulation resistance of Sauereisen is much higher than those of Ceramacast 505 and Ultratemp 516; Ceramacast 511 (Aremco Products) seems to be the best cement among the tested ones as far as insulation resistance is concerned.

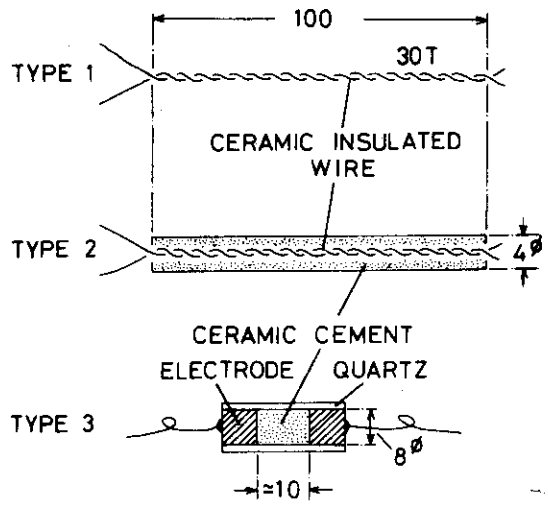

Fig. 6.3.1 Specimens for high-temperature tests

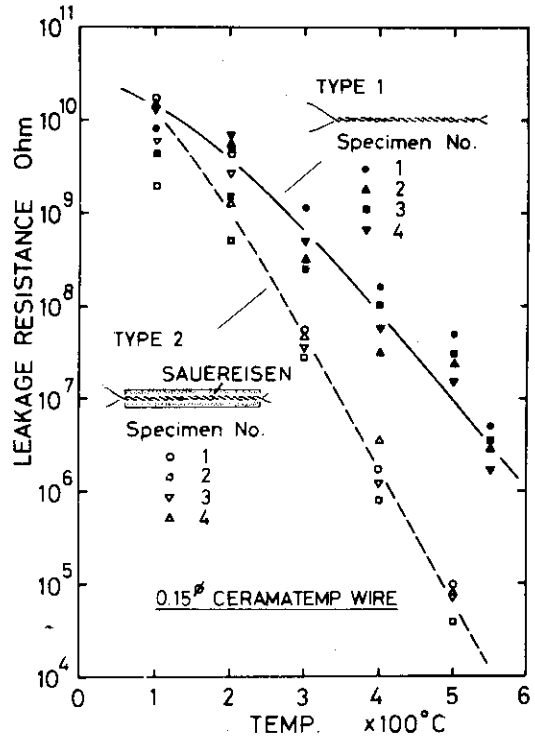

Fig. 6.3.2 Insulation resistances of specimens type 1 and 2 with 0.15ø ceramic-insulated wires

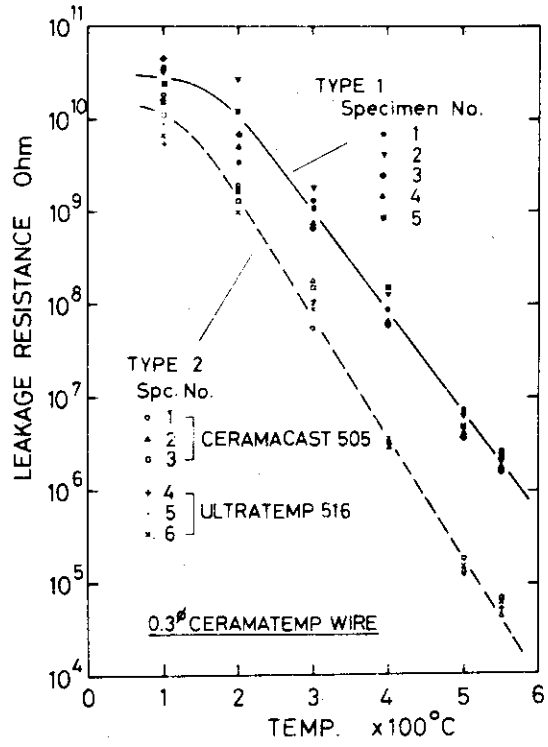

Fig. 6.3.3 Insulation resistances of specimens type 1 and 2 with 0.3ø ceramic-insulated wires

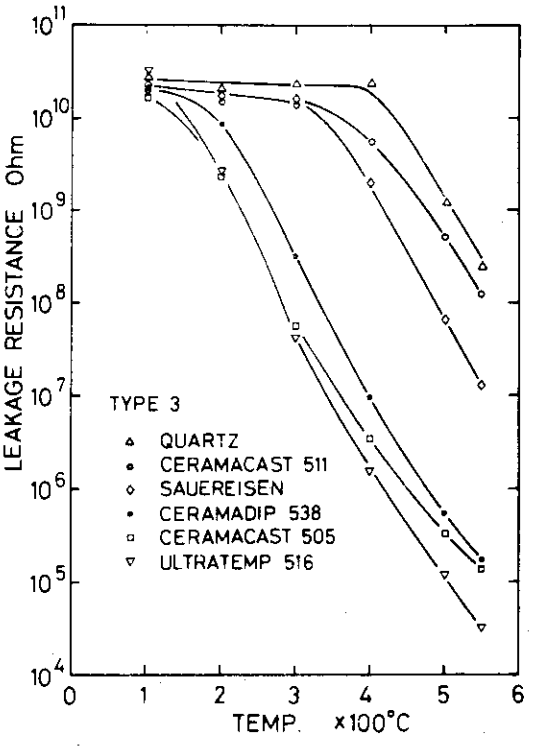

Fig. 6.3.4 Insulation resistances of ceramic cements

6.4 Test of Four Types of Fuel Failure Detection Systems Using Sodium In-Pile Loop*

E. Sakai, M. Katagiri, H. Terada, H. Itoh, T. Sukegawa* and K. Hirano*

We had been entrusted with a contract study "FFD sodium in-pile loop test (III)" from the Fast Breeder Reactor Development Project of the Power Reactor and Nuclear Fuel Development Corporation in the period between May 1, 1974 and April 30, 1975. The study consisted of the preparation and out-of-pile test of the fuel failure detection systems for the Sodium In-pile Loop. The S.I.L. is scheduled to operate with uranium oxide fuels in its irradiation section at the end of 1975.

A polyethylene moderator system was designed as a delayed neutron monitor placed on the lid of the S.I.L. and its detection efficiency of neutrons from an Am-Be source was measured. A simulated polyethylene moderator was experimented to measure the neutron detection efficiency as a function of the position of the Am-Be neutron source. The thickness of the paraffin covered on the source was varied to change the neutron spectrum. The neutron detection efficiency thus obtained simulated the detection efficiency of delayed neutrons existed in the sodium in the expansion tank of the S.I.L. A secular change in the characteristics of BF_3 counters and B-10 counters manufactured by Mitsubishi Electric Company, Ltd. were tested and no change was observed.

---

* Reactor Safety Laboratory II, Division of Reactor Safety, J.A.E.R.I.

A precipitator manufactured by Hitachi Limited was installed in the basement of the reactor room of JRR-2.

In order to measure gamma-ray spectra of fission products in cover gas, a gas reservoir whose inner volume can be changed between 100 cm^3 and 1000 cm^3 and a coaxial Ge(Li) detector of 54 cm^3 sensitive volume had been constructed. The detector has an energy resolution of 2.4 keV and a peak detection efficiency of 9 % relative to 3" x 3" NaI(Tl) detector measured at a source-to-detector distance of 25 cm for 1333 keV gamma-rays. Two kinds of on-line digital subtract units by which a peak area in the pulse height distributions could be counted had been designed and tested. A multichannel pulse height analyser, Canberra Industries model 8100, was accepted.

Some of the data analysing codes for the fuel failure detection systems of the Sodium In-pile Loop were developed.

Those results were reported in JAERI-memo 6118 (April 1975) [1]. Messrs. Naoaki Wakayama and Hideshi Yamagishi of the Reactor Instrumentation Laboratory are deeply acknowledged for their help in the polyethylene moderator simulation experiment; Mr. Tsunemi Kakuta for his help in the B-10 counter characteristics measurement.

Reference

1) Sakai, E., Katagiri, M., Terada, H., Itoh, H., Sukegawa, T. and Hirano, K.: "Performance of Fuel Failure Detection System in Sodium In-pile Loop Experiment (III)-Preparation and Out-of-pile Test of Fuel Failure Detection System-," SJ 250 75-04/JAERI-memo 6118/ SDG 75010 (Apr. 1975) (in Japanese)

6.5 Gamma-ray Spectrum Measurement in Japan Research Reactor No. 3 Using a Portable Ge(Li) Spectrometer

E. Sakai, H. Terada, S. Suzuki*, M. Katagiri and E. Shirai#

Gamma-ray spectra at various positions in the Japan Research Reactor No. 3 have been measured using a portable Ge(Li) spectrometer. The peak detection efficiency and the energy resolution for 1333 keV gamma-rays were 2.6 % relative to 3" x 3" NaI(Tl) detector and 3.5 keV, respectively. At all the measured points in JRR-3, gamma-rays from natural radionuclides such as K-40, Tl-208, Bi-214, and from Co-60 which was one of the induced radionuclides of the reactor-constructing-materials were observed. During the reactor in operation, gamma-rays from Ar-41, the induced radionuclide of argon in air, were observed also at all the points. High energy gamma-rays from the neutron capture reaction in iron and from N-16 induced by O-16(n,p)N-16 reaction of oxygen in heavy water coolant were found in the first floor of the reactor room; the former seems to originate around the monochrometer crystals of the neutron diffractometers. Gamma-rays from noble gas fission products were observed in helium cover gas of the F.F.D. system. In JAERI-M 6024[1], pulse height distributions and counting rates

---

* Student of the Reactor Engineering School, J.A.E.R.I.; on leave from Japan Atomic Power Company, Tokaimura, Nakagun, Ibarakiken, Japan

JRR-3 Operation Section, Division of Research Reactor Operation, J.A.E.R.I.

of those gamma-rays are listed; the detail of the spectrometer as well as a brief description of JRR-3 are given. The results were presented at 1974 Fall Meeting on Reactor Physics and Engineering of the Atomic Energy Society of Japan on 17 October 1974 at Kyushu University[2].

One of the coworkers (Seishiro Suzuki) cooperated the measurement as a trainee of the Reactor Engineering School during 6 to 27 September 1974.

References

1) Sakai, E., Terada, H., Suzuki, S., Katagiri, M. and Shirai, E.: "Gamma-Ray Spectrum Measurement in Japan Research Reactor No. 3 Using a Portable Ge(Li) Spectrometer," JAERI-M 6024/SDG 75005 (Mar. 1975) (in Japanese)

2) Sakai, E., Terada, H., Katagiri, M. and Itoh, H.: "Portable Ge(Li) Gamma-Ray Spectrometer Fabrication and Application," 1974 Fall Meeting on Reactor Physics and Engineering of Atomic Energy Society of Japan, Paper C-17, at Kyushu University, Oct. 17, 1974 (in Japanese)

6.6 In-Situ Gamma-Ray Spectrum Measurement Using Portable Ge(Li) Spectrometers

E. Sakai, H. Terada, M. Katagiri and H. Itoh

The measurement of the environmental gamma-ray spectra has been carried out in the outdoors using a portable Ge(Li) spectrometers. A 33.4 cm^3 Ge(Li) spectrometer (2.6 % detection efficiency relative to 3" x 3" NaI(Tl) detector) was placed at one meter above the ground. Figure 6.6.1 shows the gamma-ray pulse height distribution obtained by a 10 hr measurement made on the lawn between the Research Laboratory Building No. 2 and the Reactor Engineering School Building. Gamma-rays from natural radionuclides in the soil such as K-40, Tl-228 (daughters of Th-232), and Bi-214 (daughter of U-238) were observed as well as Cs-137 (one of the fallout nuclides) and Ar-41 (originated by nuclear reactors). A similar measurement made at the Parking Lot near the Research Laboratory Building No. 3 showed a smaller gamma-ray peak of Cs-137; this means that Cs-137 does not stay because of the disturbed surface of the soil by a blast of wind or traffic, or new sand covered the soil surface to hinder the gamma-radiations from Cs-137. On the contrary, the soil under the lawn is not disturbed at all and keeps the fallout nuclides undisturbed. The fact that a very weak peak of Ar-41 could be observed in Fig. 6.6.1 suggests that the in-situ Ge(Li) spectrometer is a powerful tool to distinguish gamma-rays of man-made radionuclides from those originated by naturally-occurring radionuclides.

The 2.6 % detection efficiency of the 33.4 cm^3 Ge(Li) detector is very small so that a 10hr measurement is needed.

The secondly-made 73 cm^3 Ge(Li) detector gave 17.5 % detection efficiency relative to 3" x 3" NaI(Tl) detector and only a 2 hr measurement was enough to obtain almost the same counts as those shown in Fig. 6.6.1. Gamma-ray spectrometry at the L-Pit of the Waste Disposal Area showed that the main radiations came from Co-60 and Cs-137 and also the presence of Ag-110 m; this measurement was requested from the health physics point of view to confirm the safety of the workers who entered into the Pit.

The measurement of the peak detection efficiency of the detector as a function of the direction of incident gamma-rays will be performed and the concentrations of the radionuclides in the soil and the exposure rates at the detector position will be deduced by analysing the pulse height distributions.

Reference

1) Sakai, E., Terada, H., Katagiri, M. and Itoh, H.: "Portable Ge(Li) Gamma-Ray Spectrometer Fabrication and Application," 1974 Fall Meeting on Reactor Physics and Engineering of Atomic Energy Society of Japan, Paper C-17, at Kyushu University, Oct. 17, 1974 (in Japanese)

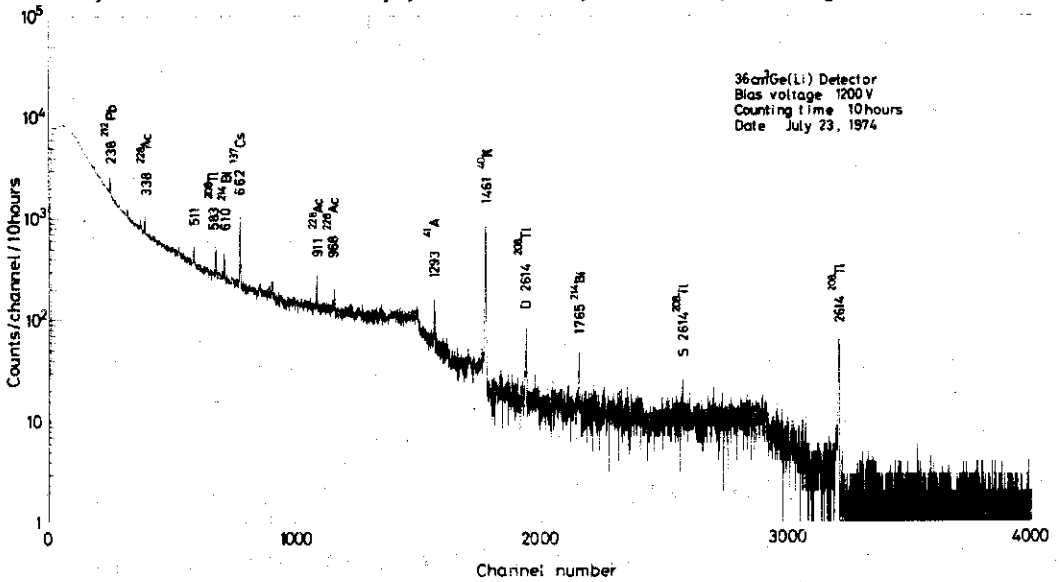

Fig.6.6.1 Outdoor measurement of background gamma-ray spectrum near the laboratory building NO. 2 in JAERI

6.7 Temperature Cycling Test of a Hyper-Pure Germanium Detector

E. Sakai, H. Terada, M. Katagiri and H. Itoh

A hyper-pure germanium detector manufactured by NRD (PHYGE model 05005B serial no. 100P5P3) was tested during temperature cycles. The detector specification shows 50 mm^2 entrance window, 5 mm thickness, and 3.5 keV energy resolution for 625 keV electrons. The detector has a construction shown in Fig. 6.7.1; the p-contact (Ni-evaporated) of the detector is pressed through an indium ring to an aluminum case which has an open entrance for charged particles. The n^+-contact (Li-diffused) is pressed by a spring soldered to the center lead of a microdot connector. The detector case has a small diameter hole by which air can enter into the case.

The detector was mounted on a cold finger in a cryostat (Cryogenic Associates SD-170J), then an aluminum end-cap was fastened, evacuation started, and the vacuum valve was closed off. The leakage current and capacitance dependence on bias voltage, and energy resolution and peak detection efficiency for gamma-rays were measured after every temperature cycle from room temperature to 77 K. The temperature cycling test was performed as shown in Table 6.7.1; liquid nitrogen was filled firstly at 11:00 on December 4, 1974 and various characteristics of the detector at 77 K were measured. The detector started to warm up to room temperature at 17:00 on December 12, 1974 and left there for 16.5 hr until liquid nitrogen was filled at 9:30 on December 13, 1974. Then, the detector characteristics were measured, and so on ---. The experimental results obtained

before the seventh cycle had been reported in JAERI-M 5988.[1] The results of the experiments including the eighth and the ninth temperature cycles were reported at 1975 Annual Meeting on Reactor Physics and Engineering of the Atomic Society of Japan on April 3, 1975.[2]

A summary of the results is as follows: The leakage current vs. applied voltage characteristics exhibited a variation in a small range, as shown in Fig. 6.7.2, but, the magnitude of the leakage current itself was about 10 pA which did not effect the energy resolution of the detector. The capacitance vs. applied voltage characteristics did not change until the seventh cycle, but, at the eighth cycle, the capacitance at applied voltages lower than 300 V increased; this might mean an increase in the net carrier concentration in the depleted region near the n^+-layer (Li-diffused) of the detector. The capacitances at applied voltages larger than 300 V did not change during the temperature cycles. Figure 6.7.3 shows the leakage current, capacitance, absolute peak detection efficiency (source-to-detector distance 10 cm) and FWHM energy resolution for 356 keV gamma-rays from Ba-133 as a function of the duration of the detector at room temperature. It shows that the detector performance except the leakage current did not change during 1376.5 hr at room temperature; the change in the leakage current was not large enough to degrade the energy resolution of the detector. The detector had been at room temperature for more longer duration than 1376.5 hr if one considers the fact that NRD tested the detector on October 21, 1974.

From the results explained above, it can be said that the hyper-pure germanium detector we tested is very stable against

the temperature cycling in vacuum between room temperature and 77 K. The possibility of a change in the depleted region near the n^+-layer (Li-diffused) during room temperature period can not be excluded. The detector is at present exposed to the air at room temperature and tests will be continued.

References

1) Sakai, E., Terada, H., Katagiri, M. and Itoh, H.: "Temperature Cycling Test of a Hyper-Pure Germanium Detector," JAERI-M 5988/SDG 75003 (Feb. 1975) (in Japanese).

2) Sakai, E., Terada, H., Katagiri, M. and Itoh, H.: "Temperature Cycling Test of a Hyper-Pure Germanium Detector," 1975 Annual Meeting on Reactor Physics and Engineering of Atomic Energy Society of Japan, Paper B43/SDG 75002, at Tokyo Institute of Technology, April 3, 1975 (in Japanese).

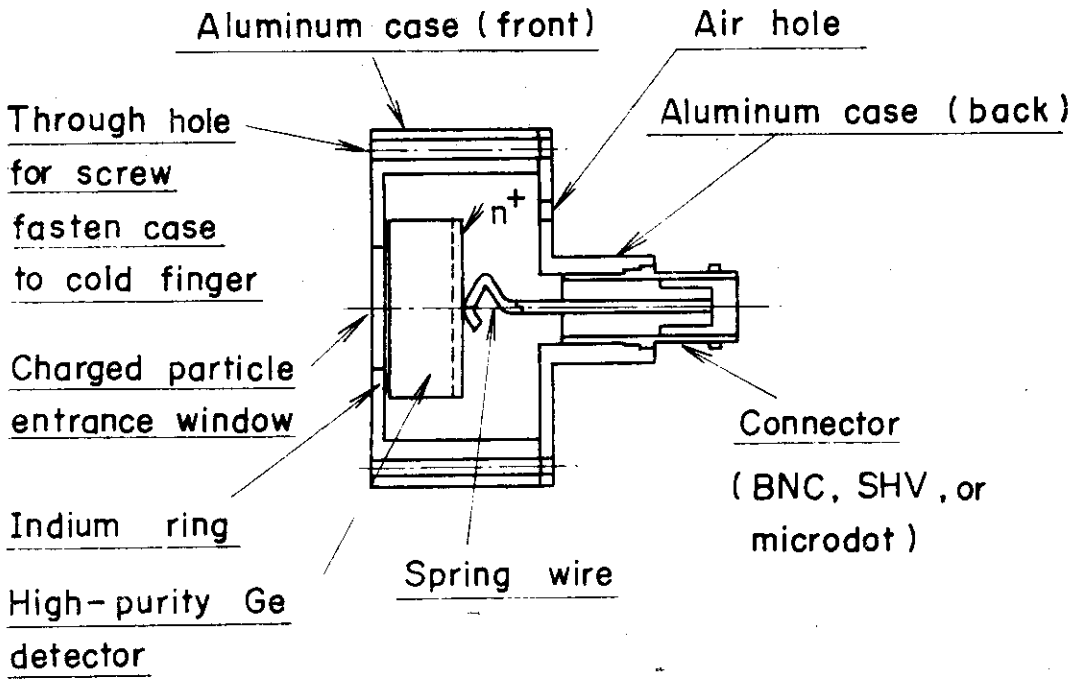

Fig.6.7.1 NRD PHYGE detector construction

Table 6.7.1 Time schedule of temperature cycling

No. of temperature cycling	Cooling cycle		Duration (hr)	
	Start	Terminate	at 77K	at room temperature
Initial	11:00 Dec. 4	17:00 Dec.12	208	
				16.5
1	9:30 Dec.13	16:30 Dec.14	31	
				41.0
2	9:30 Dec.16	18:30 Dec.16	9	
				22.5
3	17:00 Dec.17	18:10 Dec.19	49	
				22.0
4	16:00 Dec.20	14:00 Dec.21	20	
				25.0
5	15:00 Dec.22	14:30 Dec.23	23.5	
				20.5
6	11:00 Dec.24	10:00 Dec.27	71.0	
				192.5
7	10:30 Jan. 4	9:00 Jan.22	430.5	
				893.5
8	14:30 Feb.28	15:00 Mar. 8	192.5	
				143.0
9	14:00 Mar.14			
Total			1034.5hr	1376.5hr

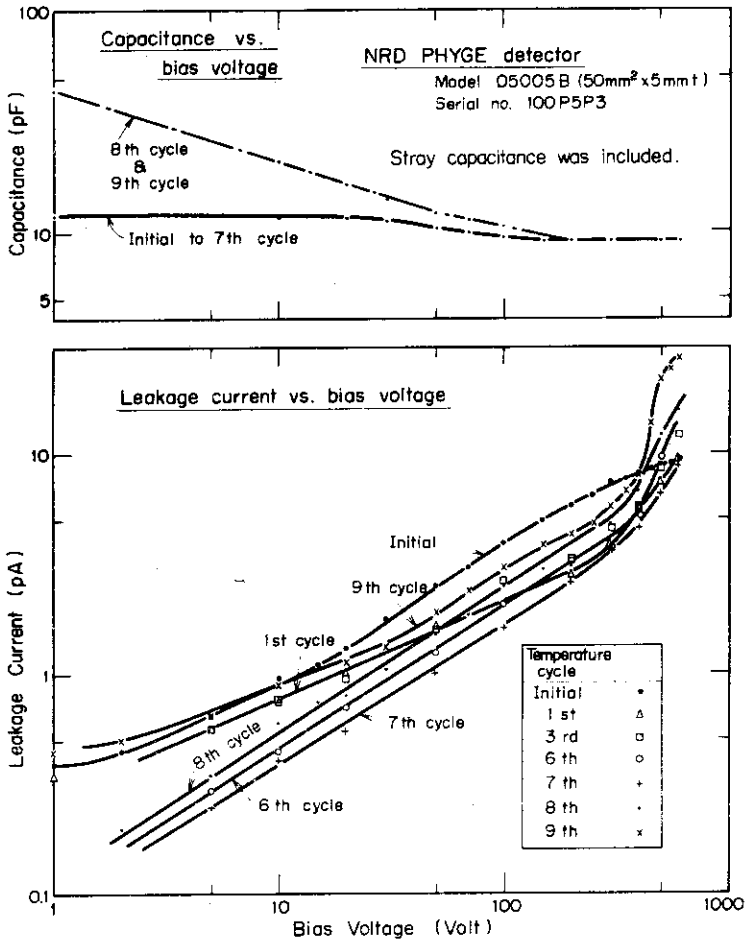

Fig.6.7.2 Capacitance and leakage current vs. bias voltage characteristics of PHYGE model 05005B detector

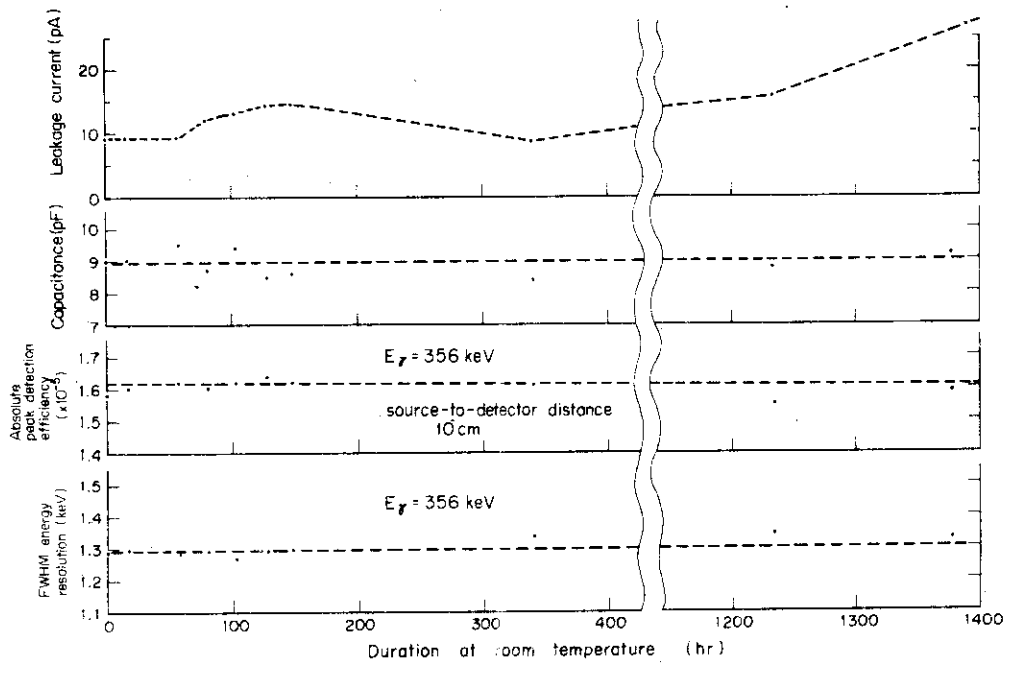

Fig.6.7.3 Detector performance at 600V bias vs. duration of detector at room temperature

6.8 Silicon Detector Fabrication by N^+ Ion Implantation

M. Katagiri, H. Itoh and E. Sakai

Some of diodes, transistors, and I.C.s are manufactured using ion implantation technique by several manufacturers. This technique can be applied to make thin, rugged contacts on semiconductor detectors. Ions of B, Al, Ga, In can be implanted to make p^+-contacts and Li, N, P, As, Sb ions to make n^+-contacts. We tried to determine whether N^+ ion implantation onto p-type silicon wafers could make p-n^+ junction or not using 2 MeV Van de Graaff accelerator of the Physics Division of J.A.E.R.I.; the accelerator can accelerate only N^+ and Ar^+ ions at present.

One mm thick boron-doped p-type silicon wafers (200 ohm) of 25 mm diameter were etched with etchant HNO_3(2) + HF (1), attached onto an irradiation mount (irradiation window area 0.5 cm^2), and irradiated by 1.1 MeV N^+ ions of 1.5 μA. Some of the wafers were irradiated by 2×10^{16} ions/cm^2 and the others by 6×10^{16} ions/cm^2. The temperature of the irradiated wafers might reach about 100 °C.

A thin gold film (10 μg/cm^2) was evaporated onto a 0.3 cm^2 area of the irradiated surface to confirm a good surface conductivity. As an ohmic contact to the p-type silicon, indium was pressed to the lapped surface of the silicon. The leakage current and capacitance vs. bias voltage characteristics of the detector made by 3×10^{16} N^+ ions/cm^2 implantation are shown in Fig. 6.8.1; the leakage current at 100 V bias was 20 μA. The pulse height distribution of alpha-particles from Am-241 obtained by the implanted detector is shown in Fig. 6.8.2. The FWHM energy resolution of the alpha peak reached 700 keV whereas good

silicon detectors shows FWHM less than 20 keV. The degradation of the energy resolution seems to be caused by the large leakage current and thick window of the detector. For the 6 x 10^{16} ions/cm^2 implanted silicon, the leakage current at 100 V was 50 μA and larger than 20 μA of the 3 x 10^{16} ions/cm^2 implanted silicon detector.

From the results described above, it was found that the implantation of 1.1 MeV N^+ ions into p-type silicon could make p-n junction detectors. The effect of the energy and dose of the ions and annealing on detector performance will be investigated. Boron implantation will be also tried to make thin p^+-contacts on hyper-pure germanium crystals.

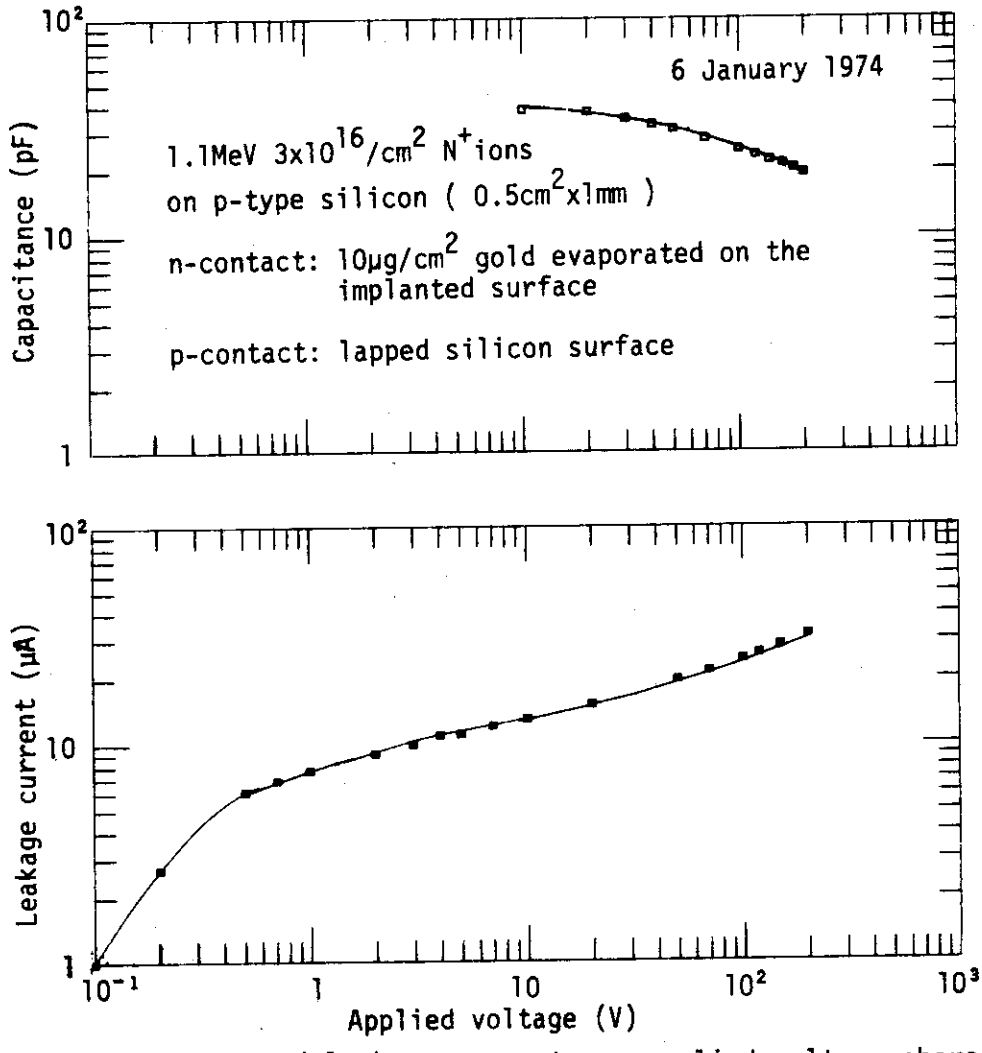

Fig.6.8.1 Capacitance and leakage current vs. applied voltage characteristics of 1.1 MeV N^+ ion implanted silicon detector

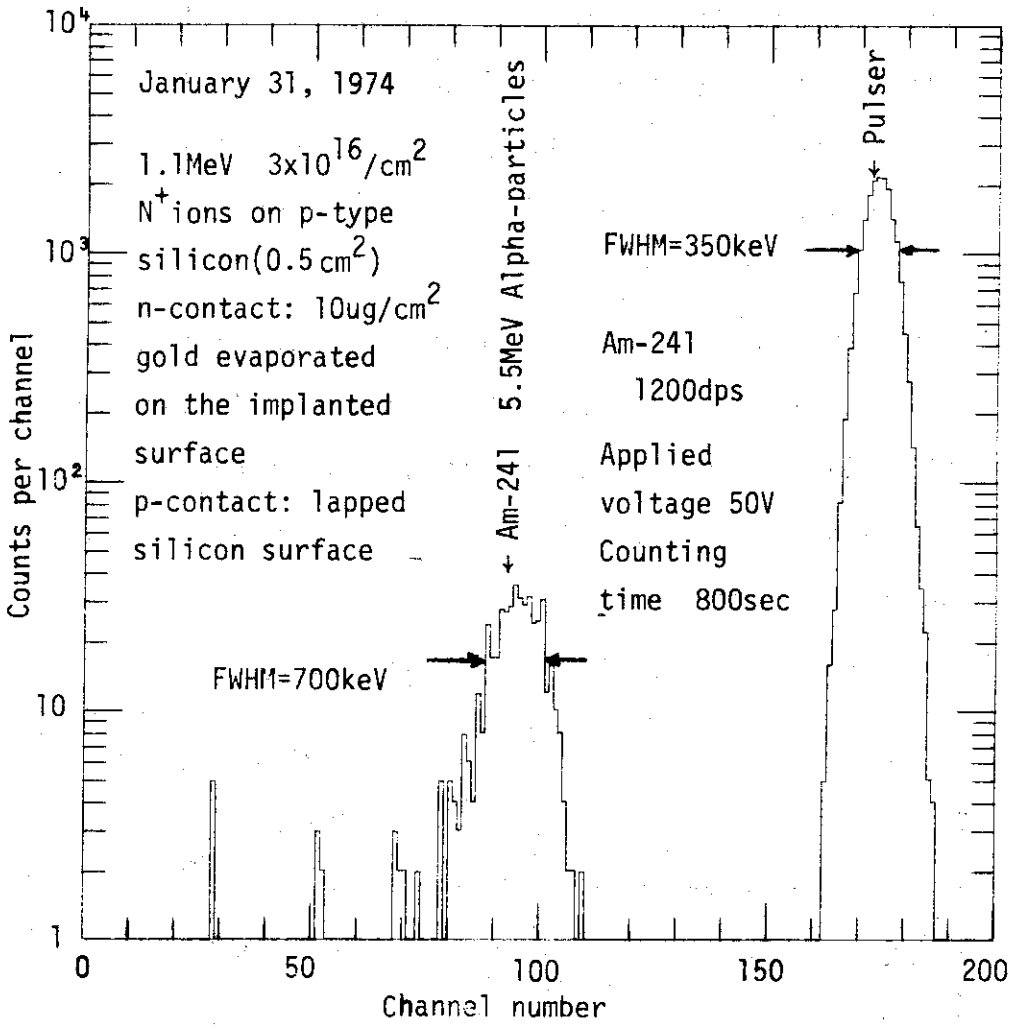

Fig.6.8.2 5.5MeV alpha-particle pulse height distribution obtained by N^+ ion implanted silicon detector

6.9 The Relation between Light Conversion Efficiency and Stopping Power of Charged Particles in Thermoluminescence Dosimeter[1)]

Y. Furuta and S. Tanaka

The response of thermoluminescence(TL) material to charged particles is not only an interesting problem itself but also very important for knowing its response to neutrons, because the response to neutrons is related from the migration of charged particles produced by interaction of neutrons with composite nuclei of TL material.

The purpose of the present study is to obtain the general method for estimating the energy response of any thermoluminescence dosimeter(TLD) to neutrons. To perform this purpose, the relation between luminescence efficiency and stopping power or linear energy transfer(LET) of charged particle was studied, and it was found that there were some problems in the published reports relating the efficiency with LET.

In this study, two types of efficiency, the differential (conversion) efficiency and the mean (conversion) efficiency, were proposed, and they were related with the mass stopping power. They are suitable not only for mere charged particles but also for those produced or recoiled by neutrons.

The differential efficiency η' is defined as

$$\eta' = dG_0/dE, \qquad (1)$$

where dG_0 is the differential contribution to the integral glow intensity by the energy loss dE of a charged particle (including charged particle produced or recoiled by neutron in TL material).

The mean efficiency $\bar{\eta}$ for a charged particle whose initial energy is E_0 is also defined as

$$\bar{\eta} = -\frac{1}{E_0}\int_{E_0}^{0} \eta' dE. \qquad (2)$$

The relations between these efficiencies and the mass stopping power obtained by the present study are shown in Fig. 6.9.1. In the published reports, confused utilization is seen for these efficiencies.

The mean efficiency is practically useful to obtain the thermoluminescence response of TLD to neutrons and charged particles, and the differential efficiency may serve for theoretical treatments of the thermoluminescence mechanism which will be subject in future investigation.

Figure 6.9.2. shows one of the results of comparison between the experimental results of neutron energy response and the calculated results using the mean efficiency obtained by the present study.

In addition to estimating the energy response of any TLD to neutrons or charged particles, the results of the present study may serve to develop a new type of TLD with desirable response such as "rem" response to neutrons.

References

1) Furuta, Y., Tanaka, S.: "The Relation between Light Conversion Efficiency and Stopping Power of Charged Particles in Thermoluminescence Dosimeter," Proceedings of 4th International Conference on Luminescence Dosimetry, Kraków, Aug. 27-31, 1974, p.97.

2) Jähnert, B.: "Thermoluminescent Research of Protons and

Alpha-Particles with LiF (TLD - 700),"
Proceedings of 3rd International Conference on Luminescence Dosimetry, Risø, Oct. 11-14, 1971, p.1031.

3) Lucas, A.C., Rainbolt, C.: "Response of Calcium Fluoride and Lithium Fluoride to Alpha Particles,"
Proceedings of 2nd International Conference on Luminescence Dosimetry, Gatlinburg, Sept. 23-26, 1968, p.456.

4) Harvey, J.R., Townsend, S.: "The Measurement of Dose from a Plane Alpha Source,"
Proceedings of 3rd International Conference on Luminescence Dosimetry, Risø, Oct. 11-14, 1971, p.1015.

5) Furuta, Y., Tanaka, S.: Nucl. Instr. and Meth., 104, 365 (1972).

6) Wingate, C.L., Tochilin, E., Goldstein, N.: "Response of Lithium Fluoride to Neutrons and Charged Particles,"
Proceedings of 1st International Conference on Luminescence Dosimetry, Stanford, June 21-23, 1965, p.421.

7) Goldstein, N., Miller, W.G., Rago, P.F.: Health Phys., 18, 157 (1970).

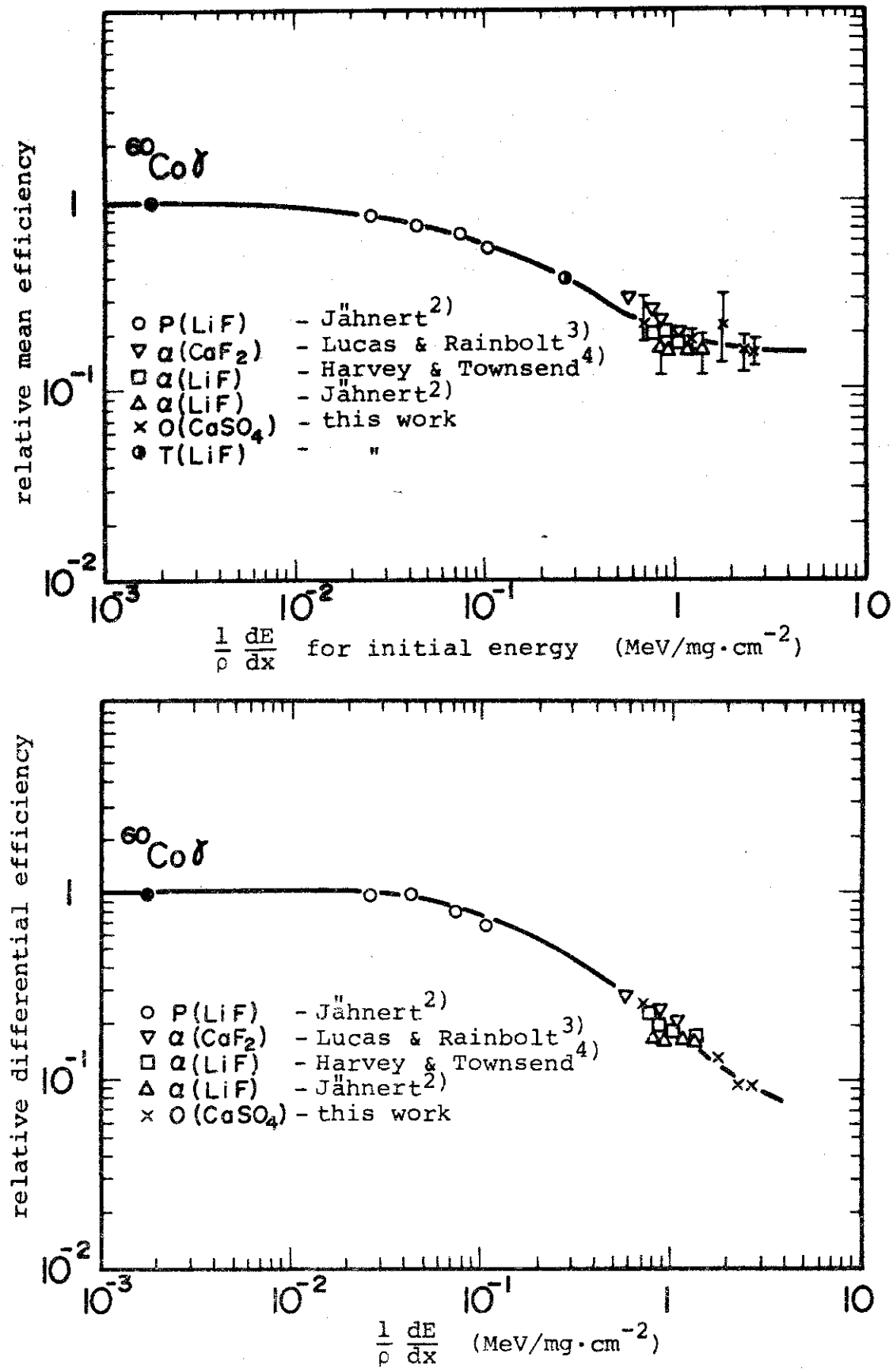

Fig. 6.9.1 Mean efficiency and differential efficiency of thermoluminescence dosimeter normalized to the values of ^{60}Co gamma rays

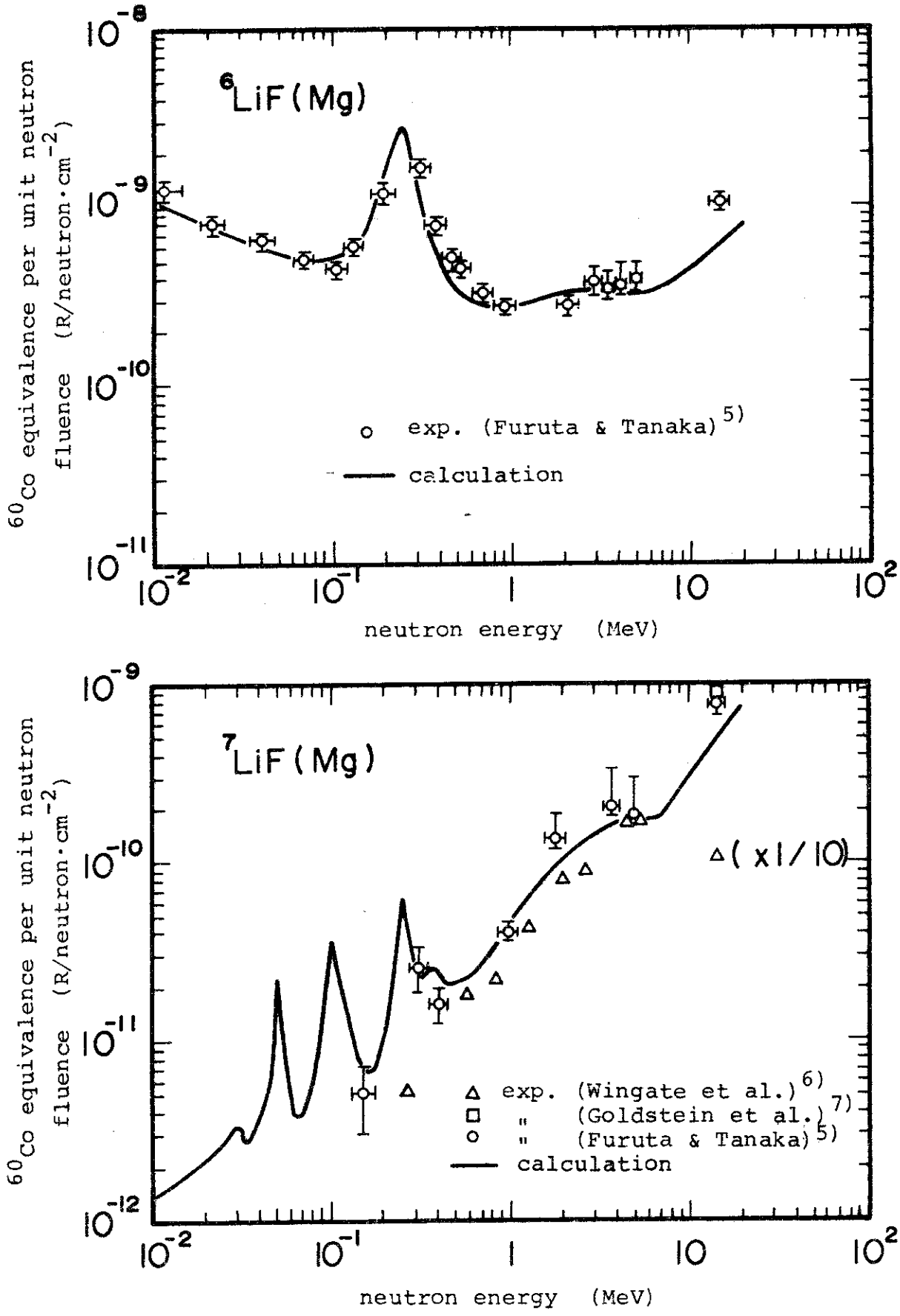

Fig. 6.9.2 Energy responses of ^{6}LiF(Mg) and ^{7}LiF(Mg) thermoluminescence dosimeters

6.10 Neutron Responses of Thermoluminescence Dosimeters, BeO(Na), $CaSO_4$(Tm), and Its Mixture with ^{6}LiF or ^{7}LiF[1)]

S. Tanaka and Y. Furuta

The present authors have reported the energy responses of ^{6}LiF and ^{7}LiF Thermoluminescence dosimeters (TLD's) to neutrons.[2)] In this work, the energy responses of TLD's, BeO(Na), $CaSO_4$(Tm), and its mixture with non-activated ^{6}LiF or ^{7}LiF powder, were obtained experimentaly for mono-energetic neutrons of energies from several ten keV to about 15 MeV. The experimental results were compared with the kerma of TLD to neutrons, and the over-all conversion efficiencies to estimate the integral thermoluminescence from the kerma were decided for each TLD as follows :

BeO(Na) : 4.2×10^{-3} R ^{60}Co equivalence/erg g^{-1},

$CaSO_4$(Tm) : 3.0×10^{-3} R ^{60}Co equivalence/erg g^{-1},

UD-136N* : 2.2×10^{-3} R ^{60}Co equivalence/erg g^{-1},

UD-137N** : 2.1×10^{-3} R ^{60}Co equivalence/erg g^{-1},

UD-2ooS*** : 3.0×10^{-3} R ^{60}Co equivalence/erg g^{-1}.

As examples of the present results, the energy responses and the kerma of BeO(Na) and $CaSO_4$(Tm) TLD's to neutrons are shown in Fig.6.10.1 and Fig.6.10.2. As seen in the figures, the over-all conversion efficiency may be available for estimating approximately the integral thermoluminescence from the kerma by a conversion constant, and it may be convenient to practical use of TLD.

---

* the mixture of $CaSO_4$(Tm) TLD and ^{6}LiF powder

** the mixture of $CaSO_4$(Tm) TLD and ^{7}LiF powder

*** $CaSO_4$(Tm) TLD of pocket dosimeter type with a γ-ray filter

The glow curves of these TLD's irradiated with various radiations were also measured. Any remarkable differences were not observed between the glow curve irradiated by gamma rays and those of other radiations differing from the case of ^{6}LiF and ^{7}LiF TLD's.

References

1) Tanaka, S., Furuta, Y. : "Neutron Responses of Thermoluminescence Dosimeters, BeO(Na), $CaSO_4$(Tm), and Its Mixture with ^{6}LiF or ^{7}LiF," Proceedings of 4th International Conference on Luminescence Dosimetry, Kraków, Aug. 27-31, 1974, p.1213.

2) Furuta, Y., Tanaka, S. : "Response of ^{6}LiF and ^{7}LiF Thermoluminescence Dosimeters to Fast Neutrons," Nucl. Instr. Meth., **104**, 365 (1972).

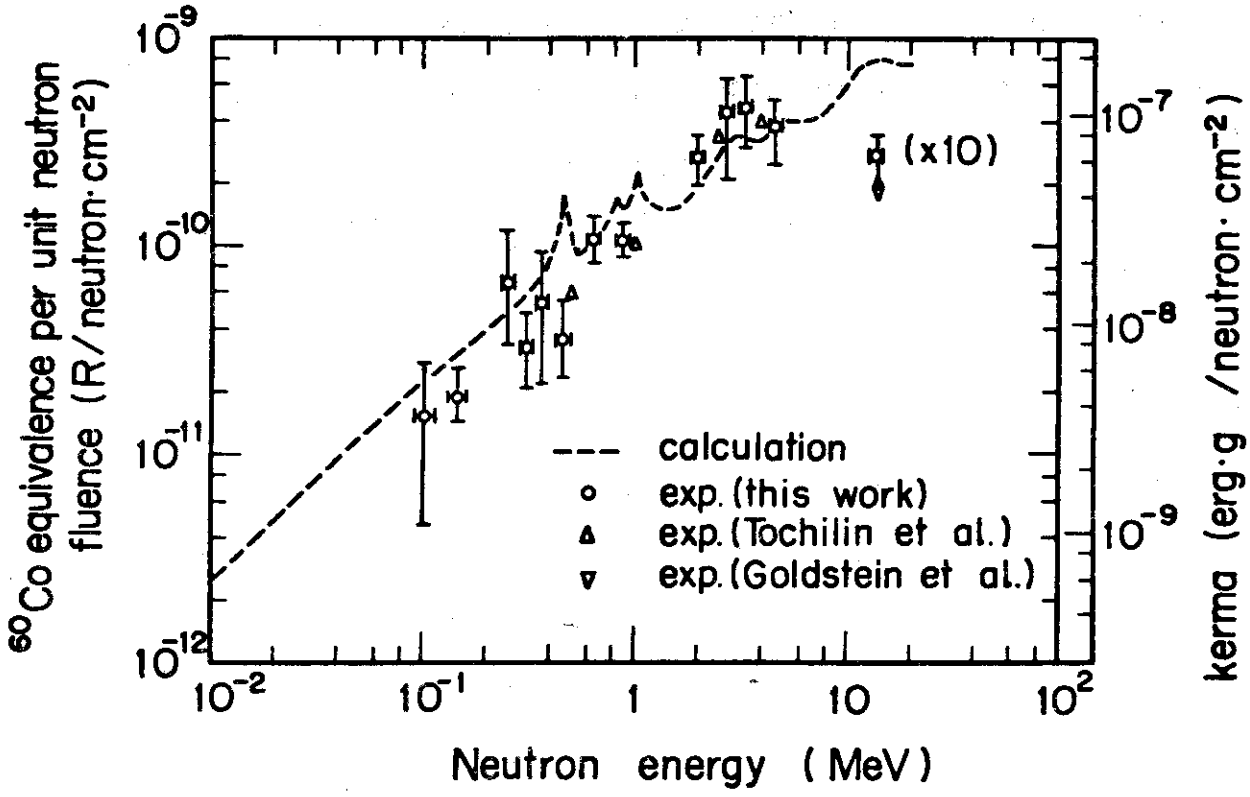

Fig.6.10.1 Energy response of integral thermoluminescence and kerma of BeO(Na) TLD to neutrons

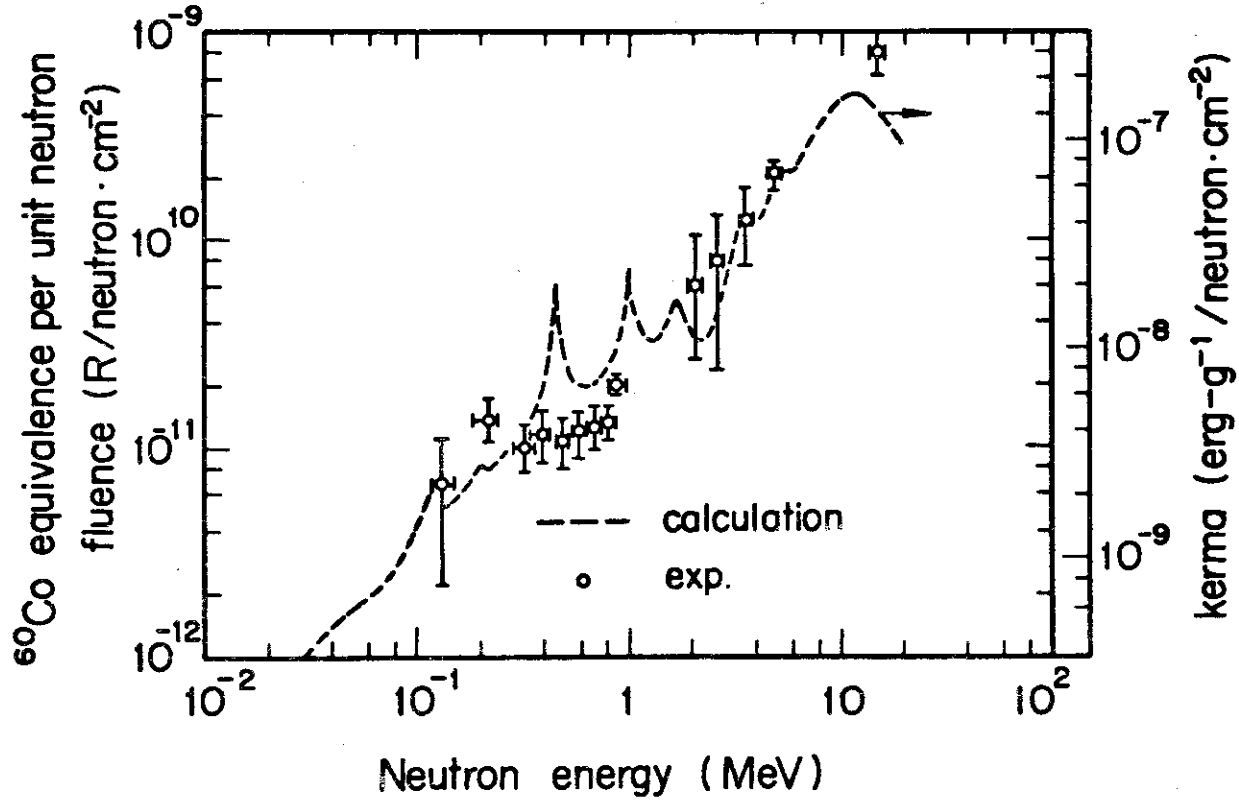

Fig.6.10.2 Energy response of integral thermoluminescence and kerma of $CaSO_4$(Tm) TLD to neutrons

6.11 Neutron Dosimetry by Thermoluminescence Dosimeter[1)]

Y. Furuta and S. Tanaka

Recently, the authors reported the relation between light conversion efficiency and stopping power of charged particles in thermoluminescence dosimeter(TLD)[2)] and the experimental results of the energy responses of some TLD's to neutrons[3)].

Using these results, possibilities of application of TLD's for neutron dose equivalent or absorbed dose measurements are suggested in this report.

1) Dose equivalent measurements

In the former report[2)], the conversion efficiency for any charged particles to obtain the integral glow intensity from the kerma were given. Using the efficiency, we may estimate the energy response to neutrons of any TLD by calculations and, furthermore, we may develop a new TLD whose response to neutrons resembles to that of the maximum dose equivalent.

The new TLD proposed in the present study, "rem" TLD, is consisted by a pair of two types of TLD having almost the same response to gamma rays; one type sensitive to neutrons while the other is not. Figure 6.11.1 shows the response of the rem TLD estimated by calculations. It was obtained by subtraction of the estimated integral glow value of the neutron insensitive TLD from that of the neutron sensitive TLD. In the same figure, the maximum dose equivalent for mono-energetic neutron of unit fluence incident normally on a 30 cm thick tissue equivalent phantom[4)] is also shown.

2) Absorbed dose measurements

As described previousely, the authors had obtained experi-

mentally the energy responses of several TLD's[3]. From the results, it was seen that the responses of some TLD's were much resembled the calculated kerma of some material. As an example, a comparison between the energy response of UD137N TLD* to neutrons obtained by experiments and the calculated kerma of iron is shown in Fig. 6.11.2. Good resemblance may be seen from the figure.

It may be concluded that if the neutron field is not disturbed by positioning a TLD, and if the contribution of gamma rays to the integral glow value of the TLD may be estimated, the absorbed dose of some material may be estimated by TLD without any information about the neutron spectrum at the position. At present, the following combinations are considered as giving good results.

material	TLD	f
aluminum	^{7}LiF	1.0×10^{2}
sodium	UD137N*	2.7×10^{2}
iron	UD137N*	5.0×10

The value of f shows a fitting factor to obtain the kerma of a material K_m in $erg \cdot g^{-1}$ from the integral glow value G_{TLD} of the corresponding TLD in R ^{60}Co equivalence for each neutron energy E_n, that is

$$K_m(E_n) = f \cdot G_{TLD}(E_n).$$

---

* mixture TLD of $CaSO_4$(Tm) TLD and ^{7}Li enriched LiF powder (made by Matsushita Electric Industrial Co., Ltd.)

References

1) Furuta, Y., Tanaka, S.: "Neutron Dosimetry by Thermoluminescence Dosimeter,"
Presented for the International Symposium on Radiation Physics, Calcutta, Nov. 30-Dec. 4, 1974.

2) Furuta, Y., Tanaka, S.: "The Relation between Light Conversion Efficiency and Stopping Power of Charged Particles in Thermoluminescence Dosimeter,"
Proceedings of 4th International Conference on Luminescence Dosimetry, Kraków, Aug. 27-31, 1974, p.97.

3) Tanaka, S., Furuta, Y.: "Neutron Responses of Thermoluminescence Dosimeters, BeO(Na), $CaSO_4$(Tm), and Its Mixture with ^6LiF or ^7LiF," ibid. p.1213.

4) "Radiation Protection Instrumentation and Its Application," ICRU Report No. 20, 1971.

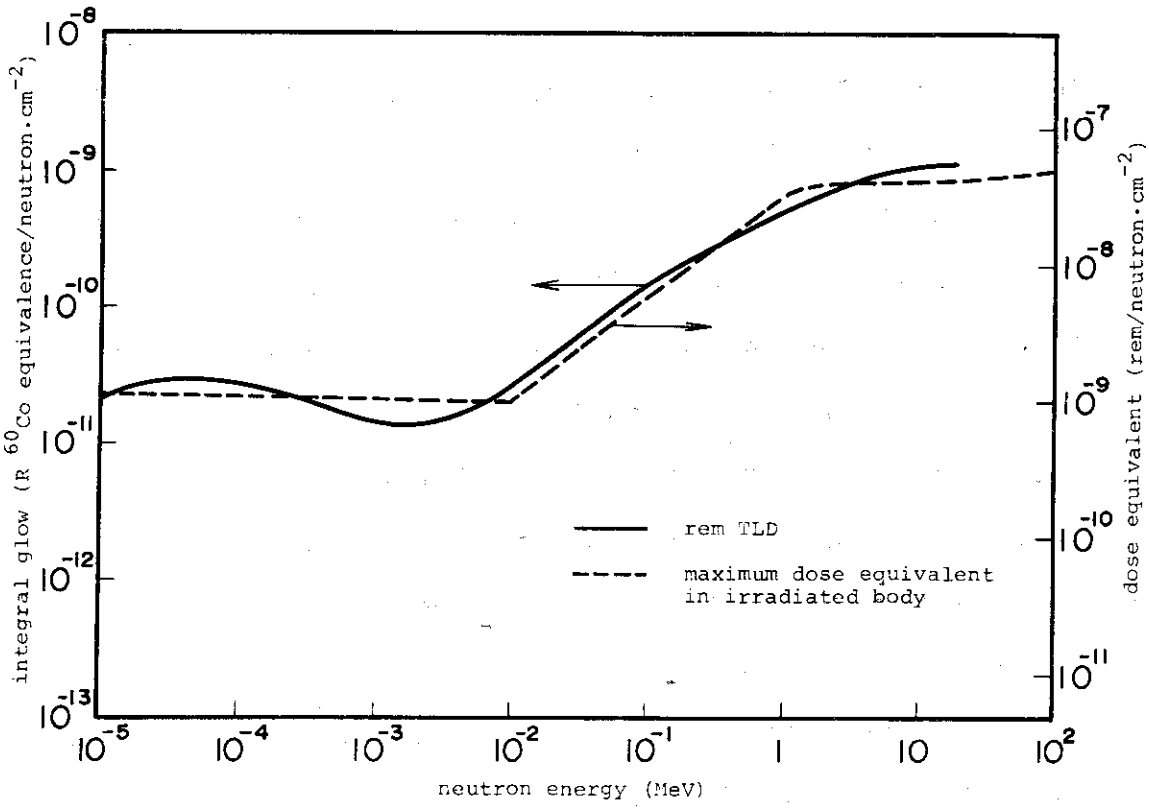

Fig. 6.11.1 Calculated energy response of a newly developing rem response thermoluminescence dosimeter

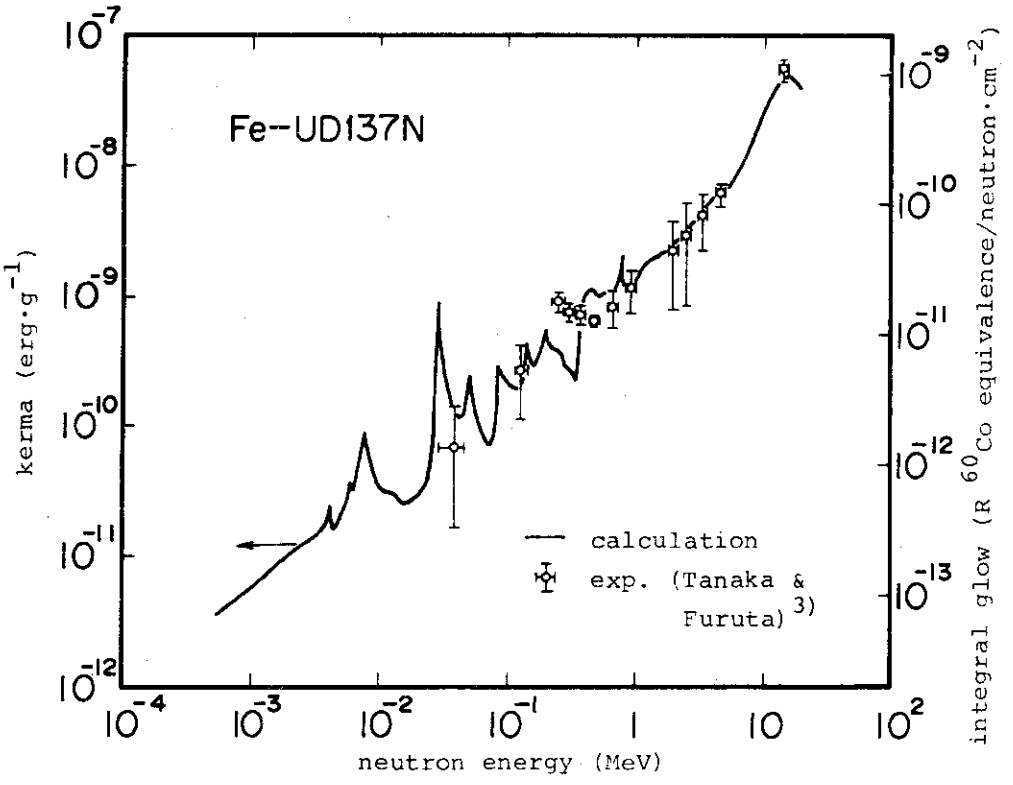

Fig. 6.11.2 Energy response of UD137N thermoluminescence dosimeter and kerma of iron

6.12 Development of Double Scintillator Fast Neutron Spectrometer

K. Shirakata, M. Cho* and T. Iijima

The double scintillator time-of-flight method has been developed as a fast neutron spectrometer, and has been applied to measurements on FCA Assembly VI-2 and a natural uranium exponential pile. The spectrometer uses two scintillator detectors, in an arragement that the 1st detector is placed as a scattering scintillator in a parallel neutron beam extracted from a pile to be measured, and that the 2nd detector is placed outside the incident neutron beam, in a position to detect neutrons scattered through 45°. The spectrometer measures the flight time between a scattering event in the 1st scintillator and the arrival of the scatterd neutron at the 2nd scintillator. As both the scattering angle and the flight path are fixed, the measured flight-time distribution is easily reduced to neutron energy spectrum of the incident beam, provided that the scattering was by a proton and occurred only once in the scattering scintillator. It is a merit of the double scintillator spectrometer, that the method is essentially one of the differential measurements of neutron energy spectra and does not need a complicated unfolding procedure for the analysis of measured data.

Fig. 6.12.1 shows the block diagram of the electronics. The upper-lower coincidence is employed both in the 1st and the 2nd detectors to decrease the time jitters for the time signals. Another coincidence between two photomultipliers is also employed for the 2nd detector to eliminate photomultiplier electronic noises. The energy dependence of the spectrometer efficiency is calibrated by two experimental means, namely the Cf-252 fission spectrum measurement and mono-energetic neutron response measurements. Fig. 6.12.2 shows the time spectra measured for mono-energetic neutrons, produced by the 5.5 MeV Van de Graaff accelerator. Fig. 6.12.3 shows the arragement of the

* Korea Atomic Energy Research Institute

detectors and equipments for the measurement of neutron spectrum at the core center of FCA Assembly VI-2. Fig. 6.12.4 shows one of time-of-flight spectra in the measurements on FCA Assembly VI-2, and the neutron spectrum deduced from the data is shown in Fig. 6.12.5, compared with a calculated result. At the present stage the applicable range of the spectrometer is 200KeV - 5MeV.

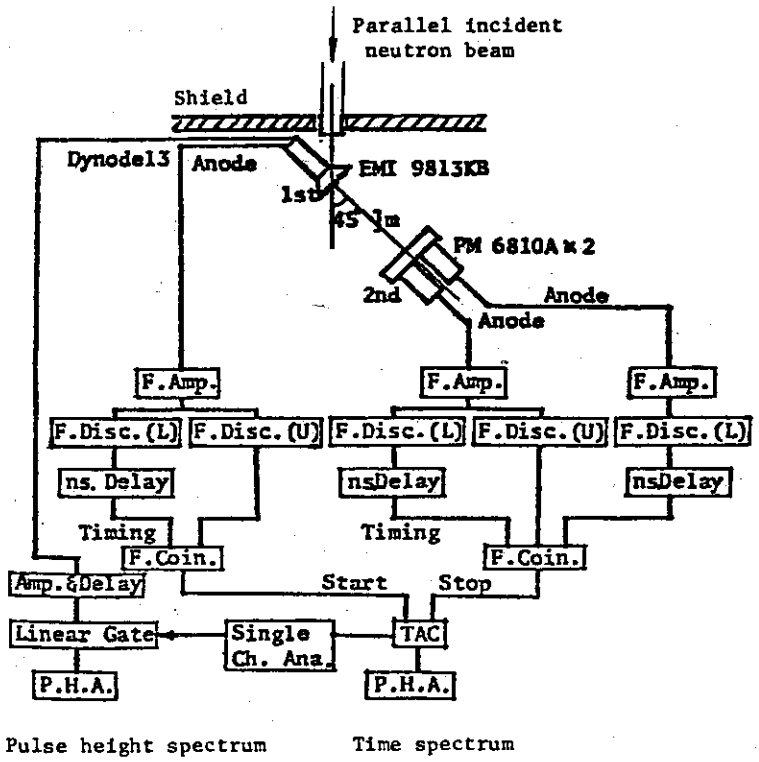

Fig. 6.12.1 Block diagram of the spectrometer electronics

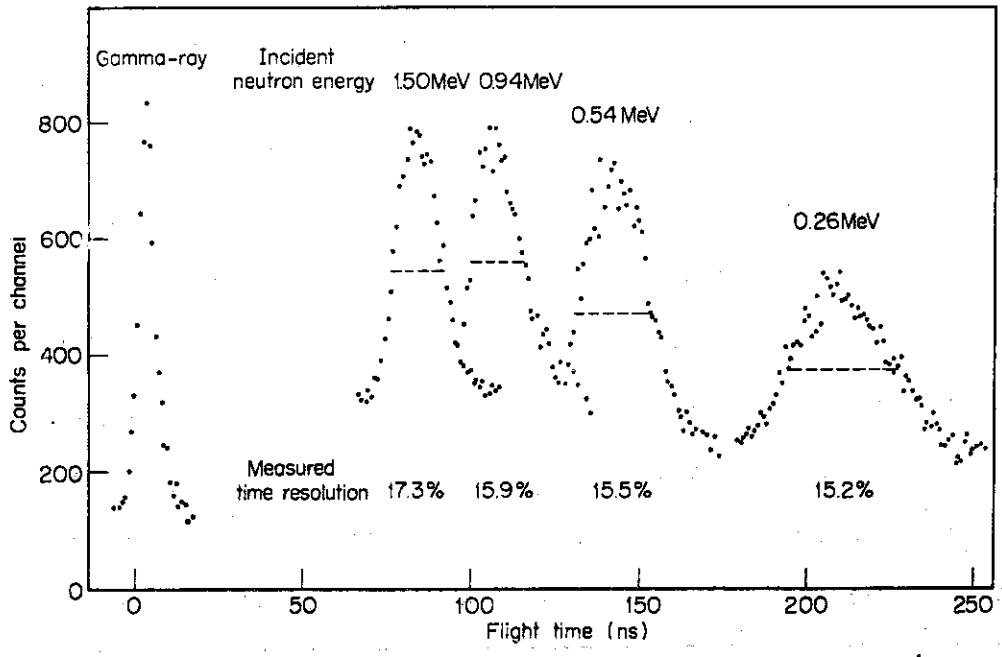

Fig. 6.12.2 Spectrometer responses to mono-energetic neutrons

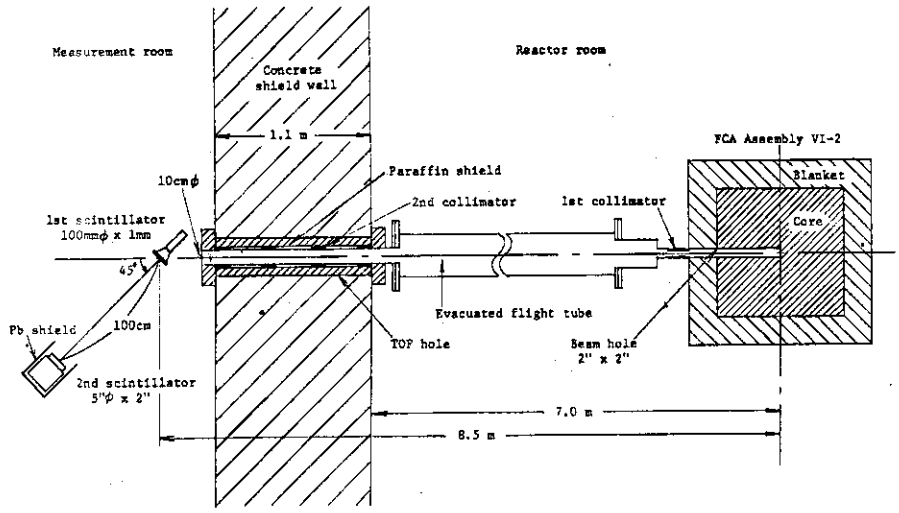

Fig. 6.12.3 Spectrometer layout for FCA core spectrum measurement

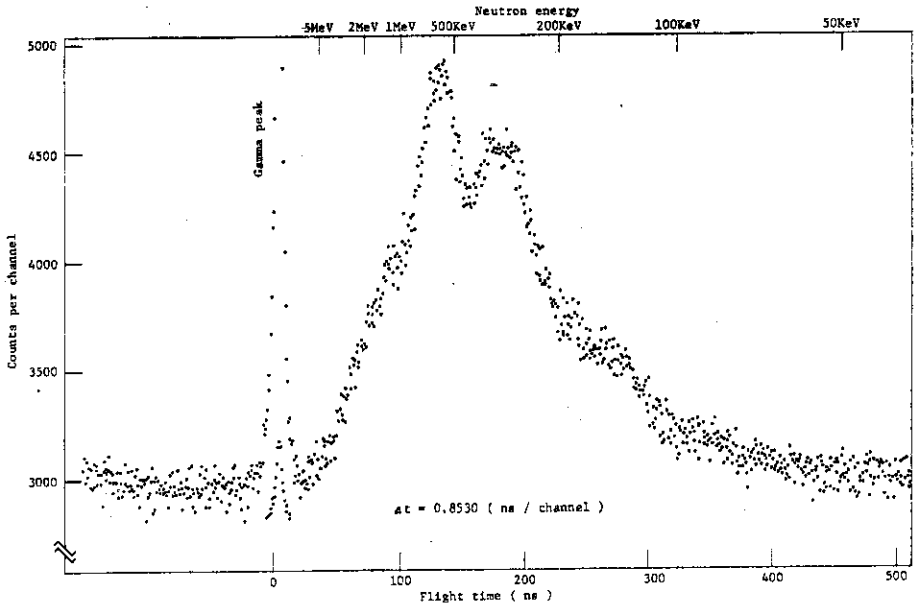

Fig. 6.12.4 Time-of-flight spectrum measurement on FCA Assembly VI-2

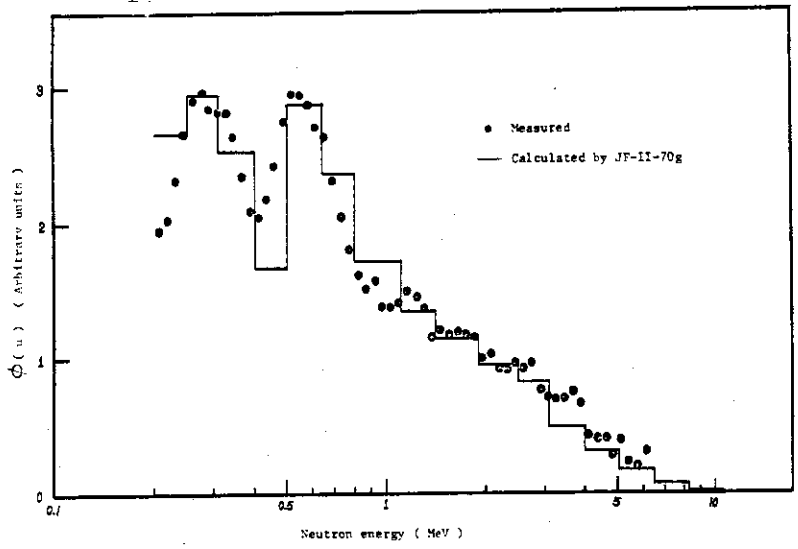

Fig. 6.12.5 Neutron spectrum at the core center of FCA Assembly VI-2

6.13 A High Resolution Cylindrical Proportional Counter for Neutron Spectrum Measurement in a Fast Critical Assembly

M. Ōbu, K. Shirakata and T. Ichimori

Compact proportional counters filled with hydrogen and with methane respectively have been constructed for measurements of fast neutron spectra in a fast critical assembly. Configuration of the electrodes is simplified by using a ceramic tube metallized on the surface, instead of the ordinary metallic tube[1]. Characteristics of the counter are compared with a counter having field tubes of a hypodermic needle type. The gas multiplication and the energy resolution in the counters were measured by $He^3(n, p)T$ reaction in filling gases. Pulse height distributions in counter responses to monoenergetic neutrons were obtained by using Van de Graaff accelerator.

Counter sizes and geometries are in Fig. 6.13.1. The methane gas was purified by a molecular sheave method. The contents of moisture and oxygen in the gas were 1 ppm after purification. The best values of the resolution (FWHM) are 3.8% and 6.5% for the hydrogen and methane counters of Type A, respectively. Resolutions in Type B are somewhat lower than Type A.

Gas multiplication saturation in counter response to monoenergetic neutrons (Gas multi.: 25) is shown in Fig. 6.13.2. The number of total electrons collected before saturation in gas multiplication occurs is about 2×10^5 when initial ionizations are highly localized. Gas multiplication saturation begins to occur above a certain value of the product of a critical gas multiplication and energy deposit[2]. The value of 14 MeV obtained from above experiments is considerably smaller than the method by obserbing the deteriorate of the resolution.

Field tubes made by metallizing ceramic seal surface are satistactory to remove recoil events in the volume defined by tubes. One of a demerit of the field tube with the hypodermic needle lies the creation of primary

ionization events at low gas multiplication due to the field tube uninsulated from the anode wire.

References

1) Ōbu, M., Ichimori, T., Shirakata, K.: JAERI-M 5466, Dec. (1973).

2) Hanna, G.C., Kirkwood, D.H., Pontecorvo, B.: Phys. Rev., 75, p.987 (1949).

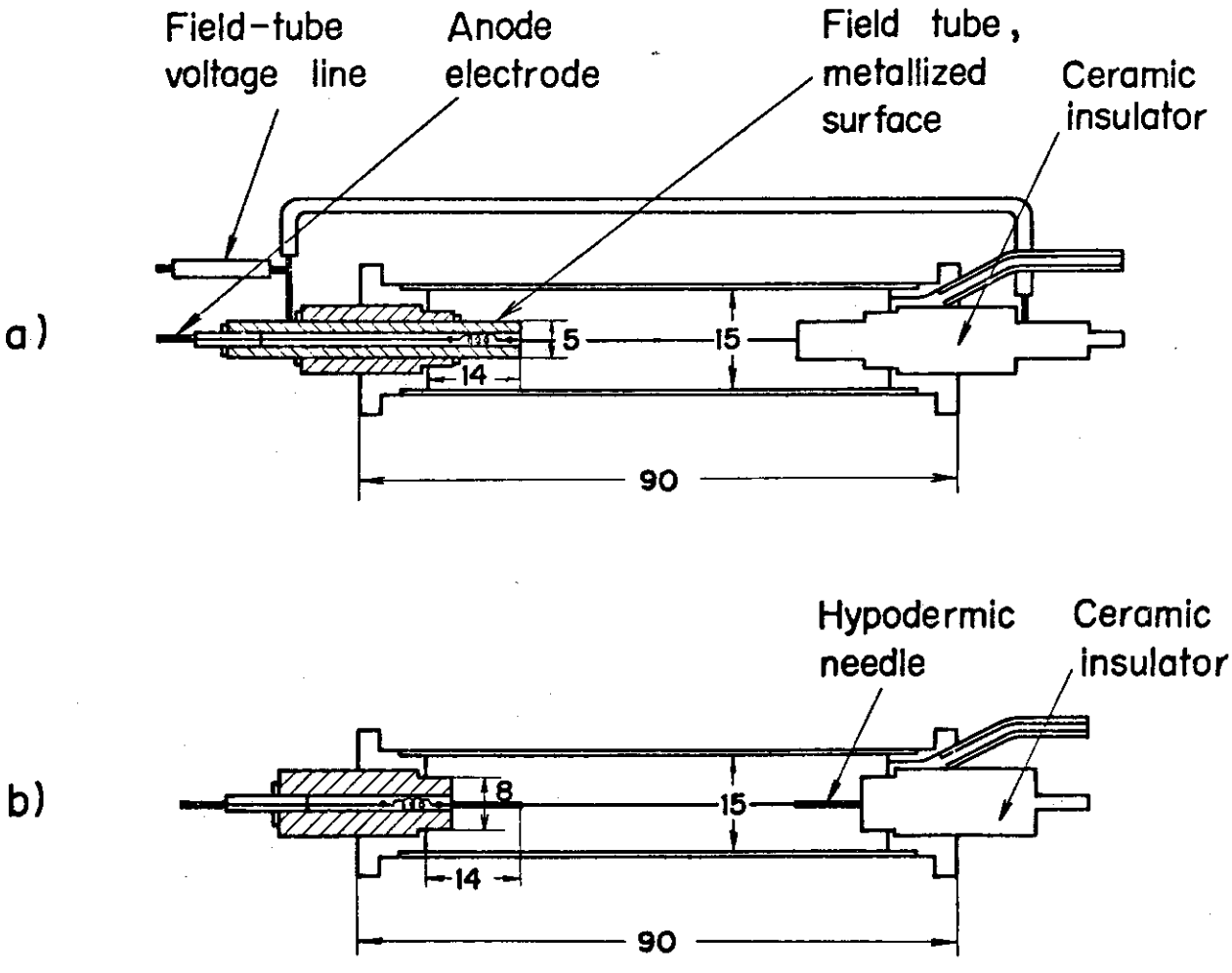

Hydrogen counter : 5.14 atm H_2, 0.258 atm CH_4, 19.1 mmHg He^3

Methane counter : 4.90 atm CH_4, 10 mmHg He^3

Fig.6.13.1 Counter sizes and geometries, a) Type A, b) Type B

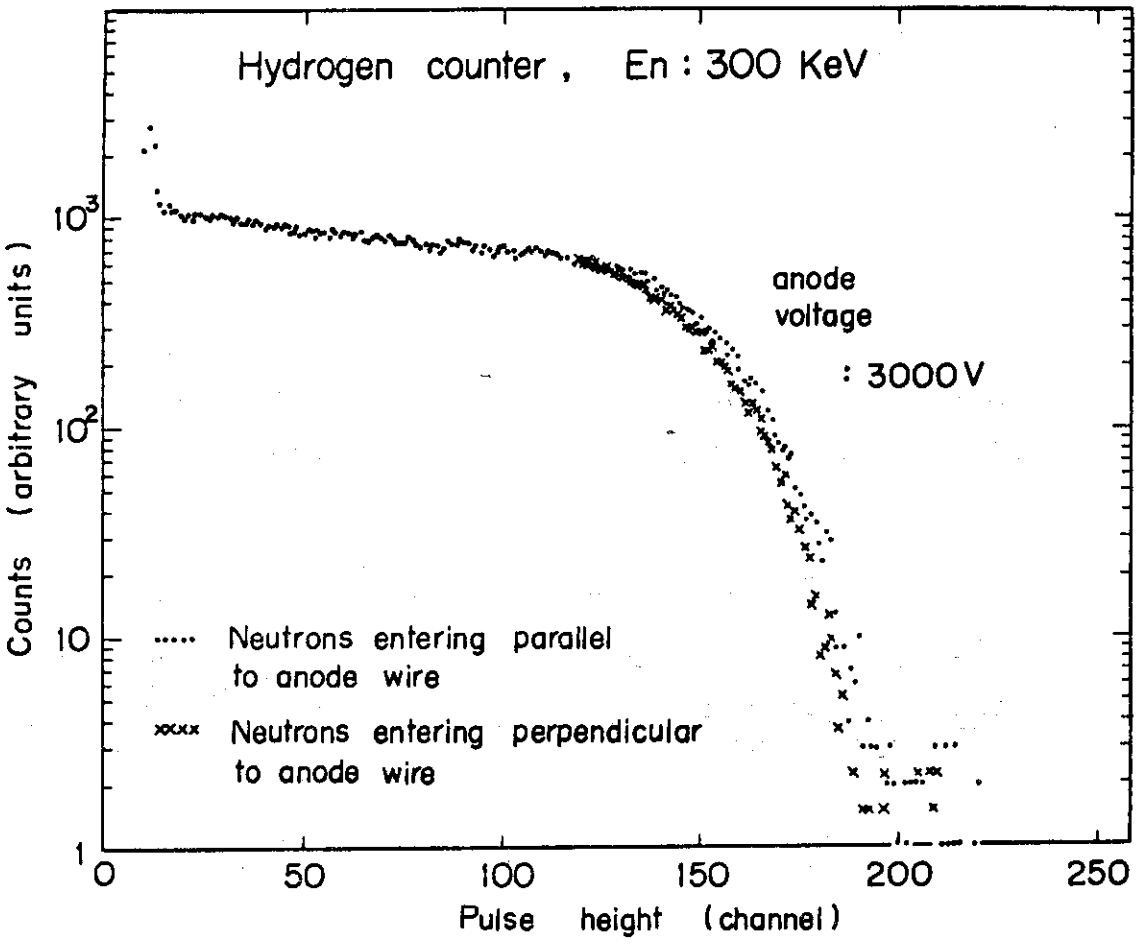

Fig.6.13.2 Pulse height saturation in counter response to monoenergetic neutrons (gas multi. : 47)

6.14 Mathematical Expressions Useful for the Evaluation of Radiation Source Strength and $^{47}Ti(n,p)^{47}Sc$ Cross Section Measurement

H. Gotoh and H. Yagi

Average Energy and Normalization Coefficient for Watt's Formula

Analytical expressions of the average energy $\overline{E}$ and the normalization coefficient C in the sense that

$$\int_0^\infty N(E)dE = 1$$

for the socalled Watt's formula

$$N(E) = C \cdot e^{-E/B} \cdot \sinh\sqrt{AE} \qquad (E \text{ in MeV}) \qquad (1)$$

on the energy distribution of fission neutrons were derived. The results are

$$\overline{E} = B \cdot \left(\frac{3}{2} + \frac{A \cdot B}{4} \right), \qquad (2)$$

and

$$C = \frac{2}{B\sqrt{\pi AB}} \cdot e^{-AB/4}. \qquad (3)$$

Self-Absorption of Gamma-Rays in a Cylindrical Sample

The knowledge on the ratio η of the unscattered gamma-ray flux from a cylindrical sample in the direction perpendicular to the axis of the sample to that from a source without self-absorption, is useful for estimating the total activity contained in the sample basing on data from gamma-ray intensity measurement. The authors derived an expression of single integral form for the ratio in cases where the distribution of the activity q(r) is represented as

$$q(r) = c + (1 - c) \cdot \left(\frac{r}{R} \right)^2 \quad \text{for } 0 \leq r \leq R. \qquad (4)$$

Here, R is the radius of the sample and c is the ratio q(0)/q(R). The result is

$$\eta = \frac{4}{\pi R\Sigma\cdot(1+c)}\cdot\left[\int_0^1 (1-e^{-2R\Sigma\sqrt{1-x^2}})\left\{1+\frac{1-c}{R^2\Sigma^2}\cdot(2R\Sigma\sqrt{1-x^2}+2)\right\}\cdot dx - \frac{\pi}{R\Sigma}\cdot(1-c)\right], \quad (5)$$

where Σ is the macroscopic cross section(cm^{-1}) of the sample material for the gamma-rays.

Activation Rate of a Cylindrical Sample by D-D Neutrons

If the center-of-mass differential cross section $d\sigma_c/d\omega_c(E_d,\mu_c)$ of d-d neutrons is assumed to be represented in the form

$$\left.\frac{d\sigma_c}{d\omega_c}\right|_{E_d,\mu_c} = \left.\frac{d\sigma_c}{d\omega_c}\right|_{E_d,1}\cdot[C_0+\mu_c^2\cdot\{C_2+\mu_c^2\cdot(C_4+\mu_c^2\cdot C_6)\}], \quad (6)$$

the activation rate Ψ(reactions/sec) of a cylindrical sample placed in axial symmetry on the forward direction of the d-d neutron source is given by

$$\begin{aligned}\Psi = 2\pi\cdot n_d\cdot N_d\cdot\left.\frac{d\sigma_c}{d\omega_c}\right|_{E_d,1}\cdot[&r\{C_0J_{10}(\mu_1,\mu_2)+C_2J_{12}(\mu_1,\mu_2)+C_4J_{14}(\mu_1,\mu_2)+C_6J_{16}(\mu_1,\mu_2)\}\\ &-s\{C_0J_{20}(\mu_1,\mu_2)+C_2J_{22}(\mu_1,\mu_2)+C_4J_{24}(\mu_1,\mu_2)+C_6J_{26}(\mu_1,\mu_2)\}\\ &+h\{C_0J_{20}(\mu_2,1)+C_2J_{22}(\mu_2,1)+C_4J_{24}(\mu_2,1)+C_6J_{26}(\mu_2,1)\}], \quad (7)\end{aligned}$$

where E_d is the energy of d^+ ions, μ_c is the cosine of the emission angle of neutrons in the center-of-mass system, r is the radius of the sample, h is the height of the sample, s is the shortest distance between the neutron source and the sample, n_d is the number of d^+ ions incident per second, N_d is the surface number density of deuterium nuclei in the D_2 target,

$$\gamma = \left(\frac{0.33456E_d}{E_d+6.538}\right)^{1/2}, \quad (8)$$

$$\mu_1 = \frac{\sqrt{1+(1-\gamma^2)r^2/s^2}-\gamma r^2/s^2}{1+r^2/s^2}, \quad (9)$$

$$\mu_2 = \frac{\sqrt{1+(1-\gamma^2)r^2/(s+h)^2}-\gamma r^2/(s+h)^2}{1+r^2/(s+h)^2}, \quad (10)$$

$$J_{1i}(x_1,x_2) = \int_{x_1}^{x_2} \mu_c^i \cdot \{1 + \frac{(\gamma+\mu_c)^2}{1-\mu_c^2}\}^{1/2} \cdot d\mu_c, \tag{11}$$

and

$$J_{2i}(x_1,x_2) = \int_{x_1}^{x_2} \mu_c^i \cdot \{1 + \frac{1-\mu_c^2}{(\gamma+\mu_c)^2}\}^{1/2} \cdot d\mu_c. \tag{12}$$

Measurement of $^{47}Ti(n,p)^{47}Sc$ Cross Section*

The activation cross section of the $^{47}Ti(n,p)^{47}Sc$ reaction at the neutron energy of 4.85 MeV was measured by irradiating a Ti-pellet with d-d neutrons from the JAERI 2.2 MeV Van de Graaff machine. The neutron flux at the sample position was monitored with an absolute neutron counter composed of a polyethylene recoil proton radiator and a silicon detector during irradiation. The result was 56.3 mb. This value is at least 15 mb smaller than the recent reported values by Meadows et al. and consistent with the evaluated values by Simons et al.

*This part of work was done in cooperation with I. Kimura and K. Kobayashi, Research Reactor Institute, Kyoto University.

6.15 PEX Network and Microcomputer System for TOKAI Online System

H. Yagi, K. Koyama, K. Asai, Y. Nakahara and T. Kumahara

An online data processing system, named TOKAI Online System, is being built in Tokai Research Establishment. The system is organized with an intelligent network (PEX Network) and various kinds of computers including the JAERI central computer, as shown in Fig.6.15.1. The network consists of packet exchange units (PEX) and communication lines connecting PEXs. Each PEX is programmed to store and forward messages to the neighboring PEXs in the network. Communication between PEXs is controlled by a pair of communication adapters (CA) through four twist pair communication lines. Two pairs are used for message transfer at 240k bps in synchronous mode, and other two pairs for control signal linking at 30k bps in asynchronous mode.

A microcomputer system (named Micro-8) was developed for PEXs and terminals connected to the PEX Network using a microprocessor, Intel 8080 or equivalent types. By a built-in microprocessor, the crate controller of CAMAC was enhanced to have an intelligent ability for online data acquisition, as shown in Fig.6.15.2. The crate controller was named CCM (Crate Controller with Microprocessor).

We are making a laboratory automation software system (JAERI LASS) for Micro-8 using the system writing language "GPL" developed for standardization of programming languages[1]. The framework of LASS has already been fixed, and I/O handling routines are prepared for all I/O devices of Micro-8 including interrupt processing routines.

Reference

1) Asai, K. : "GPL-Genken Programming Language," (in Japanese), JAERI-M 4762 (1972).

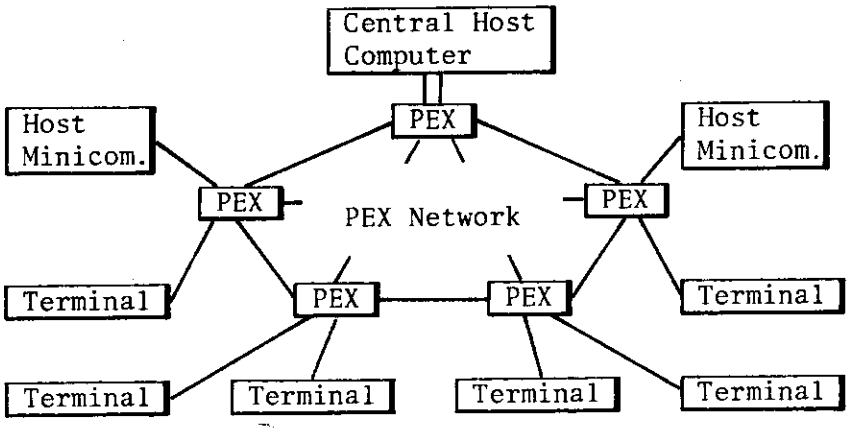

Fig.6.15.1 Configuration of TOKAI Online System

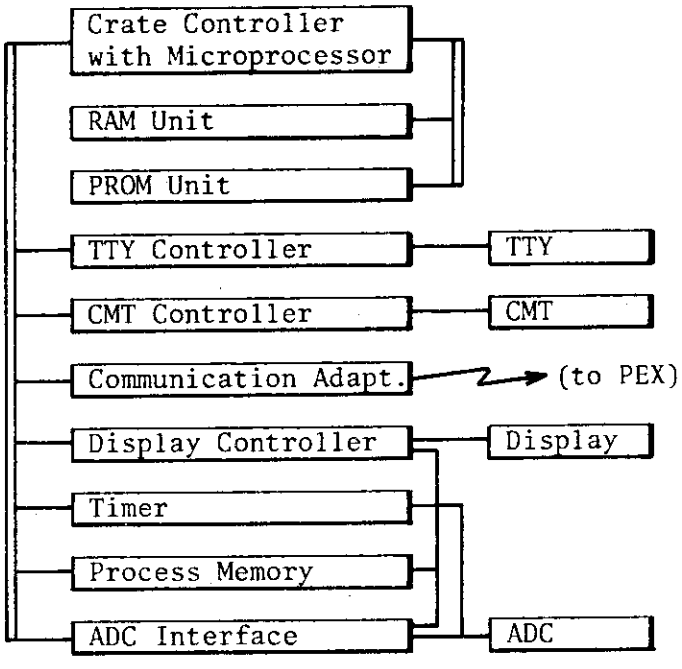

Fig.6.15.2 Typical CAMAC System

7. Dynamics Analysis and Control Method Development

7.1 Development and Study on the Control Methods for Nuclear Power Plants. -Application of a Linear Optimal Regulator.-

S. Mankin and Y. Shinohara

Now, nuclear power plants become large in the scale and have various purposes and complex characteristics. Considering the control performance in such aspects as utilities,load-following and safety, the optimal and safety control methods become more and more necessary for power plants.[1)]

However, there remain many problems for the application of the modern control theory to nuclear power plants, because of it's complex characteristics such as multi-variables and nonlinearities.[4)] Therefore, in order to use the modern control theory in practice and to realize a good performance in reactor plant control, we have been studying control methods, taking the case of the load-following control problem of the B.W.R. type reactor plant.

At the beginning, in order to obtain and discuss the conceptual design of the control system, we studied the dynamics of a B.W.R. power plant by means of analog computer simulation useing the 20-dimensional linear model. Results of the simulation study show that the change of re-circulation flow rate is effective in improving the performance of the load-following control and that the necessity of appling modern control theories is very important for solving the problem systematically.[2)] Then, we examed the application of such synthesis method as maximum principle, dynamic programming and serch-programming methods. From the results of the examination, we think that the application of L.Q.O.R.(Linear Optimal Regulator with Quadratic Performances.) is simple and easy method for solve the problem of load-following control in nuclear power plants. In this method, however, there are also many problems at the time of the application, for examples, the problem of the nonlinearity

in the object plant, the problem of the application of the regulator theory to the follow-up control, and the problem of control deviation at the case of step input. For solving or improving these problems, we modified the linear optimal regulator approach, that is, we constructed the controller based on the standard technique of the linear regulator applied to the linearized model of the plant and then modified by adding appropriate integration type action using variable gain and references.

Computer simulation suggests that this method improves the performance of the controller that is designed from the standard technique of the linear optimal regulator, relating to the problem existed in the difference between the model and the object and in the control deviation caused by the step disturbances. And we will be able to say that the linear optimal regulator technique, with simple modification mentioned above, may be easily applied to the load-following control of nuclear power plants.[4) 5)]

References

1) "Dynamic Analysis and Control of Nuclear Reactor Plant." 1974,1975 Annual Report of Electric Engineering. Electric Soci.of Japan. p.446.

2) Mankin,S and Shinohara,Y.:"Load following Control of Nuclear Power Plant -part.1-" 1971 Annual Meeting of the A.E.S.of Japan. D-46.(1971)

3) Mankin,S and Shinohara,Y.:"Synthesis methods and Problems about Load following Control for Nuclear Power Plant." JAERI memo 5420.(1973)

4) Mankin,S and Shinohara,Y.:"Load following Control of Nuclear Power Plant." 1974 Fall Meeting on Reactor Physica and Engineering of A.E.S.of J. C-36.

5) Mankin,S and Shinohara,Y.:"On the Application of Linear Optimal Regulator Technique to Control of Nuclear Power Plant." Journal of N.S.T. vol.17 No.11 (1975) [to be published.]

7.2 Software Development in The Computer Control of a Boiling Water Test Loop. - Dynamic Analysis, Development of Control Methods, and Computer Code Programming.-

S.Mankin, Y.Fujii, M.Hara and JMTR OWL-0 computer control group.

The computerized operating system of the OWL-0 (Oarai Water test Loop-No.0) had been constructed for the basic study of the computer control of power reactors in future.[1)2)] The software in the computer control has been also developed. When the project was started, dynamic analysis and simulation study of the inherent characteristics of each sub-system in OWL-0 was examined using analog computer firstly.[3)] And, the program of automatic sequence and the program of on-line caliculation were coded in machine languages.[4)5)6)] Quasi-optimal parameters of each P.I.D. control loop were sought by a search programming method, and were examined in the performance of the sampling control in the simulation study using E.A.I. hybrid computer.[7)] Considering the experience in the operation of OWL-0 and the result of the simulation study, the computer-code for control use was made, and the program SMERT and the program of operator console necessary for running the computer system were coded.[8)] These codes have been debagged, improved, and modified after the stage of construction.

Since the main object in the first step of the project was the automation by the computer system, the control method used in the system was established, based on simulation study. After the completion of the computerized system of OWL-0 , the new control methods have been studied and developed by applying the modern control theory and techniques to the OWL-0 system. The experiment of dynamic analysis was performed for estimating the accuracy of the dynamics model which was used in the simulation study.[9)] A new hierarchical control method was proposed. Concerning the new method, identification experiments for obtaining OWL-0 system model are carried out in Nov.11,1974. Synthesis and

evaluation of the control system have been tried out using the computer simulation. The results of the simulation show that the hierarchical control scheme proposed has faily well performance in comparison with the conventional one using sub-loop controllers only, though it is not strictly the optimal control method. [10][11]

References

1) Hara,M.(Ed.)"Technical Development of Computerized Operation of Water Test Loop." Reactor Engineering Div. Annual Report. JAERI-M5955.p156.

2) Hra,M.(Ed.)"Technical Development of Computer Control of OWL-0", JAERI-M 5844.(1974)

3) Mankin,S.,Nomura,Y.:"Dynamic Analysis for Computer Control of OWL-0." JAERI memo 3834. 1970 Annual Meeting of the A.E.S.of Japan. B-34.

4) Fujii,Y.,Yonekawa,I.:"JMTR OWL-0 Computer Control Programme Development." JAERI memo 3953 (1970)

5) Nomura,Y.:"On-line caliculation in the OWL-0 Computer Control." JAERI memo 4314.,1971 Annual Meeting of the A.E.S.of Japan. D-69.

6) Akutu,O. and Saruta,T.:"Design of OWL-0 Computer Control-Operation Program." 1971 Annual Meeting of the A.E.S.of Japan.D-68.

7) Mankin,S.:"Design of OWL-0 Computer Control.-Control Parameter.-" Ibid. D-70., JAERI memo 4683.(1971)

8) Fujii,Y. and Yonekawa,I.:"Design of OWL-0 Computer Control.-Operator Console.-" 1971 Annual Meeting of the A.E.S.of Japan.D-67.

9) Mankin,S.:"Dynamic Analyses and Experiments on OWL-0 for Computerized Control." JAERI-M 5336. (1973)

10) Mankin,S. and Fujii,Y.,et al.:"Experiments for improve the control Methods of OWL-0." JAERI memo 6079.,1975 Fall Meeting of the A.E.S.

11) Mankin,S. and Fujii,Y.,et al.:"A Hierarchical Control Method for Nuclear Power Plant." Journal of N.S.T. [to be published.]

7.3 Analysis of the Complex Plant Dynamics based on the Identification Technique - Application to OWL-0 Plant

R. Oguma, Y. Fujii, M. Hara and JMTR OWL-0 Computer Control Group

A method of analysing the complex plant dynamics based on the identification technique was proposed and applied to the characteristic analysis of the OWL-0 (Oarai Water Loop 0) plant dynamics. Namely, a series of identification experiments were carried out, and the time series data of observed variables obtained through these experiments were analysed by this method. Consequently, some significant characteristics of the OWL-0 plant dynamics which had not been clarified by various operating experiences performed and results analysed in earlier days, were derived by this analysis.

The way of formulating a mathematical model based on the physical laws and of executing the numerical analysis using a digital and/or analog computer is very popular as a method of dynamic system analysis up to this time. As the system becomes more complex, however, the mathematical model becomes extremely complex, so numerical analysis sometimes could not be executed without some assumption for the model reduction. Thus, when using this conventional method much works would be often needed to fabricate the mathematical model and to develop the computer code for the numerical analysis rather than to derive the distinguished characteristics about the plant dynamics.

A method of analysing the plant dynamics based on the identification technique proposed here is to apply linear system theory to the multidimensional dynamic system model obtained from the plant identification, to transform this model into the various forms(i.e. frequency and step response function and so forth), and to derive some main characteristics of the plant dynamics from these transformed functions.

These analyses are executed according to the following process using

the computer code:

1. Correlation and spectrum analysis;
   General understanding of the relation among the observed variables, and selecting the variables necessary to the analysis.
2. Autoregressive model fitting;
   Model fitting to the variables which are selected in accordance with the correlation and spectrum analysis.
3. Transformation into the step and frequency response function;
   Calculation of the step and frequency response function using an identified model and quantitative evaluation of the relation among the variables.
4. Evaluation of the model fitness;
   Comparison betwee estimated outputs calculated from the identified model and the experimental data.

A series of identification experiments were carried out and the analysis were executed in accordance with the process described above. A block diagram of the OWL-0 plant is shown in Fig. 7.3.1 and step response functions calculated from the identified model are shown in Fig. 7.3.2 ~ Fig. 7.3.6. From these response functions, the following characteristics of the OWL-0 plant dynamics can be derived; that is,

1) The manipulated variable CV12 (or CV13) has a characteristic of the reverse action to the separator level L1.
2) The separator level L1 has an inclination to saturate in response to the CV12 (or CV13) valve manipulation.
3) The plant pressure P2 is severely influenced by CV12 and CV13 valve manipulation.
4) The main cooler system is independent of other components.
5) The condenser cooler system undergoes complicated influence from some other components; i.e. main cooler, pressure regulator and so on.

Especially the characteristics of the items 3) and 5) mean the

existence of intense interaction among the components. These newly found effects should be noticed with great care when the control systems are designed and actualy used in this plant. According to the OWL-0 plant identification, the model of analysing the plant dynamics proposed here is found to be a very effective means to extract the general characteristics of the plant dynamics as a whole when applied to the complex plant. Moreover effective informations about the possibility of the system decomposition and about the qualitative evaluation of the conventional control systems are easily obtained through these analysis.

References

1) Oguma, R., Fujii, Y., Usui, H. and Watanabe, K.: "Computer Code MLCOSP for Multiple-Correlation and Spectrum Analysis with a Hybrid Computer," JAERI-M 6252 (1975).

2) Oguma, R. and Fujii, Y.: "Identification of OWL-0 Plant and Evaluation of its Control Systems," Preprints of the 14th SICE Conference (1975).

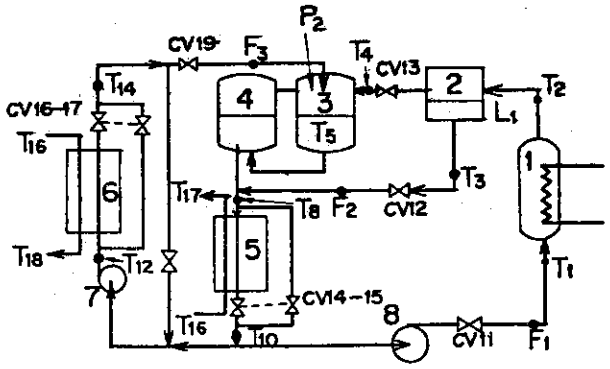

Fig. 7.3.1 Block diagram of the OWL-0 plant
1.Steam generator 2.Separator 3.Jet condenser
4.Surge tank 5.Main cooler 6.Condenser cooler
7.Condenser loop pump 8.Main loop pump

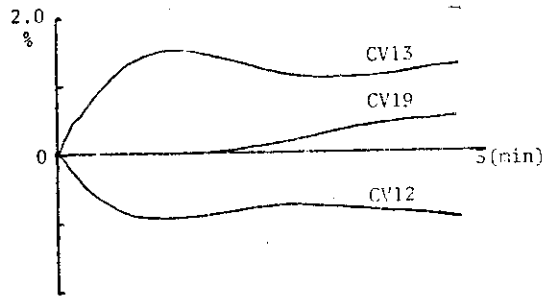

Fig. 7.3.2 Step response of separator level L1 from manipulated variables

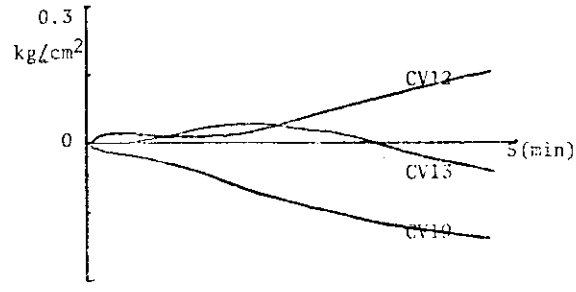

Fig. 7.3.3 Step response of pressure P2

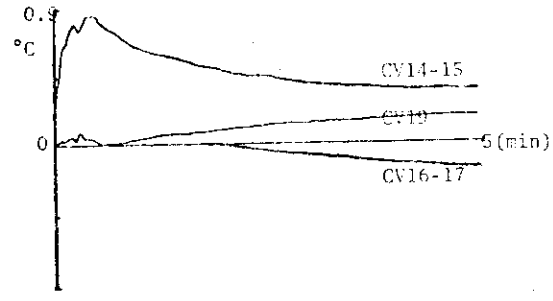

Fig. 7.3.4 Step response of main cooler outlet temperature T10

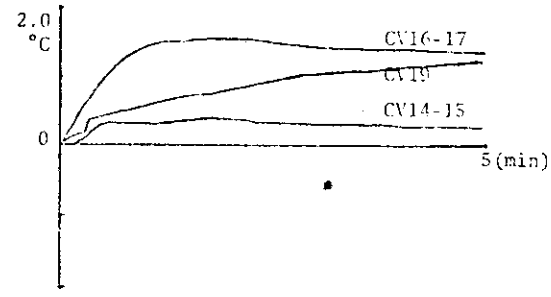

Fig. 7.3.5 Step response of condenser cooler outlet temperature T14

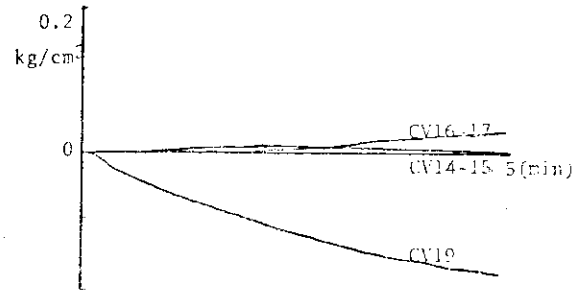

Fig. 7.3.6 Step response of pressure P2

8. Fusion Reactor Technology

8.1 Measurements of $^{238}U/^{235}U$ Fission Ratio Distribution in Spherical Hybrid Blanket Assemblies

H. Maekawa and Y. Seki

To investigate the neutronics in the fusion-fission hybrid reactor blanket, the distributions of $^{238}U/^{235}U$ fission ratio were measured in two types of hybrid Assemblies. The spherical hybrid assemblies with and without a graphite reflector are prepared by piling up lithium, natural uranium and graphite blocks in the same manner as in the previous experiments.[1),2)] A vertical cross section of the spherical hybrid assembly is shown in Fig. 8.1.1. Effective outer radii of the central cavity, natural uranium, lithium metal and graphite regions are 3.5, 10.0, 34.1 and 55.3 cm, respectively.

The 42 energy group neutron cross sections[1)] were prepared from ENDF/B-III data file by SUPERTOG code using 1/E as the weighting function. The neutron flux distribution in the spherical hybrid assemblies was calculated by the one-dimensional transport code ANISN with P_5-S_8 approximation.

The calculated results of tritium breeding ratio in the hybrid and lithium metal assemblies are summarlized in Table 8.1.1. Symbols T_6 and T_7 mean tritium breeding ratio through $^6Li(n,\alpha)T$ and $^7Li(n,n'\alpha)T$ reaction, respectively. The total tritium breeding ratio is close to unity in the hybrid assembly with graphite reflector which has a lithium region only 24 cm thick.

The experimental results of fission ratio distribution in

the hybrid assemblies with and without a graphite reflector are shown in Fig. 8.2.2 with the calculated curves.

In the assembly without a graphite reflector, the shapes of measured fission rate distribution are in fairly good agreement with those of calculation, however, there is a large difference between the measured fission ratio and calculated one. In the assembly with a graphite reflector, the measured fission ratio agrees fairly well with the calculated one except in the graphite region. These results are considerably different from the results of the previous experiments.[2] This discrepancy may be caused by the change of neutron spectrum due to the fast fission. Further analysis is being carried out.

References

1) Hiraoka, T., et al.: "Integral Experiments on a Spherical Lithium Metal Blanket System," Nucl. Fusion Special Suppl. 1974, Proc. Symp. Fusion Reactor Design Problems, p. 363, I.A.E.A. (1974).

2) Maekawa, H., et al.: Nucl. Sci. Eng. 57, 335-380 (1975).

3) Seki, Y., et al.: "Analysis of Fission Ratio Distribution in Spherical Lithium Metal Assembly with a Graphite Reflector," JAERI-M 6220 (NEACRP-L-136) (1975).

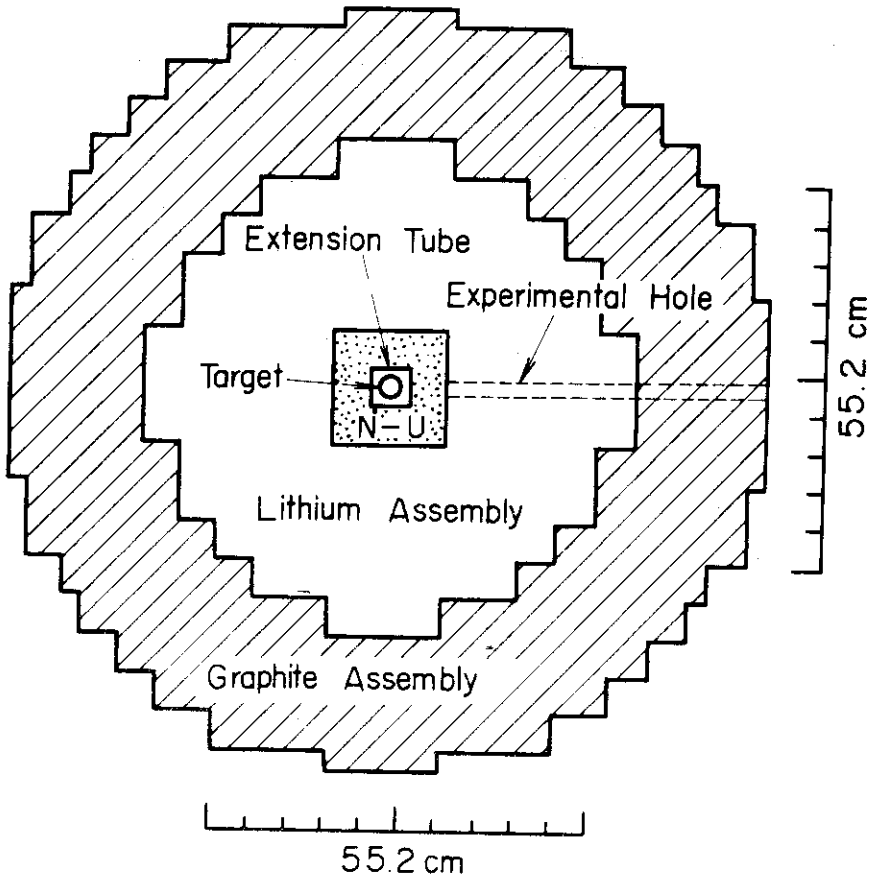

Fig. 8.1.1 Vertical cross section of the spherical hybrid assembly

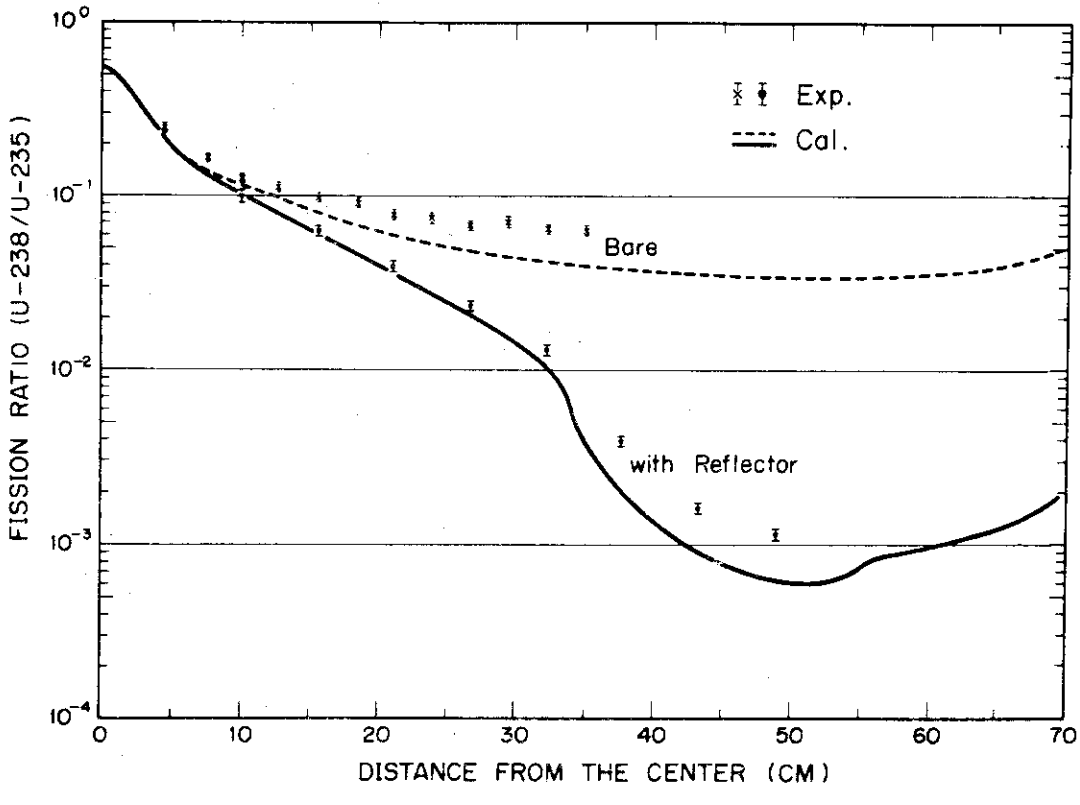

Fig. 8.1.2 Fission ratio distribution in the hybrid assemblies

8.2 A Method for Obtaining the Tritium Production Rate Distribution with a LiF Thermoluminescence Dosimeter

H. Maekawa

The measurement of tritium production rate distribution in a lithium blanket is an important subject in the neutronics experiments of fusion reactor blanket. A method for measuring the tritium production rate with a LiF thermoluminescence dosimeter (TLD) has been proposed taking note of the following facts: (1) LiF TLD contains lithium atoms in itself. (2) The half-life of tritium is 12.6 years and those of other induced radioisotopes to be expected are short enough. (3) Thermoluminescence in a TLD disappears by means of the annealing.[1)]

The TLD method is as follows: Some LiF TLD's covered with a pyrex glass are irradiated in a lithium blanket assembly. They are left for a few days in a storage where the background radiation especially that of neutron is very small. After annealing, they are left again for several days to a few months in the storage to be self-irradiated by tritium in the TLD. Thermoluminescence of TLD is read out. Then, the tritium production rate can be estimated.

The preliminary experiment was carried out at FCA. A new ^{6}LiF and ^{7}LiF TLD's were placed at the center of FCA VI-3 assembly. After irradiation, the energy of induced gamma rays from TLD's were measured by a Ge(Li) semiconductive detector. The energy spectrum is shown in Fig. 8.2.1. As main radioisotopes, ^{18}F and ^{24}Na were confirmed to exist in the TLD after the irradiation of fast neutrons. Measured decay curves of ^{18}F and ^{24}Na are shown in Figs. 8.2.2 and 8.2.3, respectively. They

should be produced by the reaction of $^{19}F(n,2n)\ ^{18}F$ and $^{24}Mn(n,p)\ ^{24}Na$. The LiF TLD contains a very small amount of magnesium. Other radio-isotope except for tritium could not be detected.

The data of ^{6}LiF irradiated by FCA are summarized in Table 8.2.1. W_H and T_H mean the integrated reactor power and self-irradiation time, respectively. The efficiency of self-dose was not considered in the calculated values. The dose of ^{7}LiF was almost equal to the back-ground. The calculated tritium production from ^{7}Li was three decades smaller than that from ^{6}Li. It was shown that the dose of the TLD was proportional to W_H and T_H. Therefore, the dose of LiF was caused by the radiation from tritium. Thus, the TLD method is feasible for the measurement of tritium production.

Reference

1) Maekawa, H. : "A Method for Obtaining the Tritium Production Rate Distribution with a LiF Thermoluminescence Dosimeter," JAERI-M 6055 (1975) (in Japanese).

Table 8.2.1 Data of ^{6}LiF irradiated by FCA

Sample NO.	W_H	T_H	Exp.	Cal.	C/E
565	65.2 W·hr	171 hr	18.9 mR	0.934 R	49.4
		665.5	73.1	3.64	49.8
		1271	144	6.96	48.3
560	16.7 W·hr	171 hr	4.4 mR	240 mR	54.0
575		665.5	20.4	933	45.7
		1271	40.8	1.78 R	43.7

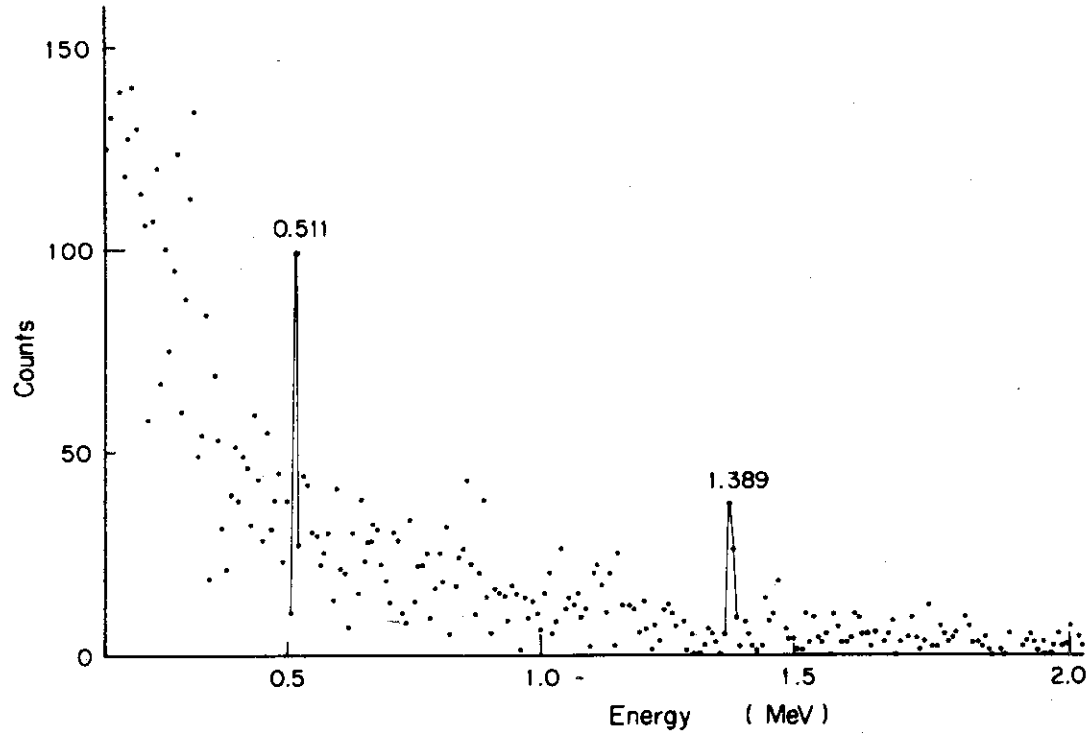

Fig. 8.2.1 Energy spectrum of gamma rays from LiF TLD after irradiation of fast neutrons

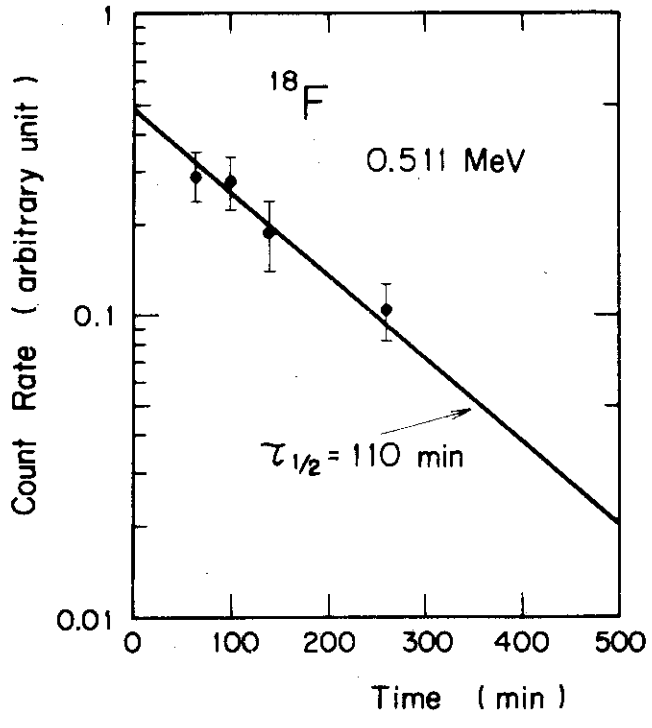

Fig. 8.2.2 Decay curve of 0.511 MeV gamma rays

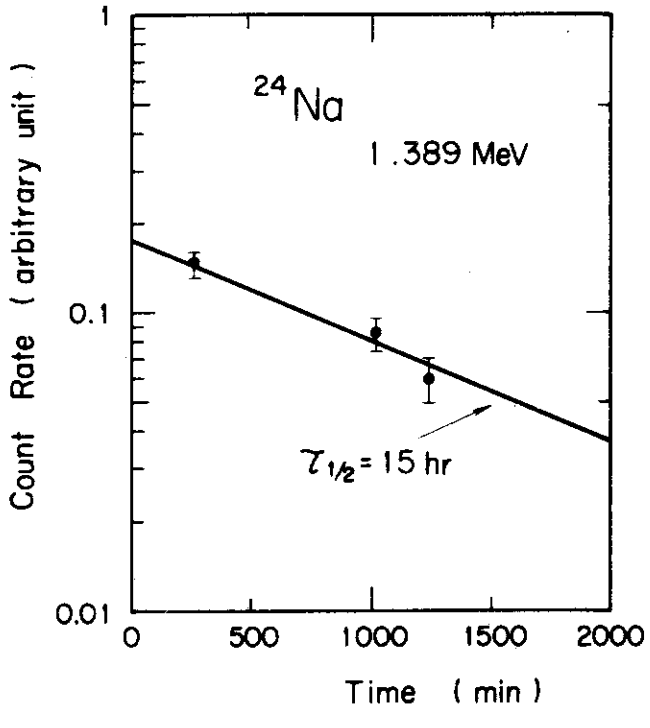

Fig. 8.2.3 Decay curve of 1.389 MeV gamma rays

8.3 Neutronics Calculation for Fusion Reactor Blanket

Y. Seki and H. Maekawa

Some improvements in the calculational method in the fusion reactor blanket neutronics have been achieved. The MACK[1] code for the calculation of neutron KERMA factors and the LAPHAN[2] code for the secondary gamma production cross section from ENDF/B have been converted for use in the computer FACOM 230/75. A graphic plotter code APPLE[3] which gives three dimensional plotting of the neutron and gamma-ray fluxes calculated by ANISN, and which also plots reaction rates has been developed.

Validity of the S_N approximation which is used for neutronics calculation of fusion reactor blankets is confirmed[4] by comparing the calculated tritium breeding ratio in the benchmark model with the recommended one[5].

The analysis of $^{238}U/^{235}U$ fission ratio distribution in the spherical lithium metal assembly with a graphite reflector is carried out[6]. Detailed calculation of the fission ratio is performed employing refined methods and with various calculational models. It is concluded that the cause of the discrepancy between experiment and calculation is most likely the uncertainties of the nuclear data of the constituents elements of the assembly.

References

1) Abdou, M.A., Maynard, C.M., Wright, R.Q.: ORNL-TM-3994, Oak Ridge National Laboratory (1973).

2) Dudziak, D.J., Bosler, G.E.: LA-4963 (ENDF-182), Los Alamos Scientific Laboratory (1973).

3) Seki, Y., Narita , H., Igarashi , M.: to be published.

4) Moriyama , M., Seki, Y., Maekawa, H.: JAERI-M 6072 (1975).

5) Steiner, D., Blow, S.: CLM-p.345, Culham Laboratory (1973).

6) Seki, T., et al.: JAERI-M 6220 (NEACRP-L-136) (1975).

8.4 JFT-2 Plasma X-ray Spectrum Measurement Using Si(Li) X-ray Spectrometer

E.Sakai, H.Terada, M.Katagiri, N.Suzuki*, K.Maeno* and N.Fujisawa*

Electron temperature measurements using a Si(Li) X-ray spectrometer have been carried out in Japan Fusion Tokamak No.2 (medium-beta-value torus experimental apparatus). Electron temperatures were deduced from the slopes of X-ray spectra obtained by the spectrometer. The first experiment was performed in April, 1974 and the second in February, 1975.

The spectrometer system used in the second experiment is shown in Fig.8.4.1. The Si(Li) detector ($30mm^2$ x 3mm) has an entrance window of 1/3 mil (8.4 μm)thick beryllium and shows 167 eV FWHM energy resolution for 5.9 keV X-rays from Fe-55 at 12 μsec time constant of the amplifier. The output of the amplifier was carried to the ND-50/50 multichannel analyser by a 400 m cable (RG-65/U) from the JFT-2 Building to the Room No.109 of the Research Laboratory Building No.2. The ND-50/50 was modified to operate as a two-dimensional analyser of (8 x 512) channels; the eight channels correspond to the predetermined periods, Δt_1, Δt_2, ..., Δt_8, which is about 1/8 of the plasma sustaining period of about 100msec. Each 512 channel records each X-ray pulse height distribution obtained in each of the predetermined periods.

An example of experimental results is shown in Fig.8.4.2; the above picture shows an oscilloscope trace of the plasma current and one-turn voltage. The below shows the electron temperatures deduced from X-ray spectra obtained from the Si(Li)detector measurement. The electron temperatures from the Si(Li)detector and from the laser scattering were not inconsistent with each other while the former gave averaged values in space and the latter gave the values for the center of the plasmas. The future experiments are planned to compare the results obtained by the two methods.

A part of the measurements was reported at the 30th Annual Meeting of the Physical Society of Japan held at Kyoto University on April 2, 1975[1].

Reference

1) Suzuki,N., Maeno,K., Fujisawa,N., Sakai,E., Katagiri,M and Terada,H.: " Soft X-ray Measurement in JFT-2 ", The 30th Annual Meeting of Physical Society of Japan, Paper 2pC6, at Kyoto University, April 2, 1975, SDG-75007 (in Japanese)

---

* JFT-2 Group, Thermonuclear Fusion Laboratory, Tokai Research Establishment, J.A.E.R.I.

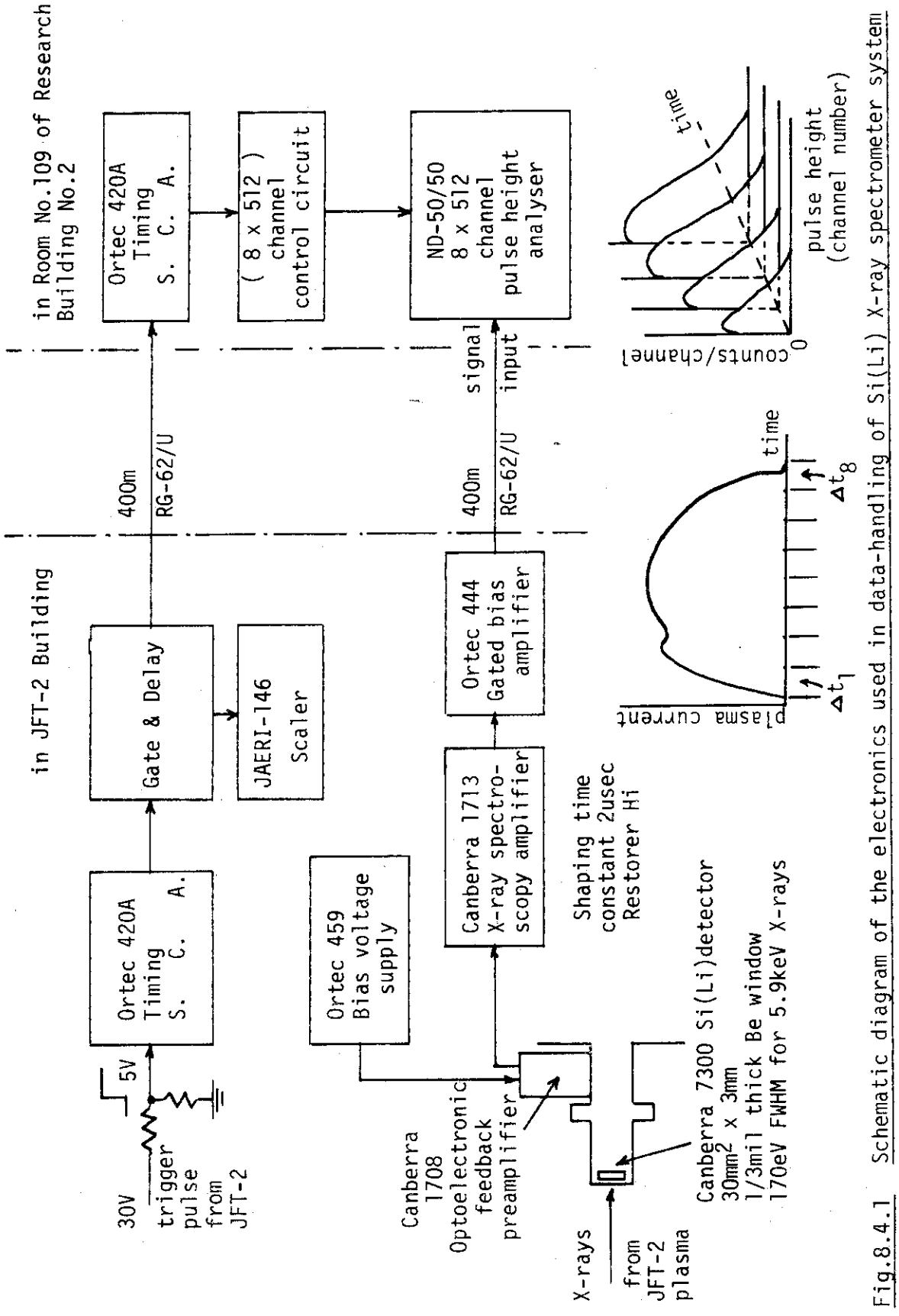

Fig.8.4.1 Schematic diagram of the electronics used in data-handling of Si(Li) X-ray spectrometer system for JFT-2 plasma electron temperature measurement

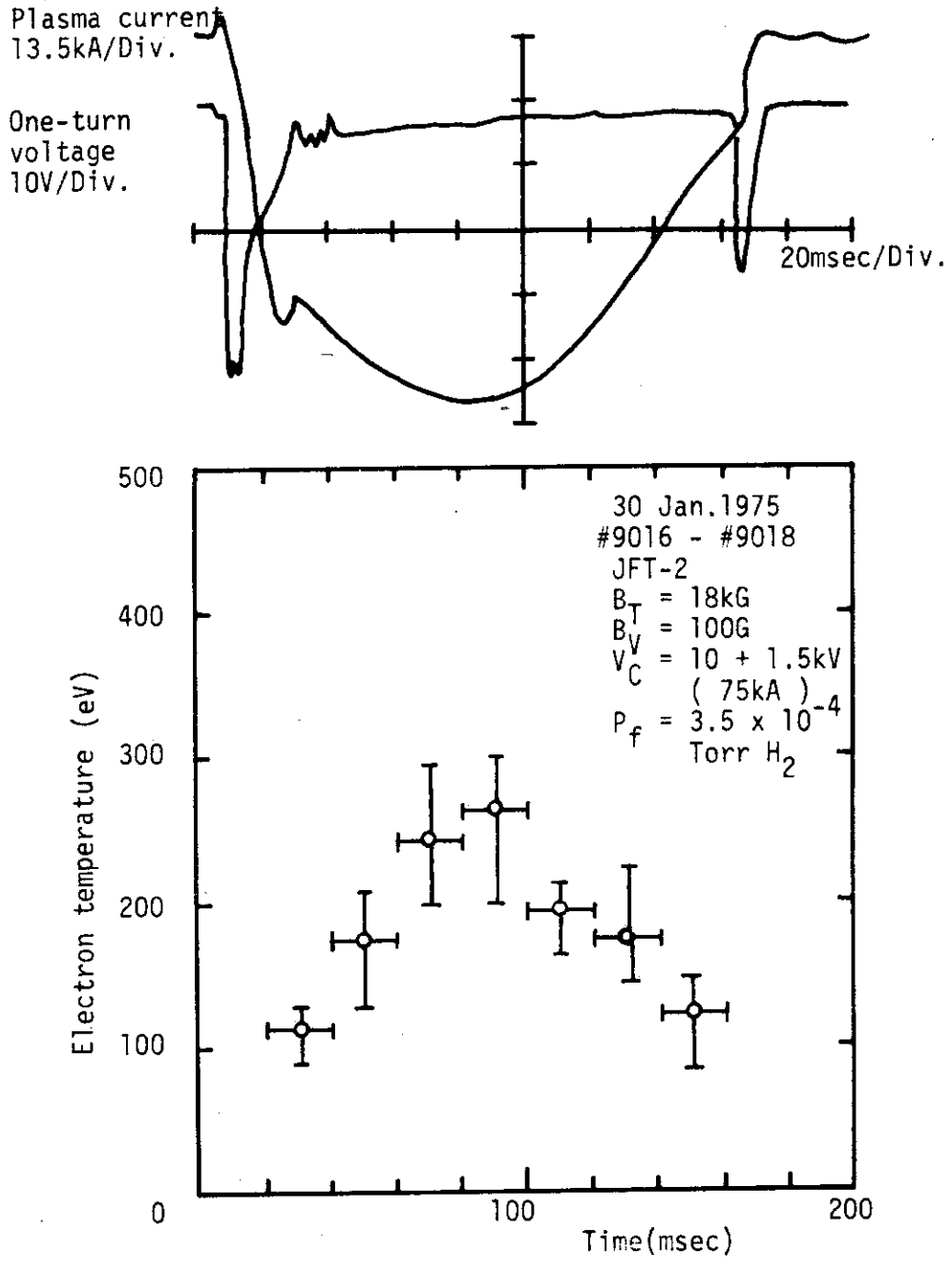

Fig.8.4.2 Plasma current waveform and electron temperature deduced from X-ray spectra

8.5 A Kinetics Model Simulating the Horizontal Displacement of a Toroidal Plasma Column

Y.Kambayashi and M.Hara

A kinetics model was constructed which simulates the horizontal displacement of a toroidal plasma column in system of the Tokamak type. The model is made up of some basic equations, that is, the equation of the motion of plasma column and those of the circuit currents which couple each other and with the plasma current.

The equations defining the conditions of equilibrium of a toroidal plasma column are the pressure-balance equation in the minor radius of the column and the equation describing the changes in the major radius of the column.

The pressure-balance can be considered as a balance between the plasma pressure, and the magnetic pressure of the toroidal field and that of the field generated by the plasma current. It was assumed in the model that the pressure-balance equation is always satisfied.

The equilibrium of the plasma column position can be considered as a balance between the expansive force due to the pressure of the magnetic field of the plasma current and the plasma pressure, and the inward force due to the interaction of the plasma current with the vertical magnetic field which is externally applied and/or generated by the current excited in the conductors at the time of plasma motion.

The equation of the motion of plasma column was considered on the assumptions that a plasma column has a circular cross-section and that the asymmetry of field distribution in the column cross-section resulting from toroidality is small.

When considering the circuit current equations, the magnetic fields and the inductances were calculated on the assumption of a cosinusoidal

current distribution in the circular cross-section coaxial with the plasma column.

The model was applied for a numerical code FLIC which calculates the frequency characteristics and for a anlogue simulator which analyzes the time response. With the numerical code and the analogue simulator, the characteristics of the apparatus JT-60 were investigated and some typical results are presented in Fig.8.5.1 and 8.5.2.

Fig.8.5.1 shows the frequency characteristics of the plasma column position to the vertical magnetic field and Fig.8.5.2 shows the time response of the plasma column position and those of circuit current at the time of 1% step change of the vertical magnetic field. The intrinsic time constant of the conductor ν is used for the parameter.

The code is useful for the parametric survey of the frequency characteristics of apparatus and the simulator serves effectively for studying the motion of plasma column and for examining the performance of control systems of plasma column position.

References

1) V.S.Mukhovatov, V.D.Shafranov: "Plasma Equilibrium in a Tokamak", Nuclear Fusion 11, 605(1971).

2) M.A.Leontovich: "Reviews of Plasma Physics, vol.2", Consultants Bureau, New York (1966).

3) J.Hugill, A.Gibson: "Servo Control of Plasma Position in CLEO-Tokamak", CLM-P382 (1974).

Fig. 8.5.1
Frequency Characteristics
Disturbance (δBd/Bvco)
⟶Plasma Position (δR/R0)

Γ_0 = 2.2

G = - 0.8

τ_ℓ = 0.03

τ_v = 1.0
0.5
0.2

τ_t = 5.0

FIG. 8.5.1-C
VECTOR DIAGRAM

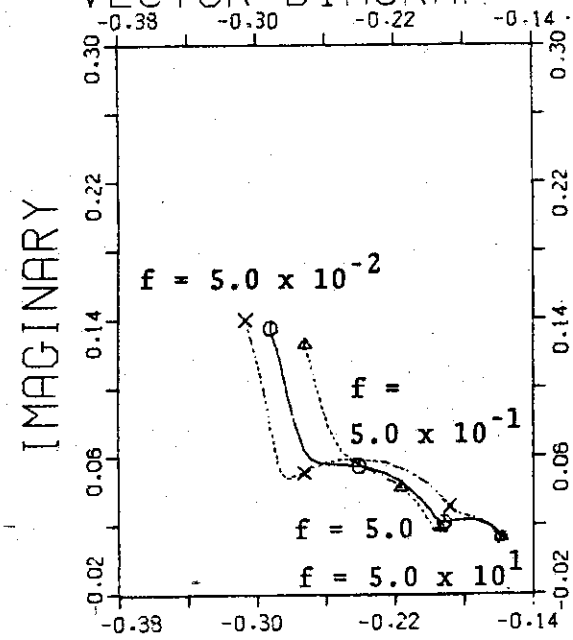

Y.KAMB

FIG. 8.5.1-A BODE DIAGRAM (GAIN)

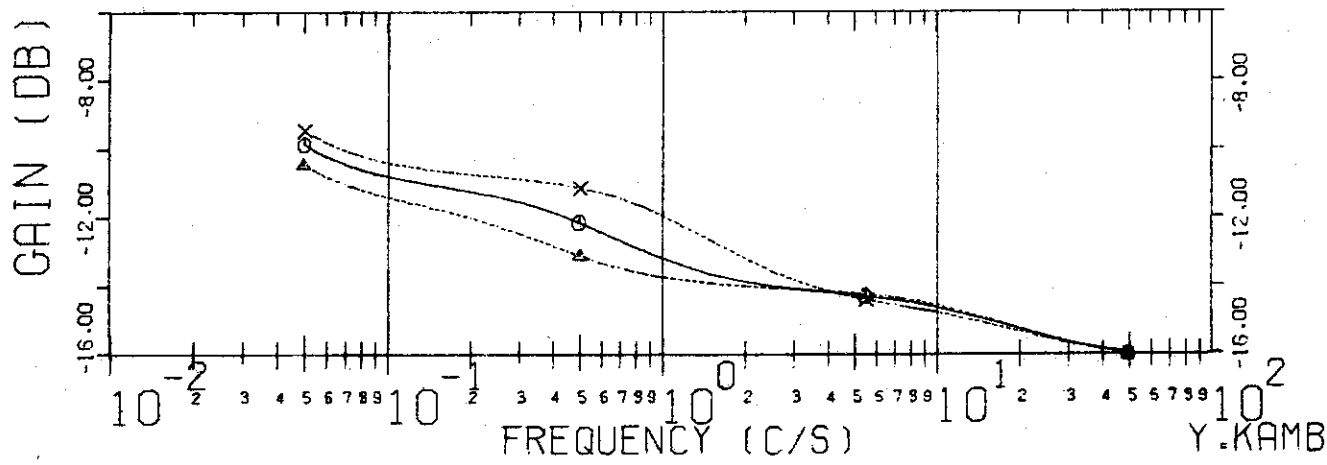

Y.KAMB

FIG. 8.5.1-B BODE DIAGRAM (PHASE)

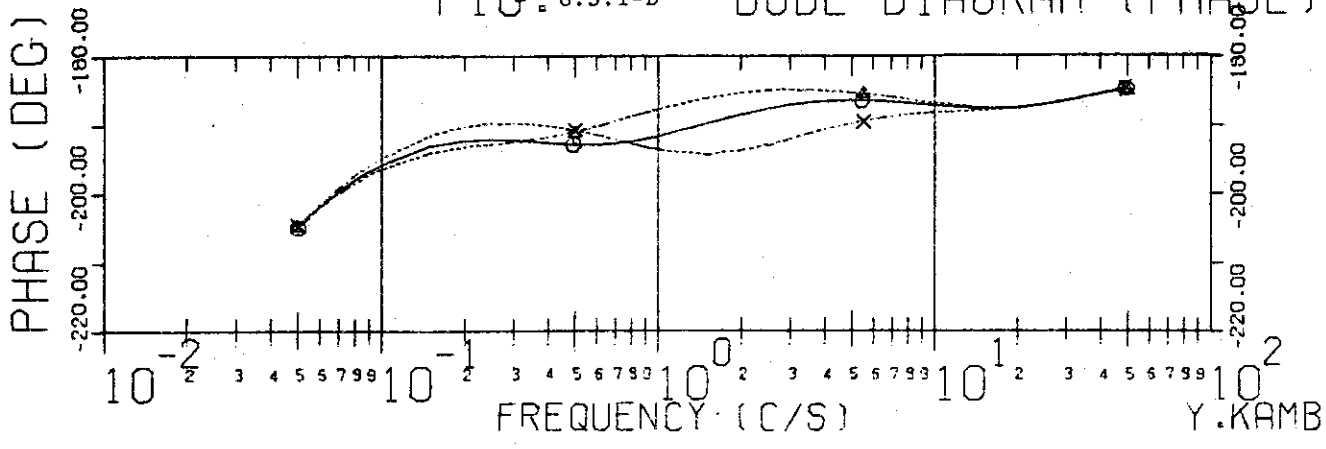

Y.KAMB

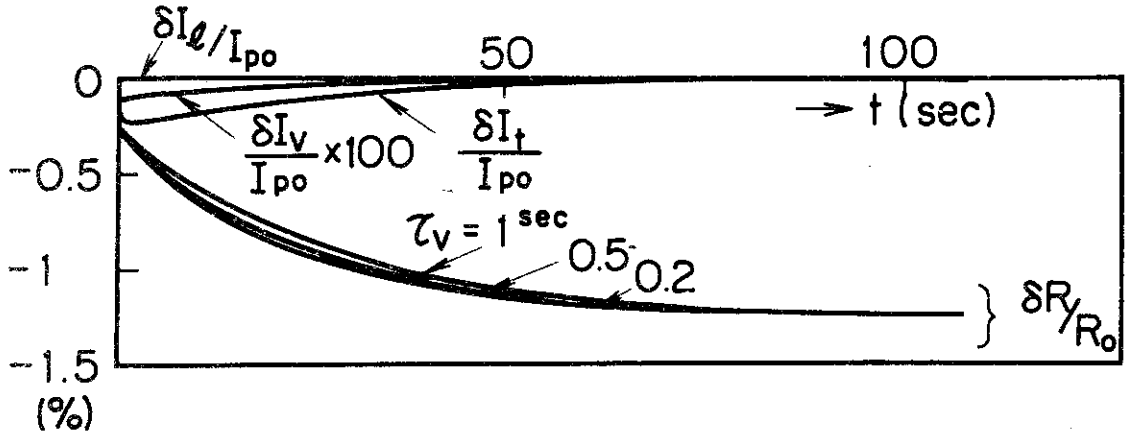

Fig. 8.5.2 Time response of plasma position to 1 % step change of virtical field
$\Gamma_0 = 2.2$ $G = -0.8$ $\tau_\ell = 0.03$ $\tau_f = 5.0$

8.6 Macroscopic Cross Sections for Analyzing the Transport of Neutrals in Plasma

T. Suzuki, Y. Taji and Y. Nakahara

An analysis of the transport of neutrals in plasmas is a fundamental problem concerned directly with the heating of plasmas and the diagnosis of the plasma ion density and temperature.

The present work intends to develop numerical algorithms to calculate the cross sections required for analyzing the neutral transport in plasmas.

When the neutral particles are injected into a plasma for the purpose of plasma heating or they diffuse into a plasma as impurities, the transport of these neutrals can be analyzed by making application of neutron transport theory, as was first tried by Greenspan.[1)]

The reaction cross section in the neutral transport equation can be defined in a way similar to those used in neutron transport equation. The neutrals are ionized by plasma ions and electrons, or exchange their charges with plasma ions. The former reactions result in the loss of neutral particles. They can, therefore, be treated analogously to absorption reaction in neutron transport phenomena. In the latter charge exchange reaction there is no net change in the number of neutrals but the energy change. This reaction has, therefore, a close analogy with the energy transition scattering of neutrons.

The reaction rate of neutrals with plasmas can be generally expressed as

$$\Sigma_j(r,E,\Omega)\phi(r,E,\Omega) = \int_E^{E+\Delta E} dE' \int_{4\pi} d\Omega' |v-v'|$$

$$\times \sigma_j(Er) N_j(r,E',\Omega') \frac{1}{|v|} \phi(r,E,\Omega), \qquad (1)$$

where j stands for the type of interactions, E is the energy of neutral particles, $\phi(r, E,\Omega)$ is the neutral flux, $\sigma_j(Er)$ is the microscopic reaction cross section[2] of neutrals with energy Er corresponding to the relative velocity of $|v-v'|$ and $N_j(r,E', \Omega')$ is the plasma density distribution.

We assume that the plasma distribution is isotropic and has a Maxwellian distribution.

In our algorithm, the integration of Eq. (1) is performed by expanding the integrand with the use of polynomials. A computer code has been made, which prints out calculational results in the FIDO format.

References

1) Greenspan, E. : "The Calculation of the Transport of Nuclear Atoms in Highly Ionized Plasmas Using Neutron Transport Methods," MATT-1001 (1973).

2) Riviere, A.C. : "Penetration of Fast Hydrogen Atoms into a Fusion Reactor Plasma," Nuclear Fusion 11 (1971).

8.7 Analysis of Neutral Particle Transport in Torus Plasma by Monte Carlo Method

S. Inoue, T. Suzuki, Y. Taji, Y. Nakahara, T. Asaoka and J. Hirota

The torus geometry is peculiar to a fusion reactor of the Tokamak type. However, because of a difficulty in analytical or numerical treatment of such a complex geometry, it is generally approximated by the cylindrical geometry in applying existing neutron transport theories to the analysis of the neutral particle transport in torus plasmas. Although this approximation may hold well for a torus with a large aspect ratio, it is necessary to estimate an error introduced by this and numerical approximations used in solving the transport equation.

The Monte Carlo method is the most powerful one for this purpose. Accordingly, we have incorporated the torus geometry routine into the Monte Carlo code MORSE.[1),2)] In addition, a subprogram has been built in it for analyzing flights paths of particles in the torus geometry.

The ionization and charge exchange reactions of neutral particles are treated, respectively, analogously to the absorption and scattering (or fission) reactions of neutrons. The spatial distribution of neutral particle density and neutral particle balance have been calculated with the use of the following model:

i) Uniform distribution of the cold neutral source (of the energy of 3 eV) on the torus surface,

ii) Two energy groups for neutrals (3 eV and 20 eV),

iii) Ten medium and geometrical regions,

iv) Plasma characteristics remains unchanged throughout the reactions, and under the following approximate conditions:

i) Ion temperature $Ti(r) \equiv 20$ eV, Electron temperature $Te(r) = 200[0.9(1-r^2/a^2) + 0.1]$eV,

ii) Plasma density $n(r) = n(0)[0.8(1-r^2/a^2) + 0.2]$ with $n(0) = 3 \times 10^{13}/cm^3$. The results are shown in Fig. 8.7.1 and Table 8.7.1 for some examples. It is remarkable that the aspect ratio (R/a) has a large effect upon the neutral particle balance. (See Table 8.7.1) It is seen that in the cylindrical approximation the leakage and ionization of primary neutral particles are much underestimated for the present case of a = 14 cm. A great difference is also seen in the balance depending on whether the source has the finite thickness or not. However, the distribution of neutral particles shows no such differences for these source conditions.

References

1) Straker, E.S., et al. : "The MORSE code – A Multigroup Neutron and Gamma-Ray Monte Carlo Transport Code," ØRNL-4585 (1970).

2) Irving, D.C., et al. : "An Amplification of Selected Portions of the Ø5R Monte Carlo Code User's Manual," ØRNL-TM-2601 (1969).

Table 8.7.1 Neutral Particle Balances (%)

Group	Reaction	R=50 cm	80 cm	200 cm	1000 cm	1000 cm *	Cylinder *
2	Leakage	19.43	22.45	28.32	32.13	16.89	16.61
	Ionization	56.95	55.00	51.27	48.82	58.39	58.83
	Charge Exch	23.62	22.55	20.41	19.05	24.73	24.56
1	Leakage	12.83	12.52	11.41	10.80	14.13	13.84
	Ionization	10.78	10.03	9.00	8.25	10.60	10.72

* Thick Source (13.65-14.0cm)

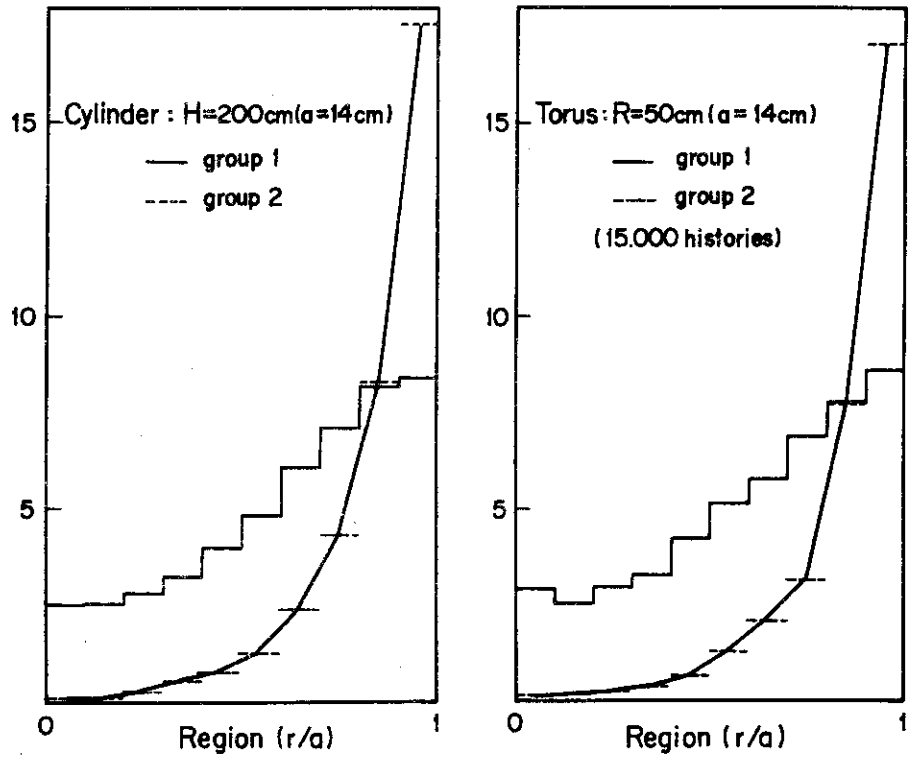

Fig. 8.7.1 Neutral Particle Density Distribution

8.8 Spherical Implosion after the Anomalous Heating by a Laser

S. Katsuragi and Y. Ishiguro

For qualitative understanding of spherical implosion in target plasma, which is induced by laser absorption, a computer program has been developed. We assume : Before a strong spherical shock reaches a spherical shell at r , the plasma is at rest and its density is given by $a r^{-\omega}$, where a and ω are constants. The equation of continuity and the equations for conservation of momentum and energy are rewritten using dimensionless velocity V , density R , pressure P and a dimensionless parameter λ , which defines the similarity line.[1),2)]

From the above, we obtain ordinary differential equations for dimensionless temperature Z , λ and R as follows:[1),2),3)]

$$\frac{dZ}{dV}=\frac{Z\left\{\begin{array}{l}\left[2(V+1)+\nu(\gamma-1)V\right](V+\delta)^2-(\gamma-1)V(V+1)(V+\delta)\\ -\left[2(V+1)-K(\gamma-1)\right]Z\end{array}\right\}}{(V+\delta)\left[V(V+1)(V+\delta)-(K+\nu V)Z\right]}, \quad (1)$$

$$\frac{d\ln\lambda}{dV}=\frac{Z-(V+\delta)^2}{V(V+1)(V+\delta)-(K+\nu V)Z}, \quad (2)$$

$$(V+\delta)\frac{d\ln R}{d\ln\lambda}=\left[-S+(k-\nu+3)V\right]-\frac{V(V+1)(V+\delta)-(K+\nu V)Z}{Z-(V+\delta)^2} \quad (3)$$

, where δ determines the similarity line $\lambda=\frac{br}{|t|^{\delta}}$ and is a constant to be determined, and K is a constant.

For obtaining a proper integral curve in (Z , V) plane, we must find singular points which represent any boundary condition or initial conditions. The computer

program finds the coordinates of these singular points and determines types of any singular points found. That is, the program examines if the point is a node, a saddle or a center point.

Because Z is not necessarily a single-valued function of V, the determination of the integral curve, which starts from a given point near any singular point, cannot be made by any usual procedure such as the Runge-Kutta formula. Finding the next point on the integral curve, we use the tangential line and the curvature. The latter is defined by the first and second order derivatives, and the second order derivative is defined through Eq. (1). The program finds in turn the proper next point on the integral curve, considering various combination of the tangential line and the curvature. A typical example is shown in Fig. 8.8.1.

References

1) Sedov, I.I. : "Similarity and Dimensional Methods in Mechanics", Academic Press, New York (1959).

2) Oswatitsch, K., Kuerti, G. : "Gas Dynamics", Academic Press, New York (1959).

3) Hayes, W., Probstein, R.F. : "Hypersonic Flow Theory", Academic Press, New York and London (1959).

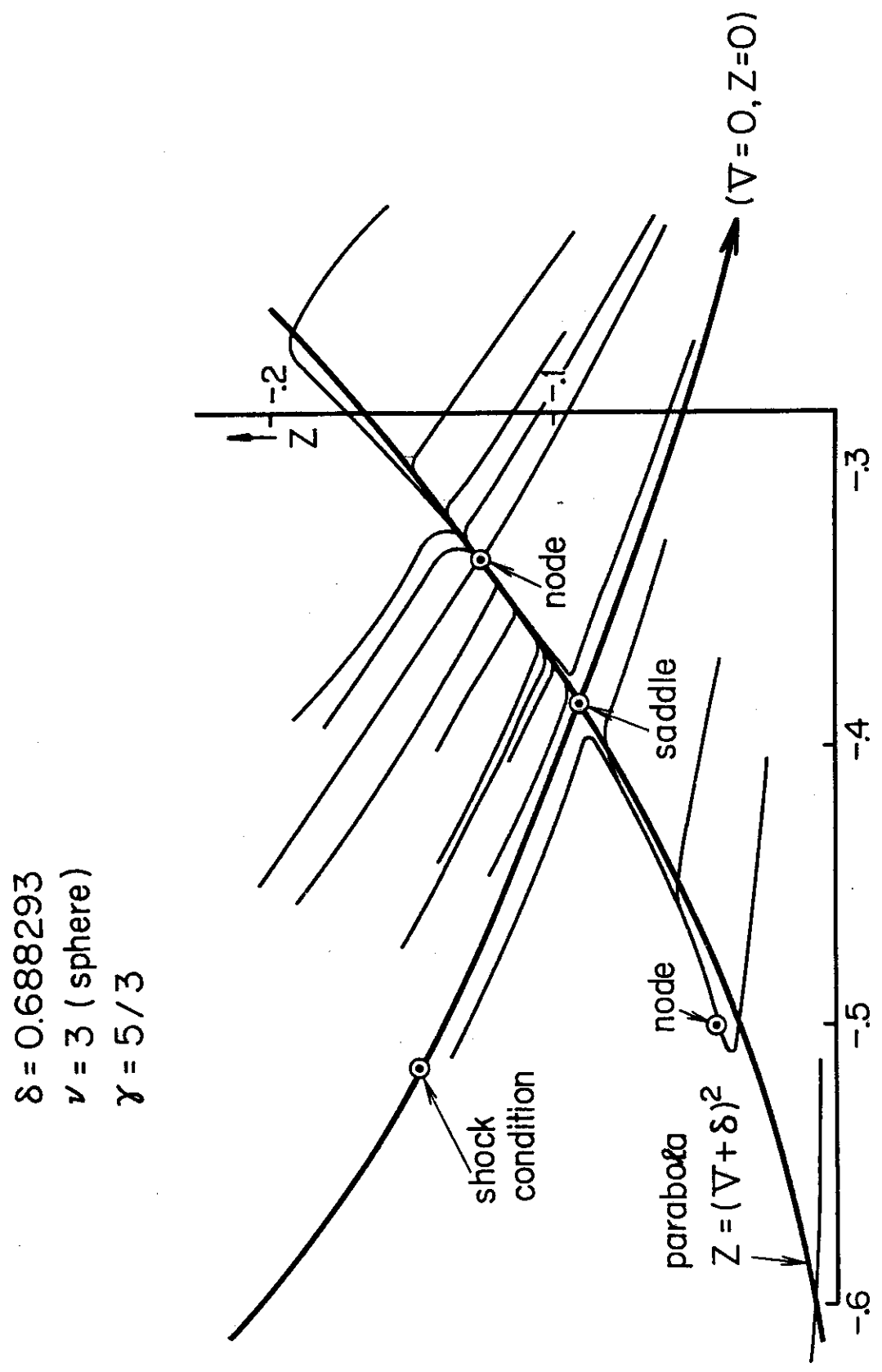

Fig. 8.8.1 The family of integral curves for ν=3, δ=0.6883, γ=513

8.9 Heat Transfer of Liquid Metal in a Magnetic Field

K. Sanokawa, H. Kawamura, M.Seki and Y. Shiina

Visual Study of Boiling Mercury in a Magnetic Field

It was found in a previous study[1] that boiling sound of liquid metal became continuous and frequency of wall temperature fluctuation became high with application of a magnetic field. These facts suggest that the bubbling is encouraged when a magnetic field is applied. So, an experiment was made in which boiling of mercury was obserbed.

A small amount of mercury was filled and boiled in a chamber with windows. The depth of the mercury was 2-3 mm. It was heated from the bottom. Figure 8.9.1 shows the boiling of mercury with and without a magnetic field. The heat input is same for the both pictures. Figure 8.9.1 indicates that the boiling is facilitated with the application of the magnetic field. The reason is being studied, and an additional experiment is in preparation.

Experimental Studies on Natural Convection of Mercury in a Magnetic Field

Experiments on natural convection heat transfer of mercury in a magnetic field have been carried on.

The apparatus is shown in Fig.8.9.2. The magnetic field was applied parallel to the heat transfer surface.

Following results were obtained.

1. The heating surface temperature was slightly affected

by the application of magnetic field.

2. Effects of magnetic field on fluid temperature were significant. When the magnetic field was increased at a constant heat flux, the fluid temperature decreased and had a minimum around 0.4 Tesla. Beyond 0.4 T, the temperature increased with increasing magnetic field.
3. The fluid temperature showed the fluctuation in the natural convection regime without magnetic field. When a weak magnetic field was applied, the fluctuation was suppressed at lower heat fluxes and the fluctuation became vigorous at heat fluxes higher than 70 W/cm^2. This vigorous fluctuation was observed only within a certain range of magnetic field intensity, and the fluctuation suppressed completely with application of higher field intensity.

Reference

(1) Kawamura, H. et al.: J. Nucl. Sci. Technol., 12-5, 280 (1975).

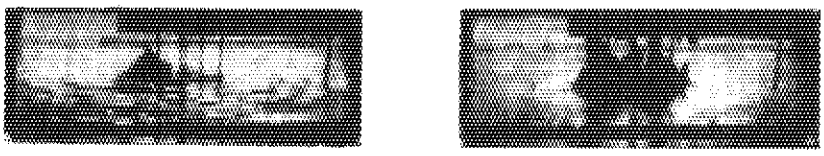

(a) (b)

Fig. 8.

	(a)	(b)	
Magnetic field	0	1.5	Tesla
Heat flux	49	49	W/cm^2

Fig. 8.9.1. Boiling of mercury with and without magnetic field

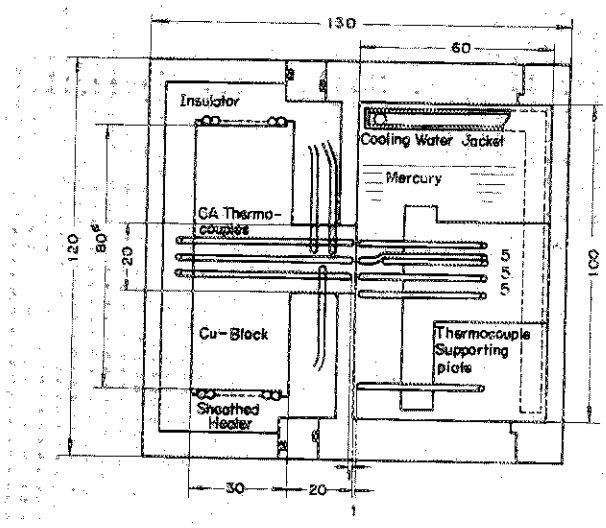

Fig. 8.9.2. Experimental apparatus of natural convection of mercury in a magnetic field

9. Activities of Computing Center

9.1 Computer Network for Radiation Measurement

M. Ishiguro, T. Yamada, Y. Nakahara, H. Yagi and K. Koyama

A computer network system shown in Fig. 9.1.1 has been developed to aid the rapidly growing laboratory works of gamma-ray spectrum measurement. The system is characterized by the hierarchical structure shown in Fig. 9.1.2. The whole system can be operated from any component in levels (A), (B) and (C).

Two terminal control programs JRSSP and JTCSP were newly developed for the minicomputer FACOM U-200.

The JRSSP is a general purpose terminal station program for the control of remote station (B) and possesses the function of data relay between the center host computer and plural data entry terminals. The program is operated under a disk based real-time monitor.

The JTCSP is a terminal control program operated under a core based realtime monitor, and is manipulated from experimenters' terminal (C) with interactive computer use. The main function of JTCSP is data taking from multi-channel pulse height analysers. The terminal (C) is also used as an independent small computer for data taking and program editing.

Reference

1) Yamada, T., et al.: "Computer Network for Radiation Measurement," Proceedings of Programming Symposium, Hakone, Jan. 1975, P.283-297 (in Japanese).

9.2 Graphic Subroutine Library PGSLIB and its Application

Y. Nakamura and Y. Onuma

Introduction

A plotter-compatible graphic subroutine library, PGSLIB bas been developed for FACOM 230-60 computer and FACOM 6233A graphic display. PGSLIB is a useful programming tool for interactive computer graphics using graphic display.

Functions of PGSLIB

PGSLIB has about 150 graphic subroutine instructions written in FACOM GSP. These instructions are classified into three packages, i.e., PGS, simplified GSP and general GSP. The functions of these packages are as follows:

(1) PGS: This package enables graphic programming in the same way with the plotter programming, as described in the last annual report [1].

(2) Simplified GSP: This package has been made from simplified FACOM GSP. Therefore, the package can display graphic figures on the CRT, and erase the displayed figures from the CRT. Moreover, it can process man-computer interaction using the CRT, lightpen and keyboards.

(3) General GSP: This package has various graphic instructions. These are graphing, lightpen-smoothing, two-dimensional drawing, three-dimensional drawing, interactive text processing, interactive computing, etc.

Application of PGSLIB

Using PGSLIB, some 30 graphic systems have been developed for the various fields in JAERI. A part of these systems was described in the last annual report. New 12 systems are indicated in Table 9.2.1.

References

1) Y. Nakamura, Y. Onuma: "Graphic Subroutine Package PGS and its Application," Reactor Engineering Division Annual Report (April 1, 1973 to March 31, 1974) (1975).

Table 9.2.1 Summary of New Graphic Systems

System	Description
GRAY-I	Analysis system of energy and directional dependence of absorbed dose due to external exposure. The absorbed dose is displayed with respect to latitude and longitude variables.
GRAY-II	Extended version of the GRAY-I system; interactive processing using lightpen and keyboard has been added.
ARCADIA-III	Interactive cross section data adjustment system. In the system, adjustment data can be entered by lightpen, keyboard and card reader.
GAME	Operations training system for graphic display. It enables playing a game and training operations of graphic display.
GTOROTO-III	Seismic simulation analysis system for block-type fuel HTGR core. It displays HTGR core in vertical view, and many parameters for displaying can be changed by lightpen and keyboard.
GTOROTO-IV	This system has the same functions with the GTOROTO-III system except that HTGR core is displayed in plan view.
GROSA-I	Interactive data analysis system for ROSA-II. It displays experimental data obtained from ROSA-II, and parameters for data correction can be changed by lightpen and keyboard.
GROSA-II	Improved version of the GROSA-I system; data scaling method and interactive processing method been improved.
GSTACK-I	Gamma ray response analysis system. It displays gamma ray response at any point along the vertical or horizontal direction of stack gas monitor for each nuclide.
GSTACK-II	Extended version of the GSTACK-I system; interactive processing using lightpen and keyboard has been added.
GTOROTO-V	This system has the same functions with the GTOROTO-III system except that HTGR itself and its core are displayed together.
GROSA-III	Extended version of the GROSA-II system; treatment for the newly included data channels has been added.

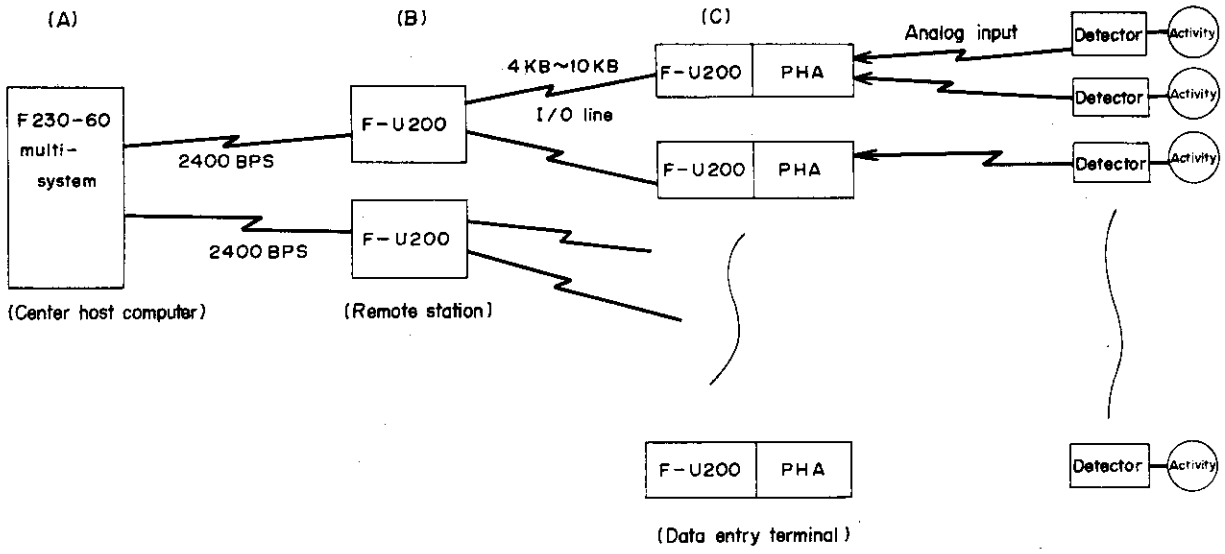

Fig. 9.1.1 Gamma-ray spectrum measuring system

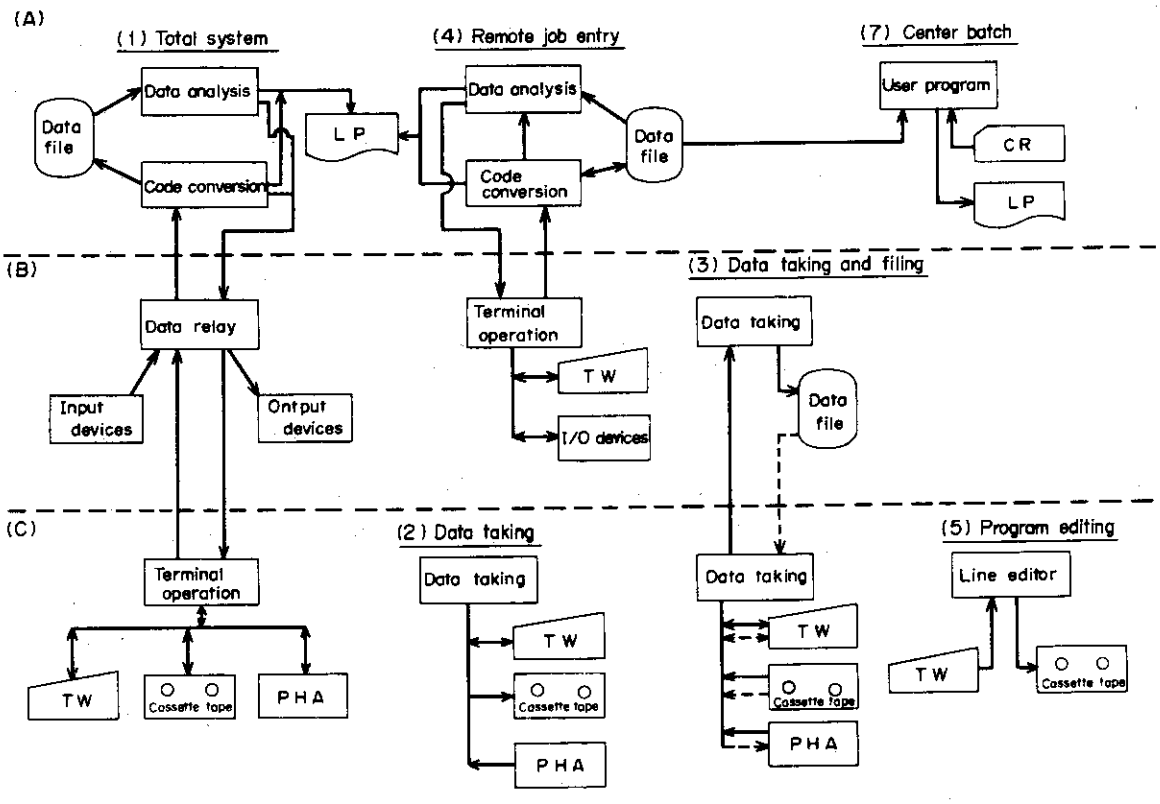

Fig.9.1.2 Examples of hierarchical system use

9.3 Current Status of Genken Programming Language

K. Asai, Y. Onuma and M. Tomiyama

History

GPL(Genken Programming Language) is a computer language designed for software description.[1,2,3]

At first a GPL compiler for FACOM230-60 computers was constructed in 1972 at JAERI computing center. In 1975 the FACOM230-60's were replaced by FACOM230-75's(upward compatible with FACOM230-60) and the compiler was immediately implemented on the FACOM230-75 with minor modifications. It has been used for these years to describe special purpose softwares such as a Fortran language processor, etc.

Needs of compilers for other machines

Recently increasing numbers of mini- and microcomputers and expanding area of applications of these computers at our institute require a considerable amount of software.

Encountering the situation we felt a need for software writing language which is common to several computers. By the language users can share their computer programs regardless of differences of computers. GPL is chosen as one of the languages. It is a modified version of PL360[4] and can specify hardware index registers explicitly in the language. Our procedures for software construction of mini- and microcomputers are as follows;

(i) at first we write programs and test the logical validity of them using GPL for large scale computers,

(ii) after the test, GPL compiler of the large scale computer produces assembly languages for the mini- or microcomputer. Thus we can debug most part of programs using large scale computers,

(iii) then the assembly language programs produced by the large scale computer are assembled to object programs of mini- and microcomputers.

At present GPL compiler for HITAC-10 minicomputer has been constructed and the construction of a compiler for INTEL8080 microcomputer is in progress.

The GPL compiler consists of two parts. One is a collection of routines ANALYSIS which reads the language and produces pseudo one-address machine instructions. The other is a routine INGEN which produces the assembly language from the pseudo instructions.

Experiences

Experiences with the GPL compilers of FACOM230-60, 75 have shown that the compiled object programs for these computers can cope with programs written in assembly languages in their memory utilization and execution efficiency.[2)]

Close investigation of assembled object programs for HITAC-10 shows that the compiled object can also cope with hand coded assembly programs. An example of GPL source language and its compiled assembly language is shown in Fig.9.3.1.

Acknowledgment

The authors wish to express their thanks to Dr. H. Betsuyaku of neutron scattering laboratory for his helpful suggestions on construction of HITAC-10 GPL compiler.

References

1) Asai, K.: "Experience with the GPL", Proceedings of the IFIP Working Conference on Machine Oriented Higher Level Languages, W.I. van der Poel et al.(Eds), Trondheim, Aug. 27-31, 1973, pp.371-376, North-Holland Publ. Co.

2) Asai, K.: "Analysis and Construction of Compiler of a Programming Language by Precedence Grammar with Precedence Functions", JAERI-M

Report 5526, Jan. 1974, Japan Atomic Energy Research Institute.

3) Asai, K. and Tomiyama, M.: "GPL - Genken Programming Language", Reactor Engineering Division Annual Report, JAERI-M 5955, Feb. 1975, Japan Atomic Energy Research Institute.

4) Wirth, N.: "PL360, A Programming Language for the 360 Computers", J.ACM, Vol.15,No.1, pp.37-74, Jan. 1968.

```
BEGIN
FOR X1=1 STEP 1 UNTIL N DO                    /* X1=I */
  BEGIN
  I=X1 *
  X4=I-1*6+I *                                /* X4=(I,I) */
  T(X4)=1.0 *
  FOR X2=I+1  STEP 1 UNTIL N DO               /* X2=J */
  BEGIN
  J=X2 *
  X4=J-1*6+I *                                /* X4=(I,J) */
  X5=I-1*6+J *                                /* X5=(J,I) */
  ((T(X4),T(X5)))=0.0 *
  END *  /* J */
  END *  /* I */
END *  /* VECTOR */
W=0.0 *
```

***** GPL-HITAC 10 SYMBOLIC CODE LIST *****

ISN	LOC.	LABEL	OPC	FLG	OPERAND
201	623		LE		X1
202	624		STE		I
203	625		L		I
204	626		S		G.02
205	627		SRDL		16
206	628		M		G•04
207	629		SLDA		16
208	630		A		I
209	631		ST		X4
210	632		LF		G.05
211	633		L		G•02
212	634		A		X4
213	635		SRDL		16
214	636		M		G•01
215	637		BAL		STF I
216	638		DC		T
217	639		L		I
218	640		A		G.02
219	641		ST		X2
220	642	J.05	L	,1	N
221	643		LE		X2
222	644		STE		T.09
223	645		S		T•09
224	646		KPA		
225	647		B		J•04
226	648		LF		X2
227	649		STE		J
228	650		L		J
229	651		S		G.02
230	652		SRDL		16
231	653		M		G•04
232	654		SLDA		16
233	655		A		I
234	656		ST		X4
235	657		L		I
236	658		S		G.02

Fig. 9.3.1 GPL source statements and compiled assembly statements

Publication List

1. Nuclear Data and Group Constants

(1) Mitani, H.: Basic Study on the Adjustment of Group Cross Sections by Means of Integral Data," JAERI-M 5767 (1974) (in Japanese)

(2) Kikuchi, Y., Hasegawa, A., Tasaka, K., Nishimura, H., Otake, I., Katsuragi, S.: "JNDC Fission Product Group Constants - Preliminary Version -," JAERI-M 6001 (1975)

(3) Tasaka, K., Sasamoto, N.: "Energy Release from the Decay of Fission Products," NEACRP-L-111 (1974)

(4) Tasaka, K., Sasamoto, N.: "Calculation of the Decay Power of Fission Products," Nucl. Sci. Eng. 54, 177 (1974)

(5) Tasaka, K.: "Calculation of the Decay Power of Fission Products Considering Neutron Capture Transformation," JAERI-M 5972 (1975) (in Japanese)

(6) Nakajima, R., Takahashi, S., Aizawa, K., Tasaka, K., Yamada, K., Iijima, S.: "After Heat from Fission Products," J. Atomic Energy Soc. Japan, 17, 3 (1975) (in Japanese)

(7) Tasaka, K.: "Nuclear Data for Calculation of Decay Power of Fission Products," JAERI-M 5997 (1975) (in Japanese)

2. Theoretical Method and Code Development

(1) Ise, T., Nakahara, Y., Akimoto, M.: "Thermal Neutron Spectrum, Prompt Negative Temperature Coefficients and Kinetics Parameters of the NSRR (Physics and Nuclear

Analysis of the Nuclear Safety Research Reactor - 1)," JAERI-M 5730 (1974) (in Japanese)

(2) Horikami, K., Nakahara, Y., Fujimura, T., Ohnishi, T.: "Finite Element Method for Solving Neutron Transport Problems in Two-Dimensional Cylindrical Geometry," JAERI-M 5793 (1974)

(3) Izui, K., Nishida, T., Furuno, S., Ohtsu, H.: "Many Wave Effects on Electron Microscope Images of Lattice Defects," JAERI-M 5829 (1974) (in Japanese)

(4) Asaoka, T., Nakahara, Y., Miyasaka, S., Horikami, K., Suzuki, T., Nishida, T., Taji, Y., Tsuchihashi, K., Gotoh, H., Seki, Y., Nakagawa, M., Hirota, J.: "Coarse Mesh Rebalance Acceleration for Eigenvalue Problems," ANL-75-2 (NEA-CRP-L-118) (1975)

(5) Kobayashi, K., Namatame, K.: "Method of Characteristics for Solving Axi-Symmetric Two-Dimensional Flows," JAERI-M 5969 (1975)

(6) Tsutsui, T., Ise, T.: "Multigroup Cross Section Production by the GGC-4 Computer Code," JAERI-M 5991 (1975) (in Japanese)

(7) Nakahara, Y.: "Neutron Thermalization," Genshiryoku Kōgyō (Atomic Energy Industries), 21, No. 4, 70 (1975) (in Japanese)

(8) Kawamura, H.: "Calculation of the Modified Bessel Functions of Integer Order and the Function Subprograms," JAERI-M 6208, (1975) (in Japanese).

(9) Ishiguro, Y.: "Multiregion Equivalence Relation for Resonance Heterogeneity Effects," Nucl. Sci. Eng., 55, 349 (1974)

(10) Kikuchi, Y., Katsuragi, S.: "Approximate Expression of Collision Density and Correction of Group Elastic Removal Cross Section Near a Wide Scattering Resonance," JAERI-M 5963 (1975)

(11) Ishiguro, Y.: "HETERO: A Code for Calculation of Resonance Heterogeneity in Fast Reactor Lattice Cells," JAERI-M 5940

(12) Nakagawa, M.: "SLAROM: A Code for Calculation of a Heterogeneous Core in Fast Reactor," JAERI-M 5916 (1974) (in Japanese)

(13) Hasegawa, A., Tsuruta, S., Ishiguro Y.: "Treatment of the Elastic Removal Cross Sections in Na-Fe Resonance Region and One-Dimensional Code EXPANDA-70 DRA," JAERI-M 6081 (1975) (in Japanese)

(14) Gotoh, Y., Tsuchihashi, K.: "The Resonance Integral of Coated Particles," Nucl. Sci. Eng., 58, 213 (1975)

(15) Gotoh, Y.: "Study of the Power Spectral Density by a Nonlinear Response to the Stochastic Input," Annals of Nucl. Energy, 2, 119 (1975)

3. Integral Experiment and Analysis

(1) Iijima, T., Hirota, J., Shirakata, K., Kobayashi, K., Fujisaki, S., Kusano, J.: "Measurement and Analysis of Density Coefficient on FCA-V," JAERI-M 5890 (1974) (in Japanese)

(2) Iijima, T., Hirota, J., Obu, M. Kusano, J., Yamagishi, K., Watanabe, H., Ogawa, N.: "Density Coefficient Measurements in FCA Assembly VI-1," JAERI-M 6062 (1975) (in Japanese)

(3) Iijima, T.: "Applicability of the Density Coefficient Method for Large Fast Reactors," JAERI-M 6063 (1975) (in Japanese)

(4) Mizoo, N., Nakano, M., Mukaiyama, T., Cho, M.: "Reactivity Measurement in a Far-Subcritical Fast System (I)," JAERI-M 6066 (1975) (in Japanese)

(5) Mukaiyama, T., Nakano, M., Mizoo, N., Cho, M.: "Reactivity Measurement in a Far-Subcritical Fast System (II)," JAERI-M 6067 (1975) (in Japanese)

(6) Kaneko, Y.: "Integral-Versions of Some Kinetic Experiments for Determining Large Negative Reactivity of Reactor," J. Nucl. Sci. Technol. 12, 402 (1975)

4. Shielding

(1) Ando, Y., Miyasaka, S., Takeuchi, K.: "Radiation Leakage of Nuclear Ship Mutsu," J. At. Energy Soc. Japan, 17, 57 (1975)

(2) Miyasaka, S., Taji, Y., Okada, T., Minami, K., Inoue, S., Ideta, T., Seki, Y., Ando, H., Iida, H., Fujimura, T., Asaoka, T., Hirota, J.: "Code System for the Radiation-Heating Analysis of a Nuclear Reactor, RADHEAT," JAERI-M 5794 (1974) (in Japanese)

(3) Miyasaka, S., Minami, K., Kuroi, H., Hirota, J.: "Sensitivity and Uncertainty Analysis for Iron Cross Sections," NEA-OECD, Paris (1975)

5. Heat Transfer and Fluid Dynamics

(1) Shimomura, H., Kawamura, H., Okamoto, Y.: "Thermal and Hydraulic Performance of High Temperature Helium Gas Loop," Winter Meeting of ASME, New York (1974)

(2) Kawamura, H., Shimomura, H., Okamoto, Y., Akino, N.: "High-Temperature Thermometry of High-Temperature Helium Gas Loop," ENEA, Petten (1974)

6. Reactor and Nuclear Instrumentation

(1) Sakai, E., Terada, H., Katagiri, M.: "Test Procedures for Germanium Gamma-Ray Detectors (A Japanese Version of IEC Publication 430)," JAERI-M 5914 (1975) (in Japanese)

(2) Sakai, E.: "Test Procedures for Germanium Gamma-Ray Detectors (Summary of IEC Publication 430)," Hoshasen (Ionizing Radiation), 2, No. 1, (1975) (in Japanese)

(3) Sakai, E., Terada, H., Katagiri, M., Itoh, H.: "Temperature Cycling Test of Hyper-Pure Germanium Detector," JAERI-M 5988 (1975) (in Japanese)

(4) Sakai, E.: "Semiconductor Radiation Detector," Text for Radioisotope School Cource - Radioisotope Application and Instrumentation, (1975) (in Japanese)

(5) Sakai, E., Terada, H., Suzuki, S., Katagiri, M., Shirai, E.: "Gamma-Ray Spectrum Measurement in Japan Research Reactor No. 3 Using A Portable Ge(Li) Spectrometer," JAERI-M 6024 (1975) (in Japanese)

(6) Sakai, E., Katagiri, M., Terada, H., Itoh, H., Sukegawa, T., Hirano, K.: "Performance of Fuel Failure Detection System in Sodium In-Pile Loop Experiment (III) - Preparation and Out-of-Pile Test of Fuel Failure Detection

System -," SJ 250 75-04 (1975) (in Japanese)

(7) Sakai, E., Terada, H., Katagiri, M., Itoh, H.: "Progress Report-Semiconductor Detector Group (April 1, 1974 to March 31, 1975)," JAERI-M 6258 (1975)

(8) Furuta, Y., Tanaka, S.: "Neutron Dosimetry by Thermoluminescence Dosimeter," International Symposium on Radiation Physics, Calcutta (1974)

(9) Furuta, Y., Tanaka, S.: "The Relation between Light Conversion Efficiency and Stopping Power of Charged Particles in Thermoluminescence Dosimeter," Proceedings of 4th International Conference on Luminescence Dosimetry, p. 97, Krakow (1974)

(10) Tanaka, S., Furuta, Y.: "Neutron Responses of Thermoluminescence Dosimeters, BeO(Na), $CaSO_4$(Tm), and Its Mixture with ^6LiF or ^7LiF," Ibid. p. 1213 (1974)

(11) Tasaka, K.: "Standard Spectrum Method for Analysis of a Gamma-Ray Spectrum and its Application to an Irradiated Fuel," JAERI-M 5947 (1974) (in Japanese)

(12) Sekiguchi, A., Natsume, H., Miki, R., Kitamori, T., Hasegawa, k., Michikawa, T., Matsuura, S., Yagi, H., Gotoh, H., Onishi, H., Takahashi, M., Tsuji, N., Onishi, K., Asakura, Y., Okuhara, H., Mori, R., Hoshino, K., Osabe, T., Tanaka, R.: "Studies on Accounting Methods of Nuclear Material for Verification in Safeguards," Nuclear Material Control Center Report (1975) (in Japanese)

(13) Gotoh, H., Yagi, H.: "Passive Gamma Assay," 4, No. 4, 4, (1975) (in Japanese)

(14) Gotoh, H.: "Activation Rate, Energy Spread of Neutrons and Semiconductor Proton Recoil Counters," KURRI-TR Report (in Japanese) (in press)

7. Dynamics Analysis and Control Method Development

(1) Oguma, R., Fujii, Y., Usui, H., Watanabe, K.: "Computer Code MLCOSP for Multiple-Correlation and Spectrum Analysis with a Hybrid Computer," JAERI-M 6252 (1975)

(2) Oguma, R., Fujii, Y.: "Identification of OWL-0 Plant and Evaluation of its Control Systems," Preprints of the 14th SICE Conference (1975)

8. Fusion Reactor Technology

(1) Hiraoka, T., Maekawa, H., Seki, Y., Hirota, J.: "Integral Experiments on Spherical Lithium Metal Blanket System," Nucl. Fusion Special Suppl. 1974, Proc. Symp. Fusion Reactor Design Problems, p. 363, I.A.E.A. (1974)

(2) Maekawa, H.: "A Method for Obtaining the Tritium Production Rate Distribution with a LiF Thermoluminescence Dosimeter," JAERI-M 6055 (1975) (in Japanese)

(3) Moriyama, M., Seki, Y., Maekawa, H.: "Neutronic Calculation on Fusion Reacctor Blanket by S_n Approximation," JAERI-M 6072 (1975) (in Japanese)

(4) Kawamura, H., Seki, M., Shiina, Y., Sanakawa, K.: "Experimental Studies on Heat Transfer dy Natural Convection and Pool Boiling of Sodium in a Strong Magnetic Field," J. Nucl. Sci. Technol. 12, 280 (1975)

9. Activities of Computing Center

(1) Ishiguro, M.: "Remote Batch Station for Paper Tape

Input," JAERI-M 5739 (1974)

(2) Tsugita,: "USC-3 Terminal Station System Program," JAERI-M 5768 (1974)

(3) Ikushima, T., Nakamura, Y., Onuma, Y.: "Seismic Simulation Analysis of Reactor Core using Graphic Display," BIT, 7, No. 1 (1975)

(4) Nakamura, Y., Onuma, Y.: GSL: A Graphic Subroutine Library for Various Graphic Input and output Devices," Proceedings of Programming Symposium, Hakone, p. 1 (1975)

(5) Ikushima, T., Onuma, Y., Nakamura, Y.: "Seismic Simulation Program using Graphic Display for Block-type Fuel HTGR Core," JAERI-M 5981 (1975)

(6) Nakamura, Y., Onuma, Y.: "PGSLIB/BASIC: A Basic Software for Graphic Programming," JAERI-M 6023 (1975)

(7) Nakamura, Y., Onuma, Y., Namatame, K., Suzuki, N.; "GROSA-II: Interactive Data Analysis System for ROSA-II using Graphic Display," JAERI-M 6237 (1975)